

Impact of physicochemical properties of lignin-based polymers on their flocculation and adsorption performance

A Thesis Presented to the
Faculty of Graduate Studies of
Lakehead University

By

Sanaz Sabaghi

Submitted in partial fulfillment of requirements
for the degree of Doctor of Philosophy in Chemical Engineering

January 2021

© Copyright Sanaz Sabaghi, 2020

Dedication

To my late father who has been my constant source of inspiration

To my spouse, Farshid Soltani, for his support and encouragement throughout my studies.

To my mother for her unfeined love and ever-present support of my personal endivorurs towards
learning

ACKNOWLEDGMENTS

My special thanks to my supervisor, Professor Pedram Fatehi, for his consistent guidance and support throughout the course of my research at Lakehead University. His support and priceless advice helped me enhance my academic experience and ability to complete this research thesis.

I am also grateful to the following people for their support and valuable suggestions during the course of this thesis:

My committee members Dr. Baoqiang Liao, Dr. Wensheng Qin and Dr. Zhaojiang Wang for their valuable input and kind support,

Mr. Michael Sorokopud, Dr. Guoseheng Wu, Mr. Martin Griffith and Mr. Greg Krepka, LUIL department for their generous help,

My previous and current lab members for their kind assistance and encouragement that provide me an ideal workplace environment.

Finally, my parents, my husband Farshid Soltani and my brother for their love and encouragement.

ABSTRACT

Industrial and municipal effluents contain colloidal charged particles, dissolved salts, heavy metals and other impurities, which may represent varied health risks and must be removed before discharge into the environment. Coagulation and flocculation techniques are highly efficient for the treatment of hydrophobic pollutants and suspended particles. Natural based polymers have been recognized as green chemicals for wastewater treatment system, which are environmentally attractive and financially feasible.

In this research, lignin, the second most abundant aromatic polymer was polymerized with cationic, anionic and non-ionic monomers to synthesize lignin-based macromolecule with desired characteristics (i.e., charge density, molecular weight, hydrodynamic radius). The successful polymerization reaction was assessed using nuclear magnetic resonance (NMR), Fourier transform infrared (FTIR) spectrophotometry, gel permeation chromatography (GPC) and elemental analyses.

The interaction of lignin-based derivatives with different suspended particles and their adsorption/flocculation performance in various waste solutions was comprehensively assessed. Moreover, a strong correlation between the molecular conformation of lignin-derivatives and their flocculation behavior was observed, in which the polymer with more extended configuration (larger hydrodynamic radius and radius of gyration) revealed the greater bridging affinity. It was also shown that the conformational changes of lignin macromolecules had a remarkable effect on its molecular weight and subsequently the flocculation performance and floc properties (e.g., size, shape and strength) when they are used in suspension systems.

The effect of chain conformation on the self-assembly of kraft lignin-based polymers in aqueous solutions was investigated using a dynamic light scattering (DLS) instrument. The viscoelastic properties of the adsorbed polymer on particles assessed by a Quartz crystal microbalance with dissipation (QCM-D), was shown to be correlated with polymer conformation. It was revealed that the polymer with flexible chain conformation had a more accelerated self-assembly, which enhanced its settling performance under both gravitational and centrifugal forces. The rheological properties of lignin-based polymers in solutions as well as their thermal behaviour were observed to be affected by different morphologies. The compact coil structure of lignin-based macromolecule restricted its free molecular movement resulted in higher T_g values.

The structure of monomers attached to the lignin backbone can also impact the polarity of lignin macromolecules after the polymerization reaction. The higher polarity and more flexible random coil chain configuration of polymers impacted the better flocculation efficiency of cationic hydrolysis lignin in aqueous solutions. The results also showed that the adsorption of lignin polymers was decreased by ionic strength increase. In the presence of urea, the hydrophobic interaction of cationic hydrolysis lignin and the particles were highlighted, which increased the adsorption efficiency of less polar polymer.

The combination of anionic and cationic lignin in a dual polymer system, as a green and effective flocculation system, for ion removals of a model effluent (i.e., Zn^{2+} , Cu^{2+} , and K^+) was comprehensively studied. The interaction of soluble ions and lignin-based polymers was investigated using a Quartz crystal microbalance (QCM), X-ray photoelectron spectroscopy (XPS) and a vertical scan analyzer (VSA). Based on adsorption, sedimentation, and floc size analyses,

the dual polymer system of anionic/cationic lignin polymers was a promising alternative for the removal of dissolved ions from solutions.

The findings of the present research prove the possibilities for use of the lignin macromolecule as flocculant or adsorbent in various wastewater system and provides more insights into how the structural changes of lignin-based derivatives would notably alter their performance in aqueous solution and suspension systems. The results shed light on the extending lignin applications via engineering the characteristics of lignin macromolecules.

Table of Contents

ACKNOWLEDGMENTS.....	iii
ABSTRACT.....	iv
List of Figures	xii
List of Tables	xvii
List of Schemes.....	xix
Chapter 1: Introduction	1
1.1 Overview	1
1.2 Objectives.....	5
1.3 References	6
Chapter 2: Literature review.....	10
2.1 Introduction	10
2.2. Background	10
2.2.1 Colloidal System.....	10
2.2.2 Kaolin characteristics	11
2.2.3 Colloidal stability of clay suspension	13
2.2.4 Polymeric flocculants	14
2.2.5 Lignin	16
2.2.6 Lignin structure and properties	16
2.2.7 Lignin production	18
2.2.8 Lignin modification.....	19
2.2.9 Free radical polymerization	19
2.2.10 Free radical copolymerization of lignin with cationic monomer	21
2.2.11 Lignin application	25
2.3 Fundamentals	26
2.3.1 Polymer adsorption.....	26
2.3.2 Effect of charge density and molecular weight	26
2.3.3 Effect of ionic strength.....	27
2.3.4 Effect of particle size.....	28
2.3.5 Effect of polymer structure.....	29
2.3.6 Relative turbidity.....	30

2.3.7 Zeta potential concept	30
2.3.8 Effect of polymer characteristics on flocculation of clay suspensions	32
2.4 Methodology.....	32
2.4.1 Charge density analysis.....	32
2.4.2 Modified polymer characterization	34
2.4.3 Clay properties	42
2.4.4 Properties of clay suspensions.....	43
2.5 Summary	51
2.6 References	52
Chapter 3: Phenomenological Changes in Lignin Following Polymerization and its Effects on Flocculating Clay Particle.....	70
3.1 Abstract.....	70
3.2 Introduction	70
3.3 Materials and Methods.....	74
3.3.1 Materials	74
3.3.2 Lignin Polymerization.....	75
3.3.3 Characterization of Macromolecules and Kaolin	76
3.3.4 Surface Tension and Contact Angle Measurements	76
3.3.5 Flocculation	77
3.4 Results and Discussions	78
3.4.1 Synthesis and Characterization of KL-METAM and KL-ATAC	78
3.4.2 Configurational Changes of Lignin Macromolecules in Aqueous Solutions.....	82
3.4.3 Behavior of Lignin Polymers in Solution Systems	84
3.4.4 Adsorption.....	85
3.4.5 Behavior of Lignin Macromolecules in Flocculation	89
3.4.6 Application	98
3.5 Conclusions	99
3.6 References	100
Chapter 4: Impact of the Chain Conformation of Lignin macromolecules on their Adsorption, Rheological Properties and Thermal behaviour	114
4.1 Abstract.....	114
4.2 Introductions.....	115
4.3 EXPERIMENTAL SECTION	117

4.3.1 Materials	117
4.3.2 Lignin polymerization.....	118
4.3.4 Characterization of Macromolecules.....	119
4.3.5 Quartz Crystal Microbalance with Dissipation (QCM-D) Studies.....	121
4.3.6 Gravitational sedimentation analysis	121
4.3.7 Centrifugal sedimentation analysis.....	122
4.3.8 DSC Analysis	123
4.3.9 Rheological Properties	123
4.4 Results and Discussions	124
4.4.1 Characterizations of KL-METAM and KL-ATAC.....	124
4.4.2 Behavior of Lignin Polymers in Solution Systems	127
4.4.3 Stability of Lignin Macromolecules.....	129
4.4.4 Adsorption Behavior	132
4.4.5 Rheological Behavior of Lignin Macromolecules	137
4.4.6 Thermal Behavior of Lignin Macromolecules	140
4.4.7 Application	142
4.5 Conclusions	143
4.6 References	144
Chapter 5: Polarity of Cationic Lignin Polymers: Physicochemical Behavior in Aqueous Solutions and Suspensions.....	155
5.1 Abstract.....	155
5.2 Introduction	156
5.3 Experimental Section	158
5.3.1 Materials	158
5.3.2 Theoretical analysis.....	159
5.3.3 Cationization of hydrolysis lignin	159
5.3.4 Characterization of HL and CHL	160
5.3.5 Adsorption test	163
5.3.6 Flocculation analysis via photometric dispersion analyzer (PDA)	164
5.3.7 Flocculation analysis via focused beam reflectance measurement (FBRM).....	165
5.4 Results and Discussion	165
5.4.1 Structure of lignin polymer	165

5.4.2 Characterization of lignin polymer.....	167
5.4.3 Properties of CHLs.....	171
5.4.4 Adsorption analysis.....	176
5.4.5 Flocculation analysis.....	180
5.5 Conclusions.....	188
5.6 References.....	189
Chapter 6: Dual Lignin-derived Polymeric Systems for Ions Removal.....	200
6.1 Abstract.....	200
6.2 Introduction.....	201
6.3 Materials and Methods.....	203
6.3.1 Materials.....	203
6.3.2 Characterization of lignin polymers.....	204
6.3.3 Coating lignin derivatives on QCM sensor.....	204
6.3.4 Synthetic ion solutions.....	205
6.3.5 Adsorption studies.....	205
6.3.6 Contact angle measurement.....	206
6.3.7 Zeta potential analysis.....	207
6.3.8 X-ray Photoelectron Spectroscopy.....	207
6.3.9 Vertical scan analyzer.....	208
6.4 Results and Discussions.....	209
6.4.1 Properties of lignin polymers.....	209
6.4.2 Adsorption analysis of single KL-METAM or KL-AA.....	212
6.4.3 Surface wettability of model surfaces.....	216
6.4.4 Surface composition changes.....	217
6.4.5 Mechanism of adsorption of ions on lignin derivatives.....	220
6.4.6 Flocculation analysis.....	223
6.4.7 Dual polymer system.....	224
6.4.8 Adsorption and flocculation in a mixed system.....	229
6.4.9 Ion removal efficiency using different materials.....	232
6.5 Conclusions.....	234
6.6 References.....	235

Chapter 7: Production and Application of Triblock Hydrolysis Lignin-based Anionic Copolymer in Aqueous Systems	245
7.1 Abstract	245
7.2 Introduction	246
7.3 Materials and methods	249
7.3.1 Materials	249
7.3.2 Synthesis and purification of HAM copolymer	249
7.3.3 Characterization of lignin polymers	250
7.3.4 Quartz crystal microbalance with dissipation (QCM-D) Studies	252
7.3.5 Rheological studies	252
7.3.6 Zeta potential analysis	253
7.3.7 Flocculation analysis	253
7.3.8 Thermogravimetric Analysis (TGA)	254
7.3.9 Differential scanning calorimetry (DSC)	254
7.4 Results and discussion	254
7.4.1 Characterization of lignin polymers	254
7.4.2 Adsorption Analysis	259
7.4.3 Rheological Characteristics	263
7.4.5 Thermal Properties	265
7.4.6 Behavior of lignin macromolecules in flocculation process	268
7.4.7 Comparison	273
7.5 Conclusions	275
7.6 References	275
Chapter 8: Conclusions and Recommendations for Future Works	286
8.1 Conclusions	286
8.2 Future work	289
Chapter 9: Appendix	291

List of Figures

Figure 2. 1 Diagrammatic sketch of the Kaolin structure	13
Figure 2. 2 The three main monomer building blocks of lignin. ³³	16
Figure 2. 3 Schematic representation of the common lignin chemical bonds. ³³	17
Figure 2. 4 Reaction scheme of lignin and METAM/ATAC.....	23
Figure 2. 5 Reaction scheme of lignin and METAC/MAPTAC.....	24
Figure 2. 6 Adsorption configuration with high and low charged cationic polymers on a particle surface with negative charge density. ^{67,68}	27
Figure 2. 7 Distribution of electrical potential in the double layer region surrounding a charged particle showing the position of the zeta potential. ⁸⁹	31
Figure 2. 8 Schematic principle of TGA measurement. ¹⁰⁴	35
Figure 2. 9 Schematic of an apparatus for measurement of static light scattering. ¹¹⁴	40
Figure 2. 10 contact angle measurement on a smooth homogeneous solid surface. ¹¹⁷	41
Figure 2. 11 Schematic representations of FBRM probe and chord length measurement. ¹³⁰	47
Figure 2. 12 Measurement principle diagram of the Turbiscan Lab Expert type stability analyzer. ¹³⁴	48
Figure 2. 13 Schematic configuration and measurement principle of the LUMiSizer®. ¹³⁸	49
Figure 2. 14 Schematic representation of QCM-D principle and related plots.....	51
Figure 3. 1 The relationship between relative turbidity and zeta potential of kaolin suspension (25 g/L kaolin suspension at pH 6)	91
Figure 3. 2 SEM images of (a) kaolin (b) kaolin/KL-ATAC (c) kaolin-KL-METAM generated at a 16 mg/g polymer dosage	93
Figure 3. 3 a) chord length and b) number of particle counts for the system at the 16 mg/g dosage of CKL/Kaolin as a function of time (conducted under the condition of 25 g/L concentration, pH 6, and stirring at 200 and 700 rpm)	95
Figure 4. 1 Double logarithmic plot of the radius of gyration (R_g) vs the molecular weight (M_w) of the KL-METAM and KL-ATAC series	126
Figure 4. 2 The dependence of shape factor to the grafting ratios of KL-METAM and KL-ATAC.....	127
Figure 4. 3 a) Contact angle and b) surface tension of water/CKL droplets.....	129
Figure 4. 4 Semi-log plot of a) destabilization index, b) sediment thickness and c) sedimentation velocity (at 127 RCF) of CKLs as a function of R_g	132

Figure 4. 5 Semi-log plot of changes in frequency and dissipation of the SiO ₂ sensor for the adsorption of CKLs at a) initial and b) late stage as a function of R _g	136
Figure 4. 6 Effect of adsorbed mass on the settling behaviour of CKLs with various M _w	137
Figure 4. 7 Semi log plot of rheological characteristics of CKLs during adsorption as a function of R _g	140
Figure 5. 1 Adsorption of CHLs on kaolin particles in the presence of salt. (100% adsorbed amount was considered with respect to the highest adsorbed amount of CHLs on kaolin; 66 and 41 mg/g for HL-METAC and HL-MAPTAC).....	178
Figure 5. 2 Adsorption of CHLs on kaolin particles in the presence of urea. (100% adsorbed amount was considered with respect to the highest adsorbed amount of CHLs on kaolin; 66 and 41 mg/g dosages for HL-METAC and HL-MAPTAC).....	180
Figure 5. 3 Stability ratio (log W) as a function of CHL dosage.....	182
Figure 5. 4 The relationship between chord length and adsorbed mass.....	185
Figure 5. 5 Influence of urea concentration (0-1000 mM) on the mean chord length and number of counts of the a,b) HL-METAC, and c,d) HL-MAPTAC samples as a function of time (pH 6, 25 °C and 25 g/L of kaolin concentration).	187
Figure 6. 1 Dissipation change of the sensors as a function of frequency changes in the adsorption of ions on a) KL-METAM and b) KL-AA; the adsorbed mass of ions on c) KL-METAM and d) KL-AA as a function of time (experiments were conducted with ionic composition at 10 mM)	216
Figure 6. 2 Mechanism model of ions adsorption using a) KL-AA and b) KL-METAM coated surface.....	223
Figure 6. 3 Dual component adsorption of CuCl ₂ , ZnCl ₂ , and KCl on a) KL-METAM surface, b) KL-AA surface (10 mM salt concentration, the control solution contained lignin derivative with the opposite charge to the lignin coated surface).....	226
Figure 6. 4 The effect of dual polymer system on the destabilization index of the model solutions (control solution contained lignin derivative with the opposite charge and no salt)	228
Figure 6. 5 Dual-component adsorption of mixed model solution (10 mM, 20 min, salt solutions are mixed with lignin polymer and adsorbed on the oppositely charged lignin coated surface).....	231
Figure 6. 6 Proposed adsorption mechanism of the dual-component adsorption in mixed model solution on QCM sensor coated with a) KL-AA and b) KL-METAM.....	231
Figure 6. 7 The effect of the dual polymer system on the destabilization index of the mixed model solutions (10 mM)	232

Figure 7. 1 Adsorption of HL, HAs, HM and HAMs on the aluminium oxide sensor: a) frequency changes, b) dissipation changes (vertical dash line shows buffer rinsing).....	261
Figure 7. 2 Plot of storage and loss modulus as a function of angular frequency for lignin samples (G' and G'' are respectively represented as solid and open symbols).	265
Figure 7. 3 a) Weight loss and b) weight loss rate of HL, HM, HAs and HAMs at a heating rate of 10 °C/min.....	268
Figure 7. 4 The change in the chord length of flocs in aluminum oxide suspension in the presence of 2.4 mg/g polymers dosage at different shear rates.....	272
Figure A. 1 Adsorption of KL and CKLs on kaolin as a function of polymer dosage under the conditions of pH 6, 25 °C and 25 g/l of kaolin concentration	296
Figure A. 2 Plots of surface tension of aqueous solution against natural logarithm.....	298
Figure A. 3 Effect of adsorbed CKLs on kaolin particles conducted under the conditions of pH 6, 25 °C and 25 g/L of kaolin concentration.....	299
Figure A. 4 Effect of CKLs adsorption on the relative turbidity of kaolin suspension conducted under the condition of pH 6, 25 °C and 25 g/L of kaolin concentration.	300
Figure A. 5 Volume fraction of kaolin particles as a function of their size	302
Figure A. 6 Effect of time on the hydrodynamic radius of a) KL-METAM and b) KL-ATAC at different grafting ratio (The Control sample is KL).	306
Figure A. 7 Effect of time on the destabilization index of a) KL-METAM and b) KL-ATAC at different grafting ratio.....	306
Figure A. 8 Stability of a) KL-METAM and b) KL-ATAC conducted under conditions of 1g/L CKL concentration, 25 °C at RCA of 5,32 and 127 (g).....	307
Figure A. 9 Dissipation change of the sensors as a function of frequency changes upon adsorption of a) KL-METAM and b) KL-ATAC on the SiO ₂ surface at different grafting ratio.....	308
Figure A. 10 (a) Theoretical adsorbed mass required for developing a monolayer CKL coverage on QCM surface. (b) Experimental adsorbed mass of CKL on the SiO ₂ surface.	309
Figure A. 11 Changes in a) frequency and b) dissipation of the SiO ₂ sensor for the adsorption of CKLs.....	310
Figure A. 12 Storage and loss modulus of a) KL-METAM and b) KL-ATAC at different grafting ratio and 25 °C as a function of frequency (The G' and G'' are respectively represented as solid and open symbols)	311
Figure A. 13 Semi log plot of storage (G') and loss modulus (G'') of CKLs at 25 °C as a function of radius of gyration.....	312

Figure A. 14 ^{31}P -NMR spectrum of a) HL, b) HL-METAC and c) HL-MAPTAC.....	313
Figure A. 15 ^1H NMR spectra of a) HL, b) HL-MAPTAC, and c) HL-METAC.....	315
Figure A. 16 FTIR spectra of HL and CHL.....	316
Figure A. 17 GPC traces for HL-MAPTAC and HL-METAC.....	317
Figure A. 18 Adsorption of CHLs on kaolin particles as a function of polymer dosage under the conditions of pH 6, 25 °C and 25 g/L of kaolin concentration.....	317
Figure A. 19 Effect of urea addition on the electrophoretic mobility of CHLs conducted under the conditions of pH 6, 25 °C and 25 g/L of kaolin concentration.....	318
Figure A. 20 Effect of CHLs adsorption on the relative turbidity of kaolin suspension conducted under the condition of pH 6, 25 °C and 25 g/L of kaolin concentration.	319
Figure A. 21 Electrophoretic mobilities of kaolin particles with CHLs in aqueous suspensions conducted under the conditions of pH 6, 25 °C and 25 g/L of kaolin concentration.....	320
Figure A. 22 Evolution of flocculation process using different CHLs conducted under the conditions of pH 6, 25 °C and 25 g/L of kaolin concentration.....	320
Figure A. 23 Stability ratio W of kaolin particles in the presence of salt conducted under the conditions of pH 6, 25 °C and 25 g/L of kaolin concentration.....	321
Figure A. 24 Influence of KCl concentration (0-100 mM) on the mean chord length and number of counts of the a,b) HL-METAC and c,d) HL-MAPTAC samples as a function of time (pH 6, 25 °C and 25 g/L of kaolin concentration).	323
Figure A. 25 Effect of salt addition on the electrophoretic mobility of CHLs conducted under the conditions of pH 6, 25 °C and 25 g/L of kaolin concentration.....	323
Figure A. 26 The changes in frequency and dissipation a result of model waste adsorption on a) KL-METAM and b) KL-AA coated sensor at different concentrations (1, 10 and 100 mM).....	328
Figure A. 27 XPS survey spectra of a) KL-METAM and b) KL-AA.....	329
Figure A. 28 The effect of KL-METAM dosage (0-10 mg/L) on destabilization index of model wastewater a) ZnCl_2 , b) CuCl_2 , and c) KCl, (wastewater concentration 10mM, polymer concentration 10 g/L, 30 °C, 30min).....	331
Figure A. 29 The effect of KL-AA dosage (0-10 mg/L) on destabilization index of model wastewater a) ZnCl_2 , b) CuCl_2 , c) and KCl (wastewater concentration 10mM, polymer concentration 10 g/L, 30 °C, 30min).....	332
Figure A. 30 Zeta potential changes of adsorbed KL-METAM and KL-AA on a) ZnCl_2 , b) CuCl_2 , and c) KCl (wastewater concentration 10mM, 25 °C).....	334

Figure A. 31 The effect of lignin-based polymers on destabilization index of mixed model wastewater containing ZnCl ₂ , CuCl ₂ , and KCl (wastewater concentration 10mM, polymer concentration 10 g/L) .	334
Figure A. 32 ¹ H-NMR spectra of a) HL, b-c) HA, d) HM and e-f) HAM polymers.	339
Figure A. 33 Dissipation change of the sensors as a function of frequency changes for adsorption of HAMs on the aluminium oxide surface	339
Figure A. 34 Surface tension of HAM polymer solution versus natural logarithm of concentration	340
Figure A. 35 Zeta potential of aluminium oxide particles in the presence of HL, HM, HAs and HAMs as a function of polymer dosage (conducted under the conditions of pH 7, 25 C and 25 g/l of aluminium oxide concentration).	341
Figure A. 36 Normal-weighted chord length distribution of particles in aluminum oxide suspension at different dosages of a) HL and b) HM c) HA1 d) HA2 e) HAM1 f) HAM2 (25 g/L concentration, pH 7 and 200 rpm).....	344

List of Tables

Table 2. 1 Various available flocculants and their applications.....	15
Table 2. 2 Percentage of different linkages in softwood lignin.	17
Table 3. 1 Characteristics of KL, KL-ATAC, and KL-METAM.....	81
Table 3. 2 Characteristics of KL, KL-ATAC, and KL-METAM.....	84
Table 3. 3 The contact angle of droplets on different surfaces and surface and interface tensions of solutions and kaolin particles.....	85
Table 3. 4 Characteristics of kaolin and modified kaolin with CKL	87
Table 3. 5 Deflocculation and reflocculation parameters for the systems of kaolin and CKLs at 16 mg/g dosages.....	98
Table 4. 1 Properties of DSC analysis for CKLs at different grafting ratio.....	141
Table 5. 1 Properties of HL and CHLs.	172
Table 5. 2 Configurational changes of lignin polymers in presence of salt and urea (10mM).....	176
Table 6. 1 Properties of KL, KL-METAM, and KL-AA	211
Table 6. 2 Contact angles of water and model solutions (10mM) on lignin coated surfaces.....	217
Table 6. 3 XPS characterization of the lignin films before and after ionic adsorption	219
Table 6. 4 Mean aggregate sizes (d) obtained for the model solutions in the single and dual polymer systems (conducted under the conditions of 10 g/L polymer solution, and 0 or 10 mM model effluent).....	229
Table 6. 5 Comparison of various polymers for the destabilization of ions in water	233
Table 7. 1 Properties of HL and HAM polymers.	256
Table 7. 2 Adsorption properties of lignin macromolecules on aluminium oxide surface at equilibrium.	261
Table 7. 3 The deflocculation and reflocculation parameters of aluminium oxide/HAMs systems under different shear rates.....	272
Table 7. 4 Comparison of various flocculants for wastewater treatment systems.	273
Table A. 1 Theoretical predictions of CKLs adsorption times.....	302
Table A. 2 The properties of KL, KL-METAM, and KL-ATAC	303

Table A. 3 Hydroxy group contents of HL and CHLs determined by ^{31}P NMR analysis.....	313
Table A. 4 Flocculation efficiency of kaolin particles in the HL-METAC, HL-MAPTAC/kaolin system (The flocculation efficiency was taken from Figure 2, $\alpha = 1/W$) ²³	318
Table A. 5 Properties of the DSC analysis.....	340
Table A. 6 Several weighting moments of the chord length distribution at 2.4 mg/g aluminium oxide/lignin polymers.....	345

List of Schemes

Scheme 3. 1 Reaction scheme of lignin and METAM/ATAC to produce a) KL-ATAC b) P-ATAC c) KL-METAM and d) P-METAM	80
Scheme 3. 2 Interaction of a) KL-METAM and b) KL-ATAC with clay particles.	96
Scheme 5. 1 Chemical structure of CHL polymers. “m” represents the number of cationic groups attached to lignin.....	171
Scheme A. 1 Cartoon model of KL-ATAC and KL-METAM chemical structure.....	293
Scheme A. 2 Proposed reaction scheme of polymerization of HL with AA, AM and AA/AM initiated by Na ₂ S ₂ O ₈ under acidic conditions.....	336

Chapter 1: Introduction

1.1 Overview

Water contamination is currently of great concern in the world, which is creating endless demand of clean water due to increase in population, urbanisation and higher level of living standards.^{1,2}

The majority of wastewater comes from domestic and Industrial sources, which is contaminated by the heavy metals, micro and macroparticles, bacteria, toxic dyes with strong color and the other organic and inorganic suspended particles. However, the removal of target contamination is challenging due to their complex nature, colloidal and charged properties, poor biodegradability and high toxicity.^{3,4} Recently, many efforts are being taken towards sustainable, efficient and cost-effective wastewater treatment methods such as flocculation, biodegradation, photocatalytic degradation, membrane filtration, ozonation and adsorption.⁵⁻¹¹ Among these, flocculation has been regarded as a promising process for treating wastewater due to its simplicity and low capital cost.^{12,13}

Previously, inorganic flocculants such as aluminum sulfate, ferric chloride, ferric sulfate and ferrous sulfate have been used in water purification and wastewater treatment, concentrating, separating a variety of colloidal dispersions, papermaking and mineral processing due to their low cost.^{14,15} However, they may produce large volume of non-biodegradable sludge that requires special handling, which also rises the overall costs of the process. Low biodegradability, pH sensitivity, and inefficiency in treating some wastewater effluents, are the other disadvantages of using inorganic flocculants in wastewater treat systems.^{16,17}

Recently, numerous petroleum-based synthetic polymers (i.e., acrylamide, diallyldimethyl ammonium chloride and polyacrylic acid) have attained extensive use in many industrial applications owing to their high water solubility. However, their usage is controversial because of their non-biodegradability and their potential public health disorder.¹⁸ Therefore, the natural polymeric flocculants has been regarded as a promising flocculant to address those problems. The low-cost, abundant, and biorenewable natural based focculants such as cellulose, starch, chitosan, rice husk, wheat straw and guar gum derivatives, have been studied in the past. However, the applications of these bio-based polymers in food processes, agricultural industries, pharmaceutical, cosmetics and papermaking hindered their availability in flocculation process.¹⁹

Lignin, an abundant natural polymer presents in lignocellulosic biomass can be an excellent candidate for flocculant productions. Despite its complex structure and low solubility at neutral pH, the existence of varied functional such as carboxyl and hydroxyl groups on its structure makes it amenable for producing inexpensive, nontoxic, and biodegradable flocculants for wastewater systems.²⁰

In order to optimize the flocculation performance, it is crucial to understand the mechanism involved in flocculation process (i.e., charge neutralization, bridging and electrostatic patch). The flocculation mechanisms are governed by the adsorption of flocculants on particle.²¹ It is worth mentioning that the adsorption capacity of polymers not only depends on the polymeric flocculant characteristics such as the molecular weight, charge density but also on the properties of the colloidal systems (i.e., pH, salt concentration, surface charge density, particle size).²² These parameters also affect the flocculation performance and floc properties, such as floc strength, structure, and sizes.²³

The main goal of this dissertation was to synthesize renewable, biodegradable, and non-toxic lignin-based polymer with unique physiochemical properties to be used as flocculant or adsorbent with comparable performance to the commercial ones. The present chapter (**chapter 1**), provide a general introduction about the current research and its importance. The objectives of this research study are also presented herein.

Chapter 2 briefly reviews the general background information on the literature related to the current studies. This chapter also discuss the various methods used in literature and in this study to analyse the physiochemical characterises of lignin polymers. The instruments that evaluate the flocculation/adsorption performance of lignin-derivatives are also discussed.

Chapter 3 centered on the polymerization of kraft lignin with [2-(acryloyloxy)ethyl]trimethylammonium chloride (ATAC) or [2-(methacryloyloxy)ethyl]trimethylammonium methyl sulfate (METAM) to synthesized the cationic kraft lignin (CKL) with similar charge densities and different molecular weights in semi dried manner. A correlation was observed between the structure of CKLs and their physiochemical properties in aqueous solution as well as their ultimate performance as flocculants for kaolin particles removals.

Chapter 4 illustrated that how monomer structure would impact the self assembly, sedimentation and interaction of CKL with solid surfaces. The polymer conformation was assessed using static light scattering technique which could alter the viscoelastic properties of lignin-based polymers in bulk solution and upon adsorption. The impact of conformational changes of lignin macromolecules on their glass transition temperature (T_g) was also evaluated.

Chapter 5 focused on the polymerization of hydrolysis lignin (HL) and with [3-(Methacryloylamino) propyl] trimethylammonium chloride (MAPTAC) or [-2-(methacryloyloxy)ethyl] trimethyl ammonium chloride (METAC) in an acidic condition to produce cationic hydrolysis lignin (CHL). CHLs with similar charge densities and molecular weights but different monomer structures facilitated the investigation on the fate of polarity of CHLs on their physicochemical performance in an aqueous system. The polarity difference of CHLs and their performance as adsorbent or flocculant was further assessed using different concentrations of salt and urea solutions.

Chapter 6 provides discussion on functionalization of lignin derivatives for ion removals to expedite their use in treating industrial wastewater. In this chapter, kraft lignin (KL) was polymerized with [2-(methacryloyloxy)ethyl]trimethylammonium methyl sulfate (METAM) or acrylic acid (AA) and the interaction of soluble ions and KL-METAM or KL-AA was investigated using a Quartz crystal microbalance (QCM), X-ray photoelectron spectroscopy (XPS) and a vertical scan analyzer (VSA). The adsorption, sedimentation, and floc size analyses of KL-AA/KL-METAM for elimination ions was also discovered in dual polymer system.

Chapter 7 describes the copolymerization of hydrolysis lignin (HL) with acrylamide (AM) and acrylic acid (AA) to produce HAM copolymers having different negative charge densities and molecular weights. The successful polymerization of HL with AM/AA was assessed using advanced tools, such as, proton nuclear magnetic resonance ($^1\text{H-NMR}$), gel permeation chromatography (GPC) and elemental analyser. The adsorption affinity of lignin-based polymers on aluminum oxide surface was probed and the viscoelasticity of adlayer was analysed. The rheological characteristics of lignin-derivatives polymers and thermal behaviour was also

investigated in this chapter. The flocculation performance of the copolymers was also analysed in terms of floc strength and reversibility of flocs.

Chapter 8 draws the overall conclusions from the results obtained in this research thesis and states some recommendations for future work.

1.2 Objectives

1. synthesize kraft lignin-METAM and kraft lignin-ATAC macromolecules via free radical polymerization in a semi-dried condition and their characterization in aqueous solution;
- 2- assess how a small group (i.e., a methyl group) on the structure of a cationic monomer (i.e., METAM) can have a substantial influence on its polymerization with lignin and subsequently on the adsorption and flocculation of kaolin particles;
- 3- study the influence of molecular architecture of KL-METAM and KL-ATAC on their chain conformation, self-assembly, sedimentation, glass transition temperature and rheological properties in the bulk solution as well as upon adsorption on SiO₂ surface
4. synthesize and characterize hydrolysis lignin-METAC and hydrolysis lignin-MAPTAC using free radical polymerization reaction in semidry manner
5. investigate how the polarity differences of METAC and MAPTAC influence on their physiochemical properties in an aqueous solution or suspension system
6. study the impact of dual polymeric system containing lignin-based macromolecules with opposite charge densities for heavy metal removals

7. synthesize and characterize hydrolysis lignin-AM-AA copolymers following free radical polymerization;
8. probe the performance of lignin-AM-AA copolymers as flocculant and adsorbent

1.3 References

- (1) Ge, Y. Li, Z., 2018. Application of lignin and its derivatives in adsorption of heavy metal ions in water: a review. *ACS Sustain. Chem. Eng.* 6(5), 7181-7192.
- (2) Elimelech, M. Phillip, W.A., 2011. The future of seawater desalination: energy, technology, and the environment. *science* 333(6043), 712-717.
- (3) Bradley, R.S., Vuille, M., Diaz, H.F. Vergara, W., 2006. Threats to water supplies in the tropical Andes. *Science* 312(5781), 1755-1756.
- (4) Sarkar, S., Gupta, A., Biswas, R.K., Deb, A.K., Greenleaf, J.E. SenGupta, A.K., 2005. Well-head arsenic removal units in remote villages of Indian subcontinent: field results and performance evaluation. *Water Res.* 39(10), 2196-2206.
- (5) Rahul, R., Jha, U., Sen, G. Mishra, S., 2014. Carboxymethyl inulin: A novel flocculant for wastewater treatment. *Int. J. Biol. Macromol.* 63, 1-7.
- (6) Song, M.L., Yu, H.Y., Chen, L.M., Zhu, J.Y., Wang, Y.Y., Yao, J.M., Zou, Z. Tam, K.C., 2019. Multibranch strategy to decorate carboxyl groups on cellulose nanocrystals to prepare adsorbent/flocculants and pickering emulsions. *ACS Sustain. Chem. Eng.* 7(7), 6969-6980.

- (7) Ajao, V., Bruning, H., Rijnaarts, H. Temmink, H., 2018. Natural flocculants from fresh and saline wastewater: comparative properties and flocculation performances. *Chem. Eng. J.* 349, 622-632.
- (8) Goswami, L., Kumar, R.V., Pakshirajan, K. Pugazhenthii, G., 2019. A novel integrated biodegradation—microfiltration system for sustainable wastewater treatment and energy recovery. *J. Hazard. Mater.* 365, 707-715.
- (9) Jorfi, S., Pourfadakari, S. Kakavandi, B., 2018. A new approach in sono-photocatalytic degradation of recalcitrant textile wastewater using MgO@ Zeolite nanostructure under UVA irradiation. *Chem. Eng. J.* 343, 95-107.
- (10) Mehrjouei, M., Müller, S. Möller, D., 2015. A review on photocatalytic ozonation used for the treatment of water and wastewater. *Chem. Eng. J.* 263, 209-219.
- (11) Wang, H., Wang, C., Tao, S., Qiu, J., Yu, Y. Gu, M., 2016. Biomimetic preparation of hybrid porous adsorbents for efficiently purifying complex wastewater. *ACS Sustain. Chem. Eng.* 4(3), 992-998.
- (12) Cai, T., Li, H., Yang, R., Wang, Y., Li, R., Yang, H., Li, A. Cheng, R., 2015. Efficient flocculation of an anionic dye from aqueous solutions using a cellulose-based flocculant. *Cellulose* 22(2), 1439-1449.
- (13) Yusoff, M.S., Aziz, H.A., Zamri, M.F.M.A., Abdullah, A.Z. Basri, N.E.A., 2018. Floc behavior and removal mechanisms of cross-linked Durio zibethinus seed starch as a natural flocculant for landfill leachate coagulation-flocculation treatment. *Waste Manag.* 74, 362-372.
- (14) Parson, S., Jefferson, B. *Introduction to Potable Water Treatment Processes*; Blackwell Publishing, Ltd: UK, 2006.

- (15) Joo, D.J., Shin, W.S., Choi, J.H., Choi, S.J., Kim, M.C., Han, M.H., Ha, T.W. Kim, Y.H., 2007. Decolorization of reactive dyes using inorganic coagulants and synthetic polymer. *Dyes Pigm.* 73(1), 59-64.
- (16) Guigui, C., Bonnelye, V., Durand-Bourlier, L., Rouch, J.C. Aptel, P., 2001. Combination of coagulation and ultrafiltration for drinking water production: impact of process configuration and module design. *Water Sci Technol Water Supply.* 1(5-6), 107-118.
- (17) Jang, N.Y., Watanabe, Y. Minegishi, S., 2005. Performance of ultrafiltration membrane process combined with coagulation/sedimentation. *Water Sci. Technol.* 51(6-7), 209-219.
- (18) Lee, C.S., Robinson, J. Chong, M.F., 2014. A review on application of flocculants in wastewater treatment. *PROCESS SAF ENVIRON* 92(6), 489-508.
- (19) Wang, J.P., Chen, Y.Z., Wang, Y., Yuan, S.J. Yu, H.Q., 2011. Optimization of the coagulation-flocculation process for pulp mill wastewater treatment using a combination of uniform design and response surface methodology. *Water Res.* 45(17), 5633-5640.
- (20) Banu, J.R., Kavitha, S., Kannah, R.Y., Devi, T.P., Gunasekaran, M., Kim, S.H. Kumar, G., 2019. A review on biopolymer production via lignin valorization. *Bioresour. Technol.* 290, 121790.
- (21) Bolto, B. Gregory, J., 2007. Organic polyelectrolytes in water treatment. *Water Res.* 41(11), 2301-2324.
- (22) Zhou, Y., Gan, Y., Wanless, E.J., Jameson, G.J. Franks, G.V., 2008. Interaction forces between silica surfaces in aqueous solutions of cationic polymeric flocculants: Effect of polymer charge. *Langmuir* 24(19), 10920-10928.

- (23) Li, R., Gao, B., Sun, J., Yue, Q., Wang, Y. Xu, X., 2016. Synthesis, characterization of a novel lignin-based polymer and its behavior as a coagulant aid in coagulation/ultrafiltration hybrid process. *Int. Biodeterior. Biodegradation* 113, 334-341.

Chapter 2: Literature review

2.1 Introduction

This chapter provides an overview of the literature relevant to the current research of the topic studied in this PhD thesis. Firstly, a fundamental knowledge about the colloidal suspension and, in particular, kaolin particles, will be discussed. Secondly, the impact of polymer characteristics on the destabilization of clay particles will be evaluated. Further, the physicochemical properties of clay particles, polymeric flocculants, and their interaction in the colloidal system will be reviewed in this chapter. A general description about lignin macromolecule, its production process, the need for modification of lignin polymer and, finally, the potential application for modified lignin employed herein.

A comprehensive description and significance of advanced methods for polymer characterization and its performance, including particle charge detector (PCD), gel permeation chromatography (GPC), nuclear magnetic resonance (NMR) spectroscopy, Brunauer-Emmett-Teller (BET) surface area analyzer, scanning electron microscopy (SEM), X-ray photoelectron spectroscopy (XPS), zeta potential analyzer, static light scattering (SLS), dynamic light scattering (DLS), vertical scan analyzer (TURBISCAN), LUMiSizer, focused beam reflectance measurement (FBRM), Quartz crystal microbalance with dissipation (QCM-D), hybrid rheometer, thermo gravimetric analyzer (TGA), and differential scanning calorimetry (DSC), which are used extensively in this work to meet the objectives, will be discussed.

2.2. Background

2.2.1 Colloidal System

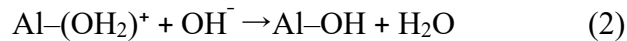
The surface forces between charged particles in an aqueous solution is a central preoccupation of colloid science. Colloid systems are present in many applications, such as membrane biology, soil

science, electrochemistry, polymers, clay dispersions in mining, as well as in the mineral and cosmetic industries. The functionality and performance of such systems depends fundamentally on solid–liquid and particle–particle interactions. The classical Derjaguin-Landau-Verwey-Overbeek (DLVO) theory has served as a backbone of colloidal chemistry, which treats colloid stability in terms of a balance of attractive van der Waals forces (VDW) and repulsive electrical double-layer (EDL) interactions.¹ Accordingly, to make unstable colloidal dispersions, the VDW interactions must overcome the EDL ones to obtain the maximum settlement of colloidal particles from suspension. Clay, and in particular kaolin, has been considered a key component in industrial effluents (i.e., waste tailings and mineral processing operations). Thus, it is crucial to gain a fundamental understanding of interactions between the colloidal particles to enhance the colloidal instability.²

2.2.2 Kaolin characteristics

Kaolin, a 1:1 tetraoctahedral aluminosilicate with chemical composition of $\text{Al}_2 \text{Si}_2 \text{O}_5 (\text{OH})_4$, consists of individual particles that cannot be divided and is a layered mineral of silicate. It is a white soil mineral formed through the chemical weathering of aluminium silicate minerals (Al_2SiO_5) such as feldspar.³ Kaolin or China clay has a low shrink–swell capacity and cation-exchange capacity. It has one tetrahedral siloxane ($-\text{Si}-\text{O}-\text{Si}-$) sheet linked through oxygen atoms to one octahedral sheet of alumina (Al_2O_3). The layers of kaolin particles are electrically neutral and bonded together via a weak van der Waals force.⁴ The neutrality of kaolin particles could be interrupted by substituting Al with some of the Si units in the tetrahedral sites of SiO_2 sheets. The basal face containing siloxane structure carries a permanent negative charge due to the isomorphous substitution of Si^{4+} by Al^{3+} . Since alumina is trivalent and silica is tetravalent, this

substitution leads to an occurrence of free electrons on the surface of the tetrahedral–octahedral layer. Considering Al substitution for every fourth Si unit in the tetrahedral basal plane, a negative charge density is generated on the basal plane. Therefore, the heteropolar characteristic of kaolin particles having two crystallographic surfaces would expose to the aqueous media: (1) a pH independent basal face containing permanent negatively charged sites and exchangeable cation, and (2) a pH-dependent edge containing positive charge density in acidic aqueous system.⁴ At the edge face of the kaolin particles, the octahedral Al and tetrahedral Si layers are disordered and the cleaved bonds subject aluminol (Al-OH) and silanol (Si-OH) groups. The edge crystals are believed to carry a positive charge owing to the protonation and deprotonation of the surface hydroxyl groups. Increasing the pH results in neutralizing the cationic sites $[\text{Al}-(\text{OH})_2^+]$ and consistent discharge of edge particles causes a negative charge density on the surface of kaolin crystals using the following reactions:⁵



This phenomenon reveals that kaolin particles can have both positive and negative charges over a wide range of pH (3.5-8.5). The diagrammatic sketch of kaolin is shown in Figure 2.1.⁶

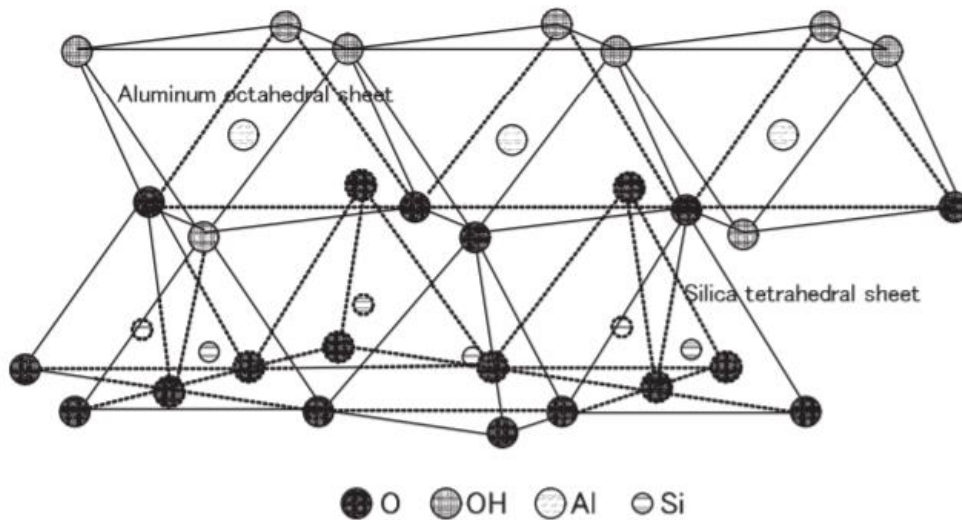


Figure 2. 1 Diagrammatic sketch of the Kaolin structure

2.2.3 Colloidal stability of clay suspension

As kaolin particles present negative charges, cationic polymers are of great interest for governing the colloidal stability in the industrial solid–liquid separation process. Kaolin clay is hard to settle and consolidate owing to its colloidal size and anisotropic shape. However, the addition of polymers can alter the complex surface properties of kaolin particles and produce a good settling performance for relatively low cost.⁷ Coagulation-flocculation process is one of the most important physicochemical methods used in industrial applications to destabilize the colloidal particles through charge neutralization, electrostatic patch and bridging or combination of these mechanisms.⁸ In this process addition of floc-forming chemical reagent to the wastewater results in agglomeration and settlement of colloidal solids. The flocculation of particle suspensions (i.e., kaolin particles) is significantly dependent on various physicochemical parameters such as particle size and distribution, solid concentration, pH and ionic strength of the suspension, charge density,

molecular weight and hydrodynamic size of the flocculants, adsorption capacity and conformation of the adsorbed flocculants.⁷

2.2.4 Polymeric flocculants

Polymeric flocculants, especially those with high molecular weight, play a crucial role in water treatment processes due to the efficient flocculation for suspensions of inorganic or organic matter. In recent years, many studies have been conducted in order to probe flocculation behavior and to elucidate the interaction between polymer and substrate. Polyacrylamides (PAMs) are used widely in many types of industrial applications, such as water treatment, paper manufacture, textile production, pharmaceuticals and detergents, building and oil field products, and mineral processing.⁹⁻¹² PAMs are organic substances that are mostly water-soluble. During the flocculation process, PAM chains adsorb onto particle surfaces to form large flocs and improve the separation method. By increasing the polymer chain length (molecular weight), more particles are involved in flocculation phenomena, resulting in better flocculation efficiency.¹³ For instance, ultra-high-molecular weight Polyacrylamide (PAM) exhibited the highest settling velocity for flocculation of kaolin suspensions compared with the other grades of synthesized PAMs with lower molecular weight.¹⁴

2-(methacryloyloxy) ethyl] trimethyl ammonium chloride (METAC) cationic reagent has been used previously to produce cationic polymers that distribute a positively charged group along the macromolecular backbone.^{15,16} The same cationic monomer was also used for preparing cationic Karaya gum (KG) (a polysaccharide extracted from the stem exudates of the plant *Sterculia urens* of family Sterculiaceae) for removing anionic dyes from aqueous solutions.¹⁷ On this subject, lignin based polymers can be synthesized and used as flocculants. The molecular

architecture multiplicity of the polymeric flocculants are related to their final application performance.^{18,19} Flocculants with certain molecular weight, charge properties and chain structure (linear or branching) can show different flocculation performance.^{19,20} Thus, the interaction of lignin-based flocculants with clay suspension should be investigated to design the novel high-performance flocculants and optimize the application conditions in wastewater treatment.

Table 2.1 lists the modification of natural polymer by copolymerizing/grafting cationic reagents to treat negatively charged particles in various effluents.

Table 2. 1 Various available flocculants and their applications

Cationic flocculant	Waste medium
Starch-g-GODAC ²¹	Kaolin suspension
Starch-AM-DMC ²²	Pulp mill effluent
Guar gum-g-PAM ²³	Tobacco wastewater
Xylan-g-METAC ²⁴	Azo dye
Xylan-g-METAC ¹⁵	Kaolin and bentonite clay suspensions
Chitosan-g-DMC ²⁵	Pulp mill wastewater
Chitosan-g- METMS ²⁶	kaolin and bentonite suspensions
Chitosan -g-PAD ²⁷	zinc phosphate contaminated wastewater
Chitosan-g-PAMA ¹⁹	Kaolin and <i>Escherichia coli</i> suspension
Lignin-g-METAC ²⁸	Kaolin suspension
Lignin-g-GTMAC ²⁹	Azo dye
Lignin-g- CHMAC ³⁰	Azo dye
Lignin-PAM-DADMAC ³¹	Reactive dyes wastewater

2.2.5 Lignin

Biomass is defined as a mixture of organic molecules containing hydrogen, oxygen, nitrogen, phosphorous and sulfur atoms as well as small quantities of alkali-, alkaline-earth metals and heavy metals. Lignocellulosic biomass consist of fibrous cellulose backbones with a hemicellulose covering, which are “glued” by lignin. Lignin, an integral part of the plant cell wall, is considered the second most natural and renewable biopolymer next only to cellulose. The key function of this complex three dimensional amorphous polymer in woody biomass is providing strength, rigidity and resistance to degradation.³² Although, the amount of lignin differs from plant to plant, it generally decreases from softwoods (24–33%) to hardwoods (19–28%) to grasses (15–25%).³³

2.2.6 Lignin structure and properties

Lignin is comprised of three primary monomers: syringyl-(S), guaiacyl-(G), and p-hydroxyphenyl-(H, also known as p-coumaryl) derived from the monolignols p-coumaryl, coniferyl, and sinapyl alcohols (Figure 2.2). The ratio between these units and the molecular weight of lignin differs significantly with the type of plant. Despite the exact polymeric structure of lignin being undetermined, the key substructures are known.^{34,35}

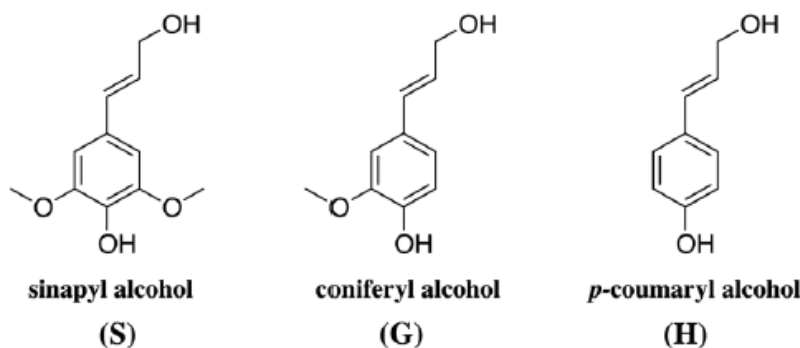


Figure 2. 2 The three main monomer building blocks of lignin.³³

The primary monomers of lignin are joined together via C–O bonds of α - and β -arylalkyl ethers.³⁶ The most predominate linkage found in a lignin macromolecule is β -O-4, accounting for roughly 50% of the linkages.

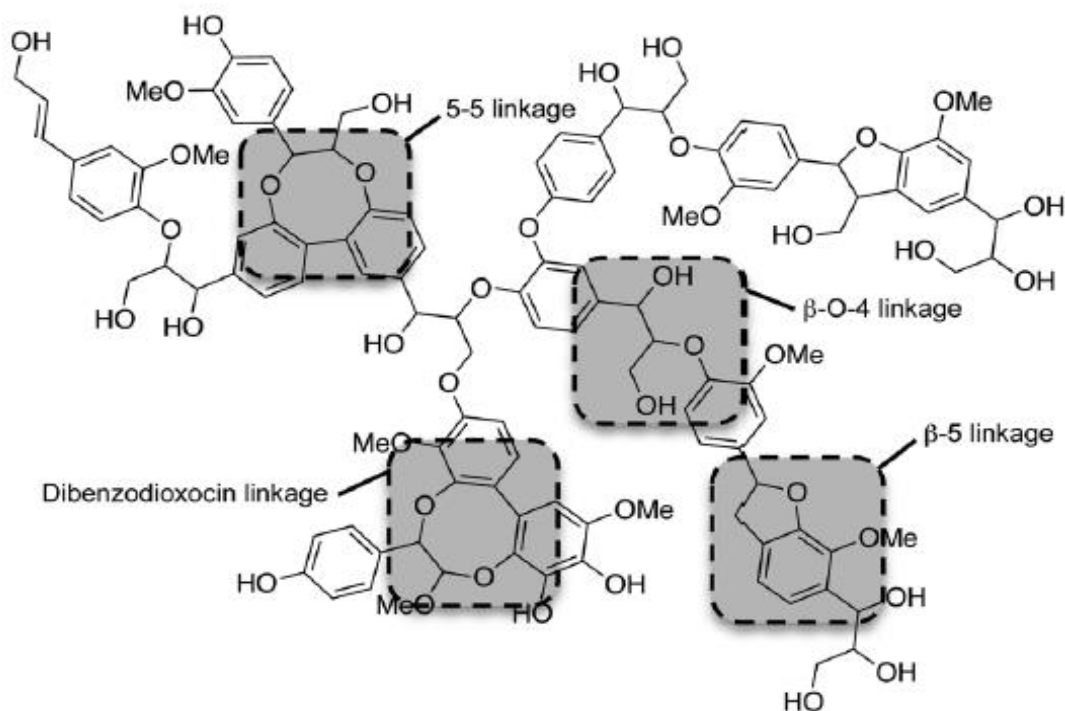


Figure 2. 3 Schematic representation of the common lignin chemical bonds.³³

The other common types of linkages are the 5-5, β -5, and the dibenzodioxocin linkage (Figure 2.3).³⁷ The ratio of linkages in softwood lignin is tabulated in Table 2.2^{38,39}

Table 2. 2 Percentage of different linkages in softwood lignin.

Linkages	Dimer structure	Distribution percentage [%]
β -O-4	Phenylpropane β -aryl ether	45-50
5-5	Biphenyl and dibenzodioxocin	18-25
β -5	Phenylcoumaran	9-12

α -O-4	henylpropane α -aryl ether	6-8
β -1	1,2-Diaryl propane	7-10
4-O-5	Diaryl ether	4-8
β - β	β - β linked structures	0-3

2.2.7 Lignin production

An enormous amount of lignin is produced annually in the kraft pulping industry. Kraft lignin, which is considered to be a non commercialized waste byproduct, is mainly incinerated as a low cost fuel in the pulping industry. However, various value-added products can be produced from lignin; these include adhesives, plasticisers, dye dispersants, stabilizers, surfactants, epoxy resins and superabsorbent hydrogels.⁴⁰ The black liquor of the Kraft pulping process contains large amounts of lignin as well as the residual pulping salts that need to be separated from pulping spent liquors effectively and selectively in order to allow the production of value-added products. For isolating lignin from black liquor, LignoBoost technology is developed to purify lignin for downstream applications .⁴¹

One of the main hindrances for the commercialization of high-performance lignin products is heterogeneous properties of lignin, including molecular weight, functionality, and thermal properties, in respect to different sources and processing methods. The inherent characteristics of lignin macromolecule significantly impact the productivity of the biorefinery processes and its potential applications. Therefore, this research focuses on the chemical modification of kraft lignin through graft copolymerization to improve its solubility in aqueous solutions. Thus, understanding the biosynthesis and structure of lignin in plant cell walls and the structural change of lignin during

the biorefinery process are essential for lignin valorization.⁴² Since the hydrophobicity and low molecular weight of kraft lignin are the two main factors hindering its application in industry,⁴³ chemical modifications of kraft lignin through graft copolymerization can be employed to overcome these difficulties.

2.2.8 Lignin modification

According to the first full proposed lignin structure,³⁷ lignin is recognized as a highly branched polymer with a variety of functional groups including aliphatic and phenolic hydroxyls, carboxylic, carbonyl and methoxyl groups.⁴⁴ The chemical structure of lignin has been determined thoroughly using different chemical and spectroscopic methods.^{45,46} These functional groups offer different possibilities for chemical modification and propose that lignin could play a crucial role as a new chemical feedstock, particularly in the formation of supramolecular architecture and aromatic chemicals. Of various kraft lignin chemical sites, OH groups of phenyl propene subunits present the most reactive sites for any reaction. However, the β -O-4 aryl ether linkages and other interior bonds can cause conspicuous steric hindrance leading to occupation of these reactive sites and subsequently limited reactivity of kraft lignin for modification.

2.2.9 Free radical polymerization

Numerous modification techniques have been carried out in the past to produce new lignin-based products for useful purposes via polymerization. These techniques include chemo-enzymes,⁴⁷ irradiations,⁴⁸ UV radiation,⁴⁹ and mechanical activation. However, free radical polymerization of lignin with functional monomers is recognized as the simplest, most economical and most efficient method that can increase both the molecular weight and the number of functional groups on lignin structure.⁵⁰ This research investigates free radical copolymerization of a lignin macromolecule

with a cationic or nonionic monomer to increase the solubility, molecular weight, charge density and hydrodynamic/gyration radius of lignin without adversely affecting its molecular structure.

Free radical polymerization is a type of chain-growth polymerization technique in which the polymer is formed following the addition of monomer molecules to an active, free radical site. Free radical polymerization initiate using chemical free radical initiator (i.e., ceric ammonium nitrate, potassium per sulfate or hydrogen peroxide) by thermal, chemical or photolytic decomposition of initiator molecules.⁵¹ It is of the utmost importance to select an initiator system to maximize the grafting efficiencies and minimize homopolymer formation during the polymerization reaction.^{28,29}

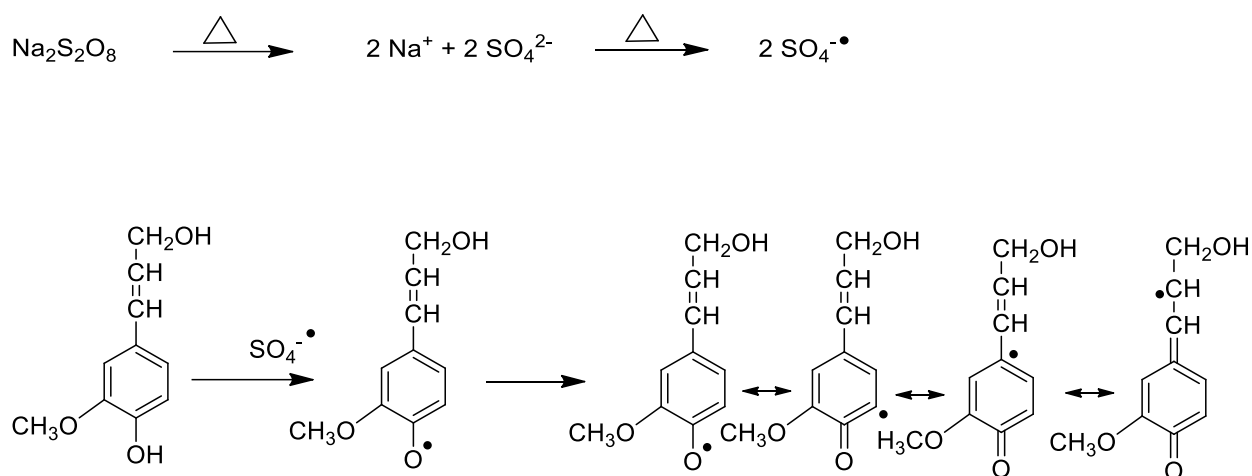
Recently, the chemical modification of natural polymers via polymerization reaction using cationic, non-ionic or both monomers in attempts to produce bio-based flocculants has been studied.^{22,26,28,52,53}

High molecular weight and charge density are two important factors in the flocculation process. Polymers of high molecular weight can form bridges between the particles using polymer adsorption on the particle surface with an extended conformation. High or medium-charge density polymers can adsorb onto the particle surface to reduce the repulsive electrostatic forces by neutralizing the surface charge of the particles.⁵⁴ To reach this goal, the bio-based flocculants of acrylamide and cationic monomers (i.e., METAC, ATAC, METAM, MAPTAC) are the most common copolymers having high molecular weight and charge density. For instance, Polyacrylamide (PAM) was grafted onto the bamboo pulp cellulose (BPC) by free-radical graft copolymerization in homogeneous aqueous solution for wastewater treatments.⁵⁵ In another report xylan was polymerized with [2-(methacryloyloxy)ethyl] trimethylammonium methyl sulfate

(METMS) in a semidry manner for kaolin and bentonite removal from model wastewater.²⁶ Similarly, a novel bio-based flocculant was also synthesized via copolymerization of [2-(acryloyloxy)ethyl]trimethylammonium chloride (ATAC) and acrylamide (AM) on chitosan backbone for treating zinc phosphate-contaminated wastewater.²⁷ This dissertation aims to study the free-radical copolymerization of kraft lignin and one or two monomers.

2.2.10 Free radical copolymerization of lignin with cationic monomer

The lignin polymers with different properties and structures can be produced in a similar way by using different cationic monomers. The polymerization of kraft lignin and [2-(methacryloyloxy)ethyl]trimethylammonium methyl sulfate (METAM) and [2-(acryloyloxy)ethyl]trimethylammonium chloride (ATAC) was carried following a free radical polymerization mechanism.⁵⁶ Compared to ATAC, METAM has one additional methyl substituent attached to its structure that may impact the efficiency of polymerization reaction. The proposed copolymerization scheme corresponding to this reaction is shown in Figure 2.4.



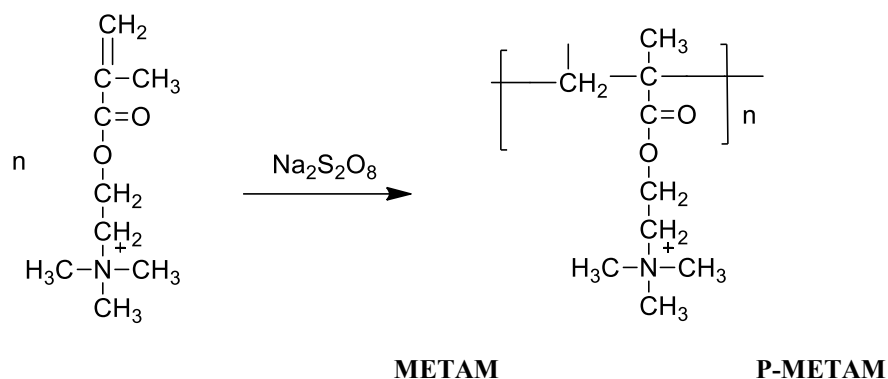
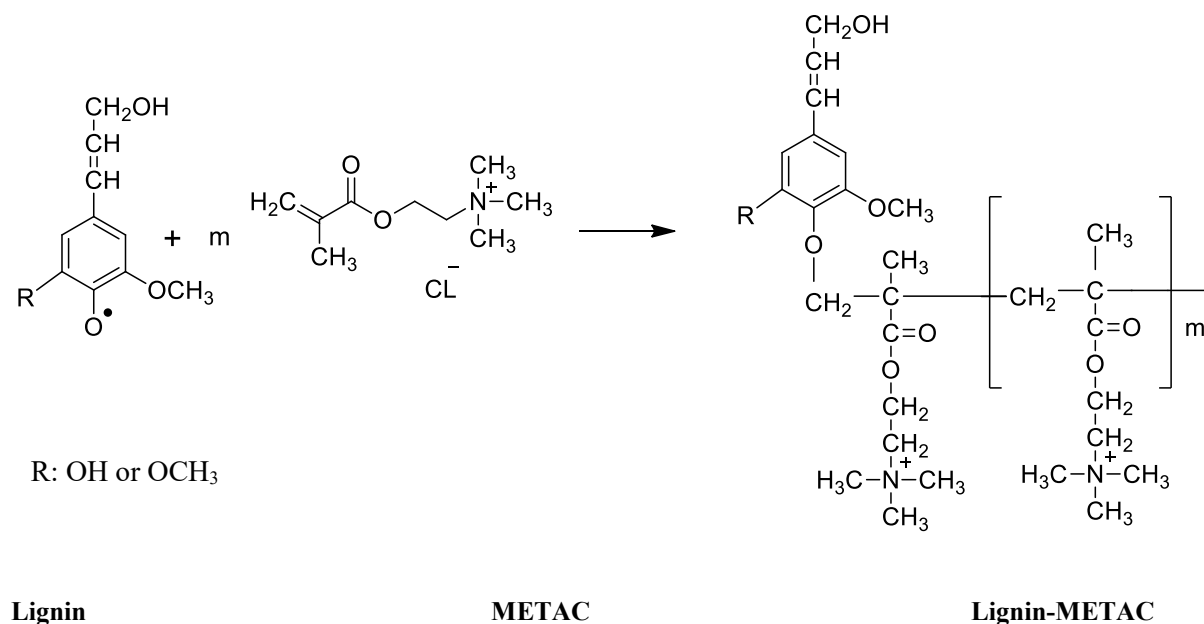
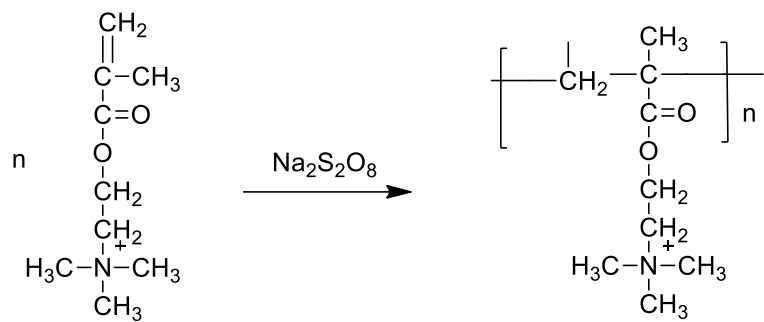


Figure 2. 4 Reaction scheme of lignin and METAM/ATAC

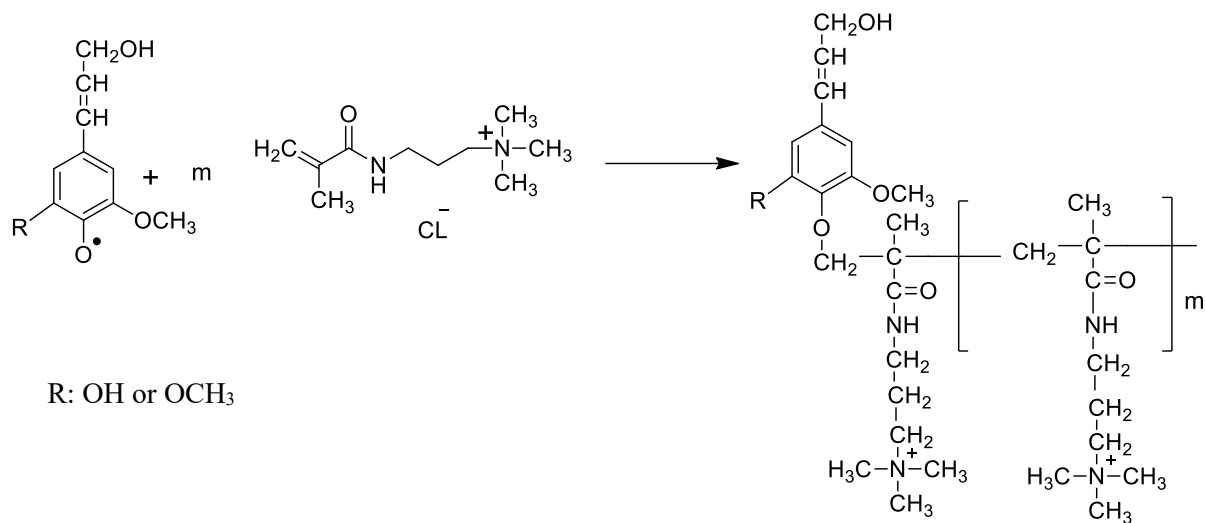
Likewise, the polymerization of lignin and [2- (methacryloyloxy)ethyl] trimethylammonium chloride (METAC) or [3-(Methacryloylamino)propyl] trimethylammonium chloride (MAPTAC) was also investigated for producing bioflocculants (Figure 2.5).⁵⁷ The structural differences of METAC and MAPTAC monomers may affect their polymerization performance and the properties of induced lignin polymers.





METAC

P-METAC

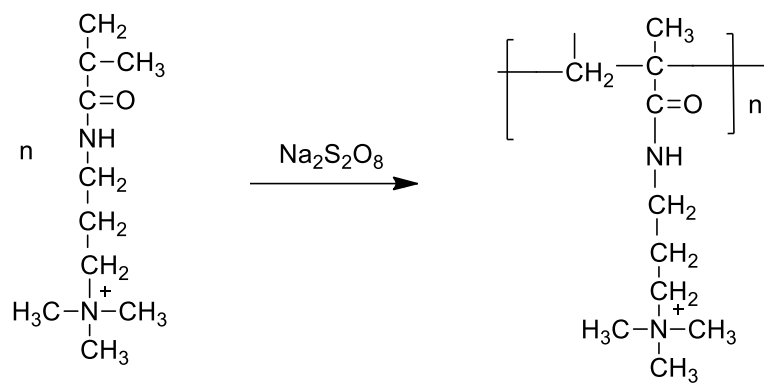


R: OH or OCH₃

Lignin

MAPTAC

Lignin-MAPTAC



MAPTAC

P-MAPTAC

Figure 2. 5 Reaction scheme of lignin and METAC/MAPTAC.

In polymerization reaction of lignin macromolecule and various cationic monomers, the sulfate radicals can initially form through heat decomposition. In this way, sulfate radicals take unstable hydrogen from phenolic hydroxyl groups of lignin to generate phenoxy radicals. These phenoxy radicals that form on the lignin backbone (free radical reaction sites) then react with the cationic reagents or propagate monomers to form cationic lignin polymers. The poly-*monomer* (PMETAM, PATAC, PMETAC, PMAPTAC) chain segments, which contain quaternary ammonium groups, existing on lignin-based macromolecule would provide cationic charges, water solubility, and a high molecular weight to lignin. Moreover, sulfate radicals can initiate the homopolymerization of cationic monomers, which are considered undesirable by-products of radical polymerization reaction.

2.2.11 Lignin application

Previously, lignin produced with [2- (methacryloyloxy)ethyl] trimethylammonium chloride (METAC) in an acidic environment confirmed that lignin-g-PMETAC polymer was indeed an excellent flocculant for kaolin suspension in which the relative turbidity of kaolin suspension reached from 1 to 0.2.²⁸ In a similar work, lignin-based multi-arm star copolymers was synthesized as a new kind of cationic flocculant via Steglich esterification of phenolated kraft lignin (KL) and subsequent RAFT polymerization with (METAC) for kaolin removal from simulated waste solution. It was reported that the lignin-based flocculant with the highest degree of polymerization effectively reduced the residual turbidity to 9.8 NTU and led to maximum removal efficiency of 96.4% within 1 h settling under the test conditions.⁵⁸ The polymerization of acrylamide (AM), (2-methacryloyloxyethyl) trimethyl ammonium chloride (DMC) and kraft lignin (KL) led to the production of a product that was able to adsorb significantly

on both kaolin and bentonite (2.58 and 1.83 mg/g) and removed the suspended particles from kaolin and bentonite suspension (76.9 and 96.2 wt%).⁵² Additionally, kraft lignin has been used industrially in carbon fiber⁵⁹ plant-derived plastics and composites,⁶⁰ binder and resins³³, adhesive⁶¹ and absorbent (Carrott et al., 2007).⁶² However, producing flocculants or adsorbent using lignin macromolecule (i.e., kraft lignin and hydrolysis lignin) was not explored fundamentally, which is, in fact, one objective of this PhD work.

2.3 Fundamentals

2.3.1 Polymer adsorption

During the flocculation process, polymer adsorption onto colloid surfaces is vital. Based on the polymer adsorption theory under equilibrium conditions, the amount of adsorbed polymer at equilibrium, suspension pH, presence of salts in the system and eventually the surface coverage of particles by polymer, are the governing factors.⁶³ In other words, the polymer adsorption can alter surface morphology and chemistry of colloidal particles that impact the magnitude of adsorption.⁶⁴ Therefore, a fundamental understanding of the interactions between the polymers and the particles in the suspensions (i.e., van der Waals attraction, hydrogen bonding and electrostatic ion exchange interaction) will help to investigate the effect of adsorption conditions on the stabilization of colloidal suspensions.

2.3.2 Effect of charge density and molecular weight

It is well-known that the charge density and molecular weight of polymers can affect their adsorption performance on clay particles and predominant flocculation mechanism.⁶³ Polymers of high molecular weight and low-medium charge density work by forming bridges between the

particles via formation of tails and loops configuration (Figure 6-a) that are extended far beyond the electrical double layer and that can be attached to other particles allowing the flocculation process.^{65,66} However, polymers of medium-low molecular weights and high charge density are adsorbed onto the particle surface with a flat conformation (known also as patches) that attract the exposed surfaces of other particles as illustrated in Figure 2.6-b.⁵⁴

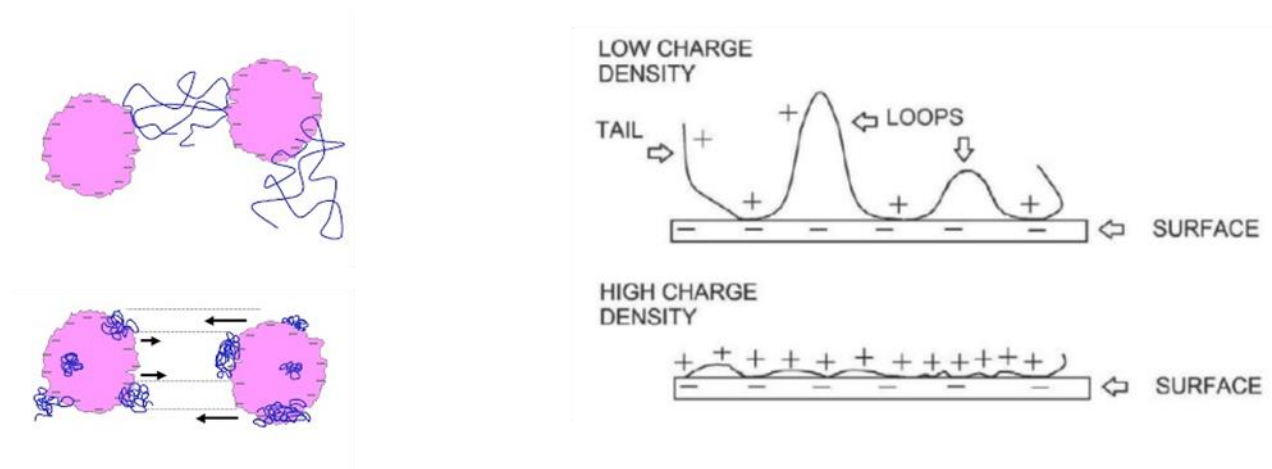


Figure 2. 6 Adsorption configuration with high and low charged cationic polymers on a particle surface with negative charge density.^{67,68}

It was reported that for polymers having low molecular weight, bridging would not be favoured due to the short macro-ion length and quick strong adsorption.¹³

On the other hand, high molecular weight polymers aid flocculation and the subsequent sedimentation process that adsorb and configure at a slower pace, hampering the adsorption of other approaching polymers from the adsorption medium on surfaces.^{13,69}

2.3.3 Effect of ionic strength

Flocculation processes would be further complicated by introducing the ionic strength to the colloidal suspension, which usually results in a remarkable loss of polymeric flocculant efficiency and a change in floc properties.⁷⁰ For high molecular weight polymer, increasing the ionic strength

may lead to shield the repulsion between charged groups along a polymer chain and enable the macromolecule to coil up into a tighter, less extended configuration that in turn weakens the bridging capability of the polymer. However, the increased ionic strength also decreases the electrical double-layer thickness of a particle, which help two particles approach one another more closely. By this approach, the bridging distance a polymer must span in order to induce flocculation will reduce. In this case, increasing the ionic strength can favor the polymer-induced flocculation. Thus, the effect of ionic strength on polymer-induced flocculation is not a straightforward process and the net effect depends on the force balance of all interactions.⁶⁴

2.3.4 Effect of particle size

The most representative parameter for analysing the flocculation performance is an enhancement in the size of the particle aggregates. Hence, one approach to indirectly monitor the flocculation process is to focus on the common factors for all flocculation mechanisms: the change in both the average size and the size distribution of the suspended particles, aggregates or floc present in the colloidal suspension. As mentioned earlier, the size of aggregated clay particle increases with increasing the molecular weight and charge density of polymers. Therefore, the size of a particle affects how fast it flocculates and how it interacts with other particles, which are important criteria in separation processes.

Moreover, the evolution of the particle size under shear conditions, after the flocculation process, allows the study of the flocs resistant to shear forces. Usually, under turbulent conditions, the flocculated particles may break either by disruption of the attachment points on a surface of particle or by the scission of covalent bonds within the bridging polymer chains.⁷¹ However, the reformation of the polymer can also be achieved when the shear forces decrease to form a patch

on the particle surface. The floc strength and degree of reflocculation is directly interconnected to the product quality and process efficiency.⁷² Floc strength, an important factor to describe floc properties,⁷³ is also related to the number and strength of the interparticle bonds.⁷⁴ Consequently, a formed floc will break if the stress applied on its surface (i.e., shear force) is greater than the bonding strength within the floc.⁷⁵ However, no straightforward technique is available to characterize the floc strength experimentally.⁷⁶ In this thesis, the effects of polymer characteristics on the floc size formed via interacting lignin polymers and clay particles as well as the floc strength in kaolin suspension system are comprehensively studied.

2.3.5 Effect of polymer structure

Properties of polymer are governed not only by the type of monomers comprising it but also on the structure of a polymer, such as a polymer chain length. The physicochemical characteristics of a polymer could be evaluated partly by chain conformation.⁷⁷ The conformational changes of polymers (i.e., shape and size) arise primarily from a balance of interactions between the monomers and with the solvent. For instance, flexible homopolymers undergo a major diminution in size, known also as “coil-to globule” transition, when the solvent quality alters from “good”, which is ideal for monomer–solvent interactions, to “poor”, which favors monomer–monomer interactions.⁷⁸ The overall balance of interactions can also control the morphology of heteropolymers, which are chemically more diverse.

Distribution of the charged groups on molecular structure of polymers can also change their configuration in aqueous systems.⁷⁹ As described in the literature, the physicochemical properties of lignin would be altered after the polymerization reaction that help to design polymers with controlled architectures.^{29,56,58} The polymers with controlled structure can be used subsequently as

flocculant and significantly improve flocculation efficiency, which is discussed fundamentally in this research work.

2.3.6 Relative turbidity

Settling rate and turbidity removal are ways to measure the performance of a flocculation process, and are governed by the floc size distribution.⁸⁰ The complex function of molecular weight, charge density, concentration of polymer and the pH of colloidal suspension are responsible for the flocculation efficiency and observed turbidity results.⁸¹ It is interesting that with an increase in flocculants doses to a certain dosage, turbidity is reduced. However, further increase in the dosage of polymer leads to an increase in turbidity again due to the re-dispersion of the formed flocs in a suspension system. High shear conditions can also increase the turbidity of a system after flocculant addition owing to breakage of formed aggregates.⁸² There is a great deal of research that is focused on the impact of flocculation properties (settling rate, sediment thickness, supernatant clarity) of clay suspensions in the presence of cationic polymer.^{26,28,83-85} Thus, in order to design an effective flocculant to reduce the turbidity of a suspension system, it is important to study the effect of flocculant properties on the settling velocity, size and compactness of formed aggregates, all of which is investigated comprehensively in this research work.

2.3.7 Zeta potential concept

Zeta potential (ζ) is an analytical technique for the determination of surface charge of particles in colloidal solution. The surface of a charged particle attracts a thin layer of an opposite charge and strongly attaches to it, forming a thin liquid layer known as Stern layer (Figure 2.7).⁸⁶ The suspended particles in solution are surrounded by an outer diffuse layer that consists of loosely associated ions leading to creation of an electrical double layer (Fig. 15.9).⁸⁷ The ζ is considered

as the electrical potential (ψ) of the double layer and determined using velocity measurement of the charged particles moving around the electrode across the sample solution in the presence of an external electric field.⁸⁸ The typical value for ζ is in the range of +100 to -100 mV that gives a prediction of the colloidal stability.⁸⁶

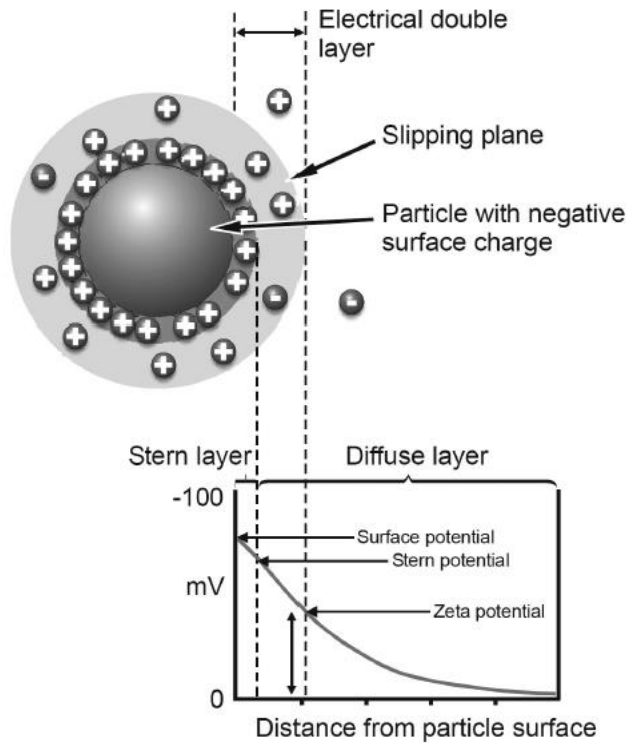


Figure 2. 7 Distribution of electrical potential in the double layer region surrounding a charged particle showing the position of the zeta potential.⁸⁹

Basically, zeta potential technique helps to estimate the surface charge, which can be employed for understanding the physical stability of particles in aqueous solution.⁹⁰ A large positive or negative value of ζ indicates good physical stability of the colloidal system owing to electrostatic repulsion of individual particles. On the other hand, a small value of zeta potential determines particle aggregation and flocculation phenomena as a result of van der Waals attractive forces

among them indicating physical instability.^{91,92} Despite the zeta potential values, solution chemistry and presence of surfactants can also affect the physical stability of colloidal dispersion.

2.3.8 Effect of polymer characteristics on flocculation of clay suspensions

As discussed in the literature, addition of cationic polymers to the negatively charged clay suspension system introduces more positive charges that can destabilize the clay particles upon adsorption, leading to sedimentation of particles from the suspensions and reducing the turbidity of the system.⁹³ As stated earlier, the maximum adsorption performance of the polymers on the surface of clay particles depends on the charge density and molecular weight of the polymers. Thus, to develop an effective cationic flocculant, positive charges and high molecular weight has proved to be favourable in flocs formation.

Suspension stability is very important in the mining and mineral industries to obtain products with desired performance. The amount of polymer addition, adsorbed capacity, surface charge density and zeta potential of solid particles are all crucial to determine the stability of examined suspensions. The surface charge of clay particles affects the flocs formation, structure and dispersed stability and will impose additional impacts on the degree of settling, stability and interaction with colloidal particles.⁹⁴ Therefore, one purpose of this PhD study is to provide an insight on the flocculation/settlement behaviour of lignin-based polymers with different charge density, molecular weight and molecular structure.

2.4 Methodology

2.4.1 Charge density analysis

To measure the charge density of cationic polymers, particle charge detectors, PCDs, have been used widely by researchers as cited in the literature.^{24,29,95} In this analysis, the appropriate amount

of cationic polymer solution is first poured in the cell of Mütek PCD 03 particle charge analyzer and titrated using a standard polymer solution of potassium polyvinylsulfate (PVSK) with opposite charge density. This analysis is based on the stoichiometric interaction of standard polymer and polymer sample.⁹³ Similarly, to measure the surface charge density of clay particles or the insoluble portion of a polymer, a back titration method is applied as reported in the past.¹⁵ Since the interactions of PVSK and PDADMAC solutions with the charges of clay particles are stoichiometrically controlled, they are employed as standard solutions in this measurement.^{96,97} First, a clay suspension system is treated with PDADMAC standard solution, having an opposite charge density compared with the charge of clay to adsorb on the clay surface. After filtration, the exact concentration of PVSK or PDADMAC solution is measured by a PCD instrument, and compared with the concentration of PVSK or PDADMAC in the control solutions (i.e. the solutions containing no clay). Considering the difference between the concentration of polymers in the filtrate and in its control solutions as a result of charge neutralization mechanism, the surface charge density of clay particles would be determined.⁹⁷

The amount of phenolic hydroxyl and carboxylate groups changed or generated during modification of lignin is determined by using potentiometric titration method as described in the literature.^{29,96} Many researchers have been using this technique to determine the concentrations of charged groups present in the unmodified and modified polymers. In this analysis, polymer solution first dissolved in KOH and then para-hydroxybenzoic acid as an internal standard. Afterward, deionized water adds to the system and is mixed with the prepared solution. The solutions then titrate against M HCl standard solution using an automatic potentiometric titrator, 785 Titrino.⁹⁵

2.4.2 Modified polymer characterization

NMR spectroscopy is a reliable and comprehensive technique to powerfully elucidate the polymer structure and dynamics of molecules.⁴² This technique probes the local magnetic environment of a nucleus with non-zero magnetic moment in terms of its chemical shift (depending on the amount of magnetic shielding and its chemical environment) and line splitting, owing to magnetic coupling to the nuclear spins of neighbouring atoms.⁹⁸ In other words, NMR spectroscopy is employed to observe the local magnetic fields around the atomic nuclei of the individual material. This provides detailed information of the electronic structure of a molecule and its individual functional groups.⁹⁹

X-ray photoelectron spectroscopy (XPS) is a very powerful surface analysis technique extensively used to determine the elemental composition and oxidation states of elements at the surface via excitation of inner orbital and bonding electrons using a focussed X-ray beam. Characteristic peaks in the XPS spectrum can be obtained by measuring the kinetic energy and quantity of electrons that are emitted from the top 1–10 nm of the material being investigated.¹⁰⁰ The energy and intensity of these signals enable identification and quantification of all elements present in the surface with the exception of hydrogen and helium. The surface sensitivity of XPS makes it a valuable tool in the study of the elemental analysis, chemical composition, and predicted particle structure.¹⁰¹

Thermogravimetry analysis (TGA) is found to be a very powerful method to characterize material weight with respect to a combination of temperature and time. TGA is a commonly used instrument for investigation of thermal characteristics of a substance under heating environments.¹⁰² The instrument can elevate the temperature up to 2000°C and analyse the specimen weight up to 1 g. TGA instrument employs a radiant heating chamber, temperature controller, gas feeding system,

and data analyzer. It also consists of a crucible sample pan supported by a precision balance in a furnace. A piece of specimen (5 mg test samples) or powder is placed in a platinum basket and the temperature is continuously recorded by a thermocouple under the basket. Basically, two types of plot will be reported as results: 1) a plot of sample weight against temperature (TGA curve), which indicate thermal decomposition temperatures with residue amount as a function of temperature, and 2) a derivative plot of the TGA curve that depicts mass loss rate depending on an increase in temperature. The other parameters, such as the kinetics of the reaction can also be extracted from those curves.¹⁰³ The schematic principle of TGA is present in Figure 2.8.

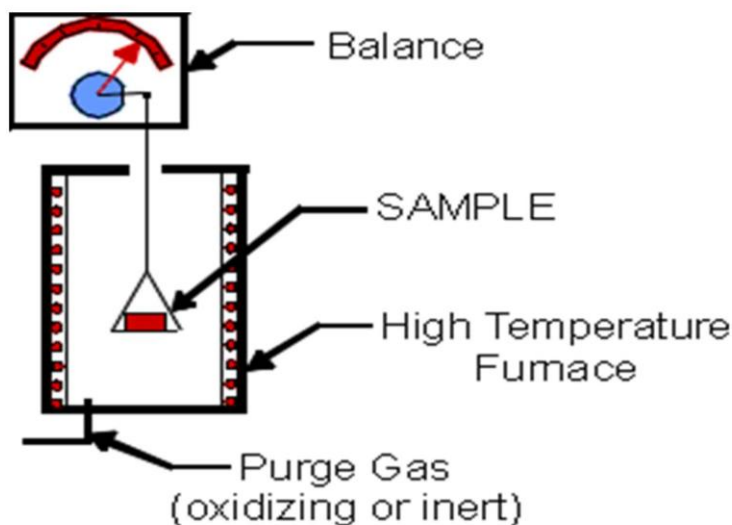


*Figure 2. 8 Schematic principle of TGA measurement.*¹⁰⁴

Differential scanning calorimetry (DSC) is one of the most frequently used techniques in the field of thermal characterization of solids and liquids that monitors heat effects associated with phase transitions and chemical reactions of materials by changing the temperature. In this analysis, the difference in heat flow to the sample and a reference at the same temperature is recorded as a function of temperature.¹⁰⁵ During the heating of a sample (i.e., from room temperature to its

decomposition temperature), peaks with positive and negative $\Delta H/dt$ may be recorded. The obtained endothermic responses are attributed to a heat effect associated with a specific process, such as crystallization or melting.¹⁰⁶ The DSC is readily employed to determine the heat capacity (C_p) and glass transition temperature (T_g). Glass transition temperature --also defined as “brittle points” -- is the temperature in which the material goes from a glassy to a rubbery state. At T_g , the physical properties of a polymer undergo dramatic changes. DSC is capable of elucidating the factors that contribute to the folding and stability of polymers. Changes in the C_p originates from the disruption of the forces stabilizing native structure of polymer.¹⁰⁷

Elemental analysis, also known as carbon hydrogen nitrogen sulfur (CHNS) analysis, is a classical destructive method to obtain information about the elemental composition of an unknown substance. The obtained results can be both qualitative (determining what elements are present) and quantitative (determining how much of each are present). In this technique, a known amount of unknown substance is converted to simple, known compounds containing only the element to be quantified.⁷⁹ It can measure the percentage of carbon, hydrogen, nitrogen, and sulfur by combustion and subsequent analysis of the gases produced. However, the elemental composition can be influenced by some factors including humidity, by-products of the reaction (i.e., homooligomers or product of the reagent) or residual compounds adsorbed or embedded in the polymer, by salts, or by different forms of ionic derivatives.¹⁰⁸ This technology is performed in many applications such as pharmaceuticals, polymers, food and chemicals.

Gel permeation chromatography (GPC) is a popular method for measuring the molecular-weight distribution of a polymer. Major advantages of GPC method include its relatively low cost, simplicity, and ability to provide accurate, reliable data about the molecular-weight distribution of

a polymer. The principle of this technique is based on separation by molecular size rather than chemical properties that enable separation of samples of polydisperse polymers into fractions of narrower-molecular-weight distribution.¹⁰⁹ In this measurement, the polymer first dissolves in a suitable solvent. Then the diluted solution is injected in a flow stream that passes through columns with different porous beads containing a rigid gel. The smaller polymer chains are temporarily entering the pores in the gel and elute slower. However, the larger polymer chains flow through the column with less pore interaction. Hence, the polymeric chains become separated based on their size.¹¹⁰ As they exit the gel columns, a refractometer detector determines the relative concentration of material. By calibrating the columns with polymers of known molecular weight, the molecular weight distribution of the polymer can be measured.

By plotting a graph between log molecular weight (M_w) and retention time for standard samples, a correlation can be made between size and molecular weight to be used for measuring the molecular weight distribution of polymers. To obtain an accurate determination of the molecular weight of polymers, the chromatogram is divided into several equidistant slices and the following parameter can be calculated using equations 1-3:¹¹⁰

$$M_w = \frac{\sum_i N_i M_i^2}{\sum_i N_i M_i} = \frac{\sum_i M_i \times w_i}{\sum_i w_i} \quad (1)$$

$$M_n = \frac{\sum_i N_i \times M_i}{\sum_i N_i} \quad (2)$$

$$PDI = \frac{M_w}{M_n} \quad (3)$$

where N corresponds to the number of polymer chains with molecular weight of M , and w_i is the weight fraction distribution. The polydispersity index (PDI) is a measure of the heterogeneity of a

sample based on size, which is the ratio of M_w over M_n . In equations 1 and 2, N_i and M_i can be obtained from the concentration of molecules measured by the viscometer and refractive index detectors associated with GPC.

Dynamic light scattering (DLS), also known as photon correlation spectroscopy (PCS), or quasi-elastic light scattering, is a sensitive, non-intrusive, and powerful analytical tool, which is used to determine the nanoparticle size in the colloidal suspension polymeric solution. DLS measures the hydrodynamic size of particles by the mechanism of the temporal fluctuations light scattering from a laser that passes through colloidal solution. This technology analyzes modulation of the intensity of scattered light as a function of time caused by hydrodynamic motions in solution.¹¹¹ The smaller particle can diffuse faster than larger ones and the DLS instrument will generate a correlation function, which is connected mathematically with particle size and its time-dependent light scattering capacity. In this measurement, DLS uses scattering angles of 90 or 173 degrees using a helium–neon laser as a source of light, and Brownian motion of individual particles can be converted into particle size using the Stokes–Einstein equation:

$$R_h = \frac{kT}{6\pi\eta D} \quad (4)$$

where, R_h is the hydrodynamic radius of particle solution (nm), D is diffusion coefficient, k is Boltzmann's constant, T is absolute temperature, η is solvent viscosity.¹¹²

DLS has been employed to analyse the particle size in colloidal systems to probe the stability of formulations, and to detect the existence of higher order structures such as aggregation or agglomeration. The advantages of DLS technique over other hydrodynamic technologies are automated operation, short time of measurement, sensitivity to aggregates, non-invasive for

colloids, no calibration and no specific sample preparation requirements in which sample analysis can be used under a wide variety of solvent conditions.¹¹³

Static light scattering (SLS), is one of the most widely used techniques that analyse the intensity of scattered light as time-averaged intensity for the determination of molar mass, and, in some cases, the size of macromolecules in solution.¹¹⁴ SLS instrument measures the angular dependence of the excess absolute time-average scattered intensity (known as the Rayleigh ratio $R_{vv}(q)$), of a dilute polymer solution at concentration C (g/mL) and the scattering angle θ (degree). Rayleigh ratio is linked to the weight-average molar mass M_w , the root-mean-square radius of gyration (R_g) as well as polymer concentration C according to:

$$\frac{KC}{R_{vv}(q)} \cong \frac{1}{M_w} \left(1 + \frac{1}{3} R_g^2 q^2 \right) + 2A_2C \quad (5)$$

where $K = 4\pi n^2(dn/dC)^2/N_A\lambda_0^4$, $q = 4\pi n/\lambda_0 \sin(\theta/2)$, N_A is Avogadro number, dn/dC is specific refractive index increment, n defines as solvent refractive index, λ_0 is wavelength of light, θ correspond to scattering angle and A_2 is considered the second virial coefficient.¹¹⁵ A laser-based light scattering photometer instrument is schematically indicated in Figure 2.9.

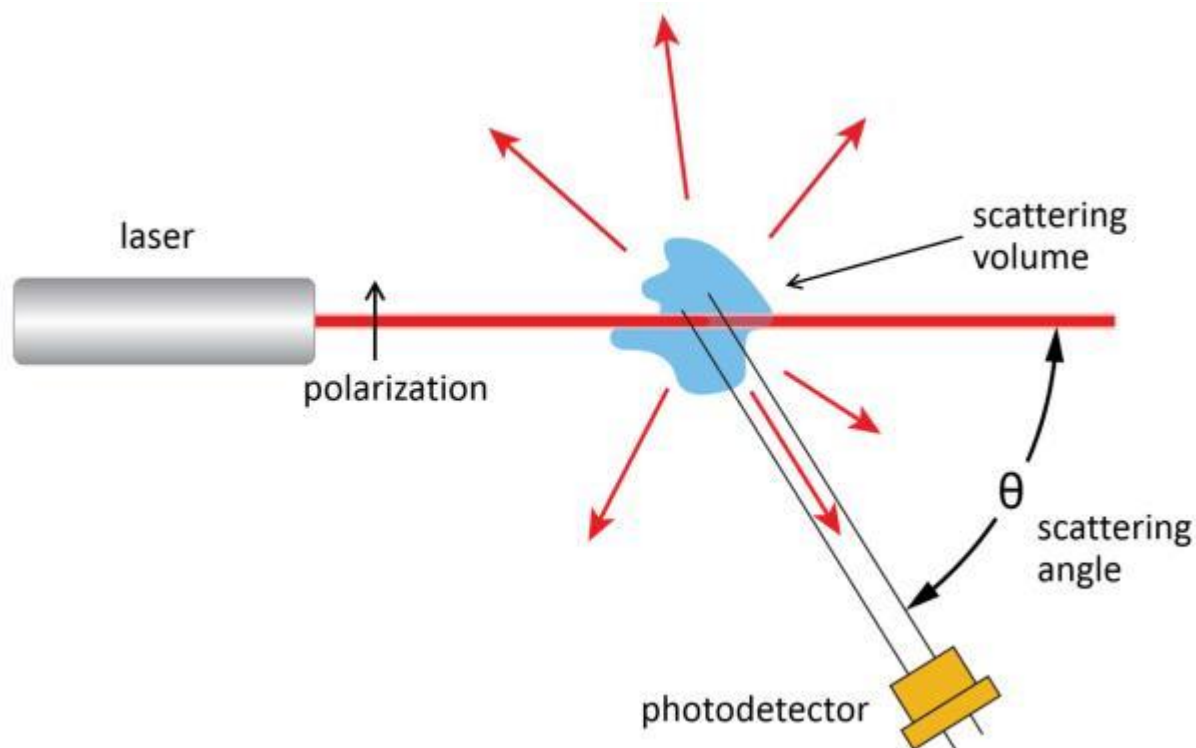


Figure 2. 9 Schematic of an apparatus for measurement of static light scattering.¹¹⁴

The radius of gyration (R_g) parameter is a geometrical quantity defined as an average root mean squared distance from the centre of the mass of a macromolecule. This parameter can also be obtained via static light-scattering studies where the intensity of scattered light is analysed.¹¹⁶

The contact angle measurement can be performed to determine the surface hydrophilicity (wettability by water) using an optical tensiometer. Wetting indicates how a liquid deposited on a solid (or liquid) substrate spreads out. In other words, it is defined as the ability of liquids to form boundary surfaces with solid states. The contact angle refers to the angle between the tangential to the liquid surface and the solid surface at a point where a liquid-vapor interface meets a solid surface as depicted in Figure 2.10. Generally, water is used as a liquid for this analysis¹¹⁷ as it quantifies the wettability of a solid surface by the liquid following Young's equation:

$$\gamma_{LG} \cos \theta_c = \gamma_{SG} - \gamma_{SL} \quad (6)$$

where γ is the interfacial tension, and the subscript SG, SL, and LG are the interface between solid-vapor, solid-liquid, and liquid-vapor, respectively and θ_c represents the contact angle.

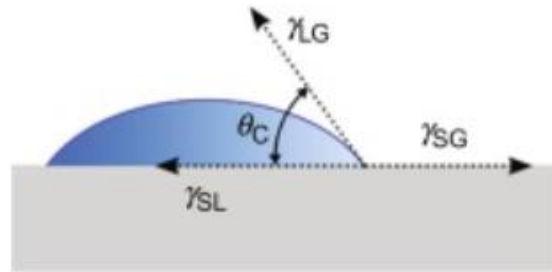


Figure 2. 10 contact angle measurement on a smooth homogeneous solid surface.¹¹⁷

Contact angle value less than 90° indicates that wetting of the surface is favorable (i.e., hydrophilic nature of solid surface). While, the contact angle larger than 90° , shows that wetting of the surface is unfavorable and solid surface is more hydrophobic in nature. Thus, the contact angle between a liquid and a solid is dependent on both the nature of the liquid and surface properties of the solid.¹¹⁸

A hybrid rheometer (TA Instruments) is employed extensively to perform the rheological studies of polymers. In this research, a rheometer device equipped with a cylindrical geometry (cone diameter, 28.03 mm; cone length, 41.96; angle, 1° ; gap, 5500 μm) was used to analyse the viscoelastic properties of lignin-based polymers. Generally, rheology is a scientific discipline that focuses on the flow of fluids. The rheology of polymeric fluids is quite complicated as these materials exhibit many unusual features related mostly to their molecular structure. Polymers usually have a viscoelastic property, which exhibits both viscous and elastic features. These characteristics are evident when a polymeric fluid is displaced slightly and then all forces acting upon it are removed. As a result, the fluid flows back slightly, but not entirely. The ability of a

material to retract to its original dimensions is defined as Elasticity. If elasticity is not detected, then the fluid is completely viscous. Storage moduli (G') is the elasticity property that describes the amount of energy stored in the elastic structure, and loss (G'') moduli represents the magnitude of energy dissipated by the material in a cycle of deformation.¹¹⁹ In addition, $G' > G''$ reflects the more elastic behavior of testing material and the crossover of G' and G'' describes the gel-like structure of polymer. The loss tangent ($\tan \delta$), which is the ratio of G''/G' comprehensively, illustrates the viscoelastic characteristics of the polymer. Basically, when $\tan \delta$ is lower than 1, then $G' > G''$, exhibiting elastic characteristics; when $\tan \delta$ is higher than unity, then $G'' > G'$, indicating viscose behaviour of a polymeric system.¹²⁰

2.4.3 Clay properties

Brunauer-Emmett-Teller (BET) method aims to indicate the physical adsorption of gas molecules on a solid surface (i.e., clay particles), which obtained from gas adsorption isotherm, (i.e., typically nitrogen) and serves as the basis for an important analysis technique for the measurement of the specific surface area of materials. This method is used widely for systems with multilayer adsorption, and usually utilizes probing gases that do not chemically react with surface of adsorbates to quantify specific surface area.¹²¹ Nitrogen is the most commonly employed gaseous adsorbate for this purpose. Specific surface area is a scale-dependent property depending on porosity, pore size distribution, shape, size, and roughness. The role of the specific surface area is critical in many applications, such as catalysis, gas storage, gas separation, drug delivery, adsorption separation, sensors, and batteries.¹²²

Specific surface area and particle size are two important factors for characterization of materials that are related to adsorption capacity and speed. Thus, the smaller the size of the material, the higher the surface area would be.¹²³

Scanning electron microscope (SEM) is an indispensable instrument for the characterization of materials in the range of nanometer to micrometer scale. SEM helps examine the microstructure morphology and chemical composition of clay particles.¹²⁴ At relative lower magnification, SEM, can provide a large field of view, while at higher magnification, it can get high-resolution images of local structures. In this analysis, a completely dried sample is coated with a 40–60 nm thick layer of carbon or metal, such as gold or palladium, under vacuum and analyzed using SEM-EDX technique.¹¹³

When this instrument is used in conjunction with other related techniques of energy-dispersive X-ray microanalysis (i.e., EDX), the specimen is bombarded with an electron beam inside the scanning electron microscope. In fact, the electron beam hits the incident electron beam of a specimen and transfers the electrons present in the inner shell of atoms to the outer shell. The void generated in the lower shell is occupied by a higher-energy electron from an outer shell of specimen atom via releasing energy in the form of X-rays. Atoms of each element in the particles emit X-rays with unique amounts of energy in the transferring process that helps identify the composition or orientation of individual crystals or features.^{113,124}

2.4.4 Properties of clay suspensions

Zeta potential represents the surface charge of colloidal particles indicating their long-term stability, which can be measured by zeta potential analyzer. According to DVLO theory, developed

by Derjaguin, Verwey, Landau, and Overbeek, the stability of particles in suspension depends on the total potential energy function V_T as presented in equation 7:

$$V_T = V_A + V_R + V_S \quad (7)$$

where V_A , V_R and V_S are the attractive forces from van der Waals interactions, the repulsive energy from the electrical double layer of particles (i.e., when they are brought close by Brownian motion), and the potential energy from the solvent, respectively. An equilibrium is reached between these two opposing forces when the particles move with constant velocity. This velocity of the particle is also named as electrophoretic mobility (μ). Accordingly, the Smoluchowski approximation is used to calculate the zeta potential (ζ) from the measured electrophoretic mobility (μ) of the samples following equation 8:

$$\mu = \varepsilon \zeta \frac{(1.5)}{\eta} \quad (8)$$

where ε is the dielectric constant and η stands for absolute viscosity of the medium.¹²⁵

The aggregation of clay particles can be monitored using a photometric dispersion analyzer (PDA). In this setup, a PDA instrument is connected to a dynamic drainage jar (DDJ) and fitted with a 70-mm mesh screen. Clay suspension is pumped from a DDJ cell through a 3mm transparent plastic tube into the photocell of the PDA that measures the fluctuations of transmitted light. Changes in the intensity of transmitted light identifies two major components: V_{DC} that represents average transmitted light intensity and V_{RMS} defines the root mean square of the fluctuations in transmitted light. The considerable increase in the proportion of V_{rms} to V_{dc} signal known as ratio (R) or flocculation index is an indicator of particle aggregation according to equation 9:¹²⁶

$$Ratio = \frac{V_{(RMS)}}{V_{(DC)}} \quad (9)$$

For dilute systems, correlation of ratio and the square root of the concentration are linear. For polydisperse systems, R value is approximately linear with radius of flocs.

$$R \approx CN^{1/2}a \quad (10)$$

Where N is the number of particles, and C is a constant.¹²⁷

After reaching equilibrium, the polymer (i.e., flocculant) added and the ratio is measured every second until it reached the plateau. As time elapses, a significant increase in the size of flocs occurs and the flocculation rate, ki , is determined. The stability ratio (W) for a specific flocculation rate is defines as:

$$W = \frac{K_{fast}}{K_i} \approx \frac{\left(\frac{dr}{dt}\right)_{fast}}{\left(\frac{dr}{dt}\right)_i} \quad (11)$$

where k_{fast} is the fastest maximum growth rate in flocculation process defined by $\log W=0$. In this system, $\log W=\infty$ represents the stable kaolin suspension.^{127,128}

Variation in the direct current (DC) voltage of the PDA instrument also expresses the flocculation behaviour of kaolin particles through changing the relative turbidity of the suspension. In this set of experiments, the addition of kaolin suspension to the photocell of PDA decreases the initial base DC voltage (V_0) to a new DC voltage (V_i). After that, varying dosages of cationic polymer are added to the cell to induce the flocculation process. This causes an increment in the DC voltage

(V_f) of the final dispersion. The relative turbidity of the system τ_r can be measured using equation 12:²⁵

$$\text{Relative turbidity, } \tau_r = \frac{\tau_f}{\tau_i} = \frac{\ln(V_0/V_f)}{\ln(V_0/V_i)} \quad (12)$$

Where τ_f and τ_i are the final and initial suspension turbidity, respectively.

Focused beam reflectance measurement (FBRM) is a versatile technique developed for ‘in situ’ particle monitoring of chord length distribution (CLD) and rate of change in crystal size in real-time. The principle of FBRM technique is presented in Figure 2.11, which works based on light backscattering using a revolving laser beam. The latter is projected inside the suspension through a sapphire window at the end of the FBRM probe. The focused beam rotates at a constant speed of 2 m/s and particles pass by the window surface. The beam intersects the edge of a particle which begins to backscatter laser light until the beam reaches its opposite edge. The reflected light from the particles is collected by the FBRM optics and converted into an electronic signal. The particle backscattering time is multiplied by the optical rotating laser scan speed and the result is a chord length. Chord length is defined as a straight line between any two points on the edge of a particle or particle structure. During the monitoring time, measured chord lengths are recorded and a chord length distribution (CLD) is obtained in real time. Thousands of chord lengths can be measured per second producing a histogram and are organized in channels (size intervals). The effect of particle shape, particle refractive index, dispersion media refractive index, focal length, suspension concentration and particle size on chord length distributions has been investigated to relate chord length distributions to the “actual” particle size distributions.^{129,130}

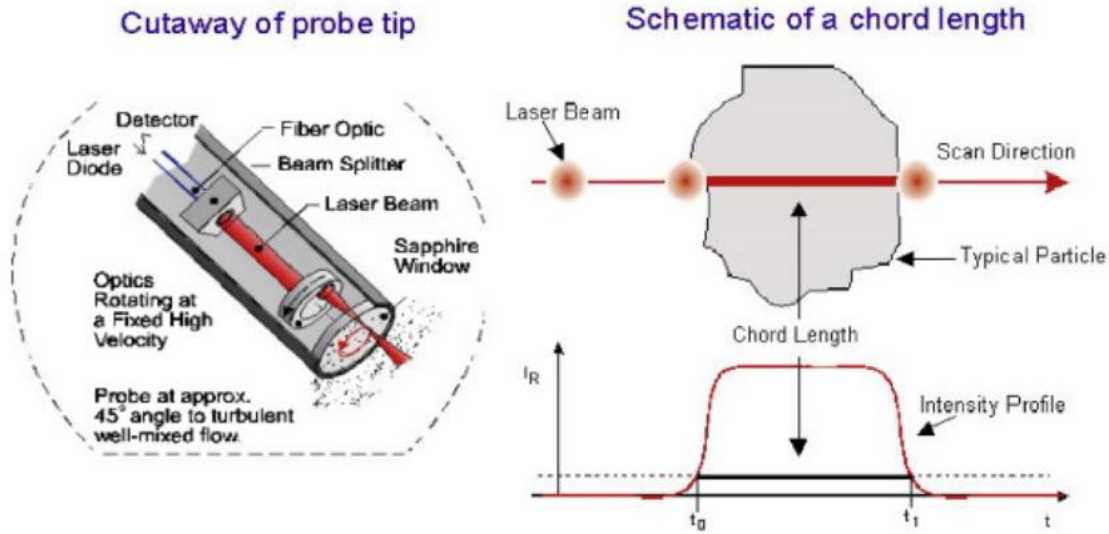


Figure 2. 11 Schematic representations of FBRM probe and chord length measurement.¹³⁰

To study suspension behaviour and to determine sedimentation speed vertical scan analyzer Formulation, France, is widely used as described in the literature.¹³¹ This optical analyser instrument can detect and measure the modifications of concentrated and opaque suspensions. It carries out step-by-step vertical scanning of the whole sample via a pulsed near-infrared light source ($\lambda = 850 \text{ nm}$) and converts the macroscopic aspects of the suspension system into two graphics. Acquiring transmission and back scattering profiles come respectively from the transmission and back scattering detectors. The former detector receives the light going across the sample (at 180° from the incident beam), while the latter obtains the light scattered backward by the sample at 45° from the incident beam (Figure 2.12).¹³² The higher transmission zone indicates less stable suspension (i.e., clay suspension) owing to the sedimentation of particles. The transmittance and backscattering profiles are recorded as a percentage of transmittance signals in regard to that of the reference chemical, silicon oil. These two profiles are also used for determining the destabilization index (DSI) and average particle diameter using the turbisoft software as presented in equation 13:¹³³

$$TSI = \sum_i \frac{\sum_h |Scan_i(h) - Scan_{i-1}(h)|}{H} \quad (13)$$

where $scan_i(h)$ and $scan_{i-1}(h)$ are the transmission signals for two consecutive time intervals at a given height (h) and H is the entire height of measuring sample.

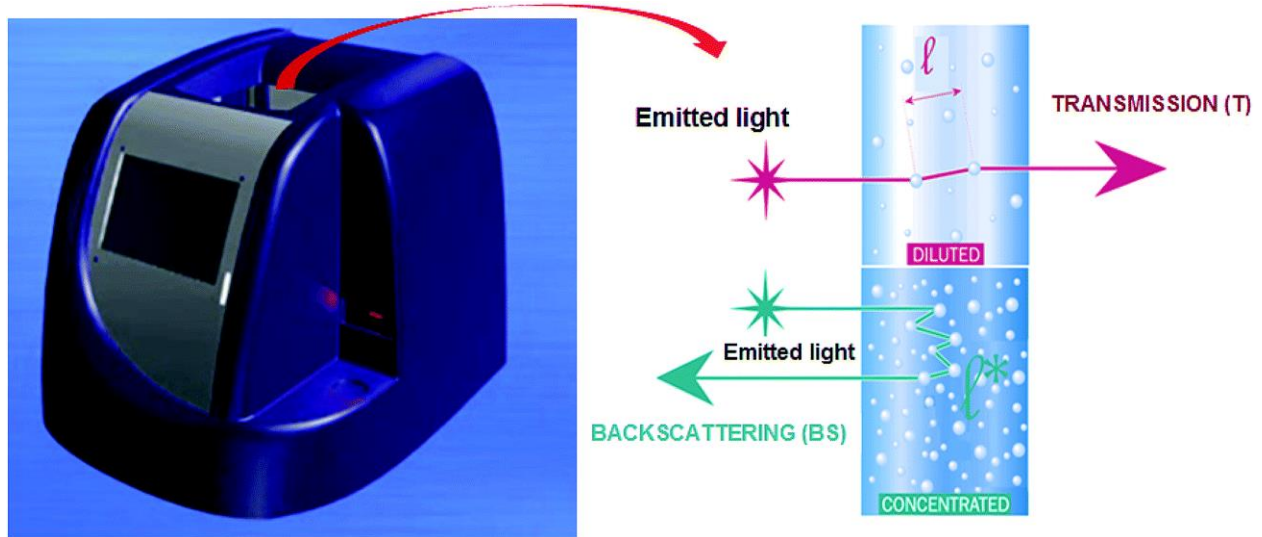


Figure 2.12 Measurement principle diagram of the Turbiscan Lab Expert type stability analyzer.¹³⁴

The evaluation of the separation behaviour of a dispersion plays a vital role in the optimization of processes and their products. LUMiSizer® is a powerful tool to assess the stability of the dispersions. LUMiSizer records the variation of transmitted light over time and space in transmission profiles and provides information on the separation process kinetics using a centrifugal separation analysis (CSA). This approach allows for the calculation of the particle migration velocity, which is intimately related to particle size distribution.¹³⁵ This technology is developed for quick characterization of any demixing phenomena (i.e., sedimentation or flotation). Using this multisample analytical centrifuge, the velocity distribution in the centrifugal field as well as of particle size distribution can be easily determined.¹³⁶ LUMiSizer® employs the STEP-Technology, to obtain space and time-resolved extinction profiles over the total range of up to 12

different samples simultaneously at constant or variable centrifugal force (up to 2300 g). Parallel near-infrared (NIR) or blue light (λ of 880 nm) illuminates the entire sample length and the transmitted light is detected by the 2087 sensors of the charge-coupled device line (CCD-line) detector.¹³⁷

The shape and progression of the transmission signals provides valuable information about the kinetics of the separation process and facilitates particle characterization. By tracing the variation in transmission profile at any part of the tested sample or the movement of any phase boundary, the separation performance of the individual samples can be compared and carefully analyzed. Considering the extinction profiles, clarification velocity, sedimentation and flotation velocity of particles, residual turbidity and separated phase volume (liquid or solid) can be quantified.¹³⁵ The measurement principle of the STEP-Technology® used in the LUMiSizer® is presented in Figure 2.13.

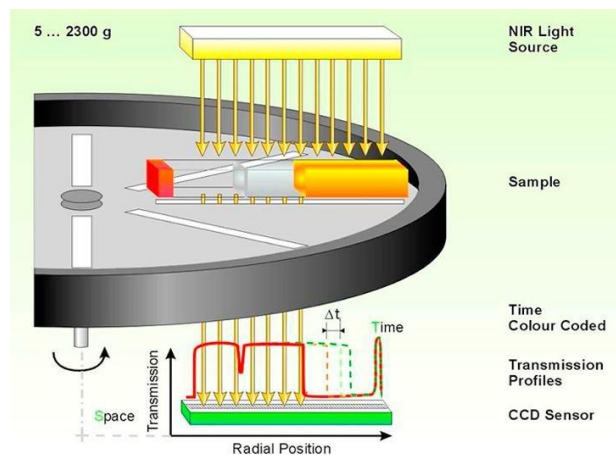


Figure 2. 13 Schematic configuration and measurement principle of the LUMiSizer®.¹³⁸

Quartz crystal microbalance (QCM) is a highly versatile and sensitive tool that uses acoustic waves generated by oscillating a piezoelectric, single crystal quartz plate to measure mass. The QCM operation associates with quartz's inherent characteristics of piezoelectricity. In this instrument, a

circular piece of quartz is sandwiched between two metal electrodes. QCM-D can monitor processes in real-time via measuring changes in frequency and energy dissipation of the system composed by the surface adsorbed on a piezoelectric quartz sensor. By applying alternating electric fields to quartz sensor a mechanical oscillation of characteristic frequency can be produced on the crystal. When a change on the mass occurred at interface, a frequency shift from the fundamental resonant frequency of the crystal (Δf) can be detected to quantify mass changes. The Sauerbrey equation correlates frequency change (Δf) and mass change (Δm), where negative frequency shift relates to the mass increase:

$$\Delta m = - \frac{C\Delta f}{n} \quad (14)$$

In this equation C is the mass sensitivity constant of crystal ($17.7 \text{ ng/ Hz} \times \text{cm}^2$) for a 5 MHz quartz crystal sensor and n is the frequency overtone number (up to the 13th overtone). This equation is applicable for the adsorbing thin film with limited viscoelastic coupling from the surrounding medium.¹³⁹ Moreover, QCM-D simultaneously monitors the viscoelastic properties of the thin film adsorbed on sensor via recording changes in the energy dissipation factor (D) following equation 15:

$$D = \frac{E_D}{2\pi E_S} \quad (15)$$

where E_D and E_S are the energy dissipated and the amount of energy stored in the oscillating system, respectively. Voigt viscoelastic model is used for model soft and thick polymer in Q-Tools software, Q-sense, Gothenborg, Sweden.¹⁴⁰ Figure 2.14 summarizes the QCM principal.

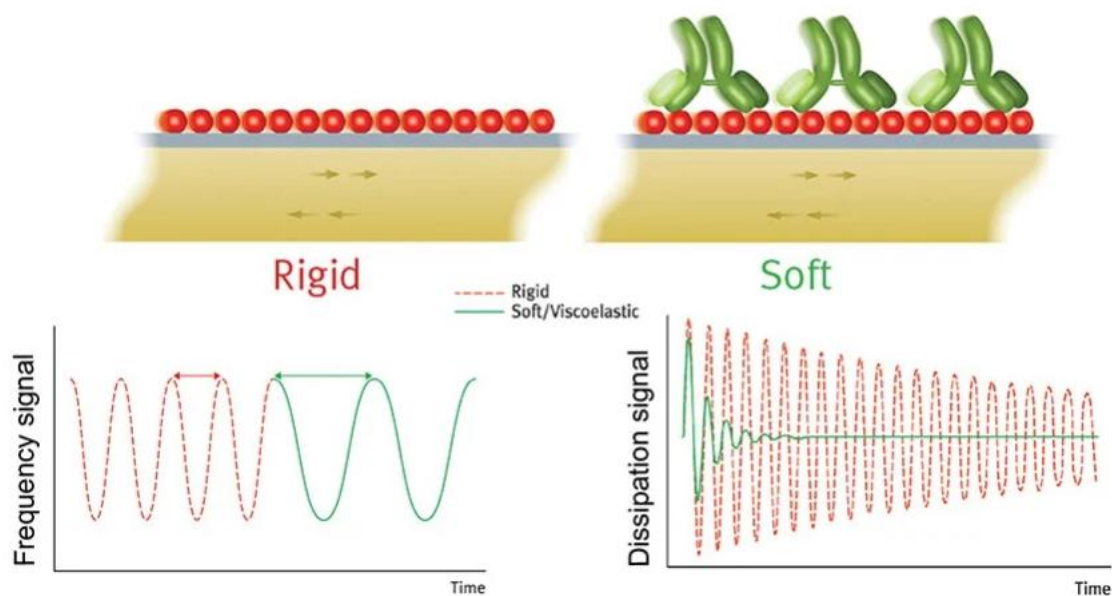


Figure 2. 14 Schematic representation of QCM-D principle and related plots

2.5 Summary

The development of sustainable processes for renewable alternatives to petroleum-based material has attracted considerable attention as a result of the increasing environmental impact and economic volatility of crude oil. Lignin, an abundant by-product of the biorefinery, has now become a promising alternative for the sustainable product development, which can be used in industrial applications. This chapter presents a review of relevant literature, which outlines the modification process of lignin macromolecule to produce cationic lignin-based products using different methods. The study framework, however, focuses on the potential application of lignin macromolecule as a flocculant or adsorbent to treat various wastewater systems. Moreover, the fundamental knowledge related to the colloidal suspension, the significance about the stabilization of clay particles and the effect of solution properties on the destabilization of model suspensions

was reviewed in this section. A fundamental understanding of the adsorption and flocculation process, along with the main mechanisms involved, were presented in this section. Furthermore, the description and significance of advanced techniques, which were extensively used in this research thesis to meet the objectives, were fundamentally discussed in this chapter.

2.6 References

- (1) Gao, Y., Evans, G. M., Wanless, E. J., Moreno-Atanasio, R. 2017. DEM modelling of particle-bubble capture through extended DLVO theory. *Colloids Surf. A Physicochem. Eng. Asp.* 529, 876-885.
- (2) Gudarzi, M. M. 2016. Colloidal stability of graphene oxide: aggregation in two dimensions. *Langmuir*, 32(20), 5058-5068.
- (3) Budhu, M. 2008. *SOIL MECHANICS AND FOUNDATIONS, (With CD)*. John Wiley & Sons.
- (4) Lee, K. E., Morad, N., Poh, B. T., Teng, T. T. 2011. Comparative study on the effectiveness of hydrophobically modified cationic polyacrylamide groups in the flocculation of kaolin. *Desalination*, 270(1-3), 206-213.
- (5) Besra, L., Sengupta, D. K., Roy, S. K., Ay, P. 2002. Flocculation and dewatering of kaolin suspensions in the presence of polyacrylamide and surfactants. *Int. J. Miner. Process.* 66(1-4), 203-232.
- (6) Choi, J. H., Anwar, A. F., Kawamura, K., Ichikawa, Y. 2009. Transport phenomena in kaolinite clay: Molecular simulation, homogenization analysis and similitude law. *Int J Numer Anal Methods Geomech.* 33(5), 687-707.
- (7) Chen, Y., Liu, S., & Wang, G. 2007. A kinetic investigation of cationic starch adsorption and flocculation in kaolin suspension. *Chem. Eng. J.* 133(1-3), 325-333.

- (8) Lee, K. E., Teng, T. T., Morad, N., Poh, B. T., Hong, Y. F. 2010. Flocculation of kaolin in water using novel calcium chloride-polyacrylamide (CaCl₂-PAM) hybrid polymer. *Sep. Purif. Technol.*, 75(3), 346-351.
- (9) Dutta, P. K., Tripathi, S., Mehrotra, G. K., Dutta, J. 2009. Perspectives for chitosan based antimicrobial films in food applications. *Food Chem.* 114(4), 1173-1182.
- (10) Tungala, K., Adhikary, P., Azmeera, V., Kumar, K., Krishnamoorthi, S. 2017. Dendritic star polymer of polyacrylamide based on a β -cyclodextrin trimer: a flocculant and drug vehicle. *New J. Chem.* 41(2), 611-618.
- (11) Halake, K., Birajdar, M., Kim, B.S., Bae, H., Lee, C., Kim, Y.J., Kim, S., Kim, H.J., Ahn, S., An, S.Y. and Lee, J., 2014. Recent application developments of water-soluble synthetic polymers. *J Ind Eng Chem.* 20(6), 3913-3918.
- (12) Kadajji, V. G., Betageri, G. V. 2011. Water soluble polymers for pharmaceutical applications. *Polymers*, 3(4), 1972-2009.
- (13) Nasser, M. S., James, A. E. 2006. The effect of polyacrylamide charge density and molecular weight on the flocculation and sedimentation behaviour of kaolinite suspensions. *Sep. Purif. Technol.* 52(2), 241-252.
- (14) Sonker, E., Tiwari, R., Adhikary, P., Kumar, K., Krishnamoorthi, S. 2019. Preparation of ultra-high-molecular-weight polyacrylamide by vertical solution polymerization technique. *Polym. Eng. Sci.* 59(6), 1175-1181.
- (15) Wang, S., Konduri, M.K.R., Hou., Q., Fatehi, P. 2016. Cationic xylan-METAC copolymer as a flocculant for clay suspensions. *RSC Adv.* 6, 40258-40269.

- (16) Pal, S., Mal, D., Singh, R.P., 2006. Synthesis, characterization and flocculation characteristics of cationic glycogen: a novel polymeric flocculant. *Colloids Surf A Physicochem. Eng. Asp.* 289, 193–199.
- (17) Preetha, B. K., Badalamoole, V. 2019. Modification of Karaya gum by graft copolymerization for effective removal of anionic dyes. *Sep. Purif. Technol.* 54(16), 2638-2652.
- (18) Wu, H., Liu, Z., Yang, H., &Li, A. 2016. Evaluation of chain architectures and charge properties of various starch-based flocculants for flocculation of humic acid from water. *Water Res.* 96, 126-135.
- (19) Li, X., Zheng, H., Wang, Y., Sun, Y., Xu, B., Zhao, C. 2017. Fabricating an enhanced sterilization chitosan-based flocculants: Synthesis, characterization, evaluation of sterilization and flocculation. *Chem. Eng. J.* 319, 119-130.
- (20) Guo, K., Gao, B., Wang, W., Yue, Q., Xu, X. 2019. Evaluation of molecular weight, chain architectures and charge densities of various lignin-based flocculants for dye wastewater treatment. *Chemosphere*, 215, 214-226.
- (21) Wei, Y., Cheng, F., Zheng, H. 2008. Synthesis and flocculating properties of cationic starch derivatives. *Carbohydr. Polym.* 74(3), 673-679.
- (22) Wang, B., Zhang, Y., Miao, C. 2011. Preparation of cationic chitosan-polyacrylamide flocculant and its properties in wastewater treatment. *J. Ocean Univ. China.* 10(1), 42-46.
- (23) Wan, X., Li, Y., Wang, X., Chen, S., Gu, X. 2007. Synthesis of cationic guar gum-graft-polyacrylamide at low temperature and its flocculating properties. *Eur. Polym. J.* 43(8), 3655-3661.

- (24) Wang, S., Hou, Q., Kong, F., Fatehi, P. 2015. Production of cationic xylan–METAC copolymer as a flocculant for textile industry. *Carbohydr. Polym.* 124, 229-236.
- (25) Wang, J. P., Chen, Y. Z., Yuan, S. J., Sheng, G. P., Yu, H. Q. 2009. Synthesis and characterization of a novel cationic chitosan-based flocculant with a high water-solubility for pulp mill wastewater treatment. *Water Res.* 43(20), 5267-5275.
- (26) Heydarifard, S., Gao, W., Fatehi, P. 2018. Generation of new cationic xylan-based polymer in industrially relevant process. *Ind. Eng. Chem. Res.* 57(38), 12670-12682.
- (27) Sun, Y., Ren, M., Zhu, C., Xu, Y., Zheng, H., Xiao, X., Wu, H., Xia, T. and You, Z., 2016. UV-initiated graft copolymerization of cationic chitosan-based flocculants for treatment of zinc phosphate-contaminated wastewater. *Ind. Eng. Chem. Res.* 55(38), 10025-10035.
- (28) Wang, S., Kong, F., Gao, W., Fatehi, P. 2018. Novel process for generating cationic lignin based flocculant. *Ind. Eng. Chem. Res.* 57(19), 6595-6608.
- (29) Kong, F., Parhiala, K., Wang, S., Fatehi, P. 2015. Preparation of cationic softwood kraft lignin and its application in dye removal. *Eur. Polym. J.* 67, 335-345.
- (30) Laszlo, J. A. 1999. Solubility and dye-binding properties of quaternized and peroxidase-polymerized kraft lignin. *Environ. Technol.* 20(6), 607-615.
- (31) Li, R., Gao, B., Guo, K., Zheng, H., Yue, Q. 2016. Floc structural characteristics of ferrum-polymer dual-coagulant for treatment of synthetic dyes wastewater: effect of solution pH, hardness and ionic strength. *RSC Adv.* 6(97), 94851-94858.
- (32) Ayyachamy, M., Cliffe, F. E., Coyne, J. M., Collier, J., Tuohy, M. G. 2013. Lignin: untapped biopolymers in biomass conversion technologies. *Biomass Convers. Biorefin.* 3(3), 255-269.

- (33) Strassberger, Z., Tanase, S., Rothenberg, G. 2014. The pros and cons of lignin valorisation in an integrated biorefinery. *RSC Adv.* 4(48), 25310-25318.
- (34) Chakar, F. S., Ragauskas, A. J. 2004. Review of current and future softwood kraft lignin process chemistry. *Ind Crops Prod.* 20(2), 131-141.
- (35) Zakzeski, J., Bruijninx, P. C., Jongerius, A. L., Weckhuysen, B. M. 2010. The catalytic valorization of lignin for the production of renewable chemicals. *Chem. Rev.* 110(6), 3552-3599.
- (36) Vanholme, R., Demedts, B., Morreel, K., Ralph, J. and Boerjan, W., 2010. Lignin biosynthesis and structure. *Plant Physiol.* 153(3), 895-905.
- (37) Adler, E. 1977. Lignin chemistry—past, present and future. *Wood Sci. Technol.* 11(3), 169-218.
- (38) Ede, R. M., Kilpeläinen, I. 1995. Homo- and hetero-nuclear 2D NMR techniques: Unambiguous structural probes for non-cyclic benzyl aryl ethers in soluble lignin samples. *Res. Chem. Intermed.* 21(3-5), 313-328.
- (39) Karhunen, P., Rummakko, P., Sipilä, J., Brunow, G., Kilpeläinen, I. 1995. Dibenzodioxocins; a novel type of linkage in softwood lignins. *tetrahedron Lett.* 36(1), 169-170.
- (40) Fatehi, P., Chen, J. 2016. Extraction of technical lignins from pulping spent liquors, challenges and opportunities. In *Production of biofuels and chemicals from lignin*, 35-54, Springer, Singapore.
- (41) Tomani, P. E. R. 2010. The lignoboost process. *Cellul. Chem. Technol.* 44(1), 53.
- (42) Yuan, T. Q., Xu, F., Sun, R. C. 2013. Role of lignin in a biorefinery: separation characterization and valorization. *J. Chem. Technol. Biotechnol.* 88(3), 346-352.

- (43) Ahvazi, B. Wojciechowicz, O., Ton-That, T.M., Hawari, J. 2011. Preparation of lignopolyols from wheat straw soda lignin. *J. Agric. Food Chem.* 59, 10505-10516.
- (44) Laurichesse, S., Avérous, L. 2014. Chemical modification of lignins: Towards biobased polymers. *Prog. Polym. Sci.* 39(7), 1266-1290.
- (45) Cazacu, G., Capraru, M., Popa, V. I. 2013. Advances concerning lignin utilization in new materials. In *Advances in natural polymers*, 255-312, Springer, Berlin, Heidelberg.
- (46) Hu, T. Q. 2008. *Characterization of lignocellulosic materials*. Blackwell.
- (47) Mai, C., Majcherczyk, A., Hüttermann, A. 2000. Chemo-enzymatic synthesis and characterization of graft copolymers from lignin and acrylic compounds. *Enzyme Microb. Technol.* 27(1-2), 167-175.
- (48) Sharif, J., Mohamad, S.F., Othman, N.A.F., Bakaruddin, N.A., Osman, H.N. and Güven, O., 2013. Graft copolymerization of glycidyl methacrylate onto delignified kenaf fibers through pre-irradiation technique. *Radiat. Phys. Chem.* 91, 125-131.
- (49) Rosu, L., Cascaval, C. N., Rosu, D. 2009. Effect of UV radiation on some polymeric networks based on vinyl ester resin and modified lignin. *Polym. Test.* 28(3), 296-300.
- (50) Fang, R., Cheng, X., Xu, X. 2010. Synthesis of lignin-base cationic flocculant and its application in removing anionic azo-dyes from simulated wastewater. *Bioresour. Technol.* 101, 7323-9.
- (51) Nesvadba, P. 2012. Radical polymerization in industry. *Encyclopedia of Radicals in Chemistry, Biology and Materials*.

- (52) Hasan, A., Fatehi, P. 2019. Cationic kraft lignin-acrylamide copolymer as a flocculant for clay suspensions:(2) Charge density effect. *Sep. Purif. Technol.* 210, 963-972.
- (53) Saeed, A., Fatehi, P., Ni, Y. 2011. Chitosan as a flocculant for pre-hydrolysis liquor of kraft-based dissolving pulp production process. *Carbohydr. Polym.* 86(4), 1630-1636.
- (54) Blanco, A., Fuente, E., Negro, C., Tijero, J. 2002. Flocculation monitoring: focused beam reflectance measurement as a measurement tool. *Can. J. Chem. Eng.* 80(4), 1-7.
- (55) Liu, H., Yang, X., Zhang, Y., Zhu, H. and Yao, J., 2014. Flocculation characteristics of polyacrylamide grafted cellulose from *Phyllostachys heterocycla*: an efficient and eco-friendly flocculant. *Water Res.* 59, 165-171.
- (56) Sabaghi, S. and Fatehi, P., 2019. Phenomenological Changes in Lignin Following Polymerization and Its Effects on Flocculating Clay Particles. *Biomacromolecules*, 20(10), 3940-3951.
- (57) Sabaghi, S. and Fatehi, P., 2020. Polarity of cationic lignin polymers: Physicochemical behavior in aqueous solutions and suspensions. *ChemSusChem*, 13(17), 4722-4734.
- (58) Liu, Z., Lu, X., Xie, J., Feng, B., Han, Q. 2019. Synthesis of a novel tunable lignin-based star copolymer and its flocculation performance in the treatment of kaolin suspension. *Sep. Purif. Technol.* 210, 355-363.
- (59) Saha, D., Payzant, E. A., Kumbhar, A. S., Naskar, A. K. 2013. Sustainable mesoporous carbons as storage and controlled-delivery media for functional molecules. *ACS Appl. Mater. Interfaces.* 5(12), 5868-5874.

- (60) Chung, H., & Washburn, N. R. 2013. Chemistry of lignin-based materials. *Green Mater.* 1(3), 137-160.
- (61) Cui, C., Sadeghifar, H., Sen, S., Argyropoulos, D. S. 2013. Toward thermoplastic lignin polymers; part II: thermal & polymer characteristics of kraft lignin & derivatives. *BioResources*, 8(1), 864-886.
- (62) Carrott, P. J. M., Carrott, M. R. 2007. Lignin—from natural adsorbent to activated carbon: a review. *Bioresour. Technol.* 98(12), 2301-2312.
- (63) Hubbe, M. A., Nanko, H., McNeal, M. R. 2009. Retention aid polymer interactions with cellulosic surfaces and suspensions: A review. *BioResources*, 4(2), 850-906.
- (64) Peng, P. and Garnier, G., 2010. Effect of cationic polyacrylamide adsorption kinetics and ionic strength on precipitated calcium carbonate flocculation. *Langmuir*, 26(22), 16949-16957.
- (65) Ödberg, L., Swerin, A., Tanaka, H. Some kinetic aspects of wet-end chemistry. In PAPERMAKERS CONFERENCE; TAPPI PRESS: 1995. 65-65.
- (66) Van de Ven, T. G. M., Alince, B. 1996. Heteroflocculation by asymmetric polymer bridging. *J. Colloid Interface Sci.* 181(1), 73-78.
- (67) Hubbe, M. *Mini-Encyclopedia of Papermaking Wet-End Chemistry: Additives and Ingredients, their Composition, Functions, Strategies for Use*; Retrieved online on Jun 4: 2011.
- (68) Roberts, J. C. *The chemistry of paper*; Royal Society of Chemistry: 2007.
- (69) Zhu, Z., Li, T., Lu, J., Wang, D., Yao, C. 2009. Characterization of kaolin flocs formed by polyacrylamide as flocculation aids. *Int. J. Miner. Process.* 91(3-4), 94-99.

- (70) Solberg, D., Wågberg, L. 2003. Adsorption and flocculation behavior of cationic polyacrylamide and colloidal silica. *Colloids Surf. A Physicochem. Eng. Asp.* 219(1-3), 161-172.
- (71) Sikora, M. D. (1981). The shear stability of flocculated colloids.
- (72) Yoon, S. Y., Deng, Y. 2004. Flocculation and reflocculation of clay suspension by different polymer systems under turbulent conditions. *J. Colloid Interface Sci.* 278(1), 139-145.
- (73) Hermawan, M., Bushell, G. C., Craig, V. S., Teoh, W. Y., Amal, R. 2004. Floc strength characterization technique. An insight into silica aggregation. *Langmuir*, 20(15), 6450-6457.
- (74) Bache, D. H., Johnson, C., McGilligan, J. F., Rasool, E. 1997. A conceptual view of floc structure in the sweep floc domain. *Water Sci. Technol.* 36(4), 49-56.
- (75) Li, T., Zhu, Z., Wang, D., Yao, C., Tang, H. 2007. The strength and fractal dimension characteristics of alum-kaolin flocs. *Int. J. Miner. Process.* 82(1), 23-29.
- (76) Jarvis, P., Jefferson, B., Gregory, J. O. H. N., Parsons, S. A. 2005. A review of floc strength and breakage. *Water Res.* 39(14), 3121-3137.
- (77) Zhang, L., Li, X., Xu, X., Zeng, F. 2005. Correlation between antitumor activity, molecular weight, and conformation of lentinan. *Carbohydr. Res.* 340(8), 1515-1521.
- (78) Petridis, L., Smith, J. C. 2016. Conformations of Low-Molecular-Weight Lignin Polymers in Water. *ChemSusChem*, 9(3), 289-295.
- (79) Das, R. K., Pappu, R. V. 2013. Conformations of intrinsically disordered proteins are influenced by linear sequence distributions of oppositely charged residues. *Proc. Natl. Acad. Sci.* 110(33), 13392-13397.

- (80) Ersoy, B. 2005. Effect of pH and polymer charge density on settling rate and turbidity of natural stone suspensions. *Int. J. Miner. Process.* 75(3-4), 207-216.
- (81) Doherty, W. O., Fellows, C. M., Gorjian, S., Senogles, E., Cheung, W. H. 2003. Flocculation and sedimentation of cane sugar juice particles with cationic homo-and copolymers. *J. Appl. Polym. Sci.* 90(1), 316-325.
- (82) Chen, W., Gao, X., Xu, H., Cai, Y., Cui, J. 2017. Influence of extracellular polymeric substances (EPS) treated by combined ultrasound pretreatment and chemical re-flocculation on water treatment sludge settling performance. *Chemosphere*, 170, 196-206.
- (83) Hasan, A. and Fatehi, P., 2018. Stability of kaolin dispersion in the presence of lignin-acrylamide polymer. *Appl. Clay Sci.* 158, 72-82.
- (84) Jaeger, W., Bohrisch, J., Laschewsky, A. 2010. Synthetic polymers with quaternary nitrogen atoms—Synthesis and structure of the most used type of cationic polyelectrolytes. *Prog. Polym. Sci.* 35(5), 511-577.
- (85) Abdollahi, Z., Frounchi, M., Dadbin, S. 2011. Synthesis, characterization and comparison of PAM, cationic PDMC and P (AM-co-DMC) based on solution polymerization. *J Ind Eng Chem.* 17(3), 580-586.
- (86) Shnoudeh, A. J., Hamad, I., Abdo, R. W., Qadumii, L., Jaber, A. Y., Surchi, H. S., Alkelany, S. Z. Synthesis, characterization, and applications of metal nanoparticles: Chapter 15- 2019.
- (87) Clogston, J. D., Patri, A. K. Zeta potential measurement. In *Characterization of nanoparticles intended for drug delivery*; Humana Press: 2011, 63-70.

- (88) Sapsford, K. E., Tyner, K. M., Dair, B. J., Deschamps, J. R., Medintz, I. L. 2011. Analyzing nanomaterial bioconjugates: a review of current and emerging purification and characterization techniques. *Analytical Chem.* 83(12), 4453-4488.
- (89) Domingues, M. M., & Santos, N. C. *Laser-Light Scattering Approach to Peptide–Membrane Interaction*; Membrane-Active Peptides: Methods and Results on Structure and Function: 2010, 147-168.
- (90) Jiang, J., Oberdörster, G., Biswas, P. 2009. Characterization of size, surface charge, and agglomeration state of nanoparticle dispersions for toxicological studies. *J Nanopart Res.* 11(1), 77-89.
- (91) Shah, R., Eldridge, D., Palombo, E., & Harding, I. 2014. Optimisation and Stability Assessment of Solid Lipid Nanoparticles using Particle Size and Zeta Potential. *J. Phys. Sci.* 25(1).
- (92) Joseph, E., Singhvi, G. *Multifunctional nanocrystals for cancer therapy: A potential nanocarrier*. In *Nanomaterials for Drug Delivery and Therapy*; William Andrew Publishing: 2019, 91-116.
- (93) Ma, J., Fu, K., Jiang, L., Ding, L., Guan, Q., Zhang, S., Zhang, H., Shi, J. and Fu, X., 2017. Flocculation performance of cationic polyacrylamide with high cationic degree in humic acid synthetic water treatment and effect of kaolin particles. *Sep. Purif. Technol.* 181, 201-212.
- (94) Al-Dawery, S. K. 2017. Degree of flocculation and Interparticles charges of conditioned Municipal Activated Sludge using Mixed Polymers. *J. Macromol. Sci. A. Part B*, 56(8), 578-594.

- (95) He, W., Gao, W., Fatehi, P. 2017. Oxidation of kraft lignin with hydrogen peroxide and its application as a dispersant for kaolin suspensions. *ACS Sustain. Chem. Eng.* 5(11), 10597-10605.
- (96) Peng, X. W., Ren, J. L., Zhong, L. X., Cao, X. F., Sun, R. C. 2011. Microwave-induced synthesis of carboxymethyl hemicelluloses and their rheological properties. *J. Agric. Food Chem.* 59(2), 570-576.
- (97) Lützenkirchen, J., Preočanin, T., Kovačević, D., Tomišić, V., Lövgren, L., Kallay, N. 2012. Potentiometric titrations as a tool for surface charge determination. *Croat. Chem. Acta.* 85(4), 391-417.
- (98) Johnston, R. L. *Metal nanoparticles and nanoalloys*. In *Frontiers of Nanoscience*; Elsevier: 3, 42, 2012.
- (99) Mohamed, M. A., Hir, Z. A. M., Mokhtar, W. N. A. W., Osman, N. S. *Features of metal oxide colloidal nanocrystal characterization*. In *Colloidal Metal Oxide Nanoparticles*; Elsevier: 83-122, 2020.
- (100) Guy, O. J., Walker, K. A. D. *Graphene functionalization for biosensor applications*. In *Silicon Carbide Biotechnology*; Elsevier: 85-141, 2016.
- (101) Hu, B., He, M., Chen, B. *Magnetic nanoparticle sorbents*. In *Solid-Phase Extraction*; Elsevier: 235-284, 2020.
- (102) Das, O., Kim, N. K., Hedenqvist, M. S., Bhattacharyya, D. *The flammability of biocomposites*. In *Durability and Life Prediction in Biocomposites, Fibre-Reinforced Composites and Hybrid Composites*; Woodhead Publishing: 335-365, 2019.

- (103) Mudalige, T., Qu, H., Van Haute, D., Ansar, S. M., Paredes, A., Ingle, T. *Characterization of Nanomaterials: Tools and Challenges*. In *Nanomaterials for Food Applications*; Elsevier: 313-353, 2019.
- (104) Gabbott P. Principles and applications thermal analysis; Blackwell Publishing Ltd, Oxford, UK: 2008.
- (105) Rafiquzzaman, S. M., Rahman, M. A., Kong, I. S. Ultrasonic-Assisted Extraction of Carrageenan. In *Seaweed Polysaccharides*; Elsevier: 75-81, 2017.
- (106) Gill, P., Moghadam, T. T., Ranjbar, B. 2010. Differential scanning calorimetry techniques: applications in biology and nanoscience. *Journal of biomolecular techniques*. 21(4), 167.
- (107) Van Holde, K. E., Johnson, W. C., Ho, P. S. .2006. Principles of physical biochemistry. *J. Chem. Educ.*
- (108) Mischnick, P., Momcilovic, D. *Chemical structure analysis of starch and cellulose derivatives*. In *Advances in carbohydrate chemistry and biochemistry*; Academic Press: 64, 117-210, 2010.
- (109) Holbrook, R. D., Galyean, A. A., Gorham, J. M., Herzing, A., Pettibone, J. *Overview of nanomaterial characterization and metrology*. In *Frontiers of Nanoscience*; Elsevier: 8, 47-87, 2015.
- (110) Lange, H., Rulli, F., Crestini, C. 2016. Gel permeation chromatography in determining molecular weights of lignins: critical aspects revisited for improved utility in the development of novel materials. *ACS Sustain. Chem. Eng.* 4(10), 5167-5180.
- (111) Lim, J., Yeap, S. P., Che, H. X., Low, S. C. 2013. Characterization of magnetic nanoparticle by dynamic light scattering. *Nanoscale Res. Lett.* 8(1), 381.

- (112) Hoo, C. M., Starostin, N., West, P., Mecartney, M. L. 2008. A comparison of atomic force microscopy (AFM) and dynamic light scattering (DLS) methods to characterize nanoparticle size distributions. *J Nanopart Res.* 10(1), 89-96.
- (113) Raval, N., Maheshwari, R., Kalyane, D., Youngren-Ortiz, S. R., Chougule, M. B., Tekade, R. K. *Importance of Physicochemical Characterization of Nanoparticles in Pharmaceutical Product Development.* In *Basic Fundamentals of Drug Delivery*; Academic Press: 369-400, 2019.
- (114) Minton, A. P. 2016. Recent applications of light scattering measurement in the biological and biopharmaceutical sciences. *Anal. Biochem.* 501, 4.
- (115) Niu, A., Li, C., Zhao, Y., He, J., Yang, Y., Wu, C. 2001. Thermal decomposition kinetics and structure of novel polystyrene clusters with mtempo as a branching agent. *Macromolecules*, 34(3), 460-464.
- (116) Stetefeld, J., McKenna, S. A., Patel, T. R. 2016. Dynamic light scattering: a practical guide and applications in biomedical sciences. *Biophys. Rev.* 8(4), 409-427.
- (117) Ismail, A. F., Khulbe, K. C., Matsuura, T. 2017. Recent Progress in Reverse Osmosis (RO) Science and Technology. *JAMST*, 21(1).
- (118) Capra, P., Musitelli, G., Perugini, P. 2017. Wetting and adhesion evaluation of cosmetic ingredients and products: correlation of in vitro–in vivo contact angle measurements. *Int. J. Cosmet. Sci.* 39(4), 393-401.
- (119) Salleh, F. M., Hassan, A., Yahya, R., Azzahari, A. D. 2014. Effects of extrusion temperature on the rheological, dynamic mechanical and tensile properties of kenaf fiber/HDPE composites. *Compos. B. Eng.* 58, 259-266.

- (120) Nigmatullin, R., Harniman, R., Gabrielli, V., Muñoz-García, J. C., Khimyak, Y. Z., Angulo, J., Eichhorn, S. J. 2018. Mechanically robust gels formed from hydrophobized cellulose nanocrystals. *ACS Appl. Mater. Interfaces*. 10(23), 19318-19322.
- (121) Nasrollahzadeh, M., Atarod, M., Sajjadi, M., Sajadi, S. M., Issaabadi, Z. *Plant-Mediated Green Synthesis of Nanostructures: Mechanisms, Characterization, and Applications*. In *Interface Science and Technology*; Elsevier: 28, 199-322, 2019.
- (122) Ambroz, F., Macdonald, T. J., Martis, V., Parkin, I. P. 2018. Evaluation of the BET Theory for the Characterization of Meso and Microporous MOFs. *Small Methods*, 2(11), 1800173.
- (123) Sinha, P., Datar, A., Jeong, C., Deng, X., Chung, Y. G., Lin, L. C. 2019. Surface Area Determination of Porous Materials Using the Brunauer–Emmett–Teller (BET) Method: Limitations and Improvements. *J. Phys. Chem. C*. 123(33), 20195-20209.
- (124) Jin, W., Xu, W., Liang, H., Li, Y., Liu, S., Li, B. *Nanoemulsions for food: properties, production, characterization, and applications*. In *Emulsions*; Academic Press: 1-36, 2016.
- (125) Pan, H., Marsh, J. N., Christenson, E. T., Soman, N. R., Ivashyna, O., Lanza, G. M., Schlesinger, P.H. Wickline, S. A. Postformulation peptide drug loading of nanostructures. In *Methods in enzymology*; Academic Press: 508, 17-39, 2012.
- (126) Chen, D., van de Ven, T. G. 2016. Flocculation kinetics of precipitated calcium carbonate induced by electrosterically stabilized nanocrystalline cellulose. *Colloids Surf. A Physicochem. Eng. Asp.* 504, 11-17.

- (127) Gaudreault, R., Di Cesare, N., Weitz, D., van de Ven, T. G. 2009. Flocculation kinetics of precipitated calcium carbonate. *Colloids Surf. A Physicochem. Eng. Asp.* 340(1-3), 56-65.
- (128) Porubská, J., Alince, B., van de Ven, T. G. 2002. Homo-and heteroflocculation of papermaking fines and fillers. *Colloids Surf. A Physicochem. Eng. Asp.* 210(2-3), 223-230.
- (129) Kumar, V., Taylor, M. K., Mehrotra, A., Stagner, W. C. 2013. Real-time particle size analysis using focused beam reflectance measurement as a process analytical technology tool for a continuous granulation–drying–milling process. *Aaps Pharmscitech*, 14(2), 523-530.
- (130) Ndoye, F. T., Alvarez, G. 2015. Characterization of ice recrystallization in ice cream during storage using the focused beam reflectance measurement. *J. Food Eng.* 148, 24-34.
- (131) Azema, N. 2006. Sedimentation behaviour study by three optical methods— granulometric and electrophoresis measurements, dispersion optical analyser. *Powder Technol.* 165(3), 133-139.
- (132) MacIver, M. R., Pawlik, M. 2017. Measurement of optical backscattering height scans from flocculated mineral sediments. *Colloids Surf. A Physicochem. Eng. Asp.* 514, 38-46.
- (133) Senoussi, H., Osmani, H., Courtois, C., el Hadi Bourahli, M. 2016. Mineralogical and chemical characterization of DD3 kaolin from the east of Algeria. *BOL SOC ESP CERAM V*, 55(3), 121-126.
- (134) Yang, H., Kang, W., Wu, H., Yu, Y., Zhu, Z., Wang, P., Zhang, X. and Sarsenbekuly, B., 2017. Stability, rheological property and oil-displacement mechanism of

- a dispersed low-elastic microsphere system for enhanced oil recovery. *RSC Adv.* 7(14), pp.8118-8130.
- (135) Fernandes, A.R., Ferreira, N.R., Fangueiro, J.F., Santos, A.C., Veiga, F.J., Cabral, C., Silva, A.M. and Souto, E.B., 2017. Ibuprofen nanocrystals developed by 22 factorial design experiment: A new approach for poorly water-soluble drugs. *Saudi Pharm J.* 25(8), pp.1117-1124.
- (136) Xu, D., Qi, Y., Wang, X., Li, X., Wang, S., Cao, Y., Wang, C., Sun, B., Decker, E. and Panya, A., 2017. The influence of flaxseed gum on the microrheological properties and physicochemical stability of whey protein stabilized β -carotene emulsions. *Food Funct.* 8(1), pp.415-423.
- (137) Zielińska, A., Martins-Gomes, C., Ferreira, N. R., Silva, A. M., Nowak, I., Souto, E. B. 2018. Anti-inflammatory and anti-cancer activity of citral: Optimization of citral-loaded solid lipid nanoparticles (SLN) using experimental factorial design and LUMiSizer®. *Int. J. Pharm.* 553(1-2), 428-440.
- (138) Gross-Rother, J., Herrmann, N., Blech, M., Pinnapireddy, S. R., Garidel, P., Bakowsky, U. 2018. The application of STEP-technology® for particle and protein dispersion detection studies in biopharmaceutical research. *Int. J. Pharm.* 543(1-2), 257-268.
- (139) Reviakine, I., Johannsmann, D., Richter, R. P. 2011. Hearing what you cannot see and visualizing what you hear: interpreting quartz crystal microbalance data from solvated interfaces. *Anal. Chem.* 83(23), 8838–8848
- (140) Yang, D., Yan, B., Xiang, L., Xu, H., Wang, X., Zeng, H. 2018. Understanding the surface properties and rheology of a silica suspension mediated by a comb-type poly

(acrylic acid)/poly (ethylene oxide)(PAA/PEO) copolymer: effect of salinity. *Soft matter*, 14(23), 4810-4819.

Chapter 3: Phenomenological Changes in Lignin Following Polymerization and its Effects on Flocculating Clay Particle

3.1 Abstract

In present work, cationic kraft lignin (CKL) macromolecules were produced via polymerizing kraft lignin (KL) with [-2-(Acryloyloxy)ethyl] trimethyl ammonium chloride (ATAC) or [-2-(methacryloyloxy)ethyl] trimethyl ammonium methyl sulfate (METAM). Despite slightly different charge densities (2.3-2.5 mmol/g) of CKL, lignin-METAM (KL-METAM) had a significantly larger molecular weight and radius of gyration. A correlation was observed between the structure of CKLs and their impacts on the surface hydrophilicity of kaolin particles. In interacting with kaolin particles, KL-METAM generated larger and stronger flocs with looser structures than did KL-ATAC. Compared to ATAC, METAM had one additional methyl substituent on its structure, which provided fundamental evidence on how a small group (i.e., a methyl group) on the structure of a cationic monomer can have a substantial influence on its polymerization with lignin and subsequently on the efficiency of the induced macromolecule as a flocculant in a kaolin suspension system.

Keywords: Lignin, Polymerization, Flocculation, Cationization, Macromolecules structure, Surface and interface

3.2 Introduction

Recently, the development of advanced wastewater treatment systems has attracted considerable attention due to the growing environmental concerns of wastewater.^{1,2} Kaolin particles have been recognized as one of the most problematic minerals in the wastewater effluent of many industries,

for instance, papermaking and mineral processes, owing to their small sizes and anisotropic shapes.¹ Kaolin particles have various properties consisting of both positive and negative charges at the edge and on the basal face of the particles.³ When interacting with flocculants, these charges would be affected. Extensive research has been carried out to treat wastewater following different pathways, such as flocculation,⁴⁻⁶ biodegradation,^{7,8} photocatalytic degradation,⁹⁻¹¹ ozonation¹², and adsorption.¹³ Of available methods, flocculation is industrially attractive and financially feasible.¹⁴⁻¹⁶ Recently, the use of natural flocculants was recognized as a green solution for treating various effluents.¹⁴⁻¹⁶

Lignin is a three-dimensional amorphous natural macromolecule that has the largest reservoir of aromatic product in the world. The most substantial volume of lignin is produced commercially in the kraft pulping process.¹⁷⁻¹⁹ The recent surge of interest for the utilization of this biodegradable and renewable resource has led to the development of various lignin products.²⁰⁻²² Although this macromolecule is quite complicated in structure, the existence of varied functional groups, in particular, carboxylic acid and hydroxyl groups, on its structure makes it amenable for modification.²³ For lignin valorization, the chemical modification is widely used to introduce reactive functional groups on lignin structure.²⁴ Among kraft lignin (KL) modification processes, amination is one of the most promising methods,^{25,26} which was considered for altering lignin's properties in this work.

Considerable research has been exploited in understanding the physicochemical properties of polymers.²⁷⁻³² Polymer characteristics depend not only on the type of monomers comprising it but also on the structure of a polymer, such as a polymer chain length.^{33,34} Numerous studies demonstrated that the physicochemical characteristics of lignin would be altered after the

polymerization reaction. For instance, various copolymers of phenolated kraft lignin-graft-poly (2-methacryloyloxyethyl) trimethyl ammonium chloride (PKL-g-PDMC) were produced with different grafting densities and arm lengths of the PDMC chain.³⁵ In an alternative approach, the polymerization of lignin and acrylic acid (AA) changed the molecular weight and molecular weight distribution of lignin macromolecule significantly.³⁶ However, two cationic monomers of [2-(acryloyloxy)ethyl]trimethyl ammonium chloride (ATAC) and [2-(methacryloyloxy) ethyl] trimethyl ammonium methyl sulfate (METAM) have not been studied for the polymerization of lignin. Compared to ATAC, METAM has one additional methyl substituent attached to its structure. This additional group may affect the polymerization of the cationic monomer with lignin and hence influence its polymerization efficiency (Scheme 3.1).

Studies are available on correlating the properties of lignin macromolecules and their behavior in solution and suspension systems. For example, the lignin-acrylic acid macromolecule had a larger hydrodynamic diameter (H_y) compared to unmodified lignin.³⁷ It was also reported that the molecular shape of lignin macromolecules was directly related to the H_y of them in that a macromolecule with a larger H_y had a looser molecular shape.^{38,39} Moreover, the radius of gyration (R_g) and size of lignin macromolecules strongly depend on the degree of polymerization of macromolecules.⁴⁰ It was observed that, for different fractions of acetylated lignin, the imperfect correlation of R_g value and molecular weight (M_n) was attributed to its varying degrees of branching.⁴¹ The chemical alteration was also used to improve the water solubility and surface activity of lignin.⁴² In one study, the impact of grafting density and molecular weight of lignin polymerized with hydrophilic monomers, such as acrylamide and acrylic acid, on the surface tensions of water was investigated.⁴³ In another study, kraft lignin-acrylamide (KAM) synthesized via polymerization with different molar masses and charge densities showed diverse surface

tensions in aqueous solutions.⁴⁴ In that study, the authors stated that KAM macromolecule with a higher molecular weight and charge density impacted the hydrophilicity of kaolin particles more dramatically by reducing its surface tension more greatly.⁴⁴ These studies suggest that the polymerization of lignin may generate lignin macromolecules with altered physicochemical behavior in aqueous systems. In this regard, it is unclear if lignin-ATAC and lignin-METAM macromolecules would behave similarly in an aqueous system.

In a flocculation process, when the particles and polymers are subjected to the shear stresses and mixing, they will move, rotate, and collide at different rates.⁴⁵ As a result of these interactions, polymeric flocculants and suspended particles can form large flocs with a three-dimensional network structure.¹⁵ Flocs generated using a polymer with a larger molecular weight can be larger and have a looser structure.^{46,47} The porosity or compactness of flocs can also affect their settling velocity as fluid can easily pass through the networks of porous flocs.^{48,49} It is interesting to note that the configurational changes of polymers caused by altering polymeric chain, chemical composition and morphology can also affect their flocculation behavior and floc properties, such as floc strength, structure, and sizes. Previously, lignin-diallyl dimethyl ammonium chloride-acrylamide (LDA), a cationic macromolecule with a broad structure, was synthesized and used as a flocculant for humic acid removal, which resulted in the formation of flocs with an open structure and strong anti-shear affinity.⁵⁰ In another work, the polymerization of lignin with acrylamide (AM) and (2-methacryloyloxyethyl) trimethyl ammonium chloride (DMC) produced a water-soluble flocculant for a clay suspension via inducing strong and large size flocs that showed high regrowth affinity at different shear rates.⁵¹ Recently, kraft lignin was polymerized with (methacryloyloxy)ethyl] trimethylammonium chloride (METAC), and its analysis confirmed that

the lignin-METAC macromolecule was a promising flocculant for treating kaolin suspensions.⁵² This work also covers the fundamental chemistry of lignin-METAC polymerization reactions.⁵²

However, there is no information available for relating the structure and performance of cationic monomers in polymerizing with lignin for novel flocculant productions. In the present study, particular emphasis was dedicated to investigating how this extra methyl group on METAM (compared to ATAC) would impact the polymerization efficiency of the monomer with lignin and ultimately the properties of the resulting lignin macromolecules. To have a better understanding of the flocculation process, the features of flocs should be analyzed fundamentally. Here, we aim to explore the properties of flocs formed in the flocculation of the kaolin suspension by the novel cationic kraft lignin (CKL) macromolecules. The primary novelties of the present work are 1) the introduction of a new cationic lignin-based flocculant, 2) the study on the impact of the methyl substituent of a cationic monomer on its polymerization with lignin and 3) the investigation on the impact of methyl substituent of CKL on the flocculation performance of CKL in a kaolin suspension. The mechanism of the flocculation process for the newly developed lignin-based macromolecules is also covered in the present study.

3.3 Materials and Methods

3.3.1 Materials

Kraft lignin (KL) was received from a Canadian mill located in Alberta, Canada. [2-(acryloyloxy) ethyl]trimethyl-ammonium chloride solution (ATAC), 80 wt.% in H₂O, poly diallyl dimethyl-ammonium chloride (PDADMAC, 100,000–200,000 g/mol), 20 wt.% in water, sodium persulfate (Na₂S₂O₈) (analytical grades), sulfuric acid and sodium hydroxide, diiodomethane, potassium

nitrate, potassium hydroxide (8 M), hydrochloric acid (37%, reagent grade), para-hydroxybenzoic acid and kaolin clay (325 mesh) were purchased from Sigma-Aldrich Company. Acetic acid was provided from Fisher Scientific company. Wako Pure Chemical company, Japan, provided potassium polyvinyl sulfate (PVSU, 100 000-200 000 g/mol, 97.7 wt.% esterified). Dialysis membrane (Cut off of 1000 g/mol) was received from Spectrum Labs. Ethanol (95 vol.%) was obtained from Fisher Scientific company. [2-(methacryloyloxy) ethyl] trimethyl ammonium methyl sulfate (METAM) was purchased from BOC science Company, USA. Deionized water (resistivity $\geq 18 \text{ M}\Omega \text{ cm}$) was used for all the experiments conducted in this study obtained from a Millipore water purification system.

3.3.2 Lignin Polymerization

In this study, lignin was polymerized with the cationic monomers in a semi-dry manner.⁵³ The amount of water was 40 wt.% (i.e., 60 wt.% solid content). A 2 g sample of KL was mixed with cationic monomers (2/1 wt./wt. cationic agent/lignin), and the desired amount of water was added to the system to make a 40 wt.% concentration in all reactions. The pH of the system was adjusted to 3. Afterward, a predetermined amount of potassium persulfate (0.03 g) was added to the system as an initiator, and the solution was deoxygenated by purging with nitrogen gas for 10 minutes. Then, the system was placed in a water bath, and the polymerization reaction was conducted at 80 °C for three hours. After completion, the system was immersed in cold water for 15 min. Ethanol (80 vol % in water) was added to the system, which precipitated cationic lignin from the reaction solution.⁵² Our previous findings confirmed that KL was not soluble in ethanol, however, the cationic homopolymers and unreacted cationic monomers were soluble in the reaction mixtures after ethanol addition.⁵² After collecting CKLs from the reaction mixtures, ethanol was added to

the CKL samples and the systems were mixed well to dissolve the remaining cationic homopolymer and unreacted cationic monomer from the collected CKLs in ethanol. After mixing, the systems were centrifuged at 3500 rpm for 10 min to precipitated treated CKLs. After that, the solution was neutralized using 0.1 M NaOH solution (pH=7) and further purification of the CKL macromolecules were conducted using membrane dialysis tubes for 48 h to remove any unreacted cationic monomers and salts from CKLs. This arrangement was conducted to ensure the best possible purification of CKLs. Then, the dialyzed cationic lignin was freeze-dried.

3.3.3 Characterization of Macromolecules and Kaolin

The charge density, molecular weight, nitrogen content, and the phenolic hydroxyl group content of KL and CKL were determined.⁵³ The radius of gyration (R_g) and hydrodynamic diameter (H_v) of macromolecules were also assessed with static and dynamic light scattering, respectively, and the details of these analyses are available in the Supplementary Materials of this work. Kaolin particles were characterized in terms of their potential in solutions, as also explained in the Supplementary materials file.

3.3.4 Surface Tension and Contact Angle Measurements

The surface tension and contact angle of samples (1 wt.% aqueous solution) were analyzed using a tensiometer instrument. The surface tension of the kaolin sample was also determined using the tensiometer's OneAttension software with the generated data of contact angle analysis. The dispersive component, σ_S^D , of the surface tension of kaolin was determined using equation 1:

$$\sigma_S^D = \frac{\sigma_L (\cos \theta_a + 1)^2}{4} \quad (1)$$

in which σ_L is the surface tension of liquid and θ_d is the contact angle between liquid and coated surface. In this equation, the data of diiodomethane (50.8 mN/m) was used for determining σ_S^D . In addition, the polar component of the surface tension of diiodomethane was determined following the Fowkes' model (equation 2):^{54,55}

$$\frac{\sigma_L (\cos \theta_w + 1)}{2} = \sqrt{\sigma_L^D \sigma_S^D + \sigma_L^P \sigma_S^P} \quad (2)$$

where σ_L is the overall surface tension of the liquid (in this case, water), θ_w , is the contact angle between water and coated surface, σ_L^D (26.4 mN/m) and σ_L^P (46.4 mN/m) are dispersive and polar components of water, and σ_S^P represent polar components of the surface energy of the solid surface.⁵⁶ By considering σ_S^D and σ_S^P , the total surface energy of solid surface, σ_S , was determined. The interfacial tension between kaolin and droplets of CKL containing solutions was then determined following the Young equation (3):

$$\sigma_L \cos \theta_p = \sigma_S + \sigma_{SL} \quad (3)$$

wherein σ_L and σ_S are the overall surface tension of liquid (CKL) and solid (kaolin) respectively, σ_{SL} is the interface tension between solid and liquid (polymer solution) and θ_p is the contact angle between the polymer solution and the kaolin surface.

3.3.5 Flocculation

The flocculation analysis was performed using a photometric dispersion analyzer (PDA 3000, Rank Brothers Ltd), which was attached to a dynamic drainage jar (DDJ). The flocculation behaviour of the suspension and floc properties were also analyzed under different conditions by monitoring the chord length distribution of particles in the suspension in real-time using a focused

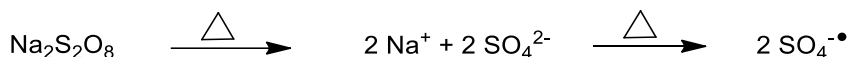
beam reflectance measurement, FBRM, Mettler Toledo, E25 as explained in the Supplementary Materials.

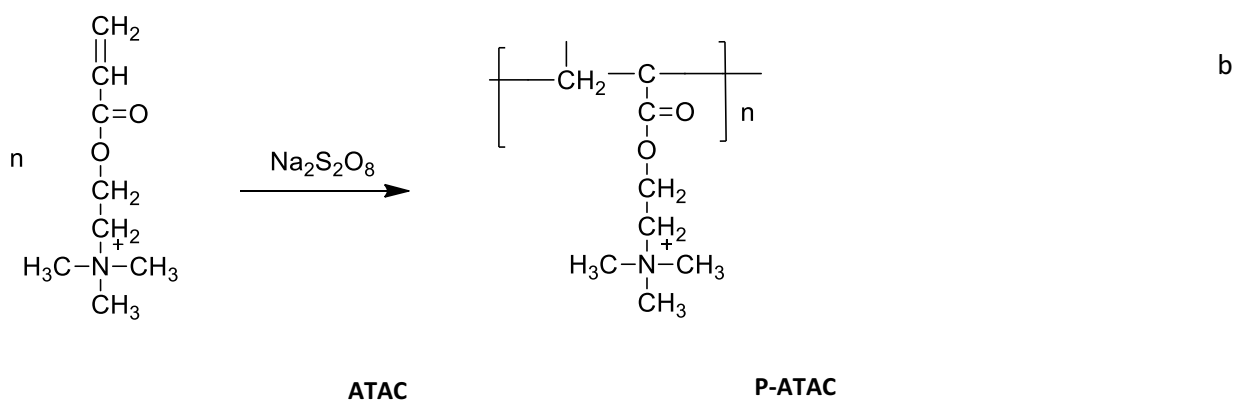
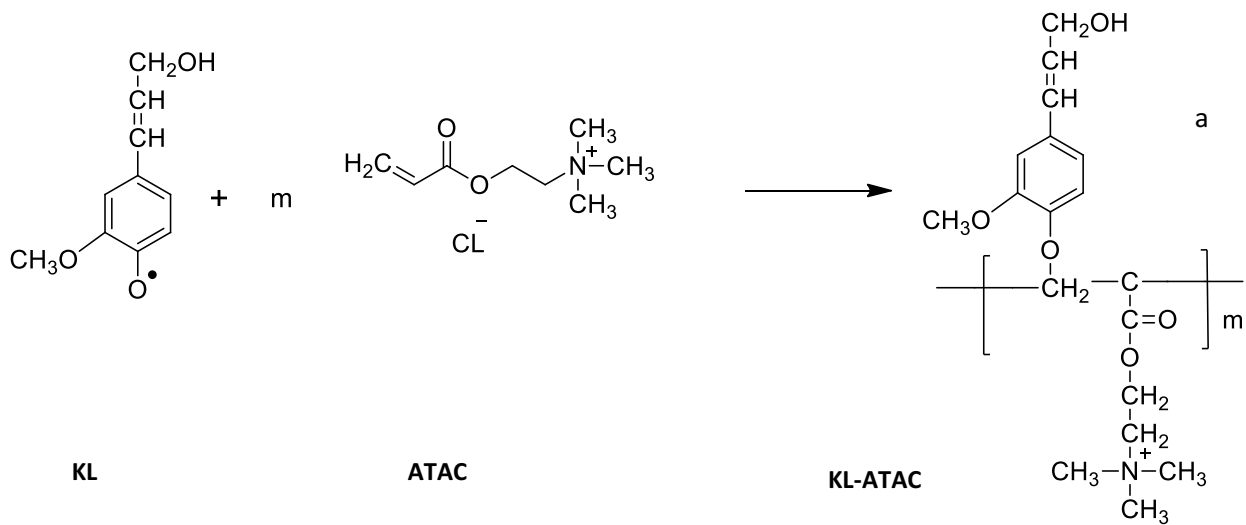
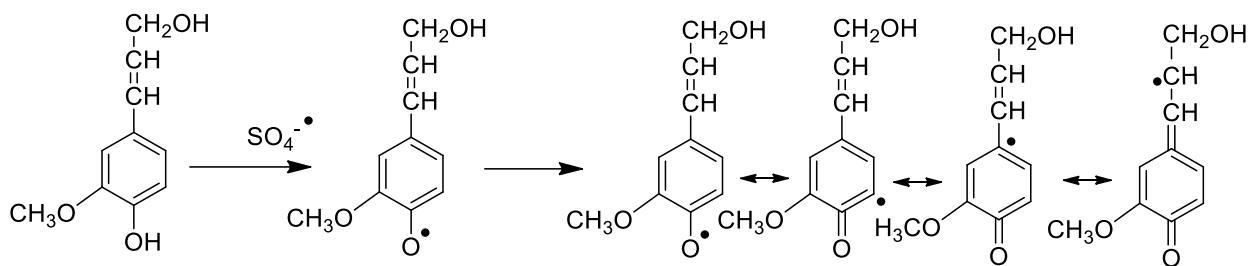
3.4 Results and Discussions

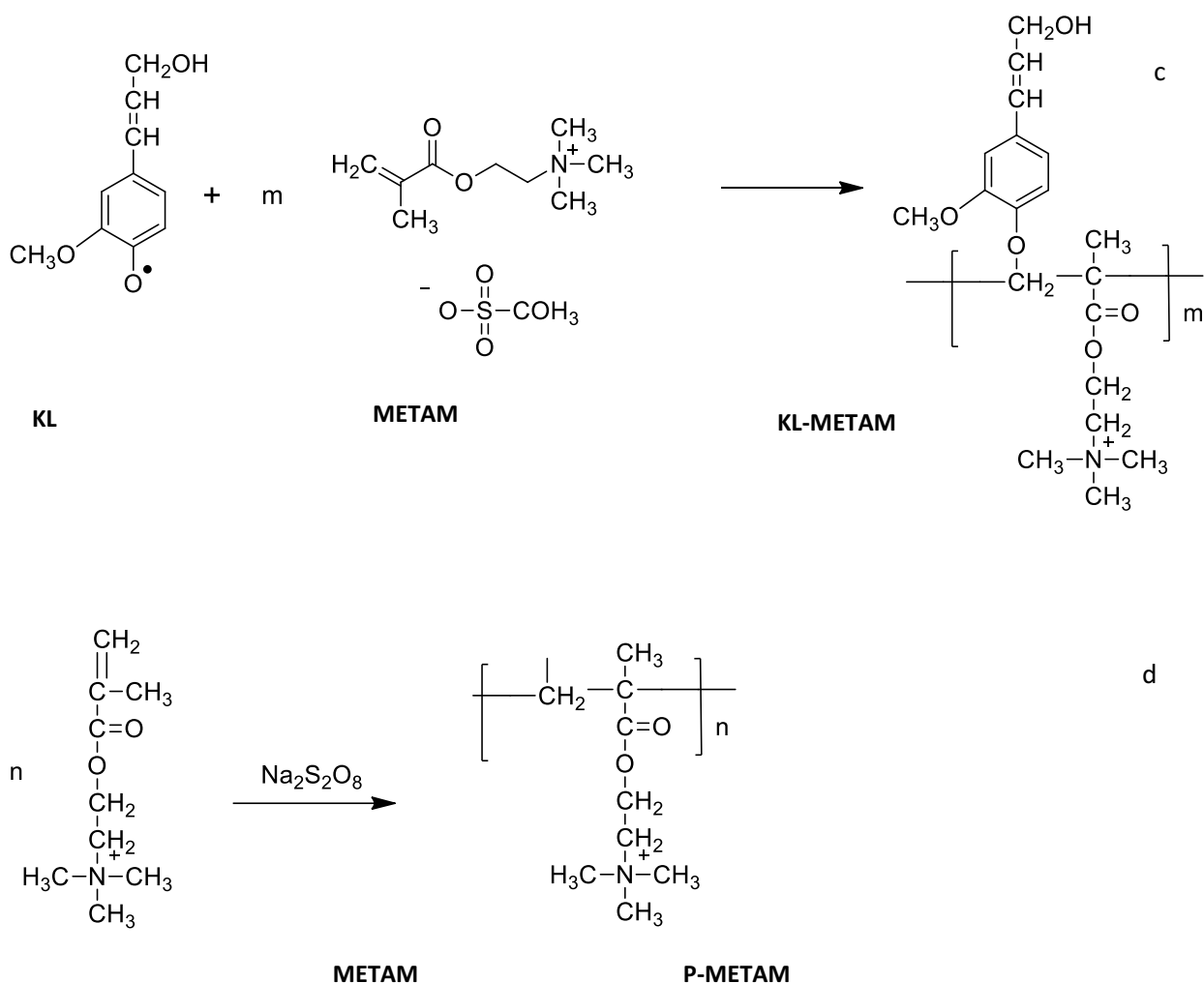
3.4.1 Synthesis and Characterization of KL-METAM and KL-ATAC

Polymerization was performed under the conditions of cationic agents/lignin ratio of 1.6 mol/mol, 3 h reaction time, 80 °C reaction temperature, pH 3 and 60 wt.% KL concentration in water. These conditions were reported to be optimum for the polymerization of kraft lignin with METAC, which has a similar chemical structure to METAM.⁵² The details of the polymerization mechanism are available in Scheme 3.1. As can be seen, these cationic macromolecules have only one quaternary ammonium group in their repeating unit, but different chain lengths and structures.

Table 3.1 lists the properties of cationic lignin macromolecules. The charge densities of KL-ATAC and KL-METAM were 2.3 and 2.5 mmol/g, while their grafting ratios were 43 and 45 mol%, respectively. The alkenyl group of METAM monomer is more stable when forming radicals due to the existence of neighboring atoms that can donate an electron. Thus, the polymerization efficiency of METAM was higher, which yielded a higher grafting ratio and slightly higher charge density for KL-METAM than for KL-ATAC. Our previous results confirmed a 20-30% homopolymerization yield during the cationic polymerization of unmodified kraft lignin (KL) with METAC under similar reaction conditions.⁵² However, we did not record the yield of homopolymerization reaction (P-METAM and P-ATAC, Scheme 3.1) in this work.







Scheme 3. 1 Reaction scheme of lignin and METAM/ATAC to produce a) KL-ATAC b) P-ATAC c) KL-METAM and d) P-METAM

KL was highly soluble in water at pH 7. In the past, acid washed lignin was reported to be insoluble in water,⁵² but as our lignin source was unwashed and deprotonated (i.e., in sodium form), and it had 90% solubility in water at a 10 g/L concentration. The solubility of lignin did not change after polymerization implying that CKLs had similar solubilities in water. Results also demonstrated that the nitrogen contents of KL-METAM originating from cationic agents attached to the polymers was slightly higher than that of KL-ATAC. The phenolic hydroxy group content of lignin was decreased from 1.63 mmol/g for KL to 0.55 and 0.77 mmol/g for KL-METAM and KL-ATAC, respectively. KL-METAM had a higher molecular weight (824×10^3 g/mol) compared to

KL-ATAC (657×10^3 g/mol) implying that the extra methyl group notably contributed to the molecular weight enhancement of the cationic macromolecule. It is worth mentioning that the higher molecular weight of KL compare to what was reported in other studies,^{36,42,52} may originated from its high content of impurities, which are generated during the extraction process. To have insights into the effect of $-\text{CH}_3$ on the molecular weight of CKL macromolecules, the number of PMETAM or PATAC-side chains of KL-METAM and KL-ATAC were determined theoretically.⁵² Considering the grafting ratio and the molecular weight of C_9 unit of lignin as well as that of METAM and ATAC, the molecular weight of lignin that had only one group of METAM or ATAC attached to it was determined to be 258 and 247 g/mol, respectively. Based on the M_n of KL-METAM and KL-ATAC macromolecule, M_n of KL (Table 3.1) and M_n of KL-METAM and KL-ATAC subunits, the number of repeating monomer units of METAM and ATAC in KL-METAM and KL-ATAC was determined to be 747 and 644, respectively. These results confirmed that the existence of one extra $-\text{CH}_3$ on the METAM improved its chain growth on lignin.

Table 3. 1 Characteristics of KL, KL-ATAC, and KL-METAM

Sample	KL	KL-ATAC	KL-METAM
Charge density, mmol/g	-1.7 ± 0.11	$+2.3 \pm 0.13$	$+2.5 \pm 0.1$
Solubility, wt. %	90 ± 0.5	90 ± 0.5	93 ± 0.73
Nitrogen, wt. %	0	4.7 ± 0.1	4.8 ± 0.1
Phenolic hydroxyl group, mmol/g	1.63 ± 0.1	0.77 ± 0.05	0.55 ± 0.08
Grafting ratio, mol %	0	42.6 ± 0.06	45.5 ± 0.07
M_w , g/mol	$49 \pm 6.4 \times 10^3$	$657 \pm 84.2 \times 10^3$	$824 \pm 107.5 \times 10^3$
M_n , g/mol	$28 \pm 6.02 \times 10^3$	$187 \pm 43.8 \times 10^3$	$221 \pm 51.6 \times 10^3$
M_w/M_n	1.7 ± 0.15	3.5 ± 0.024	3.7 ± 0.091

Moreover, a larger polydispersity index (PDI) of cationic lignin macromolecules than KL is probably related to the inconsistent size, shape, and mass distribution of lignin macromolecules after the polymerization reaction. In this case, KL-METAM macromolecule with a larger PDI showed a wider molecular weight distribution. Thus, due to steric hindrance of methyl group, the final configuration of KL-METAM macromolecule might be looser and bulkier in aqueous solution.

Theoretically, the nitrogen content of the macromolecules can help determine the charge density of CKL. In this case, the theoretical charge densities of KL-METAM and KL-ATAC were 1.9 and 1.8 mmol/g. In the same vein, the number of repeating monomers in CKL can facilitate the determination of the charge density of CKL. This approach resulted in the theoretical charge densities of 3.4 and 3.3 mmol/g for KL-METAM and KL-ATAC, respectively. These results confirm that there is a discrepancy between the experimental and theoretical charge density determination. The difference should be associated with experimental errors involved in each pathway to determine the characteristics of CKLs. For example, the molecular weight analysis by GPC depends on the fractionation of the polymers based on their sizes, while experimental charge density analysis relies on the interaction of two oppositely charged polymers in the titration analysis. Interestingly, all methods confirm that the charge densities of CKL were similar.

3.4.2 Configurational Changes of Lignin Macromolecules in Aqueous Solutions

The most commonly used parameters to describe the molecular size and configuration of polymers are hydrodynamic radius and radius of gyration. According to Table 3.2, the hydrodynamic diameter (H_y) of CKL macromolecules increased from 14.3 nm for KL to 30.2 and 37.6 nm for KL-ATAC and KL-METAM, respectively. The grafted METAM and ATAC monomers onto the

lignin structure altered the compact shape of the lignin molecule due to the detachment of its ionizable ammonium group and increased lignin's molecular weight.⁵⁷ It was reported that H_y of kraft lignin was proportional to its molecular size.^{38,39}

The radius of gyration (R_g) of a polymer is a geometrical quantity defined as an average square distance of the chain segments from the center of the mass of the chain of a polymer segment.⁵⁸⁻⁶⁰ As the radius of gyration of polymers is very sensitive to their geometry and molecular structure,⁶¹ this property can also be used as an indicator for polymer configuration in solutions. For polymers, R_g and chain length are proportionally related.^{62,63} A larger R_g of KL-METAM macromolecule (78.5 nm) than KL-ATAC macromolecule (R_g of 57 nm) was observed (Table 3.2), which may show its more three-dimensional structure. On the other hand, the looser and bulkier configuration of KL-METAM created larger hydrodynamic radius and three-dimensional structure in aqueous solutions. A strong dependency of R_g on the molecular weight of synthetic polymers was observed in the literature ($R_g \propto M_w$).⁶⁴⁻⁶⁸ One possible reason for the larger R_g and H_y for KL-METAM is the higher molecular weight of KL-METAM, and another reason is the steric hindrance that the extra CH_3 made on the KL-METAM, which would stretch the KL-METAM macromolecule more than KL-ATAC.

By analyzing R_g and H_y , the change in the structure macromolecules can be determined via shape factor (R_g/H_y) analysis.^{69,70} This ratio provides information about the spatial density distribution of colloid and the degree of draining of a scattering object in solutions.^{71,72} In our case study, the ratio of R_g/H_y is related to the shape of CKL in solutions where the lignin molecules undergo a morphological evolution with introducing different cationic monomers. It is known that the shape factor value of ~ 0.774 corresponds to a uniform hard (non-draining) sphere (where the R_g is smaller

than H_y), the value of 1.0-1.3 relates to a hyperbranched polymer cluster or a soft sphere (depending on the branching degree), the value of 1.5-1.8 is for a flexible random coil chain (depending on the chain polydispersity), and R_g/H_y value of >2 indicates a rigid rod structure.⁷³⁻⁷⁷ In Table 3.2, the R_g/H_y value for KL (2.96) implied a rigid rod shape structure. Interestingly, this value dropped to 1.88 and 2.08 for KL-ATAC and KL-METAM, respectively, postulating that the conformation of lignin changed from rod-like to flexible random coil chain after polymerization reaction. Also, KL-METAM macromolecule had a less coiled structure than did KL-ATAC, which might be due to 1) more extended polymerization of METAM than ATAC with lignin and 2) the steric hindrance that the extra methyl substituent on METAM imparted to lignin-METAM.

Table 3. 2 Characteristics of KL, KL-ATAC, and KL-METAM

Sample	KL	KL-ATAC	KL-METAM
H_y , nm	14.28±1.9	30.22±1.8	37.63±2.7
R_g , nm	42.3±7.1	57±2.6	78.5±3.9
Shape factor	2.96±0.1	1.88±0.026	2.08±0.046

3.4.3 Behavior of Lignin Polymers in Solution Systems

Surface Properties

The results for contact angle and surface tension of droplets containing CKLs were tabulated in Table 3.3. A water droplet on the glass slide created the contact angle of 21° , which is similar to what was reported previously.⁴⁴ However, the contact angles of droplets of solutions containing CKL (10 g/L) on the glass slides were 14.3° and 17.2° for KL-METAM and KL-ATAC, respectively, depicting that CKL improved the interaction of water and the glass surface. The higher hydrophilicity of droplets containing CKLs originated from the -COO, -OH and quaternary

ammonium groups attached to CKLs. Results also imparted that the contact angle of solutions was altered on different substrates. As seen, the droplets containing water and CKLs made the surface of kaolin coated slides more hydrophilic than glass slides through developing attraction force between water/CKL molecules and kaolin. The surface tension of KL was measured to be 72.0 ± 0.01 mN/m. It is also seen that the surface tension of the CKL solution was very close to that of water (72.8 mN/m).⁷⁸ In another study, the contact angles of water on thin films coated with Kraft lignin samples were different, but the surface tensions of a solution containing lignin samples made similar results.⁷⁹ Contact angle measurement can also be used to investigate the interfacial tension between the liquid and solid surfaces. As illustrated in Table 3.3, the interfacial tension between kaolin and water was 4.95 mN/m. CKL samples did not reduce the interface tension between kaolin and water significantly, indicating that the wettability of solutions containing CKL to kaolin surface was very close to that of water. CKL did not affect the interface tension of kaolin and water, similar to negligible alteration they made on the surface tension of water. Results showed that the configurational changes of CKLs marginally impacted the surface properties.

Table 3. 3 The contact angle of droplets on different surfaces and surface and interface tensions of solutions and kaolin particles

Solution	Contact angle, ° (CKL on a glass slide)	Surface tension, mN/m	Contact angle, ° (CKL on kaolin coated slide)	Interfacial tension, mN/m
Water	21.02 ± 0.03	72.8 ± 0.01	17.14 ± 0.52	4.95 ± 0.5
KL-METAM	14.26 ± 0.11	71.25 ± 0.03	11.33 ± 0.23	4.63 ± 0.2
KL-ATAC	17.16 ± 0.09	71.61 ± 0.01	13.42 ± 0.52	4.78 ± 0.5

3.4.4 Adsorption

The adsorption kinetics of KL and CKLs on kaolin particles are presented in Figure A1. The adsorption of KL on the surface of kaolin particles was limited to 0.47 mg/g. The adsorption of KL on kaolin particles could be attributed to hydrophobic interaction, van de Waals and hydrogen bonding development. As the adsorption of KL was limited (Figure A1), these factors did not facilitate the adsorption of KL on kaolin particles. However, the maximum adsorption of KL-ATAC and KL-METAM on kaolin particles was 54 and 46.4 mg/g, respectively (at 128 mg/g dosage of polymer/kaolin). Also, no saturation level of CKLs adsorption was observed on the surface of kaolin particles within the scope of the adsorption study (Figure A1). In this case, CKLs might have developed charge interaction, hydrogen bonding, van de Waals attraction and hydrophobic interaction with multilayer adsorption on kaolin particles. This phenomenon was observed elsewhere as well.⁸⁰ It should be emphasized that, if the dosage of CKLs was continuously increased, the adsorption kinetic might reach to an equilibrium level. This trend was observed in the adsorption of cationic polyacrylamide on the surface of precipitated calcium carbonate.⁸¹ Since the main focus of this study was to compare the structural differences of CKLs and its effect on the polymerization and flocculation behaviour, we didn't investigate the saturation level of CKLs adsorption on kaolin particles.

Table 4 lists the surface area of kaolin particle before and after adsorbing CKL. Results exhibited that kaolin had a large specific surface area (SSA) of 52.55 m²/g with the pore volume of 0.14 cm³/g. Upon adsorption of CKLs on kaolin, the pore volume and SSA decreased, which confirmed the diffusion of CKLs into the pores of kaolin particles. The total surface area of kaolin particles decreased more dramatically for KL-ATAC/kaolin (40.15 m²/g) than for KL-METAM/kaolin (45.37 m²/g).

The pore volume of kaolin dropped from 0.14 cm³/g to 0.06 and 0.07 cm³/g when the distinct amount of KL-ATAC and KL-METAM adsorbed on the surface of kaolin, respectively. As KL-ATAC has a more coiled structure and smaller size than KL-METAM (Table 3.2), a higher adsorption and diffusion of KL-ATAC into the pores of kaolin particles was observed, which reduced the pore size of clay particles more greatly. The diffusion of polymers into pores of kaolin particles is inversely related to the size of polymers.^{38,39} The average pore size of the particles was also estimated from the total pore volume, and results depicted that the KL-METAM macromolecule probably covered the pores of kaolin surface to a greater extent. As a result, the average pore size of kaolin particles in Kaolin/KL-METAM (29.53 nm) system was smaller than that in the Kaolin/KL-ATAC (31.02 nm) system. It can also be stated that the depletion in the accessible surface sites on kaolin particles for KL-METAM can be another factor for its lower adsorption.⁸²

Table 3. 4 Characteristics of kaolin and modified kaolin with CKL

Label	Surface area, m ² /g	Total pore volume, cm ³ /g	Average pore size, nm
Kaolin	52.55±1.7	0.14±0.08	53.12±1.2
Kaolin/KL-ATAC	40.15±1.3	0.06±0.017	31.02±1.6
Kaolin/KL-METAM	45.37±1.1	0.07±0.023	29.53±1.8

Considering the average pore size of kaolin particles (53.12±1.2), centrifugation can also be considered as an alternative approach for isolation of clay particles from model waste suspension. Centrifugation process is one of the most rapid and reliable methods for clay removal, but its high cost and energy demandingness, hamper its implementation at large-scale. Furthermore, kaolin is not the only component in industrial effluents. The other impurities present in industrial wastewater can be in the form of soluble effluent such as dissolved/colloidal organic matter and

heavy metals. Therefore, flocculation process is assumed to be more efficient than centrifugation technique in industrial application, which allows treating large volumes of wastewater without consuming much energy.

To understand the fundamentals of the adsorption of CKL on kaolin particles, the surface area occupied by each molecule of CKL was calculated. To determine the surface occupancy of each molecule on a particle, the surface excess density (Γ) of the molecule should be assessed. The surface excess density can directly be calculated from the slope of surface tension (σ_L) of the polymer as a function of its concentration (C) (the results are available in Figure A2 in Supplementary Materials) according to Gibbs adsorption isotherm (equation 4):

$$\Gamma = -(RT)^{-1} \times \left(\frac{d\sigma_{CKL}}{d \ln C} \right) \quad (4)$$

where R is the universal gas constant (J/molK), and T is the absolute temperature (K).

According to Figure A2, the surface tension decreased linearly with increasing the natural logarithm of polymer concentration. The maximum surface (excess) concentration of polymers at the air/water interface determined to be 1.39×10^{-6} and 1.70×10^{-6} mol/m² for KL-METAM and KL-ATAC solutions, respectively. It was reported that the surface activity of a polymer is related to the surface excess density (Γ).⁸³ Therefore, the smaller Γ value of KL-METAM resulted in a decrease in the surface activity of this polymer. Considering the surface excess density value, the surface area occupied by each molecule on kaolin particles can be estimated following equation 5:

$$a = \frac{10^{20}}{\Gamma N} \quad (5)$$

where a is surface area per molecule (Å²), and N is the Avogadro constant.^{84,85}

KL-METAM polymer occupied a larger area compared to KL-ATAC (97.3 \AA^2) when adsorbing on kaolin particle (118.93 \AA^2). The higher surface occupancy of KL-METAM was due to its larger H_y (Table 3.2), which developed larger tail and loop configurations upon adsorbing on kaolin particles. Moreover, KL-METAM macromolecule with a larger R_g value (Table 3.2) can form a more three-dimensional structure than KL-ATAC on the surface of the particle.

3.4.5 Behavior of Lignin Macromolecules in Flocculation

Zeta Potential

The impact of CKL on the zeta potential of kaolin suspension as a function of adsorbed macromolecules are presented in Figure A3. The zeta potential of kaolin suspension changed from negative to positive as adsorbed amounts of CKL on kaolin particles increased. This increment in the zeta potential of the suspension was very close for both lignin macromolecules.⁸⁶ The zeta potential of the suspension reached to the isoelectric point at a slightly lower dosage of KL-METAM than that of KL-ATAC. In this case, the slightly higher charge density of KL-METAM affected the overall zeta potential of kaolin suspension a bit stronger. These results confirm how the methyl group of KL-METAM could impact the overall charge density of the lignin macromolecules that would impact the zeta potential of the kaolin suspension.

Flocculation

The relative turbidity of kaolin suspension as a function of adsorbed CKLs was investigated, and the results are available in Figure A4. As the adsorption of the CKL increased, the relative turbidity of kaolin decreased to the minimum level. The slight increase in the relative turbidity at a higher polymer dosage is attributed to the electrostatic repulsion between the generated flocs. The relative turbidity of kaolin suspension decreased significantly from 1 to 0.18 and 0.31 when 16 mg/g of

KL-METAM and KL-ATAC adsorbed on the kaolin particles, respectively (Figure A4 in Supplementary Materials). As the adsorption level and charge density of these macromolecules were similar, the better performance of KL-METAM is attributed to its higher molecular weight (Table 3.1) and H_y (Table 3.2), which facilitated more effective bridging. It is worth mentioning that, since the lowest level of relative turbidity obtained when 16 mg/g of CKLs adsorbed on the kaolin particles, this dosage was selected as the optimum dosage for further analysis in this work (e.g., further evidence is available in Figure A5 in Supplementary Materials).

To study the mechanism involved in flocculating of kaolin particles by CKLs, the relative turbidity of kaolin suspension was plotted against its zeta potential in Figure 3.1. The gradual decrease in the relative turbidity of kaolin suspension when the zeta potential of kaolin was negative indicated that CKLs facilitated the removal of particles via bridging and patching. Therefore, charge neutralization was not the main mechanism for the flocculation process, as the zeta potential and flocculation of the systems were not changed in a similar fashion at different dosages of CKLs. The more reduction in the relative turbidity of the kaolin suspension via KL-METAM macromolecule confirmed the higher efficiency of this macromolecule in the flocculating the particles.

The greater flocculation efficiency of KL-METAM than KL-ATAC might be due to the larger molecular weight and three-dimensional structure (i.e., more efficient bridging affinity) of this macromolecule. By adsorbing KL-METAM on the kaolin surface, the hydrophilicity of kaolin particles was enhanced (contact angle results in Table 3.3). Also, the more three-dimensional (i.e., stretched) structure of KL-METAM than KL-ATAC may provide more influential bridging affinity for kaolin particles. In a similar work, a polyacrylamide grafted carboxymethyl guar gum (CMG-g-PAM) with a higher R_g was a more efficient flocculant for a kaolin system.⁸⁷

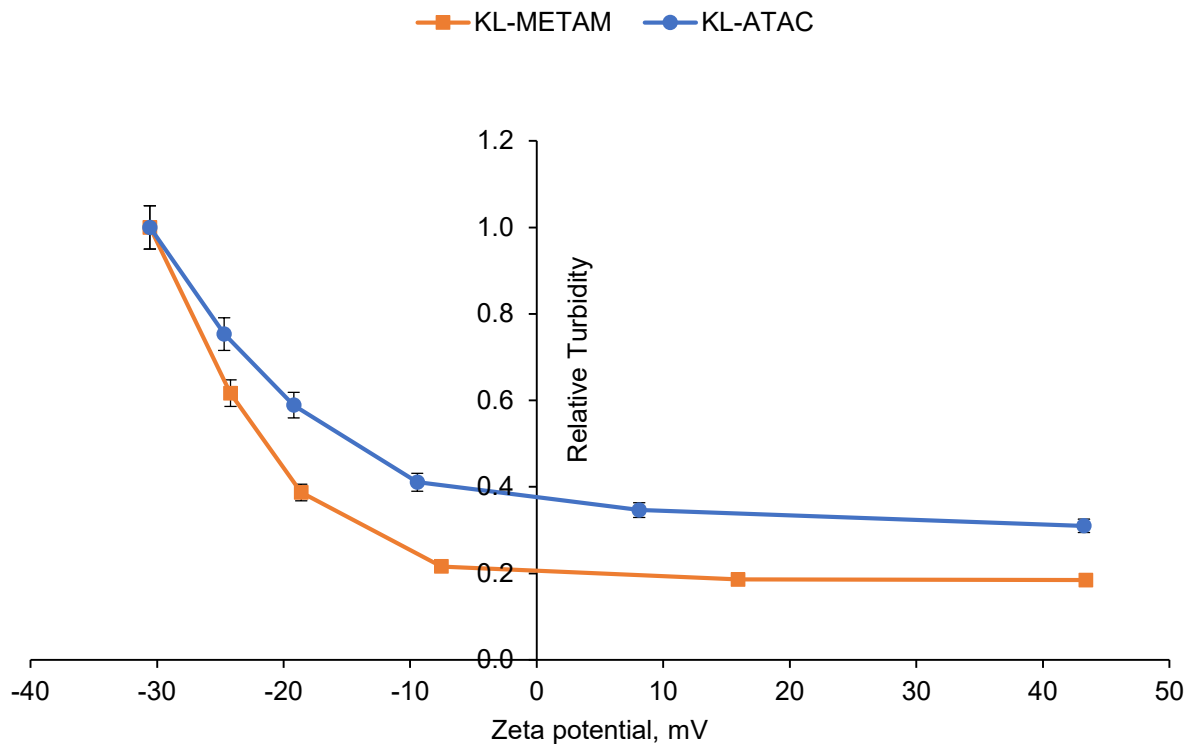


Figure 3. 1 The relationship between relative turbidity and zeta potential of kaolin suspension (25 g/L kaolin suspension at pH 6)

Kinetic of Flocculation

To have a fundamental understanding of the kinetics of the flocculation process, the adsorption of CKLs on particles during flocculation was investigated. Adsorption of CKLs on kaolin particles and their flocculation is an orthokinetic (shear-induced) interaction of unequal spheres. In this system, large flocs are formed by maximizing the polymer-particle interaction and particle-particle collision (caused by external shear stirring) via polymer adsorption and flocculation process, and by minimizing the floc breakage.^{71,72,88,89} According to Smoluchowski's theory, the flocculation rate constant (k_{sm}) can be calculated via following equation 6:

$$K_{sm} = \frac{4}{3}G(a_1 + a_2)^3 \quad (6)$$

where G is the velocity gradient of the flow in a 3 mm tube of PDA instrument (84 1/s), a_1 and a_2 are the radius of kaolin particles (2.1 μm) and the H_y of lignin macromolecules (Table 3.2), respectively.^{90,91} Knowing the K_{sm} value, the required time, τ_{ads} for adsorption of CKL on kaolin particles can be estimated following equation 7:

$$\tau_{ads} = \frac{1}{\alpha_{ads}K_{sm}n_c n_0} \quad (7)$$

where α_{ads} is the adsorption efficiency of CKL on kaolin particles (assumed to be 1), n_c is the number of kaolin particles per unit volume, and n_0 defines as the initial amount of polymer in the suspension relative to the maximum amount of polymer that can adsorb on the surface of kaolin particles. The value of dimensionless, n_0 , was obtained from the experimental results of adsorption (Γ_{max}) following equation 8:

$$n_0 = \frac{C_{polymer}}{A n_c \Gamma_{max}} \quad (8)$$

where $C_{polymer}$ is the concentration of CKLs (mg/g), A is the surface area of kaolin particles and Γ_{max} is the maximum adsorption of CKL on kaolin particles.^{45,88}

Based on equation 8, at a lower polymer concentration where CKLs had the same adsorption performance, the required time for their adsorption was almost identical (Table A5 in Supplementary Materials). At 16 mg/g of CKLs adsorption in which the optimum flocculation efficiency achieved (Figure A4), τ_{ads} was 36.6 and 37s for KL-METAM and KL-ATAC, respectively. However, at higher polymer dosages, longer time needed for adsorption of lignin macromolecules. Adopting the results of Figure A1, the longest time for macromolecule

adsorption in the scope of this study were 106.4 and 125.1 s for KL-METAM and KL-ATAC at 128 mg/g dosage, respectively.

The longer τ_{ads} of KL-ATAC on kaolin particles might be due to the slower diffusion of KL-ATAC into the kaolin's pores. It is worth noting that the time of adsorption for both macromolecules in a well-mixed system is the same. However, the adsorption time of CKL in flocculation process depends on the bridging efficiency and diffusion of CKLs into the pores of kaolin particles. As stated earlier, CKL formed flocs via the bridging mechanism and KL-METAM with the higher flocculation efficiency formed larger flocs with more tail and loop configurations on the surface of particles. The surface morphology of kaolin and kaolin/CKL particles are shown in Figure 3.2. The SEM images showed that the kaolin particles (blank sample) possessed a larger size when KL-METAM was used.

In the present work, KL-METAM having lower τ_{ads} and higher flocculation efficiency was more effective in bridging the kaolin particles. The variation in τ_{ads} of two flocculants (especially at higher dosages) reflected the differences of their physicochemical behavior in aqueous solutions originating from the altered configurations of the CKLs.

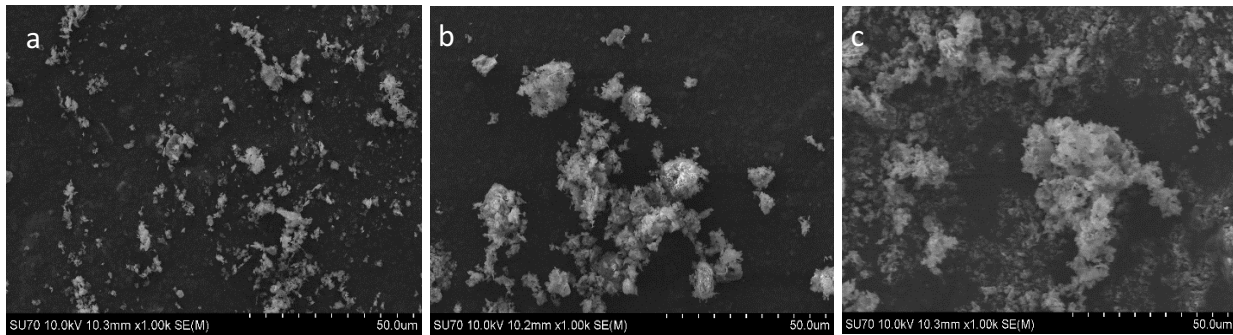
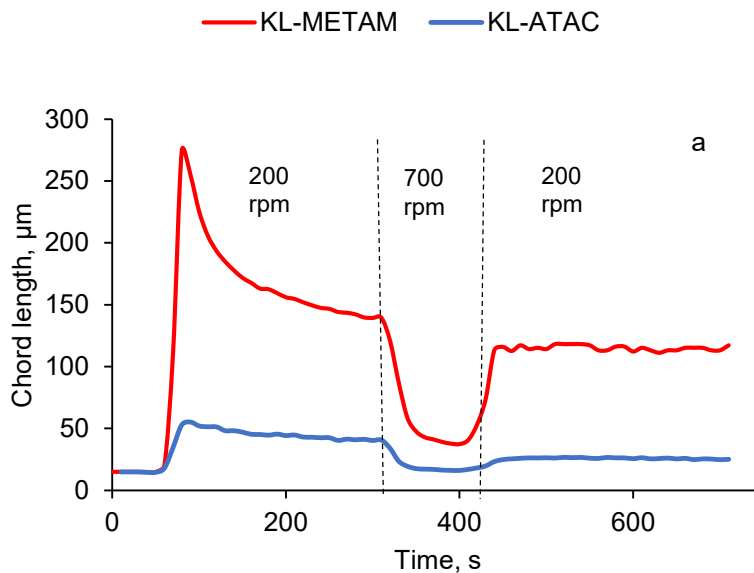


Figure 3. 2 SEM images of (a) kaolin (b) kaolin/KL-ATAC (c) kaolin-KL-METAM generated at a 16 mg/g polymer dosage

Floc Formation

The flocculation of kaolin particles with the cationic macromolecules was also studied by FBRM. As the maximum reduction in the relative turbidity of KL-METAM and KL-ATAC was obtained at 16 mg/g, this dosage was selected for the FBRM analysis. Figure 3.3 presents the number of the formed flocs (in counts) and chord length distribution of the formed flocs as a function of time for CKL/kaolin system. After 50 s of stabilizing the system (at 200 rpm), the CKLs were added that induced larger flocs but reduced the number of particles in the system. KL-METAM with the higher molecular weight (Table 3.1) and greater bridging affinity (Figure 3.2) created larger flocs at 16 mg/g, leading to the lowest number of particles in the suspensions (Figures 3a and 3b).



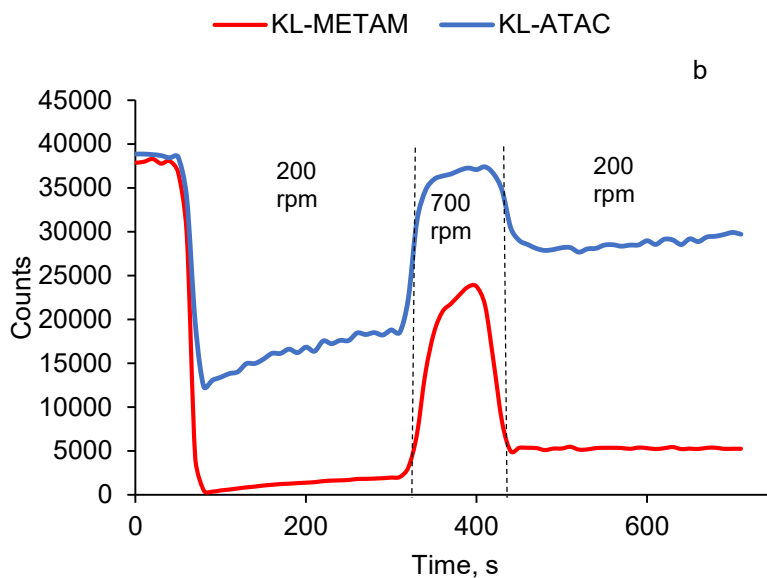
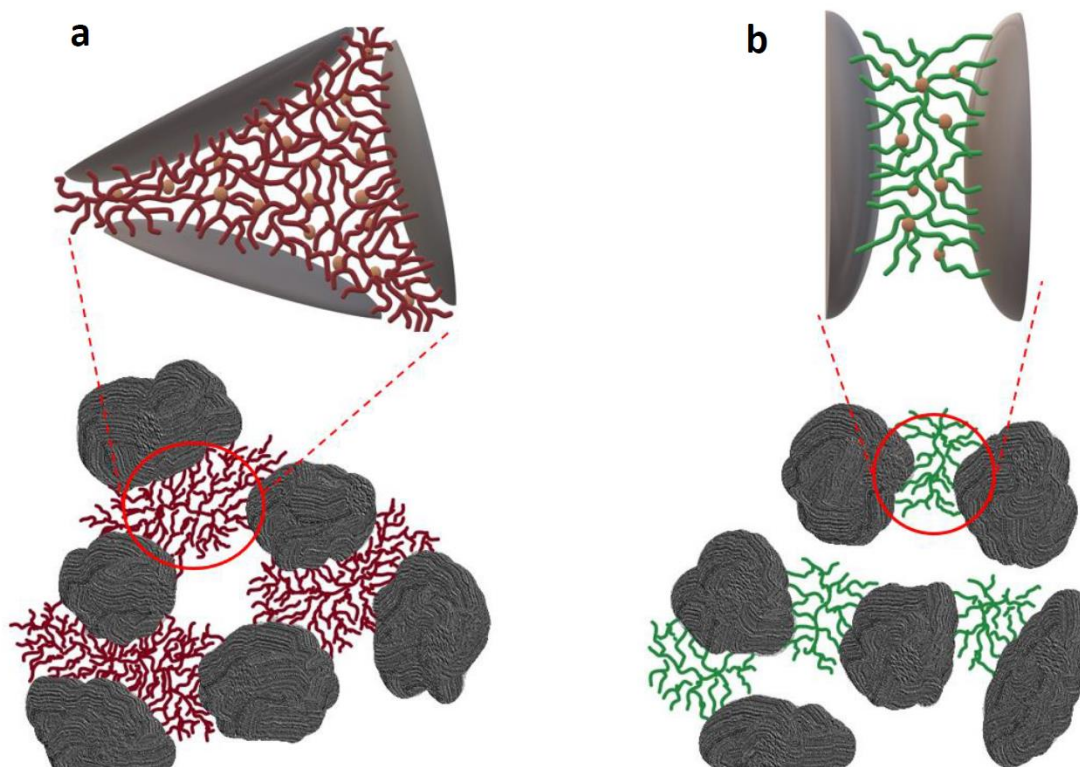


Figure 3. 3 a) chord length and b) number of particle counts for the system at the 16 mg/g dosage of CKL/Kaolin as a function of time (conducted under the condition of 25 g/L concentration, pH 6, and stirring at 200 and 700 rpm)

On the other hand, KL-ATAC formed more stable flocs as the chord length of formed flocs remained constant at a fixed mixing condition (200 rpm) (Figure 3.3-a). This behavior confirmed the weaker bridges probably with shorter tail and loop configurations between KL-ATAC macromolecule and kaolin particles, which could be more resistant to external shear forces. The number of particles also decreased dramatically when KL-METAM macromolecule was added to the kaolin suspension. It was pointed out that the grafted copolymers having more repeating units (or with more grafted flexible chains) showed better flocculation performance.⁹² In the present work, the grafting of METAM and ATAC monomers to the rigid-like lignin decreased the rigidity (stiffness) of lignin molecule (as seen in the shape factor analysis in Table 3.2), facilitating the interaction and adsorption of lignin macromolecules with colloidal particles (i.e., clay particles) and hence improving their flocculation characteristics. The reason for better flocculation performance of KL-METAM than KL-ATAC could be due to the higher surface occupancy of the

former macromolecule upon adsorption on the clay particles. This higher occupancy could be attributed to 1) the larger molecular weight of KL-METAM that improved its bridging performance, and 2) the larger shape factor implying its less flexibility and larger R_g implying its more three-dimensional effectiveness in interacting with clay particles (Scheme 3.2).



Scheme 3. 2 Interaction of a) KL-METAM and b) KL-ATAC with clay particles.

Floc Strength

After 300 s, the shear force in FBRM analysis was increased to 700 rpm (from 200 rpm) decreasing the chord length of the flocs and increasing the number of flocs (Figure 3.3). At high shear rates, the formed flocs break due to the disruption of bridging. Once the shear force diminishes, the crushed particles may agglomerate.⁹³ In this case, when the shear rate decreased to the initial level

(200 rpm), only partial reflocculation was achieved for the macromolecules depicting an increment in chord length and a decrement in floc counts.^{94,95} In the present study, the deflocculation and reflocculation of particles were studied by fitting the data of Figure 3.3 into equations 9 and 10, respectively.^{96,97}

$$Y = C_0 + Ae^{\frac{-t}{T_{df}}} \quad (9)$$

$$Y = C_\infty - Ke^{\frac{-t}{T_{rf}}} \quad (10)$$

where Y is mean chord size, t is a time in second, C₀ and C_∞ are numerical constant (μm), A and K are pre-exponential factors, T_{df} is deflocculation parameter (s), and T_{rf} stands for reflocculation parameter (s).

Table 5 depicts the flocculation parameters obtained via fitting the data into equations 9 and 10. In flocculation processes, there is an equilibrium between the formation and breakage of flocs. The higher T_{df} value of KL-METAM (54 s) is due to the higher strength of formed flocs and can be considered as the strength of flocs. It is known that the patching mechanism causes flocs with relatively weak strength, whereas bridging forms stronger ones.⁹⁸ Therefore, it might be concluded that, compared with KL-METAM, KL-ATAC generated flocs via more patching than bridging. It is noteworthy that the higher floc strength of KL-METAM is attributed to grater bridging efficiency (due to its higher molecular weight) and three-dimensional effectiveness (as seen as larger R_g) of this polymer owing to its higher molecular weight (Scheme 3.2).

However, T_{rf} can describe the reflocculation performance of the broken flocs after reducing the shear rate. The larger T_{rf} of the KL-METAM system indicates the lower tendency of this system to reflocculate and slower reversibility of the flocculation system.^{94,95} Although the flocs formed

using KL-METAM via tail and loop configurations (i.e., higher bridging efficiency) were stronger, the formed flocs could not reach to their initial sizes after deflocculation and reflocculation (i.e., they had weaker reversibility in size). In this case, KL-METAM was probably reconfigured on the surface of kaolin particles after the deflocculation process, and thus it lost its bridging performance when the reflocculation process occurred. In KL-ATAC/kaolin system, smaller flocs with more reversibility in the floc size was detectable after deflocculation and reflocculation process, which is an indicator of the patching flocculation mechanism.⁹⁹ In another study, the larger flocs broke more easily via shear forces and the flocculation process was less reversible.^{100,101}

Table 3. 5 Deflocculation and reflocculation parameters for the systems of kaolin and CKLs at 16 mg/g dosages.

Flocculant	T_{df} , s		T_{rf} , s	
KL-METAM	54.0	$R^2 = 0.93$	43.1	$R^2 = 0.97$
KL-ATAC	38.7	$R^2 = 0.98$	36.6	$R^2 = 0.98$

3.4.6 Application

The results in Figure 3.3 revealed that KL-METAM was more efficient in the flocculation of kaolin particles than did KL-ATAC and it formed stronger (Table 5) and larger (Figure 3.3) flocs. Also, KL-METAM seems to function effectively in the flocculation systems with a low agitation intensity. This macromolecule may be more suitable for use in sedimentation tanks and large clarifiers operating at a low agitation intensity. Although KL-ATAC was not as effective as that of KL-METAM, it can still be used as a flocculant for some flocculation systems. As documented in Table 5, KL-ATAC made weaker flocs with more size reversibility (Figure 3.3) under different agitation intensities, which may be suitable for flocculation systems that occur in more confined (e.g., pipes) and well agitated systems (e.g., mixing tanks).

3.5 Conclusions

New cationic lignin-based flocculants, KL-ATAC and KL-METAM, were synthesized in a semi-dried condition for the first time, which had slightly different charge densities (2.3-2.5 mmol/g) and different molecular weights (657×10^3 and 824×10^3 g/mol). The molecular weight of repeating units of KL-ATAC and KL-METAM were 644 and 747, respectively, indicating the remarkable effect of an extra methyl group associated with METAM on its polymerization efficiency. The higher grafting ratio of KL-METAM than KL-ATAC is attributed to the fact that METAM monomer produced more stable radicals in polymerization reaction. The H_y and R_g of lignin increased after polymerization, and KL-METAM exhibited a larger size and three-dimensional structure. The decrease in the R_g/H_y of CKLs revealed that the structure of lignin macromolecules changed from rigid-rod to more flexible random coil chain after the polymerization reaction. KL-METAM improved the hydrophilicity of kaolin surface more greatly than did KL-ATAC. With a larger size, the surface excess density of KL-METAM was smaller than that of KL-ATAC, but its area of occupancy on the kaolin surface was larger. CKLs impacted the diffuse double layer of the kaolin particles in a similar fashion. However, the zeta potential of the suspension containing KL-METAM with a slightly higher charge density reached to the isoelectric point at a slightly lower dosage. Moreover, a strong correlation between CKLs' structures and flocculation behavior were observed. Due to the large surface occupancy and three-dimensional structure of KL-METAM, its bridging affinity was more remarkable than even though KL-ATAC adsorbed more greatly on kaolin particles. In this case, KL-METAM created a larger chord length and fewer number of flocs than did KL-ATAC. The kinetic studies revealed that τ_{ads} were 36.6 and 37s for KL-METAM and KL-ATAC at 16 mg/g of CKLs adsorption, respectively. Furthermore, KL-METAM formed stronger flocs that were more resistant to the external shear forces (T_{df} of 54.05 s). However, if

KL-METAM/kaolin flocs were broken, they were not able to reflocculate to their original sizes. This behaviour can make KL-METAM macromolecule an appropriate candidate for flocculating kaolin particles in sedimentation tanks and thickeners with low agitation intensities. Overall, the results confirmed that only one extra methyl group would play a vital role in the characteristics of lignin-based macromolecules (CKL), which would notably alter the performance of CKL as a flocculant for kaolin suspension systems.

3.6 References

- (1) Kang, X., Xia, Z., Chen, R., Liu, P., Yang, W. 2019. Effects of inorganic cations and organic polymers on the physicochemical properties and microfabrics of kaolinite suspensions. *Appl. Clay Sci.* 176, 38-48.
- (2) Liu, Z., Lu, X., Xie, J., Feng, B., Han, Q. 2019. Synthesis of a novel tunable lignin-based star copolymer and its flocculation performance in the treatment of kaolin suspension. *Sep. Purif. Technol.* 210, 355-363.
- (3) Lee, K. E., Morad, N., Poh, B. T., Teng, T. T. 2011. Comparative study on the effectiveness of hydrophobically modified cationic polyacrylamide groups in the flocculation of kaolin. *Desalination* 270(1), 206-213.
- (4) Rahul, R., Jha, U., Sen, G., Mishra, S. 2014. Carboxymethyl inulin: A novel flocculant for wastewater treatment. *Int. J. Biol. Macromol.* 63, 1-7.
- (5) Song, M. L., Yu, H. Y., Chen, L. M., Zhu, J. Y., Wang, Y. Y., Yao, J. M., Zou, Z., Tam, K. C. 2019. Multibranch strategy to decorate carboxyl groups on cellulose nanocrystals to prepare adsorbent/flocculants and pickering emulsions. *ACS Sustain. Chem. Eng.* 7(7), 6969-6980.

- (6) Ajao, V., Bruning, H., Rijnaarts, H., Temmink, H. 2018. Natural flocculants from fresh and saline wastewater: comparative properties and flocculation performances. *Chem. Eng. J.* 349, 622-632.
- (7) Park, Y. I., Labrecque, M., Lavoie, J. M. 2013. Influence of Elevated CO₂ and Municipal Wastewater Feed on the Productivity, Morphology, and Chemical Composition of *Arthrospira* (*Spirulina*) *platensis*. *ACS Sustain. Chem. Eng.* 1(11), 1348-1356.
- (8) Goswami, L., Kumar, R. V., Pakshirajan, K., Pugazhenti, G. 2019. A novel integrated biodegradation—microfiltration system for sustainable wastewater treatment and energy recovery. *J. Hazard. Mater.* 365, 707-715.
- (9) Jorfi, S., Pourfadakari, S., Kakavandi, B. 2018. A new approach in sono-photocatalytic degradation of recalcitrant textile wastewater using MgO@ Zeolite nanostructure under UVA irradiation. *Chem. Eng. J.* 343, 95-107.
- (10) Chen, D., Chen, Q., Ge, L., Yin, L., Fan, B., Wang, H., Lu, H., Xu, H., Zhang, R., Shao, G. 2013. Synthesis and Ag-loading-density-dependent photocatalytic activity of Ag@ TiO₂ hybrid nanocrystals. *Appl. Surf. Sci.* 284, 921-929.
- (11) Khanna, A., Shetty, V. 2013. Solar photocatalysis for treatment of Acid Yellow-17 (AY-17) dye contaminated water using Ag@ TiO₂ core–shell structured nanoparticles. *Environ. Sci. Pollut. R.* 20(8), 5692-5707.
- (12) Mehrjouei, M., Müller, S., Möller, D. 2015. A review on photocatalytic ozonation used for the treatment of water and wastewater. *Chem. Eng. J.* 263, 209-219.

- (13) Wang, H., Wang, C., Tao, S., Qiu, J., Yu, Y., Gu, M. 2016. Biomimetic Preparation of Hybrid Porous Adsorbents for Efficiently Purifying Complex Wastewater. *ACS Sustain. Chem. Eng.* 4(3), 992-998.
- (14) Yusoff, M. S., Aziz, H. A., Zamri, M. F. M. A., Abdullah, A. Z., Basri, N. E. A. 2018. Floc behavior and removal mechanisms of cross-linked *Durio zibethinus* seed starch as a natural flocculant for landfill leachate coagulation-flocculation treatment. *Waste. Manage.* 74, 362-372.
- (15) Yang, Z., Yan, H., Yang, H., Li, H., Li, A., Cheng, R. 2013. Flocculation performance and mechanism of graphene oxide for removal of various contaminants from water. *Water Res.* 47(9), 3037-3046.
- (16) Cai, T., Li, H., Yang, R., Wang, Y., Li, R., Yang, H., Li, A. 2015. Cheng, R. Efficient flocculation of an anionic dye from aqueous solutions using a cellulose-based flocculant. *Cellulose* 22(2), 1439-1449.
- (17) Van Heiningen, 2006. A. Converting a kraft pulp mill into an integrated forest biorefinery. *Pulp Pap. Canada* 107(6), 38-43.
- (18) Nagy, M., Kosa, M., Theliander, H., Ragauskas, A. J. 2010. Characterization of CO₂ precipitated Kraft lignin to promote its utilization. *Green Chem.* 12(1), 31-34.
- (19) Agrawal, A., Kaushik, N., Biswas, S. 2014. Derivatives and applications of lignin—An insight. *The SciTech.* 1(7), 30-36.
- (20) Løhre, C., Laugerud, G. A. A., Huijgen, W. J. J., Barth, T. 2018. Lignin-to-Liquid-Solvolysis (LtL) of Organosolv Extracted Lignin. *ACS Sustain. Eng. Chem.* 6(3), 3102-3112.

- (21) Ragauskas, A. J., Beckham, G. T., Biddy, M. J., Chandra, R., Chen, F., Davis, M. F., Davison, B. H., Dixon, R. A., Gilna, P., Keller, M., Langan, P., Naskar, A. K., Saddler, J. N., Tschaplinski, T. J., Tuskan, G. A., Wyman, C. E. 2014. Lignin valorization: improving lignin processing in the biorefinery. *Science* 344(6185), 1246843.
- (22) Gharekhani, S., Zhang, Y., Fatehi, P. 2019. Lignin-derived platform molecules through TEMPO catalytic oxidation strategies. *Prog. Energy Combust. Sci.* 72, 59-89.
- (23) Yuan, T. Q., Xu, F., Sun, R. C. 2013. Role of lignin in a biorefinery: separation characterization and valorization. *J. Chem. Technol. Biotechnol.* 88(3), 346-352.
- (24) Laurichesse, S., Avérous, L. 2014. Chemical modification of lignins: Towards biobased polymers. *Prog Polym Sci.* 39(7), 1266-1290.
- (25) Ruihua, H., Bingchao, Y., Zheng, D., Wang, B. 2012. Preparation and characterization of a quaternized chitosan. *J. Mater. Sci.* 47(2) 845-851.
- (26) Wahlström, R., Kalliola, A., Heikkinen, J., Kyllönen, H., Tamminen, T. 2017. Lignin cationization with glycidyltrimethylammonium chloride aiming at water purification applications. *Ind. Crop. Prod.* 104, 188-194.
- (27) Zhang, B., Mei, J. Q., Chen, B., Chen, H. Q. 2017. Digestibility, physicochemical and structural properties of octenyl succinic anhydride-modified cassava starches with different degree of substitution. *Food Chem.* 229, 136-141.
- (28) Jeddou, K. B., Chaari, F., Maktouf, S., Nouri-Ellouz, O., Helbert, C. B., Ghorbel, R. E. 2016. Structural, functional, and antioxidant properties of water-soluble polysaccharides from potatoes peels. *Food Chem.* 205, 97-105.

- (29) Wang, Z. J., Xie, J. H., Shen, M. Y., Tang, W., Wang, H., Nie, S. P., Xie, M. Y. 2016. Carboxymethylation of polysaccharide from *Cyclocarya paliurus* and their characterization and antioxidant properties evaluation. *Carbohydr. Polym.* 136, 988-994.
- (30) Xu, Y., Du, Y. 2003. Effect of molecular structure of chitosan on protein delivery properties of chitosan nanoparticles. *Intl. J. Pharm.* 250(1), 215-226.
- (31) Pang, Y. X., Qiu, X. Q., Yang, D. J., Lou, H. M. 2008. Influence of oxidation, hydroxymethylation and sulfomethylation on the physicochemical properties of calcium lignosulfonate. *Colloids Surf A Physicochem Eng Asp.* 312(2-3), 154-159.
- (32) Sweedman, M. C., Tizzotti, M. J., Schäfer, C., Gilbert, R. G. 2013. Structure and physicochemical properties of octenyl succinic anhydride modified starches: A review. *Carbohydr. Polym.* 92(1), 905-920.
- (33) Mark, J. E., Ed., *Physical Properties of Polymers Handbook*; Springer: New York, 2007, 1076, 825.
- (34) Kang, H., Uddin, M. A., Lee, C., Kim, K. H., Nguyen, T. L., Lee, W., Li, Y., Wang, C., Woo, H.Y., Kim, B. J. 2015. Determining the role of polymer molecular weight for high-performance all-polymer solar cells: its effect on polymer aggregation and phase separation. *JACS* 137(6), 2359-2365.
- (35) Liu, Z., Lu, X., Xie, J., Feng, B., Han, Q. 2019. Synthesis of a novel tunable lignin-based star copolymer and its flocculation performance in the treatment of kaolin suspension. *Sep. Purif. Technol.* 210, 355-363.

- (36) Kong, F., Wang, S., Price, J. T., Konduri, M. K., Fatehi, P. 2015. Water soluble kraft lignin–acrylic acid copolymer: Synthesis and characterization. *Green Chem.* 17(8), 4355-4366.
- (37) Kong, F., Wang, S., Gao, W., Fatehi, P. 2018. Novel pathway to produce high molecular weight kraft lignin–acrylic acid polymers in acidic suspension systems. *RSC Adv.* 8(22), 12322-12336.
- (38) Garver, T. M., Callaghan, P. T. 1991. Hydrodynamics of kraft lignins. *Macromolecules* 24(2), 420-430.
- (39) Gilardi, G., Cass, A. E. 1993. Associative and colloidal behavior of lignin and implications for its biodegradation in vitro. *Langmuir* 9(7), 1721-1726.
- (40) Petridis, L., Smith, J. C. 2016. Conformations of Low-Molecular-Weight Lignin Polymers in Water. *ChemSusChem* 9(3), 289-295.
- (41) Clauss, M. M., Weldin, D. L., Frank, E., Giebel, E., Buchmeiser, M. R. 2015. Size-Exclusion Chromatography and Aggregation Studies of Acetylated Lignins in N, N-Dimethylacetamide in the Presence of Salts. *Macromol. Chem. Phys.* 216(20), 2012-2019.
- (42) Yang, D., Huang, W., Qiu, X., Lou, H., Qian, Y. 2017. Modifying sulfomethylated alkali lignin by horseradish peroxidase to improve the dispersibility and conductivity of polyaniline. *Appl. Surf. Sci.* 426, 287-293.
- (43) Gupta, C., Washburn, N. R. 2014. Polymer-grafted lignin surfactants prepared via reversible addition–fragmentation chain-transfer polymerization. *Langmuir* 30(31), 9303-9312.
- (44) Hasan, A., Fatehi, P. 2018. Stability of kaolin dispersion in the presence of lignin-acrylamide polymer. *Appl. Clay Sci.* 158, 72-82.

- (45) Gaudreault, R., van de Ven, T. G., Whitehead, M. A. 2005. Mechanisms of flocculation with poly (ethylene oxide) and novel cofactors. *Colloid Surf. A Physicochem. Eng. Asp.* 268(1-3), 131-146.
- (46) Hogg, R. 2000. Flocculation and dewatering, *Intl. J. Miner. Process.* 58(1), 223-236.
- (47) Guo, K., Gao, B., Wang, W., Yue, Q., Xu, X. 2019. Evaluation of molecular weight, chain architectures and charge densities of various lignin-based flocculants for dye wastewater treatment. *Chemosphere* 215, 214-226.
- (48) Heath, A. R., Bahri, P. A., Fawell, P. D., Farrow, J. B. 2006. Polymer flocculation of calcite: Relating the aggregate size to the settling rate. *AIChE J.* 52(6), 1987-1994.
- (49) Filipenska, M., Vasatova, P., Pivokonska, L., Cermakova, L., Gonzalez-Torres, A., Henderson, R. K., Naceradska, J., Pivokonsky, M. 2019. Influence of COM-peptides/proteins on the properties of flocs formed at different shear rates. *J. Environ. Sci.* 80, 116-127.
- (50) Li, R., Gao, B., Sun, J., Yue, Q., Wang, Y., Xu, X. 2016. Synthesis, characterization of a novel lignin-based polymer and its behavior as a coagulant aid in coagulation/ultrafiltration hybrid process. *Intl Biodeterior. Biodegrad.* 113, 334-341.
- (51) Hasan, A. Fatehi, P. 2019. Cationic kraft lignin-acrylamide copolymer as a flocculant for clay suspensions:(2) Charge density effect. *Sep. Purif. Technol.* 210, 963-972.
- (52) Wang, S., Kong, F., Gao, W., Fatehi, P. 2018. Novel Process for Generating Cationic Lignin Based Flocculant. *Ind. Eng. Chem. Res.* 57(19), 6595-6608.
- (53) Heydarifard, S., Gao, W., Fatehi, P. 2018. Generation of new cationic xylan-based polymer in industrially relevant process. *Ind. Eng. Chem. Res.* 57(38), 12670-12682.

- (54) Chassin, P., Jounay, C., Quiquampoix, H. 1986. Measurement of the surface free energy of calcium-montmorillonite. *Clay Miner.* 21(5), 899.
- (55) Rudawska, A., Danczak, I., Müller, M., Valasek, P. 2016. The effect of sandblasting on surface properties for adhesion. *Intl. J. Adhe. Adhes.* 70, 176-190.
- (56) Ito, N. M., Antunes, R. A., Teixeira, F. D. S., Salvadori, M. C., Santos, D. J. D. 2018. The peeling resistance of flexible laminated food packaging: Roles of the NCO: OH ratio and aluminum surface aging times. *J. Adhes.* 94(10), 784-798.
- (57) Vainio, U., Maximova, N., Hortling, B., Laine, J., Stenius, P., Simola, L. K., Gravitis, J., Serimaa, R. 2004. Morphology of dry lignins and size and shape of dissolved kraft lignin particles by X-ray scattering. *Langmuir* 20(22), 9736-9744.
- (58) Kosmas, M. K. 1981. On the mean radius of gyration of a polymer chain. *J. Phys. A. Math. Gen.* 14(10), 2779.
- (59) Nygaard, M., Kragelund, B. B., Papaleo, E., Lindorff-Larsen, K. 2017. An efficient method for estimating the hydrodynamic radius of disordered protein conformations. *Biophys. J.* 113(3), 550-557.
- (60) Rouhi, S., Alizadeh, Y., Ansari, R. 2015. On the wrapping of polyglycolide, poly (ethylene oxide), and polyketone polymer chains around single-walled carbon nanotubes using molecular dynamics simulations. *Braz J. Phys.* 45(1), 10-18.
- (61) Kaasalainen, M., Aseyev, V., von Haartman, E., Karaman, D. Ş., Mäkilä, E., Tenhu, H., Rosenholm, J., Salonen, J. 2017. Size, stability, and porosity of mesoporous nanoparticles characterized with light scattering. *Nanoscale Res. lett.* 12(1), 74.

- (62) Thomas, H. R., Phillips, D. J., Wilson, N. R., Gibson, M. I., Rourke, J. P. 2015. One-step grafting of polymers to graphene oxide. *Polym. Chem.* 6(48), 8270-8274.
- (63) Russo, D., De Angelis, A., Garvey, C. J., Wurm, F. R., Appavou, M. S., Prevost, S. 2019. Effect of Polymer Chain Density on Protein–Polymer Conjugate Conformation. *Biomacromolecules* 20(5), 1944-1955.
- (64) Ba, X., Wang, H., Zhao, M., Li, M. 2002. Conversion dependence of the z-average mean square radii of gyration for hyperbranched polymers with excluded volume effect. *Macromolecules* 35(10), 4193-4197.
- (65) Gibis, M., Schuh, V., Allard, K., Weiss, J. 2017. Influence of molecular weight and degree of substitution of various carboxymethyl celluloses on unheated and heated emulsion-type sausage models. *Carbohydr Polym.* 159, 76-85.
- (66) Lee, H., Venable, R. M., MacKerell Jr, A. D., Pastor, R. W. 2008. Molecular dynamics studies of polyethylene oxide and polyethylene glycol: hydrodynamic radius and shape anisotropy. *Biophys. J.* 95(4), 1590-1599.
- (67) Li, Y., Shen, H., Lyons, J. W., Sammler, R. L., Brackhagen, M., Meunier, D. M. 2016. Size-exclusion chromatography of ultrahigh molecular weight methylcellulose ethers and hydroxypropyl methylcellulose ethers for reliable molecular weight distribution characterization. *Carbohydr. Polym.* 138, 290-300.
- (68) Mendichi, R., Šoltés, L., Giacometti Schieron, A. 2003. Evaluation of radius of gyration and intrinsic viscosity molar mass dependence and stiffness of hyaluronan. *Biomacromolecules* 4(6), 1805-1810.

- (69) Ruckdeschel, P., Dulle, M., Honold, T., Förster, S., Karg, M., Retsch, M. 2016. Monodisperse hollow silica spheres: an in-depth scattering analysis. *Nano Res.* 9(5), 1366-1376.
- (70) Li, W., Cui, S. W., Wang, Q. 2006. Solution and conformational properties of wheat β -D-glucans studied by light scattering and viscometry. *Biomacromolecules* 7(2), 446-452.
- (71) Nie, T., Zhao, Y., Xie, Z., Wu, C. 2003. Micellar Formation of Poly (caprolactone-b lock-ethylene oxide-b lock-caprolactone) and Its Enzymatic Biodegradation in Aqueous Dispersion. *Macromolecules* 36(23), 8825-8829.
- (72) W. Schärtl, *Light scattering from polymer solutions and nanoparticle dispersions*; Springer Science & Business Media: 2007.
- (73) Zhang, G., Liu, L., Zhao, Y., Ning, F., Jiang, M., Wu, C. 2000. Self-Assembly of Carboxylated Poly (styrene-b-ethylene-co-butylene-b-styrene) Triblock Copolymer Chains in Water via a Microphase Inversion. *Macromolecules* 33(17), 6340-6343.
- (74) Szwengiel, A., Lewandowicz, G., Górecki, A. R., Błaszczak, W. 2018. The effect of high hydrostatic pressure treatment on the molecular structure of starches with different amylose content. *Food Chem.* 240, 51-58.
- (75) Niu, A., Li, C., Zhao, Y., He, J., Yang, Y., Wu, C. 2001. Thermal decomposition kinetics and structure of novel polystyrene clusters with mtempo as a branching agent. *Macromolecules* 34(3), 460-464.
- (76) Barthel, M.J., Rinkenauer, A.C., Wagner, M., Mansfeld, U., Hoepfener, S. Czaplowska, J.A., Gottschaldt, M., Träger, A., Schacher, F.H., Schubert, U.S. 2014. Small but powerful: co-assembly

of polyether-based triblock terpolymers into sub-30 nm micelles and synergistic effects on cellular interactions. *Biomacromolecules* 15(7), 2426-2439.

(77) Baek, J., Wahid-Pedro, F., Kim, K., Kim, K., Tam, K. C. 2019. Phosphorylated-CNC/modified-chitosan nanocomplexes for the stabilization of Pickering emulsions. *Carbohydr Polym.* 206 520-527.

(78) Wu, H., Chen, F., Feng, Q., Yue, X. 2012. Oxidation and sulfomethylation of alkali-extracted lignin from corn stalk. *BioRes.* 7(3), 2742-2751.

(79) Notley, S. M., Norgren, M. 2010. Surface energy and wettability of spin-coated thin films of lignin isolated from wood. *Langmuir* 26(8), 5484-5490.

(80) Hamdaoui, O., Naffrechoux, E. 2007. Modeling of adsorption isotherms of phenol and chlorophenols onto granular activated carbon: Part I. Two-parameter models and equations allowing determination of thermodynamic parameters. *J. Hazard. Mater.* 147(1-2), 381-394.

(81) Peng, P., & Garnier, G. 2010. Effect of cationic polyacrylamide adsorption kinetics and ionic strength on precipitated calcium carbonate flocculation. *Langmuir* 26(22), 16949-16957.

(82) Fatehi, P., Xiao, H. 2008. Adsorption characteristics of cationic-modified poly (vinyl alcohol) on cellulose fibers—A qualitative analysis. *Colloid. Surf. A Physicochem. Eng. Asp.* 327(1-3), 127-133.

(83) Matsushita, Y., Imai, M., Iwatsuki, A., Fukushima, K. 2008. The relationship between surface tension and the industrial performance of water-soluble polymers prepared from acid hydrolysis lignin, a saccharification by-product from woody materials. *Bioresour. Technol.* 99(8), 3024-3028.

- (84) Zhang, T., Marchant, R. E. 1996. Novel polysaccharide surfactants: the effect of hydrophobic and hydrophilic chain length on surface active properties. *J. Colloid Interf. Sci.* 177(2), 419-426.
- (85) Adamson, A. W., Gast, A. P. 1967. Physical chemistry of surfaces, *New York: Interscience*, (150), 180.
- (86) Huang, Y., Zhang, X., Fu, K., Li, H., Huang, C., Yuan, S. 2015. Synthesis and application of cationic spherical polyelectrolyte brushes as retention and drainage aid in bleached eucalyptus kraft pulp. *J. Ind. Eng. Chem.* 31, 309-316.
- (87) Pal, S., Ghorai, S., Dash, M. K., Ghosh, S., Udayabhanu, G. 2011. Flocculation properties of polyacrylamide grafted carboxymethyl guar gum (CMG-g-PAM) synthesised by conventional and microwave assisted method. *J. Hazard. Mater.* 192(3), 1580-1588.
- (88) Gaudreault, R., Di Cesare, N., Weitz, D., van de Ven, T. G. 2009. Flocculation kinetics of precipitated calcium carbonate. *Colloid. Surf A Physicochem. Eng. Asp.* 340(1-3), 56-65.
- (89) McFarlane, A. J., Bremmell, K. E., Addai-Mensah, J. 2005. Optimising the dewatering behaviour of clay tailings through interfacial chemistry, orthokinetic flocculation and controlled shear. *Powder Technol.* 160(1), 27-34.
- (90) Higashitani, K., Nakamura, K., Shimamura, T., Fukasawa, T., Tsuchiya, K., Mori, Y. 2017. Orders of magnitude reduction of rapid coagulation rate with decreasing size of silica nanoparticles. *Langmuir* 33(20), 5046-5051.
- (91) Gaudreault, R., Di Cesare, N., van de Ven, T. G., Weitz, D. A. 2015. Structure and strength of flocs of precipitated calcium carbonate induced by various polymers used in papermaking. *Ind. Eng. Chem. Res.* 54(24), 6234-6246.

- (92) Higashitani, K., Nakamura, K., Shimamura, T., Fukasawa, T., Tsuchiya, K., Mori, Y. 2017. Orders of magnitude reduction of rapid coagulation rate with decreasing size of silica nanoparticles. *Langmuir* 33(20), 5046-5051.
- (93) Yoon, S. Y., Deng, Y. 2004. Flocculation and reflocculation of clay suspension by different polymer systems under turbulent conditions. *J. Colloid Interf. Sci.* 278(1), 139-145.
- (94) Blanco, A., De La Fuente, E., Negro, C., Monte, M. C., Tijero, J. 2002. Focused beam reflectant measurement as a tool to measure flocculation. *Tappi J.* 1(10), 14-20.
- (95) Antunes, E., Garcia, F. A. P., Blanco, A., Negro, C., Rasteiro, M. G. 2015. Evaluation of the flocculation and reflocculation performance of a system with calcium carbonate, cationic acrylamide co-polymers, and bentonite microparticles. *Ind. Eng. Chem. Res.* 54(1), 198-206.
- (96) Alfano, J. C., Carter, P. W., Whitten, J. E. 1999. Use of scanning laser microscopy to investigate microparticle flocculation performance. *J pulp pap sci* 25(6), 189-195.
- (97) Blanco, A., Fuente, E., Negro, C., Tijero, J. 2002. Flocculation monitoring: focused beam reflectance measurement as a measurement tool. *Can. J. Chem. Eng.* 80(4), 734-740.
- (98) Yang, Z., Li, H., Yan, H., Wu, H., Yang, H., Wu, Q., Li, H., Li, A., Cheng, R. 2014. Evaluation of a novel chitosan-based flocculant with high flocculation performance, low toxicity and good floc properties. *J. Hazard Mater.* 276, 480-488.
- (99) Zheng, H., Feng, L., Gao, B., Zhou, Y., Zhang, S., Xu, B. 2017. Effect of the cationic block structure on the characteristics of sludge flocs formed by charge neutralization and patching. *Materials* 10(5), 487.

(100) Antunes, E., Garcia, F. A., Ferreira, P., Blanco, A., Negro, C., Rasteiro, M. G. 2008. Effect of water cationic content on flocculation, flocs resistance and reflocculation capacity of PCC induced by polyelectrolytes. *Ind. Eng. Chem. Res.* 47(16), 6006-6013.

(101) Korhonen, M. H., Rojas, O. J., Laine, J. 2015. Effect of charge balance and dosage of polyelectrolyte complexes on the shear resistance of mineral floc strength and reversibility. *J. Colloid Interfa. Sci.* 448, 73-78.

Chapter 4: Impact of the Chain Conformation of Lignin macromolecules on their Adsorption, Rheological Properties and Thermal behaviour

4.1 Abstract

Cationic kraft lignin (CKL) polymers were synthesized via polymerizing kraft lignin (KL) with [2-(acryloyloxy)ethyl]trimethylammonium chloride (ATAC) or [2-(methacryloyloxy)ethyl]trimethylammonium methyl sulfate (METAM) in an acidic environment to investigate how monomer structure would impact the self assembly, sedimentation and interaction of CKL with solid surfaces. Results suggested that KL-METAM had a flexible chain conformation while KL-ATAC exhibited a more compact coil structure. KL-METAM with more three-dimensional structure (i.e., R_g and R_h) had a more accelerated self assembly. The structural differences of CKLs had an influence on their surface hydrophilicity in which KL-METAM decreased the surface tension of water more greatly than KL-ATAC. The sedimentation analysis under both gravitational and centrifugal forces proved that the KL-METAM had a higher tendency to settle with a larger settling velocity as a result of greater self-aggregation than KL-ATAC. Below and at equilibrium, KL-METAM could adsorb more greatly and generated bulkier and more viscoelastic adlayer on the rigid surface. In the Quartz crystal microbalance analysis, the alteration in the slope of $\Delta D/\Delta F$ curve in the early and late stages of adsorption was assigned to the conformational changes of CKLs by increasing R_g . The steeper slope of $\Delta D/\Delta F$ at the early stage of KL-METAM adsorption was due to its greater adsorption affinity on SiO_2 surface, while the more rigid conformation of KL-ATAC resulted in a more significant slope change in the late adsorption stage. Higher storage modulus (G') was observed for KL-METAM at bulk solution, which represented its more resistance to oscillation. The compact coil structure of KL-ATAC

restricted free molecular movement of the lignin polymer resulted in higher T_g values. The findings of this study showed that a small group in the cationic monomers can affect the structure of CKLs so significantly that the lignin polymers would have different chain conformations and thermal properties, rheological properties in solutions, adsorption performance and altered viscoelastic adlayers upon adsorption. These altered characteristics would impact their potential applications remarkably.

Keywords: Lignin, Polymerization, Macromolecules conformation, Self-assembly, Adsorption, Viscoelasticity

4.2 Introductions

Recently, the environmental issues and the increment in the energy demand have promoted the development of chemicals from renewable resources such as cellulose, hemicellulose, lignin and chitosan.¹ Among them, lignin, an abundant polymer of aromatic units, was recognized as one of the most promising natural polymers owing to its eco-friendliness, availability and biodegradability.² Annually, a large volume of lignin is produced in the pulping industry. Despite the complicated structure of lignin, the existence of various functional groups on its structure (i.e., methoxy, carboxylic acid and hydroxyl groups) makes it amenable for modification through different pathways.³⁻⁸ Of kraft lignin (KL) modification processes, amination was assigned as one of the most auspicious methods to alter lignin's properties.

It is well-known that the physicochemical characteristics of a polymers could be evaluated by their chain conformation.⁹ The distribution of the charged groups on the molecular structure of polymers as well as the balance of polymer-solvent interactions^{10,11} can change the conformational

characteristics of polymers (i.e., shape and size) in aqueous solutions.¹² Several studies revealed that the physicochemical properties of lignin would be altered after the polymerization reactions, and the polymers with controlled architectures could be synthesized.^{3,13,14} Also, lignin macromolecule has been exhibited to aggregate in aqueous solutions,^{15,16} which would remarkably affect its applications.¹⁷⁻¹⁹ However, little attention has been paid to a fundamental understanding of the impact of grafting monomers on the physicochemical characteristics of lignin polymers and their subsequent behaviors in aqueous solutions, which is the first objective of this work.

The polymer adsorption onto a model substrate has received significant attention and developed various fundamental concepts in colloidal stability, flocculation/dispersion systems and drug carriers.²⁰⁻²² Numerous studies demonstrated that the adsorption behavior of lignin polymers on model substrates (i.e., silica or alumina) is governed by their structural conformation.²³ For instance, sulfonated lignin showed excellent adsorption performance on the surface of cation dye by expanding its structural conformation on the dye surface, which enhanced the electrostatic interactions, as well as the π - π interactions of lignin macromolecules with the model substrate.²⁴ Likewise, the studies on the adsorption behaviour and surface properties of a kraft lignin-acrylamide (KAM) with various molecular weights on the gold surface revealed that the high molecular weight KAM with extended configuration elevated the intermolecular hydrogen bonding (i.e., self-assemble) by forming loose agglomerates.¹⁸ However, little information is available on the adsorption characteristics of cationically modified lignin polymers with different structures on a rigid surface, which is the second objective of present work.

Understanding the rheological properties of polymers plays a fundamental role in their viscoelastic response in different media, processability and ultimately in altered potential applications.²⁵

Polymer conformation and inter-molecular interactions can influence the rheological properties (i.e., viscoelasticity) of polymers in solutions.^{26,27} Previously, the viscoelastic functions of ABS (acrylonitrile-butadiene-styrene) polymers were reported to be depended strongly on grafting degree, which in turn improved the stability of colloidal solutions.²⁷ However, the correlation between the chain conformation of cationic kraft lignin (CKL) macromolecules and their viscoelastic characteristics in the aqueous solution and after adsorption remain unclear, which is the third objective of this study.

In our previous work, the [2- (acryloyloxy)ethyl]trimethyl ammonium chloride (ATAC) and [2- (methacryloyloxy) ethyl] trimethyl ammonium methyl sulfate (METAM) monomers was polymerized with kraft lignin to produce cationic kraft lignin samples (CKL).³ Present research aims to investigate the correlation between the chain conformation of CKL macromolecules and their short- and long-term colloidal stabilities, bulk and adsorbed viscoelastic properties as well as the adsorption behaviour at various grafting densities. This work also studies the impact of the molecular conformation of CKL polymers on their thermal behavior. The primary novelties of this work are the study on the impact of the molecular architecture of the cationic lignin macromolecules on their self-association which can 1) alter the colloidal behaviour of CKLs in aqueous solution, 2) produce surfaces with different morphologies, 3) change the thermal properties as well as the rheological characteristics of CKLs in bulk solution and upon adsorption.

4.3 EXPERIMENTAL SECTION

4.3.1 Materials

Softwood Kraft lignin (KL) generated by the LignoForce technology was received from a mill located in Alberta, Canada. [2-(Acryloyloxy)ethyl]trimethylammonium chloride solution (ATAC), 80 wt % in H₂O, sodium persulfate (Na₂S₂O₈) (analytical grades), sodium hydroxide, potassium nitrate (KNO₃), potassium hydroxide (8 M), hydrochloric acid (37%, reagent grade), sulfuric acid, para-hydroxybenzoic acid and poly(diallyldimethylammonium chloride) (PDADMAC, 100000–200000 g/mol), 20 wt % in water, were all purchased from Sigma-Aldrich Co. Fisher Scientific Co. provided acetic acid and ethanol (95 vol %). Potassium poly (vinyl sulfite) (PVSK, 100000–200000 g/mol, 97.7 wt % esterified) was purchased from Wako Pure Chemical Co., Japan. [2-(Methacryloyloxy)ethyl]-trimethylammonium methyl sulfate (METAM) was obtained from BOC Science Co., USA. The dialysis membrane of cellulose acetate (cutoff of 1000 g/mol) was received from Spectrum Laboratories. Deionized water with the resistivity of less than 18 MΩ/cm used throughout this study was obtained from a Millipore water purification system.

4.3.2 Lignin polymerization

Cationic kraft lignin (CKL) was synthesized in a semidry manner according to the reported method with a minor modification.³ Briefly, 2 g of KL was dissolved in the desired amount of water and then mixed with various amounts of cationic monomers (0.5-3/1 w/w cationic agent/lignin) to produce a 40 wt % concentration in all reactions. The pH of the reaction was set to 3.6 ± 0.2 using H₂SO₄ (1 M) and then potassium persulfate (0.03 g) was used to initiate the free radical polymerization. Afterward, the nitrogen gas was purged into the reaction suspension for 10 min. The polymerization reaction was then carried out at 80 °C for 3 h. Upon completion of the reaction, the reaction was cooled to room temperature. After that, cationic lignin was precipitated from the

reaction mixture using ethanol (80 vol % in water).²² The final product was dialyzed against deionized water for 2 days. The sample was subsequently dried by a freeze-dryer.

4.3.4 Characterization of Macromolecules

Charge density analysis

The charge density of the samples was determined using a Particle Charge Detector, Mütek PCD 04 titrator (Arzbergerstrae, Herrsching, Germany). A 1 wt % CKL polymer suspension was prepared and shaken at 300 rpm for several hours at room temperature. After centrifuging at 1000 rpm for 5 min, the collected supernatants were titrated against a PVSK standard solution (0.005 mol/L) to determine the charge density of soluble CKL.²⁸

Phenolic hydroxy group content

An aqueous potentiometric titration technique was used to determine the phenolic hydroxy group of CKL using an automatic potentiometer titrator (785 DMP Titrino, Metrohm, Switzerland). In this experiment, 0.06 g of lignin polymer was dissolved in 100 mL deionized water containing 1 mL of potassium hydroxide (0.8 M) and 0.02 g of para-hydroxybenzoic acid (as internal standard). After mixing, the titration was carried out against 0.1 M HCl standard solution.²⁹

Elemental analysis

The elemental analysis of KL and CKLs was performed using an elemental analyser (Vario EL Cube, Elemental Analyzer, Germany). The content of nitrogen element was obtained through combustion of 2 mg of dried sample at 1200 °C. The grafting ratio of ATAC and METAM monomer to lignin corresponding with the nitrogen content of CKL was calculated according to following equation 1:

$$\text{Grafting ratio (mol \%)} = \frac{N_{14} \times M_w}{100 - (N_{14} \times M_w)} \quad (1)$$

Where N (wt %) is the nitrogen content of polymers, and M_w stands for the molecular weight of METAM and ATAC monomers, which are 173 and 152 g/mol, respectively.

Molar mass analysis

The weight-average molecular weight (M_w) and the root-mean-square radius of gyration (R_g) of KL and CKL were measured using a static light scattering (SLS) technique that was attached to a goniometer, Brookhaven BI-200SM, Holtsville, NY, USA. In this analysis, the different concentrations of lignin solutions (0.2-2 wt %) were prepared in sodium hydroxide aqueous solutions (0.5 M) containing 10 mM KNO_3 (to avoid aggregation) at room temperature. Afterward, the samples were passed through a nylon syringe filter with 30 mm diameter and 0.45 μm pore opening prior to the measurement. The experiment was conducted at the wavelength of 637 nm and the scattering intensities of samples were set at different angles (15 °C - 155 °C). BIC Zimm Plot software was performed for determining M_w and R_g of the samples.

Surface tension and contact angle determination

The surface tension and contact angle of CKL solutions at the concentration of 1 g/L was measured using a Theta Lite Optical tensiometer, TL100 (Biolin Scientific), which was equipped with a USB2 digital camera and light-emitting diode light source. A droplet of CKL solution (5 μL) was dispensed on the tip of a Hamilton syringe equipped with a needle and the images of three replicate drops were acquired using a digital camera. The pendant drop method of Attension software was then used for surface tension measurement using drop dimensions at the air-water interface by fitting the dimensions into the Young-Laplace equation.

Similarly, the contact angle analysis of CKLs was conducted by placing 5 μL of liquid droplets of CKLs (1g/L) on a clean glass wafer following a static contact angle measurement with the sessile drop method. Each analysis repeated three times, and the average values were reported.

4.3.5 Quartz Crystal Microbalance with Dissipation (QCM-D) Studies

The adsorption mechanisms of CKLs on the SiO_2 surface and the properties of the adsorbed layer was determined using a Quartz crystal microbalance with dissipation (QCM-D 401, E1, Q-Sense Inc. Gothenborg, Sweden). The details of QCM-D technique were fundamentally discussed elsewhere.³⁰ Briefly, it tracks the changes of the resonance frequency, f , caused by physically adsorbed onto the SiO_2 crystal sensors over time. The viscoelastic properties of an attached layer were also measured by the energy loss in the oscillating Quartz crystal system according to equation 2:

$$D = \frac{E_D}{2\pi E_S} \quad (2)$$

herein E_D is the energy dissipated and E_S determines the amount of energy stored in the oscillating system. Basically, a soft material adsorbed on the sensor crystal exhibits more deformation during the oscillation, indicating a higher dissipation value. However, a rigid material has a lower dissipation value.³¹ The adsorption behaviour of CKLs (1 g/L) on the SiO_2 sensor was monitored by introducing a buffer solution (i.e. Mili-Q water) at ambient temperature to generate the baseline in the experiments. Then, the CKL solutions were pumped at a flow rate of 0.15 mL/min to carry out the adsorption analysis.

4.3.6 Gravitational sedimentation analysis

The short-time storage stability of KL and CKL solutions was assessed by a vertical scan analyzer, Turbiscan (Lab Expert, Formulaction) under non-stirring conditions. In this analysis, 20 mL of lignin solution (1g/L) was added into a flat-bottomed cylindrical glass cell of the instrument and scanned from the bottom to the top using electro luminescent diode light at 880 nm at 40 μm height intervals. The sample scanning was conducted every 25s for 1h to report kinetic stability of the solution.

By comparing the transmittance signals generated by the samples with those generated by a silicon oil (calibration chemical), Turbiscan stability index (TSI) was calculated using Turbisoft 2.1 software³² following equation (3):

$$TSI = \sum_i \frac{\sum_h |Scan_i(h) - Scan_{i-1}(h)|}{H} \quad (3)$$

where $scan_i(h)$ and $scan_{i-1}(h)$ represent the transmission signals for two consecutive time intervals at a specified height (h) and H exhibits the total height of samples.

4.3.7 Centrifugal sedimentation analysis

The long-time storage stability of KL and CKL solutions was evaluated by a dispersion analyzer (LUMiSizer 611, LUM GmbH, Berlin, Germany) at room temperature using polyamide cuvettes. The LUMiSizer analytical photo centrifuge is a microprocessor-controlled instrument that measures the intensity of near-infrared light as a function of time and position from top to bottom of the cell length simultaneously using space and time resolved extinction profiles (STEP) technology.³³ The progression of these transmission profiles contains information on the kinetics of any concentration changes as a result of sedimentation, flocculation, coalescence, phase separation or creaming.³⁴ Measurements were conducted at 25°C for 1 g/L polymer dispersions

and wavelength of 865 nm at 200, 500 and 1000 rpm. The experimental time was set at 1000 s with 5 s time intervals between recordings.

By means of a centrifugal separation analysis (CSA), the changes in the intensity of the transmitted near-infrared light over time and position was recorded in transmission profiles that would yield information on the separation process kinetics, allowing the calculation of particle migration rate (i.e., velocity), which would be associated with the particle size distribution.^{35,36}

4.3.8 DSC Analysis

Glass transition temperature (T_g) and heat capacity (C_p) values of the lignin samples were analysed using a differential scanning calorimetry (DSC, TA Instruments Q2000). The experiment was conducted according to the methods published previously.^{37,38} First, a 5 mg dried lignin sample was placed in a DSC pan, and then the samples were treated in the temperature range of 0 °C and 200 °C, while the heating rate was set at 3 °C/min.³⁸ After heating the samples to 200 °C, they were cooled down to 0 °C and reheated again to 200 °C. The values of T_g and C_p of KL and CKL were assessed in the second heating cycle.³⁷

4.3.9 Rheological Properties

The rheological behaviour of CKLs were analysed using a hybrid rheometer (TA Instruments) equipped with a cylindrical geometry (cone diameter, 28.03 mm, cone length, 41.96, angle, 1°, gap, 5500 μ m) at room temperature. Approximately 25 mL of CKL aqueous suspension at the 4 wt % concentration was placed inside the cell of the instrument. The samples were equilibrated (a 3 min pre shear at 100 1/s) prior to the test. In contrast to the other experiments, the higher concentration of CKLs (4 wt %) was essential for meaningful results to be obtained by rheometer

instrument. Dynamic strain sweep measurements were performed at a frequency of 6.28 rad/s to discover the linear viscoelastic region (LVR). Then, frequency sweep measurements (0.01–100 rad/s) were carried out for all the samples at a strain value of 1% from the linear viscoelastic region. The experiment was performed at room temperature.

4.4 Results and Discussions

4.4.1 Characterizations of KL-METAM and KL-ATAC

The polymerization reaction of lignin and METAM or ATAC was carried out via free radical polymerization under the conditions of 3 h reaction time, 80 °C reaction temperature, pH 3, and 60 wt % lignin concentration in water. Our previous findings proved that these conditions were optimum for the polymerization of kraft lignin with METAM and ATAC monomers.^{3,22} However, to produce CKLs with different grafting ratio (ranging from 35 mol % to 125 mol %), various cationic monomers/lignin ratios (0.5-3/1 w/w METAM or ATAC/lignin) were considered in the reaction. The reaction schemes of lignin polymerization with METAM or ATAC are available in Supporting Information (Scheme 3.1). Table A2 lists the properties of CKL macromolecules. The charge density, nitrogen content (originating from cationic monomers attached to the lignin structure) and grafting ratio of KL-METAM and KL-ATAC increased gradually with increasing the cationic monomer contents of the lignin derivatives. The reduction in the content of phenolic hydroxy group of CKLs also confirmed the successful attachment of METAM or ATAC to lignin backbone (Table A2). Results also revealed that the grafting ratio of KL-METAM samples were slightly higher than those of KL-ATAC and the value of phenolic hydroxy groups of KL-METAM was lower than that of KL-ATAC samples. The molecular weight (M_w) and radius of gyration (R_g)

of CKLs were also tabulated in Table A2. Accordingly, KL-METAM polymers had a higher molecular weight compared to KL-ATAC samples, demonstrating the more successful polymerization of METAM and lignin. The reason for this phenomenon can be attributed to the existence of an extra methyl group in METAM 's structure, which notably contributed to the better polymerization efficiency of this monomer with lignin macromolecule.³ The radius of gyration (R_g) is very sensitive to the geometry and molecular structure of polymers.³⁹ It was reported that the molecular weight of polymers was correlated with the mean square radius of gyration.⁴⁰ Figure 4.1 shows the logarithmic plot of the molecular weight dependence of the R_g and M_w of CKLs. This figure facilitates the determination of scaling factor (ν) in $R_g \propto M_w^\nu$ relationship.⁴¹ The exponent ν represents the compactness of a polymer. It is known that the scaling factor of $\nu = 0.33$ represents the compact coils (collapsed globules) in a theta solvent, the ν values of approximately 0.5 and 0.6 for random coils in a favorable solvent and $\nu = 0.7$ corresponds to a relatively stiff rod-like conformation in good solvent.^{11,42} In the present study, the value of ν for KL-METAM was found to be 0.46 indicating a relatively flexible chain conformation and 0.37 for KL-ATAC polymer suggesting its compact coil chains in water. The more flexibility of polymer chain in the KL-METAM macromolecule could be due to the steric hindrance that the extra CH_3 substituent of METAM imparted to KL-METAM.

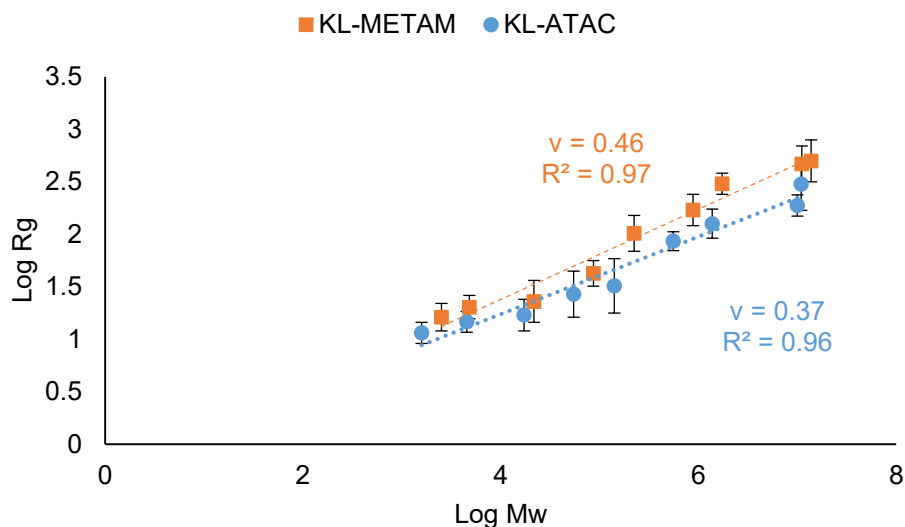


Figure 4. 1 Double logarithmic plot of the radius of gyration (R_g) vs the molecular weight (M_w) of the KL-METAM and KL-ATAC series

The changes in the conformation of macromolecules as a result of increasing their grafting ratios can also be determined via structure-sensitive shape factor (ρ) analysis, which is the ratio of R_g/R_h .^{43,44} Generally, the shape factor shows the density distribution of colloid and the degree of draining of a scattering object in solution or dispersion.^{45,46} According to the literature, the ρ value of approximately 0.774 is for a polymer chain existing as a uniform hard sphere, 1-1.3 for a hyperbranched polymer chain, 1.5-1.8 for flexible random coil chain, and $\rho > 2.0$ is for an extended rigid rod.⁴⁶⁻⁴⁸ It should be stated that the kraft lignin displayed a rod-like structure with R_g/R_h of 2.04.³ Figure 4.2 presents the shape factor of CKLs where they undergo a morphological evolution with raising grafting ratio. As seen, the conformation of lignin macromolecules altered from hyperbranched to rigid rod structure as the grafting ratio of CKLs increased. The R_g/R_h ratio of CKLs was in the range 1.04 -1.15 for KL-METAM or KL-ATAC with grafting ratios were increased to 72 and 80 mol %, respectively, indicating the highly branched and dense structure of polymers due to insufficient amount of grafted chains to lignin backbone. More extensive grafting

of cationic monomer to KL (77.9-98.6 mol % and 95.5-10.5 mol % for KL-METAM and KL-ATAC, respectively) extended the polymer chains with flexible random coil structure. The rigid rod-like shape was also observed for CKLs at elevated grafting ratios and Mw. As stated earlier, the extra methyl substituent in METAM structure created greater steric barrier in KL-METAM structure as compared with KL-ATAC resulted in looser structure of the former polymer at the lower grafting ratios.

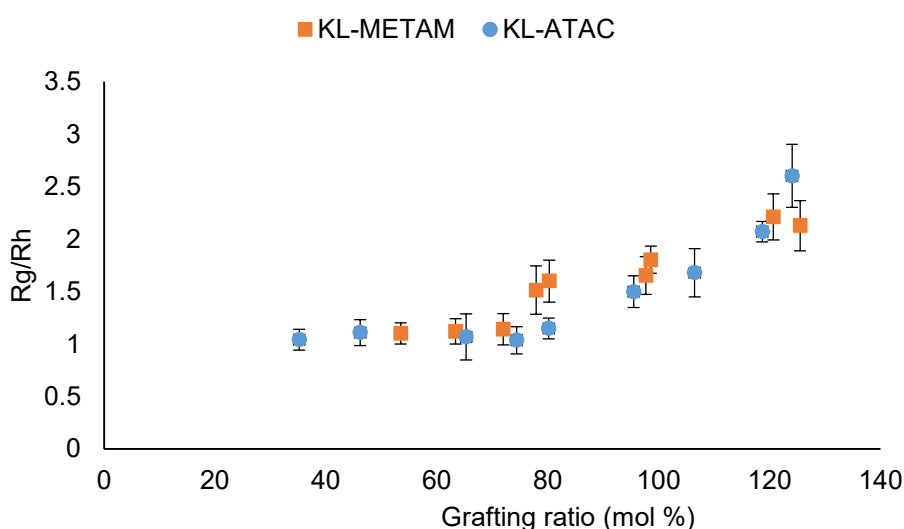


Figure 4. 2 The dependence of shape factor to the grafting ratios of KL-METAM and KL-ATAC.

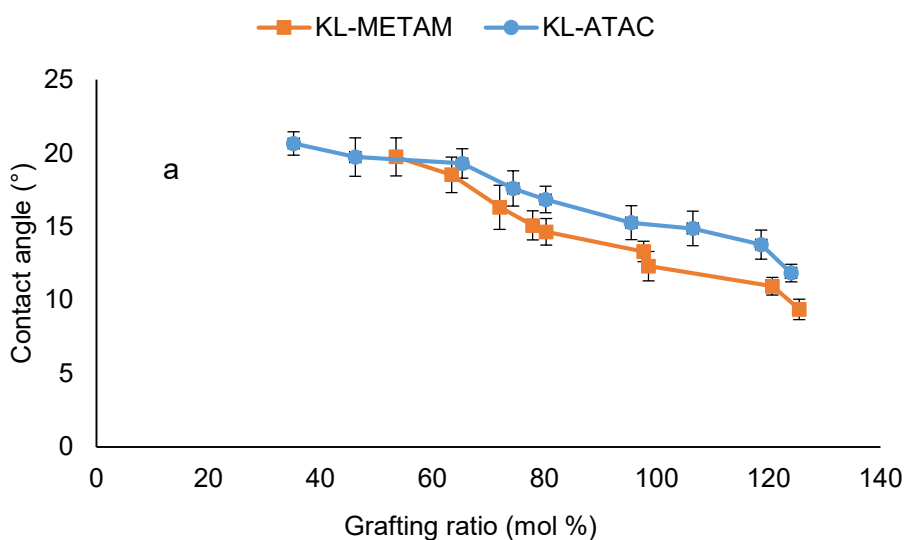
4.4.2 Behavior of Lignin Polymers in Solution Systems

Surface properties

The surface tension and contact angle of droplets containing CKLs as a function of their R_g are illustrated in Figure 4.3. The contact angle of water droplet on glass slide was 21° , similar to the results reported previously.⁴⁹ However, the hydrophilicity of the glass surface was improved when the droplets of solutions containing CKL were placed on the surface owing to the more interactions of water and CKL molecules with glass surface via $-\text{COOH}$, $-\text{OH}$ and NR_4^+ (R: alkyl or aryl)

group interaction. Moreover, the wettability of CKL on the glass surface elevated by increasing the grafting ratio and the introduction of more charged groups attached to lignin backbone (Table A2).

The surface tension of pure water was determined to be 72.8 mN/m.⁵⁰ Similar to contact angle results, the surface tension of water containing CKLs dropped as CKL concentration increased in the solution. As mentioned above, the presence of a number of functional groups in CKL structure could change the interactions among water molecules and thus lowering the surface tension of water.⁵¹ It is worth noting that the higher reduction in the surface tension of water containing KL-METAM samples compared to that of KL-ATAC at any grafting ratio could be attributed to the higher charge density of the former polymer (Table A2). These results illustrated that how the methyl group of KL-METAM could influence the surface properties of lignin macromolecules by altering their overall charge densities.



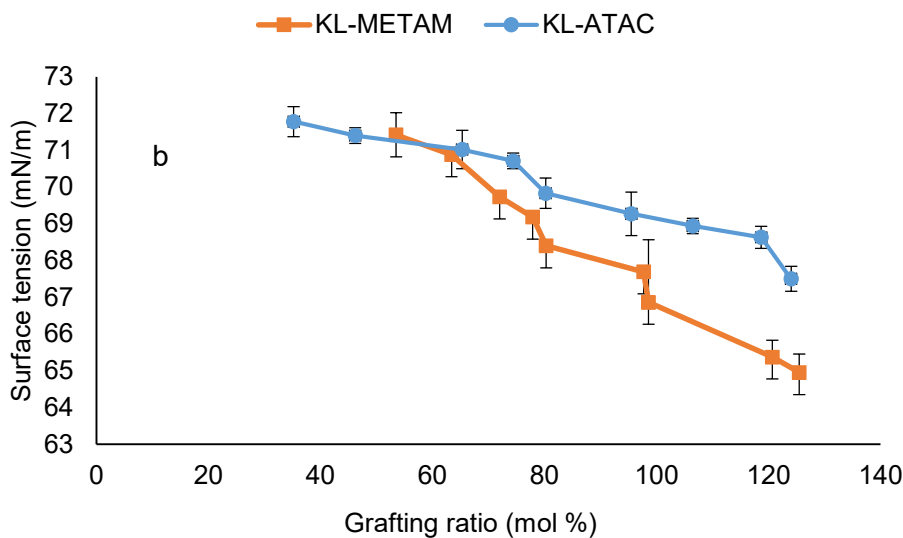


Figure 4. 3 a) Contact angle and b) surface tension of water/CKL droplets

4.4.3 Stability of Lignin Macromolecules

Self assembly and settlement

To understand the self-assembly behaviour of the lignin macromolecules, the changes in the hydrodynamic radius of CKLs in the aqueous solutions were also investigated as a function of time, and results are shown in Figure A6. As observable, the hydrodynamic radius of CKLs increased gradually with time. This time dependence evolution of the R_h indicated that individual lignin polymers agglomerated in the aqueous solution and generated larger clusters. However, KL-METAM polymers created larger aggregates compared to KL-ATAC, in which the largest R_h obtained for CKLs at their highest grafting ratios were 522 and 425 nm, respectively. Accordingly, the polymers with a higher grafting ratio and molecular weight may be engaged more greatly in hydrogen bonding than the smaller ones owing to their greater hydroxyl and amino group contents (Table A2). It was stated that the noncovalent interactions play a significant role in the stabilization of lignin through self-association.⁵² Increasing the M_w of lignin polymers can also promote the self

assembly of CKLs through lowering the surface energy of lignin (i.e., inter-unit interactions) and thus enhance surface properties, such as, van der Waals forces.⁵²

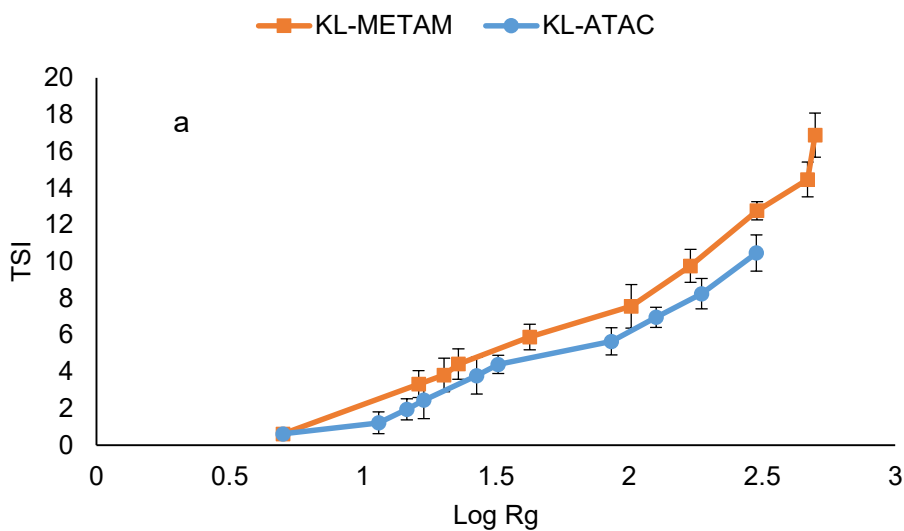
The sedimentation behaviour of CKLs as a function of R_g under regular and accelerated gravitation was illustrated in Figure 4.4. As seen in Figure 4.4-a, the destabilization index of CKLs monotonically increased with increasing R_g , and the maximum TSI values of 16.8 and 10.46 (in a 1 h experiment) were obtained for KL-METAM and KL-ATAC, respectively. The results from Figure 4.1 and Table A2 revealed that, the higher the molecular weight and charge density, the larger the R_g of the resultant lignin polymers would be. This indicated that CKLs with higher molecular weights could form larger aggregates with faster settling performance (i.e., higher TSI as time elapsed, Figure A7).

The sediment layer formed at the bottom of the measurement vial was also thickened by increasing the R_g of CKLs as time elapsed (Figure 4.4-b). Results showed that the self-assembly of KL-METAM was more intense compared to that of KL-ATAC due to its higher molecular weight that manifested by higher TSI value and thicker sediment layers (Figure 4.4-b).

Analytical centrifugation was used to evaluate the long-term colloidal stability of CKLs at various relative centrifugal force (RCF), and results are available in Figure A8. Instability phenomena is directly correlated with a migration rate of particles (i.e., sedimentation) and changing the particle size distribution.⁵³ As reported in the literature,³⁵ considering a spherical shape for the self-assembled particles, the use of the accelerated gravitation technique enables the application of the equation (4):

$$KR^2 = v_m \quad (4)$$

where k is a constant, R is the size of the aggregate and v_m is the sedimentation velocity. This equation indicates a quadratic relation between sedimentation velocity and size of aggregates.^{54,55} Since the largest destabilization index of CKLs was observed at the highest RCF (Figure A8), the sedimentation velocity of lignin macromolecules investigated at 127 RCF and results were shown in Figure 4.4-c. Similar to the sedimentation analysis at non-stirring condition, the precipitation of KL-METAM was more detectable compared to that of KL-ATAC (Figures S3). Owing to more three-dimensional structure of KL-METAM and larger M_w , larger aggregates would be produced when they are exposed to centrifugal rotation, accelerating their precipitation (Figure 4.4-c).



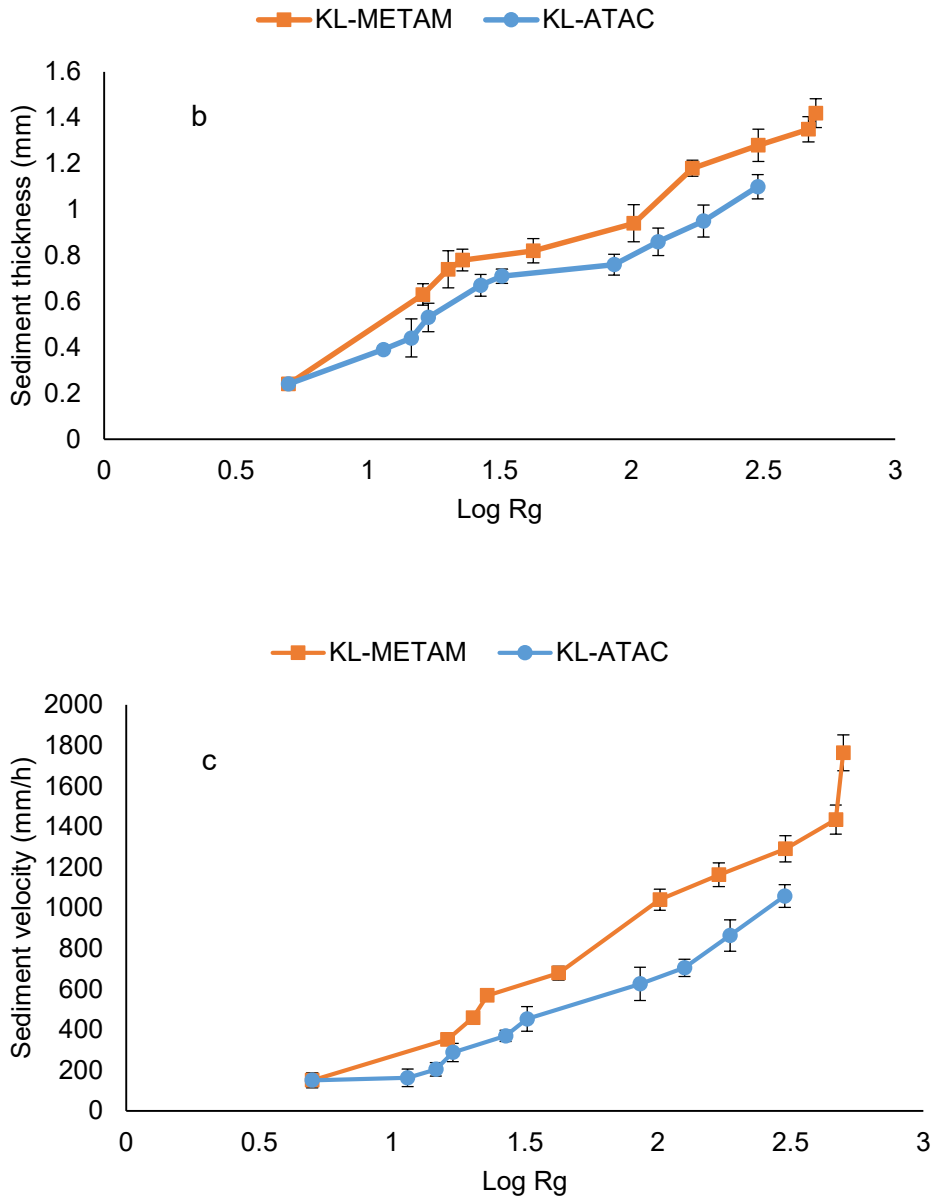


Figure 4. 4 Semi-log plot of a) destabilization index, b) sediment thickness and c) sedimentation velocity (at 127 RCF) of CKLs as a function of R_g .

4.4.4 Adsorption Behavior

Figure A9 shows the changes in the frequency, Δf , and dissipation, ΔD , in the CKL adsorption onto the SiO_2 sensor of QCM to probe the impact of CKL adsorption on the viscoelastic

characteristics of adsorbed layer. Generally, the slope of $\Delta D/\Delta f$ was much steeper for the uptake of CKLs with a higher molecular weight indicating a soft and dissipative film. In contrast, a lower $\Delta D/\Delta f$, as a result of mass addition without a significant dissipation change, was observed for the lower molecular weight samples suggesting a fairly rigid characteristic of adsorbed layer. However, between CKLs, KL-METAM created a more viscose adsorbed layer on silica. In this case, the higher $\Delta D/\Delta f$ ratio reflects more loops of the adsorbed polymer through extended configuration, which would help more water entrapment within the adsorbed adlayer.

As seen in Figure A9, the driving force for CKL adsorption on the QCM sensor is related to hydrogen bonding and electrostatic attractions between the amino group of CKLs and deprotonated silanol groups on the silica surface.⁵⁶ Since the polymerization reaction of METAM with lignin was more significant than that of ATAC monomer (at the same reaction condition), it generated polymers with a higher charge density (Table A2). Obviously, the higher charge density of KL-METAM polymers developed more adsorption of this polymer on the crystal sensor (electrostatic attraction).

The deposition of KL-METAM on the silica surface improved the hydrophilicity of SiO₂ sensor (Figure 4.2-a) more greatly than did KL-ATAC. Moreover, the more three-dimensional structure of KL-METAM may have contributed to its higher dissipation resulting in a bulkier adsorbed layer (Figure 4.1). The higher adsorbed mass and thickness of KL-METAM (233 ng/cm², 2.1 nm) than KL-ATAC (162 ng/cm², 1.2 nm) confirmed the stronger interaction and deposition of KL-METAM on the surface.⁵⁷ Considering the hydrodynamic radius of lignin macromolecules, the theoretical adsorbed mass of CKLs (ΔM) deposited on the QCM sensor was calculated following equation 5:

$$\Delta M_{Theoretical} = \frac{A_s}{4\pi\left(\frac{R_h}{2}\right)^2} \cdot \frac{M}{N} \quad (5)$$

wherein, A_s represents the surface area of QCM sensor (cm^2), R_h expresses the hydrodynamic radius of CKLs (nm), M is the molecular weight of lignin polymer (g/mol), and N represents the Avogadro number (1/mol). The theoretical and experimental adsorbed mass of CKLs upon adsorption on the QCM surface was presented in Figure A10. $\Delta M_{Theoretical}$ results showed that a higher mass was required at lower R_h for a full monolayer coverage of CKLs on the QCM sensor (Figure 4.5-a). However, the experimental adsorption results indicated the greater adsorbed mass of CKL ($\Delta M_{Experimental}$ is about 10^3 times greater than $\Delta M_{Theoretical}$) on SiO_2 surface (Figure A10-b). This could be due to the uneven adsorption of CKLs on the QCM surface and the creation of electrostatic attraction forces between CKLs and SiO_2 surface.⁵⁸ The higher adsorbed mass obtained from QCM experiment, was also suggested the multilayer formation of CKLs on SiO_2 surface even at lower R_h .

Considering the smaller R_h of KL-ATAC (Figure A6), its $\Delta M_{Theoretical}$ was larger than that of KL-METAM. In contrast, the experimental results showed higher adsorbed mass for KL-METAM compared to that of KL-ATAC. That would be interpreted as evidence for the entrapment of more water molecules within its more three-dimensional structure of KL-METAM during the course of adsorption. To have insights into the effect of polymer configuration on its adsorption behaviour, the changes in the slope of frequency and dissipation of the silica sensor at the initial and saturation stages of CKL adsorption was plotted as a function of R_g in Figure 4.5. Accordingly, the polymers with the larger R_g can adsorb more on silica surfaces (i.e., a large negative frequency), while creating a more viscose adsorbed layer (i.e., higher dissipation) in both stages of adsorption process. In addition, the larger R_g of KL-METAM macromolecule, which is correlated with the

more space occupied by the polymer chain⁵⁹ could entrap more water molecule through flexible polymer chain, resulting in a thicker adsorbed layer with more viscoelastic characteristics (more hydrogen bond formation).

The larger R_g of KL-METAM than KL-ATAC also enhanced its adsorption behaviour (Figure A11) through more extensive mechanical entanglement with silica surface, which raised their physical interactions.

As seen in Figure 4.5-a, the fast adsorption of the CKLs occurred at an initial stage of adsorption (steeper $\Delta D/\Delta F$ slope of the curve), and the surface of SiO_2 sensor was gradually covered with polymers as the adsorption proceeded. This might be due to the more accessible sites for adsorption of CKLs at the initial adsorption of adsorption indicating a more dissipative and softer adlayer. The changes in the $\Delta D/\Delta F$ slope in the early and later stages of adsorption of CKLs were attributed to the conformational changes of lignin macromolecules in the adsorbed layer when they possessed different R_g .⁶⁰ The reduction in the slope of the curve (Figure 4.5-b) is an indication that the layer becomes more rigid due to increased packing density at the later stage of adsorption.²³ This analysis highlighted the fate of the molecular structure of CKLs on their adsorption and viscoelastic properties at interface.

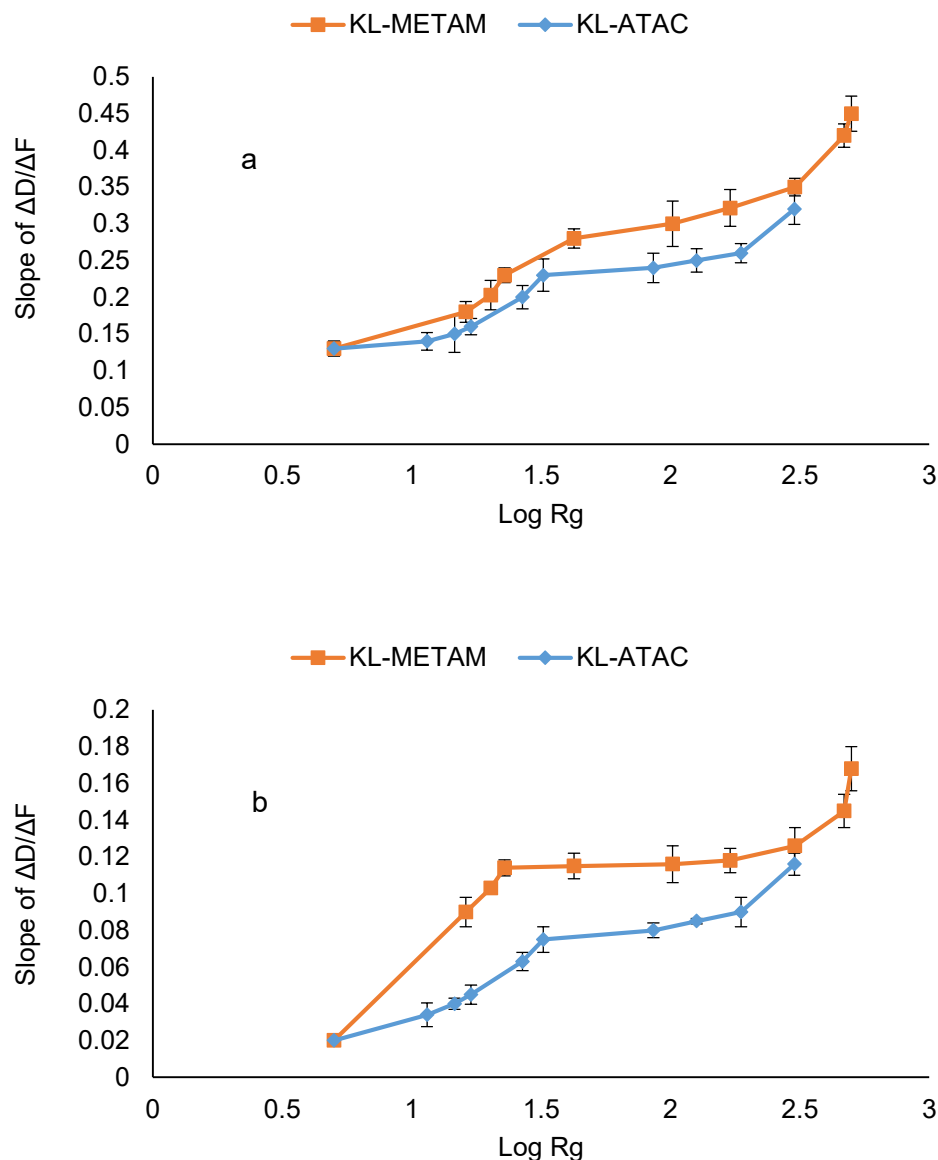


Figure 4. 5 Semi-log plot of changes in frequency and dissipation of the SiO_2 sensor for the adsorption of CKLs at a) initial and b) late stage as a function of R_g

To examine the correlation between adsorption behaviour of CKLs and their stability performance as a result of the self-assembly of the polymers in aqueous solutions, the sediment thickness of CKL was plotted over their adsorbed mass on QCM sensor and results presented in Figure 4.6. Generally, the electrostatic deposition of CKL polymers at solid-liquid interfaces was

demonstrated to be extremely efficient in producing thick sediment layer in aqueous solution (high values of $\Delta M_{\text{Experimental}}$ in Figure A10-b). As stated earlier, the instability of polymer solutions and their adsorption behaviour are directly associated with their surface properties. The higher charge density and molecular weight of CKLs facilitate their self-aggregations via non-covalent interactions (i.e., hydrogen bonding, π - π stacking, chain entanglement, etc), which enable the formation of particles with significant R_h (Figure A6). KL-METAM polymers with larger R_g and R_h showed higher adsorbed mass and adsorbed layer thickness (Figure A10), which in turn generated thicker sediment in the aqueous solution. Considering the higher dissipation values of KL-METAM than KL-ATAC polymers upon adsorption (Figure A11), it can be postulated that the sediment compactness of KL-METAM was lower than KL-ATAC. Owing to its more three-dimensional structure, KL-METAM would trap more water molecules leading to reduce the sediment concentration.

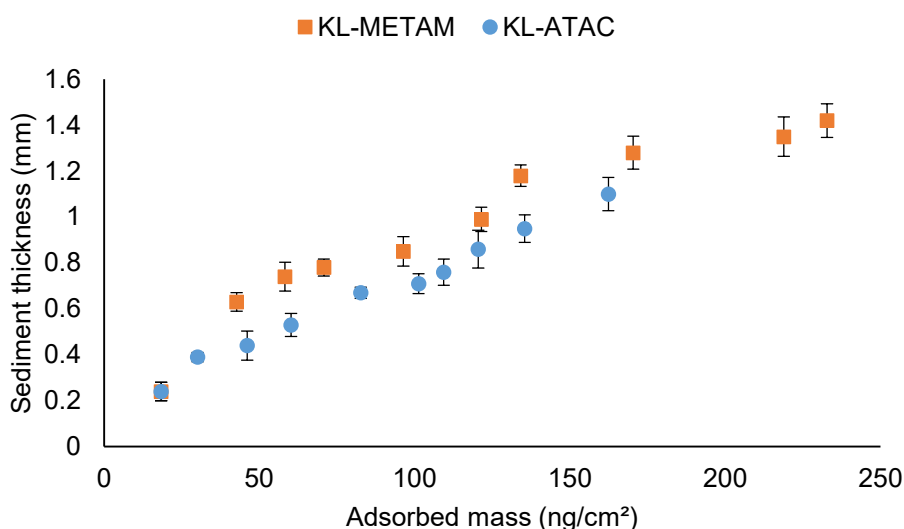


Figure 4. 6 Effect of adsorbed mass on the settling behaviour of CKLs with various M_w

4.4.5 Rheological Behavior of Lignin Macromolecules

The rheological behaviour of macromolecules can be correlated with their chemical structures and polymer chain conformations in solutions.^{42,61,62} The bulk viscoelastic properties of CKLs (4 wt %) at ambient temperature as a function of frequency (ω) are illustrated in Figure A12. Storage moduli (G') is the elasticity property that describes the amount of energy stored in the elastic structure and loss (G'') moduli represents the magnitude of energy dissipated by the material in a cycle of deformation.⁶³ Generally, increasing the grafting ratio of polymers led to an increase in both elastic and viscous moduli of CKLs as a consequence of more attachments of cationic monomer to lignin backbone. In addition, $G' > G''$ reflected the more elastic behavior of CKLs. The changes in G' and G'' were more highlighted in their high frequency regions. The crossover of G' and G'' defined as the gel-like structure of polymer was observed for all the samples at the lower frequency regions (<20 rad/s) and suggested the transition of samples from a liquid-phase dominated to a solid-phase dominated viscoelastic behavior.⁶⁴ This transition also reflected the formation of an interconnected network of polymer chains (i.e., self-organization of polymers in solutions) as discussed in section 3.2.

The higher storage modulus of KL-METAM (Figure A12), specially at the maximum grafting ratio, indicated that its more three dimensional structure than KL-ATAC developed more entanglement between KL-METAM chains. This behavior leads to the topological restriction of molecular motion, decreasing the relative slippage between chains and formation of a stable network structure.

The impact of polymer conformation on the bulk rheological behaviour of CKL solution was further studied, and the changes of storage and loss modulus as a function of R_g was presented in Figure A13. The values of G' or G'' reported in this graph were selected at the highest frequency

region (100 rad/s), in which the changes of storage and loss modulus were more observable. As expected, the viscoelastic properties of CKL solutions was strongly influenced by the molecular weight of the polymer. Generally, CKLs with larger M_w and R_g (as a result of higher grafting ratio), exhibited the higher values of G' and G'' since longer chains led to a higher amount of entanglements present in the tested solutions. However, compared to KL-ATAC, KL-METAM polymer chains with having a larger R_g at any grafting ratio started to lose their mobility and could store more energy when they subjected to oscillation.

To compare the bulk and adlayer viscoelastic properties of CKLs at different molecular sizes (Figure A13), the storage and loss modulus of CKLs from QCM experiment was depicted as a function of R_g (Figure 4.7). In contrast to bulk viscoelastic properties, the loss modulus of CKLs was larger than its storage modulus postulating less elastic behaviour of lignin macromolecules owing to high water content in the adlayer and formation of hydrogen bonding of lignin solution with silica surface.⁶⁵ The greater G'' and lower G' of KL-METAM compared to those of KL-ATAC could be due to higher adsorption affinity of former polymer with SiO_2 surface and its more dissipation values (Figures S6 and 5) as a result of higher charge density and more three dimensional structure of KL-METAM polymer.⁶⁶ It should be stated that the higher values of G' and G'' for the adsorbed adlayer compared with those of bulk CKL solutions is attributed to the higher concentration of lignin macromolecules adsorbed on the surface of the QCM sensor than those in the bulk solution.

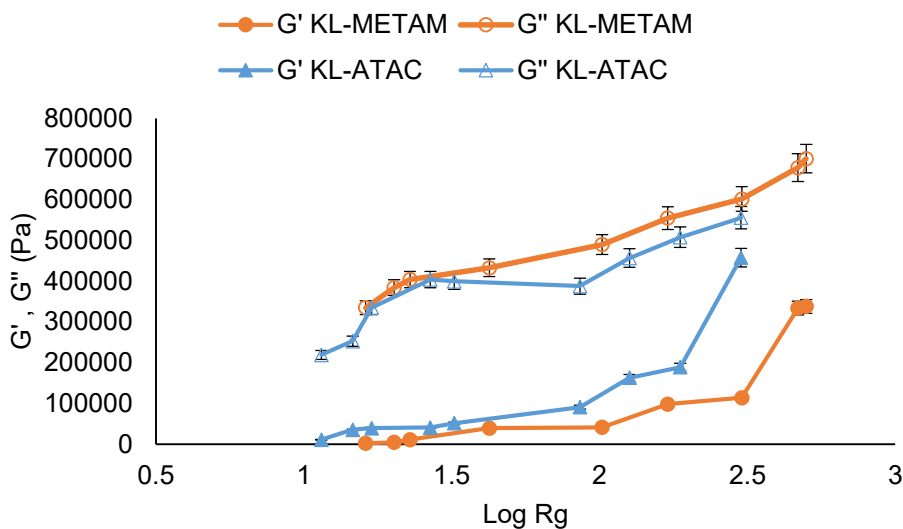


Figure 4. 7 Semi log plot of rheological characteristics of CKLs during adsorption as a function of R_g .

4.4.6 Thermal Behavior of Lignin Macromolecules

In the process of agglomerate formation of lignin, noncovalent interactions can also affect the thermal properties of lignin, in which strong interactions result in a decrease in the thermal molecular motion of the lignin macromolecule.⁵² Thus, the molecular structure of CKLs can significantly contribute to their thermal behaviour.

The glass transition temperature (T_g) and heat capacity (C_p) of polymers were also summarized in Table 4.1, and an increase in T_g value of CKLs were observed with the increase in the monomer content. The T_g of unmodified softwood kraft lignin was reported to be 155°C.⁶⁷ The addition of METAM or ATAC monomer to lignin structure after the polymerization reaction raised the molecular weight of CKLs leading to a reduction in the flexibility and mobility of the polymer chain and enhancement in T_g values.^{68,69} In comparison to KL-METAM, KL-ATAC showed higher T_g values at various grafting ratios. This behaviour can be ascribed to the more compact coil structure of KL-ATAC macromolecule that restricted free molecular movement of main chain.

However, KL-METAM polymer with an extra $-CH_3$ in its structure and more three-dimensional conformations (higher R_g) expressed a higher molecular motion, resulting in a lower T_g at entire grafting ratios. The similar trends were observed elsewhere.⁷⁰

The T_g of a polymer can also be used as an indicator for miscibility of the material. According to the literature, a single T_g demonstrates miscibility between the components (in polymers or composites) while two or more T_g values imply immiscibility (or lower interactions between the components).⁷¹ The results in Table 4.1 suggested that, lignin polymer had more homogenous structure up to approximately 80 wt % grafting ratio. However, an increase in the cationic monomer content to the lignin core yielded a lower uniformity of CKLs because they showed two T_g , the lower T_g value corresponded to the METAM and the higher T_g associated with lignin.

Although T_g of CKLs were altered smoothly as a function of grafting ratio, the values of heat capacity difference at T_g (ΔC_p) were scattered in a range from 0.018 to 0.25 J/g°C. According to the literature,⁷² a high ΔC_p illustrates the high molecular mobility of polymer chains results in a decrease in T_g value. Considering the fact that ΔC_p values of amorphous polymers (i.e., lignin) are in the range of 0.2 to 0.4,⁷³ the lower ΔC_p values of CKLs suggested that their molecular motion was restricted either to the lignin or cationic monomer part.⁷⁴

Table 4. 1 Properties of DSC analysis for CKLs at different grafting ratio.

Sample	Grafting ratio, mol %	T_{g1} (°C)	T_{g2} (°C)	C_{p1} (J/g°C)	C_{p2} (J/g°C)
KL-METAM	53.5	90.8	-	0.052	-
KL-METAM	63.4	91	-	0.45	-
KL-METAM	72	91.1	-	0.042	-

KL-METAM	77.9	91.2	-	0.036	-
KL-METAM	80.3	91.2	141	0.032	0.15
KL-METAM	97.7	91.3	134	0.03	0.12
KL-METAM	98.6	91.5	131	0.024	0.084
KL-METAM	120.7	91.6	133.4	0.02	0.075
KL-METAM	125.5	92.1	161.0	0.018	0.07
KL-ATAC	35.2	92.1	-	0.047	-
KL-ATAC	46.2	92.2	-	0.047	-
KL-ATAC	65.3	92.3	-	0.045	-
KL-ATAC	74.4	92.3	119.2	0.042	0.25
KL-ATAC	80.2	92.4	115.7	0.042	0.21
KL-ATAC	95.5	92.5	171.4	0.041	0.211
KL-ATAC	106.5	92.6	125.9	0.04	0.206
KL-ATAC	118.7	92.7	123.7	0.041	0.2
KL-ATAC	124.04	92.8	108.9	0.04	0.194

4.4.7 Application

Results revealed that KL-METAM polymer with more three dimensional configuration was more efficient in the stability of the system by forming large agglomerates (Figures 3 and S2), which may be beneficial for some applications where the precipitation and removal of suspended materials are crucial such a sedimentation tanks or clarifiers in wastewater treatment plants.⁷⁵ Moreover, KL-METAM adsorbed more on SiO₂ sensor and generated thicker film (Figures 5 and

S6). This macromolecule may be suitable for some applications where bulkiness of the film is critical to adsorb a higher amount of suspended particles (i.e., ions, dye molecules, proteins).⁷⁶ The bulky structure of the film may offer some optical and mechanical.^{77,78} The higher solid-like behaviour of KL-METAM than KL-ATAC in bulk solution (Figures 7 and S8) can make KL-METAM macromolecule an appropriate candidate for producing composites with high mechanical properties.⁷⁹

4.5 Conclusions

In this work, the effect of chain conformation on surface properties, colloidal stability, adsorption capacity and viscoelastic characteristics of lignin polymers was investigated. Double logarithmic plot of R_g as the function of M_w illustrated that KL-METAM might adopt a flexible chain conformation while KL-ATAC exhibited a more compact coil configuration owing to more steric hindrance of extra methyl group of METAM monomer on KL-METAM. The shape factor parameter also revealed that with increasing the monomer content, the morphology of the CKLs transformed from hyperbranched polymer cluster to rigid-rod structure. The contact angle and surface tension of water containing KL-METAM were smaller than those of KL-ATAC for the whole range of R_g . It was observed that the self-assembly of CKL was enhanced with time in which the KL-METAM with larger R_h was aggregated more aggressively than KL-ATAC. The sedimentation studies demonstrated that the destabilization index and settling velocity of KL-METAM solution increased progressively with increasing R_g at both regular and accelerated gravitation owing to its higher self-association capability. At initial and later stages of adsorption, KL-METAM deposited more greatly and generated a bulkier adsorbed layer on the SiO_2 surface due to its higher charge density, three-dimensional structure and more water adsorption. A strong

correlation between the R_g of CKLs and storage (G') or loss modulus (G'') was observed when CKLs oscillated in bulk solution and during course of adsorption. CKLs exhibited more solid-like behaviour in the bulk solution, while they behaved more viscoelastically upon adsorption on SiO_2 . The more three-dimensional structure of KL-METAM and higher chain entanglement in bulk solution resulted in the higher elastic characteristic of KL-METAM. The higher T_g values of KL-ATAC confirmed that its molecular chain movement was restricted due to the more compact conformation of this polymer, enhancing its rigidity. The fundamental understanding on the effect of molecular architecture on the lignin-based polymers will allow for the molecular design of lignin macromolecules with desired characteristics that are crucial for different applications.

4.6 References

- (1) Guo, K., Gao, B., Wang, W., Yue, Q., Xu, X. 2019. Evaluation of molecular weight, chain architectures and charge densities of various lignin-based flocculants for dye wastewater treatment. *Chemosphere* 215, 214-226.
- (2) Naseem, A., Tabasum, S., Zia, K. M., Zuber, M., Ali, M., Noreen, A. 2016. Lignin-derivatives based polymers, blends and composites: A review. *Int. J. Biol. Macromol.* 93, 296-313.
- (3) Sabaghi, S., Fatehi, P. 2019. Phenomenological Changes in Lignin Following Polymerization and Its Effects on Flocculating Clay Particles. *Biomacromolecules* 20(10), 3940-3951.
- (4) Kong, F., Wang, S., Gao, W., Fatehi, P. 2018. Novel pathway to produce high molecular weight kraft lignin–acrylic acid polymers in acidic suspension systems. *RSC Adv.* 8(22), 12322-12336.

- (5) Fang, R., Cheng, X., Xu, X. 2010. Synthesis of lignin-base cationic flocculant and its application in removing anionic azo-dyes from simulated wastewater. *Bioresour. Technol.* 101(19), 7323-7329.
- (6) He, W., Zhang, Y., Fatehi, P. 2016. Sulfomethylated kraft lignin as a flocculant for cationic dye. *Colloids Surf. A Physicochem. Eng. Asp.* 503, 19-27.
- (7) Fang, Z., Sato, T., Smith Jr, R. L., Inomata, H., Arai, K., Kozinski, J. A. 2008. Reaction chemistry and phase behavior of lignin in high-temperature and supercritical water. *Bioresour. Technol.* 99(9), 3424-3430.
- (8) Yang, D., Li, H., Qin, Y., Zhong, R., Bai, M., Qiu, X. 2015. Structure and properties of sodium lignosulfonate with different molecular weight used as dye dispersant. *J Dispers Sci Technol.* 36(4), 532-539.
- (9) Zhang, L., Li, X., Xu, X., Zeng, F. 2005. Correlation between antitumor activity, molecular weight, and conformation of lentinan. *Carbohydr. Res.* 340(8), 1515-1521.
- (10) Vainio, U., Maximova, N., Hortling, B., Laine, J., Stenius, P., Simola, L. K., Gravitis, J., Serimaa, R. 2004. Morphology of dry lignins and size and shape of dissolved kraft lignin particles by X-ray scattering. *Langmuir* 20(22), 9736-9744.
- (11) Petridis, L., Smith, J. C. 2016. Conformations of Low-Molecular-Weight Lignin Polymers in Water. *ChemSusChem* 9(3), 289-295.
- (12) Das, R. K., Pappu, R. V. 2013. Conformations of intrinsically disordered proteins are influenced by linear sequence distributions of oppositely charged residues. *Proc. Natl. Acad. Sci.* 110(33), 13392-13397.

- (13) Liu, Z., Lu, X., Xie, J., Feng, B., Han, Q. 2019. Synthesis of a novel tunable lignin-based star copolymer and its flocculation performance in the treatment of kaolin suspension. *Sep. Purif. Technol.* 210, 355-363.
- (14) Kong, F., Wang, S., Price, J. T., Konduri, M. K., Fatehi, P. 2015. Water soluble kraft lignin–acrylic acid copolymer: Synthesis and characterization. *Green Chem.* 17(8), 4355-4366.
- (15) Contreras, S., Gaspar, A. R., Guerra, A., Lucia, L. A., Argyropoulos, D. S. 2008. Propensity of lignin to associate: light scattering photometry study with native lignins. *Biomacromolecules* 9(12), 3362-3369.
- (16) Deng, Y., Feng, X., Zhou, M., Qian, Y., Yu, H., Qiu, X. 2011. Investigation of aggregation and assembly of alkali lignin using iodine as a probe. *Biomacromolecules* 12(4), 1116-1125
- (17) Zhao, W., Xiao, L. P., Song, G., Sun, R. C., He, L., Singh, S., Simmons, B.A., Cheng, G. 2017. From lignin subunits to aggregates: insights into lignin solubilization. *Green Chem.* 19(14), 3272-3281.
- (18) Hasan, A., Fatehi, P. 2019. Flocculation of kaolin particles with cationic lignin polymers. *Sci. Rep.* 9(1), 1-12.
- (19) Norgren, M., Edlund, H. Lignin: Recent advances and emerging applications. 2014. *Curr. Opin. Colloid Interface Sci.* 19(5), 409-416.
- (20) Van der Gucht, J., Spruijt, E., Lemmers, M., Stuart, M. A. C. 2011. Polyelectrolyte complexes: Bulk phases and colloidal systems. *J. Colloid Interface Sci.* 361(2), 407-422.
- (21) Farrokhpay, S. 2009. A review of polymeric dispersant stabilisation of titania pigment. *Adv. Colloid Interface Sci.* 151(1-2), 24-32.

- (22) Wang, C., Yan, F., Meng, X., Qiao, Y., Qiu, D. 2018. Regulating polymer adsorption on colloid by surface morphology. *Soft Matter*. 14(46), 9336-9342.
- (23) Palmqvist, L., Holmberg, K. 2008. Dispersant adsorption and viscoelasticity of alumina suspensions measured by quartz crystal microbalance with dissipation monitoring and in situ dynamic rheology. *Langmuir* 24(18), 9989-9996.
- (24) Li, J., Li, H., Yuan, Z., Fang, J., Chang, L., Zhang, H., Li, C. 2019. Role of sulfonation in lignin-based material for adsorption removal of cationic dyes. *Int. J. Biol. Macromol.* 135, 1171-1181.
- (25) Pérez-Orozco, J. P., Sánchez-Herrera, L. M., Ortiz-Basurto, R. I. 2019. Effect of concentration, temperature, pH, co-solutes on the rheological properties of *Hyptis suaveolens* L. mucilage dispersions. *Food Hydrocoll.* 87, 297-306.
- (26) Ikeda, S., Murayama, D., Tsurumaki, A., Sato, S., Urashima, T., Fukuda, K. 2019. Rheological characteristics and supramolecular structure of the exopolysaccharide produced by *Lactobacillus fermentum* MTCC 25067. *Carbohydr. Polym.* 218, 226-233.
- (27) Aoki, Y. 1987. Dynamic viscoelastic properties of ABS polymers in the molten state. 5. Effect of grafting degree. *Macromolecules* 20(9), 2208-2213.
- (28) Liu, L., Parameswaran, S., Sharma, A., Grayson, S. M., Ashbaugh, H. S., Rick, S. 2014. Molecular Dynamics Simulations of Linear and Cyclic Amphiphilic Polymers in Aqueous and Organic Environments. *W. J. Phys. Chem. B.* 118, 6491.
- (29) Gharekhani, S., Ghavidel, N., Fatehi, P. 2018. Kraft Lignin–Tannic Acid as a Green Stabilizer for Oil/Water Emulsion. *ACS Sustain. Chem. Eng.* 7(2), 2370-2379.

- (30) Sakai, K. *Quartz Crystal Microbalance with Dissipation Monitoring (QCM-D)*, In *Measurement Techniques and Practices of Colloid and Interface Phenomena*; Springer, Singapore: 45-50, 2019.
- (31) Feiler, A. A., Davies, P. T., Vincent, B. 2011. Adsorption of anionic gold nanoparticles by a layer of cationic microgel particles deposited on a gold-coated, quartz surface: studied by quartz crystal microbalance and atomic force microscopy. *Soft Matter*. 7(14), 6660-6670.
- (32) Mengual, O., Meunier, G., Cayre, I., Puech, K., Snabre, P. 1999. Characterisation of instability of concentrated dispersions by a new optical analyser: the TURBISCAN MA 1000. *Colloids Surf. A Physicochem. Eng. Asp.* 152(1-2), 111-123.
- (33) Parker, B. R., Derry, M. J., Ning, Y., Armes, S. P. 2020. Exploring the Upper Size Limit for Sterically Stabilized Diblock Copolymer Nanoparticles Prepared by Polymerization-Induced Self-Assembly in Non-Polar Media. *Langmuir* 36(14), 3730-3736.
- (34) Tan, C., Feng, B., Zhang, X., Xia, W., Xia, S. 2016. Biopolymer-coated liposomes by electrostatic adsorption of chitosan (chitosomes) as novel delivery systems for carotenoids. *Food Hydrocoll.* 52, 774-784.
- (35) Zielińska, A., Martins-Gomes, C., Ferreira, N. R., Silva, A. M., Nowak, I., Souto, E. B. 2018. Anti-inflammatory and anti-cancer activity of citral: Optimization of citral-loaded solid lipid nanoparticles (SLN) using experimental factorial design and LUMiSizer®. *Int. J. Pharm.* 553(1-2), 428-440.
- (36) Fangueiro, J. F., Andreani, T., Egea, M. A., Garcia, M. L., Souto, S. B., Souto, E. B. 2012. Experimental factorial design applied to mucoadhesive lipid nanoparticles via multiple emulsion process. *Colloids Surf. B.* 100, 84-89.

- (37) Sammons, R.J., Harper, D.P., Labbe, N., Bozell, J.J., Elder, T., Rials, T.G. 2013. Characterization of organosolv lignins using thermal and FT-IR spectroscopic analysis. *BioResources* 8(2): 2752-2767.
- (38) Persson, J., Dahlmon, O., Albertsson, A.C. 2012. Birch xylan grafted with PLA branches of predictable length. *BioResources* 7(3), 3640-3655.
- (39) Russo, D., De Angelis, A., Garvey, C. J., Wurm, F. R., Appavou, M. S., Prevost, S. 2019. Effect of Polymer Chain Density on Protein–Polymer Conjugate Conformation. *Biomacromolecules* 20(5), 1944-1955.
- (40) Ba, X., Wang, H., Zhao, M., Li, M. 2002. Conversion dependence of the z-average mean square radii of gyration for hyperbranched polymers with excluded volume effect. *Macromolecules* 35(10), 4193-4197.
- (41) Kato, T., Okamoto, T., Tokuya, T., Takahashi, A. 1982. Solution properties and chain flexibility of pullulan in aqueous solution. *Biopolymers* 21(8), 1623-1633.
- (42) Cai, W. D., Qiu, W. Y., Ding, Z. C., Wu, L. X., Yan, J. K. 2019. Conformational and rheological properties of a quaternary ammonium salt of curdlan. *Food Chem.* 280, 130-138.
- (43) Ruckdeschel, P., Dulle, M., Honold, T., Förster, S., Karg, M., Retsch, M. 2016. Monodisperse hollow silica spheres: an in-depth scattering analysis. *Nano Res.* 9(5), 1366-1376.
- (44) Li, W., Cui, S. W., Wang, Q. 2006. Solution and conformational properties of wheat β -D-glucans studied by light scattering and viscometry. *Biomacromolecules* 7(2), 446-452.
- (45) Schärfl, W. *Light Scattering from Polymer Solutions and Nanoparticle Dispersions*, Springer Science & Business Media: 2007.

- (46) Nie, T., Zhao, Y., Xie, Z., Wu, C. 2003. Micellar Formation of Poly (caprolactone-b lock-ethylene oxide-b lock-caprolactone) and Its Enzymatic Biodegradation in Aqueous Dispersion. *Macromolecules* 36(23), 8825-8829.
- (47) Baek, J., Wahid-Pedro, F., Kim, K., Kim, K., Tam, K. C. 2019. Phosphorylated-CNC/modified-chitosan nanocomplexes for the stabilization of Pickering emulsions. *Carbohydr. Polym.* 206 520-527.
- (48) Barthel, M.J., Rinkenauer, A.C., Wagner, M., Mansfeld, U., Hoepfner, S., Czaplewska, J.A., Gottschaldt, M., Träger, A., Schacher, F.H., Schubert, U.S. 2014. Small but powerful: co-assembly of polyether-based triblock terpolymers into sub-30 nm micelles and synergistic effects on cellular interactions. *Biomacromolecules* 15(7), 2426-2439.
- (49) Binks, B. P., Clint J. H. 2002. Solid wettability from surface energy components: relevance to Pickering emulsions, *Langmuir* 18,1270-1273.
- (50) Zhang, Z., Wang, W., Korpacz, A. N., Dufour, C. R., Weiland, Z. J., Lambert, C. R., Timko, M. T. 2019. Binary Liquid Mixture Contact-Angle Measurements for Precise Estimation of Surface Free Energy. *Langmuir* 35(38), 12317-12325.
- (51) Szymczyk, K., Jańczuk, B. 2011. Wettability of polymeric solids by aqueous solutions of anionic and nonionic surfactant mixtures, *J. Adhes. Sci. Technol.* 25, 2641–2657.
- (52) Mishra, P. K., Ekielski, A. 2019. The self-assembly of lignin and its application in nanoparticle synthesis: A short review. *Nanomaterials* 9(2), 243.
- (53) Fernandes, A. R., Ferreira, N. R., Figueiro, J. F., Santos, A. C., Veiga, F. J., Cabral, C., Silva, A.M., Souto, E. B. 2017. Ibuprofen nanocrystals developed by 22 factorial design experiment: A new approach for poorly water-soluble drugs. *Saudi Pharm J.* 25(8), 1117-1124.

- (54) Chang, C. W., Liao, Y. C. 2016. Accelerated sedimentation velocity assessment for nanowires stabilized in a non-Newtonian fluid. *Langmuir* 32(51), 13620-13626.
- (55) Lim, A. S., Roos, Y. H. 2015. Stability of flocculated particles in concentrated and high hydrophilic solid layer-by-layer (LBL) emulsions formed using whey proteins and gum Arabic. *Food Res. Int.* 74, 160-167.
- (56) Alagha, L., Wang, S., Xu, Z., Masliyah, J. 2011. Adsorption kinetics of a novel organic–inorganic hybrid polymer on silica and alumina studied by quartz crystal microbalance. *J. Phys. Chem. C.* 115(31), 15390-15402.
- (57) Long, Y., Wang, T., Liu, L., Liu, G., Zhang, G. 2013. Ion specificity at a low salt concentration in water–methanol mixtures exemplified by a growth of polyelectrolyte multilayer. *Langmuir* 29(11), 3645-3653.
- (58) Groot, R. D. 2003. Electrostatic interactions in dissipative particle dynamics—simulation of polyelectrolytes and anionic surfactants. *J. Chem. Phys.* 118(24), 11265-11277.
- (59) Yang, D., Yan, B., Xiang, L., Xu, H., Wang, X., Zeng, H. 2018. Understanding the surface properties and rheology of a silica suspension mediated by a comb-type poly (acrylic acid)/poly (ethylene oxide)(PAA/PEO) copolymer: effect of salinity. *Soft matter.* 14(23), 4810-4819.
- (60) Kikkawa, Y., Yamashita, K., Hiraishi, T., Kanetsato, M., Doi, Y. 2005. Dynamic adsorption behavior of poly (3-hydroxybutyrate) depolymerase onto polyester surface investigated by QCM and AFM. *Biomacromolecules* 6(4), 2084-2090.
- (61) Boyle, B. M., Heinz, O., Miyake, G. M., Ding, Y. 2019. Impact of the Pendant Group on the Chain Conformation and Bulk Properties of Norbornene Imide-Based Polymers. *Macromolecules* 52(9), 3426-3434.

- (62) Ye, J., Hua, X., Zhao, Q., Zhao, W., Chu, G., Zhang, W., Yang, R. 2020. Chain conformation and rheological properties of an acid-extracted polysaccharide from peanut sediment of aqueous extraction process. *Carbohydr. Polym.* 228, 115410.
- (63) Salleh, F. M., Hassan, A., Yahya, R., Azzahari, A. D. 2014. Effects of extrusion temperature on the rheological, dynamic mechanical and tensile properties of kenaf fiber/HDPE composites. *Compos. B. Eng.* 58, 259-266.
- (64) Weng, L., Chen, X., Chen, W. 2007. Rheological characterization of in situ crosslinkable hydrogels formulated from oxidized dextran and N-carboxyethyl chitosan. *Biomacromolecules* 8(4), 1109-1115.
- (65) Spruijt, E., Biesheuvel, P. M., de Vos, W. M. 2015. Adsorption of charged and neutral polymer chains on silica surfaces: The role of electrostatics, volume exclusion, and hydrogen bonding. *Phys. Rev. E.* 91(1), 012601.
- (66) Lucklum, R., Behling, C., Hauptmann, P. 1999. Role of mass accumulation and viscoelastic film properties for the response of acoustic-wave-based chemical sensors. *Anal. Chem.* 71(13), 2488-2496.
- (67) Kubo, S., Kadla, J. F. 2005. Kraft lignin/poly (ethylene oxide) blends: effect of lignin structure on miscibility and hydrogen bonding. *J. Appl. Polym. Sci.* 98(3), 1437-1444.
- (68) Zhang, Y., Li, X., Li, H., Gibril, M. E., Han, K., Yu, M. 2013. Thermal and rheological properties of cellulose-graft-polyacrylamide synthesized by in situ graft copolymerization. *RSC Adv.* 3(29), 11732-11737.
- (69) Nejad, F. M., Nazari, H., Naderi, K., Karimiyan Khosroshahi, F., Hatefi Oskuei, M. 2017. Thermal and rheological properties of nanoparticle modified asphalt binder at low and intermediate temperature range. *Pet Sci Technol.* 35(7), 641-646.

- (70) Shi, Y., Cao, X., Luo, S., Wang, X., Graff, R. W., Hu, D., Guo, R., Gao, H. 2016. Investigate the glass transition temperature of hyperbranched copolymers with segmented monomer sequence. *Macromolecules* 49(12), 4416-4422.
- (71) Mousavioun, P., Halley, P. J., Doherty, W. O. 2013. Thermophysical properties and rheology of PHB/lignin blends. *Ind Crops Prod.* 50, 270-275.
- (72) Li, H., McDonald, A. G. 2014. Fractionation and characterization of industrial lignins. *Ind Crops Prod.* 62, 67-76.
- (73) Hatakeyama, T., Hatakeyama, H. 1995. Effect of chemical structure of amorphous polymers on heat capacity difference at glass transition temperature. *Thermochim. Acta.* 267, 249-257.
- (74) Hatakeyama, T., Yamashita, S., Hatakeyama, H. 2019. Thermal properties of lignin-based polycaprolactones. *J. Therm. Anal. Calorim.* 1-9.
- (75) Ge, Y., Li, Z. 2018. Application of lignin and its derivatives in adsorption of heavy metal ions in water: a review. *ACS Sustain. Chem. Eng.* 6(5), 7181-7192.
- (76) Alipoormazandarani, N., Fatehi, P. 2020. Interaction Mechanism of Anionic Lignin and Cationic Soft Surface in Saline Systems. *J. Phys. Chem. B.* 124(39), 8678-8689.
- (77) Janshoff, A., Galla, H. J., Steinem, C. 2000. Piezoelectric mass-sensing devices as biosensors—an alternative to optical biosensors?. *Angew. Chem. Int. Ed.* 39(22), 4004-4032.
- (78) Dixon, M. C. 2008. Quartz crystal microbalance with dissipation monitoring: enabling real-time characterization of biological materials and their interactions. *J Biomol Tech.* 19(3), 151.

- (79) Gupta, A., Simmons, W., Schueneman, G. T., Hylton, D., Mintz, E. A. 2017. Rheological and thermo-mechanical properties of poly (lactic acid)/lignin-coated cellulose nanocrystal composites. *ACS Sustain. Chem. Eng.* 5(2), 1711-1720.

Chapter 5: Polarity of Cationic Lignin Polymers: Physicochemical Behavior in Aqueous Solutions and Suspensions

5.1 Abstract

The structure of cationic monomers would significantly impact the polarity of lignin after polymerization. Cationic hydrolysis lignin (CHL) polymers were produced via polymerizing hydrolysis lignin (HL) with [3-(Methacryloylamino) propyl] trimethylammonium chloride (MAPTAC) or [-2-(methacryloyloxy)ethyl] trimethyl ammonium chloride (METAC). METAC monomer had oxygen atom with larger electronegativity on its molecular structure while MAPTAC monomer contained nitrogen atom as well as an extra non-polar group of CH₂ facilitating the investigation on the fate of polarity of CHLs on their physicochemical performance in an aqueous system. CHL polymers were analyzed and their interaction with clay particles was determined in colloidal systems. CHLs were designed to have similar charge densities (2.1-2.2 mmol/g) and molecular weights (55,000 – 60,000 g/mol). The hydrodynamic radius, H_y, and radius of gyration, R_g, of HL-METAC were larger than those of HL-MAPTAC implying the more 3-dimensional structure of HL-METAC in aqueous solutions. The stability ratio of kaolin particles affirmed the better performance of HL-METAC than HL-MAPTAC, which would reflect the better flocculation efficiency of HL-METAC. The results also revealed that salt and urea aqueous solutions affected the H_y, R_g and configuration of CHL polymers, which would alter the flocculation efficiency of HL-METAC and HL-MAPTAC polymers in kaolin suspensions.

Keywords: Lignin, Polarity, Adsorption, Flocculation, Polymer structure

5.2 Introduction

Flocculation processes have great uses in many industrial applications, such as water and wastewater treatment, mineral recovery, and paper manufacturing. Clay, and in particular kaolin, has been recognized as one of the most problematic minerals in the wastewater treatment of different industries due to the formation of highly stable suspensions and challenging separations.¹⁻³ In this context, the stability of kaolin suspension is stemmed from the colloidal size, anisotropic shape, and the negatively charged basal faces of kaolin particles.^{4,5} As kaolin particles carry slightly negative charges, cationically charged polymers are generally used for the flocculation of kaolin particles in suspensions.^{6,7} Recently, natural polymeric flocculants have received great attention to destabilize colloidal systems.⁸⁻¹⁰ As a natural macromolecule, lignin is one of the abundant resources of aromatic compounds with a three-dimensional structure composed of phenylpropane connected by various linkages.^{11,12} Enzymatically hydrolyzed lignin, which is called hydrolysis lignin (HL), is a by-product of an enzymatic process for sugar production from lignocellulosic biomass, but it has a limited industrial use currently.¹³⁻¹⁵ To valorize this lignin, cationic polymerization has been a promising method as it improves the water solubility and charge density of hydrolysis lignin.¹⁶ Our previous studies focused on the polymerization of kraft lignin with [2-(acryloyloxy)ethyl]trimethyl ammonium chloride (ATAC), [2-(methacryloyloxy)ethyl] trimethyl ammonium methyl sulfate (METAM) and [2-(methacryloyloxy)ethyl] trimethylammonium chloride (METAC) in an acidic environment to produce cationic flocculants for simulated wastewater effluents.^{17,7} However, to the best of our knowledge, [3-(Methacryloylamino)propyl] trimethylammonium chloride (MAPTAC) has not been studied for producing bioflocculants. Although both METAC and MAPTAC monomers contain amino groups

to introduce cationic charges to lignin, their structures are different, which may affect their polymerization performance and the properties of induced lignin polymers. The structure of polymers imparts varied polarities to polymers, which may affect their behavior in aqueous solutions. In the past, strategies were developed to design polymers with different polarities and solubilities through polymerization reactions.^{18,19} The polarity of polymers may also affect their hydrogen bonding development and electrostatic interaction with other colloidal particles.^{20,21} The first objective of this work was to study how different polarities of the generated cationic lignin-based polymers would affect their physicochemical properties in aqueous solutions. Furthermore, studies reported the impact of the polarity of polymers on the flocculation efficiency and stability of colloidal particles. Recently, the effect of chitosan's polarity on the particle agglomeration, floc sizes, zeta potential, and turbidity of kaolinite suspension was investigated.²² The results showed the direct relationship between the size and degree of polarity of formed flocs.²² In another study, sulfonated polystyrenes with varied sulfonation degrees were produced to precipitate a model asphaltene suspension, and the polymers with greater polarities had better flocculation performance.²³ These studies suggest that the polarities of polymers may directly affect their performance in interacting with other particles in suspensions. In this regard, the impact of lignin-based polymers (with different polarities) on the flocculation of kaolin suspension is unclear, which is the second objective of the current study.

To investigate the mechanism of flocculation, salts and urea have been used in the past.^{24,25} Salts generally screen the charges of colloidal particles revealing the influence of charges in the interaction of colloidal particles.²⁶ Urea has also been extensively utilized for diminishing hydrogen bonding and exposing hydrophobic interaction of colloidal particles in aqueous systems. For example, in one study linoleic modified chitosan (LA-chitosan) was prepared and its

adsorption on trypsin and the particle size of LA-chitosan/trypsin in salt and urea environment were investigated.²⁷ It was reported that the adsorption efficiency of LA-chitosan on trypsin dropped as salt and urea concentration increased.²⁷ The third objective of this study was to utilize salt and urea in the aqueous suspension system for understanding the adsorption and flocculation performance of the lignin-based polymers. The main novelties of the present study were the exploitation of the role of the polarity of cationic lignin-based polymers in altering their structures in colloidal systems, and ultimately in their interaction and flocculation of kaolin particles.

5.3 Experimental Section

5.3.1 Materials

Enzymatically hydrolyzed lignin (HL) used in this study was received from FPIInnovations, Pointe-Claire, QC, Canada, which was derived from hardwood chips. However, the purity of HL source was not defined. [2-(methacryloyloxy) ethyl] trimethyl ammonium chloride solution (METAC), 80 wt.% in H₂O, [3-(Methacryloylamino) propyl] trimethylammonium chloride (MAPTAC), 50 wt.% in H₂O, sodium persulfate (Na₂S₂O₈), poly diallyl dimethyl-ammonium chloride (PDADMAC, 100,000–200,000 g/mol), 20 wt.% in water, deuterated chloroform (CDCl₃), pyridine (C₅H₅N), cyclohexanol (C₆H₁₂O), chromium(III) acetylacetonate, 2-chloro-4,4,5,5-tetramethyl-1,3,2-dioxaphospholane, d₆-dimethyl sulfoxide (d₆-DMSO), deuterium oxide (D₂O), urea, potassium chloride (KCl), sulfuric acid, sodium hydroxide and kaolin clay were all purchased from Sigma-Aldrich company. Ethanol (95 vol.%) was received from the Fisher Scientific company. Potassium polyvinyl sulfatate (PVSK, 100,000–200,000 g/mol, 97.7 wt.% esterified) was obtained from Wako Pure Chem. Ltd., Osaka, Japan. Dialysis membrane (Cut off of 1,000 g/mol)

was provided by Spectrum Labs. Deionized water with a resistivity of less than 18 M Ω /cm was generated using a Millipore water purification system, and it was used in all the experiments.

5.3.2 Theoretical analysis

The Gaussian 09 software Rev. D.01 (Gaussian, Wallingford, CT, USA)²⁸ with the density functional theory (DFT) method at the B3LYP/6-311++G (d, p) theory level was used to determine the dipole moment of a lignin unit attached to cationic monomer (METAC or MAPTAC).

5.3.3 Cationization of hydrolysis lignin

Cationic hydrolyzed lignin (CHL) was synthesized in a semi-dried condition based on the method developed in the previous work [17]. In this set of experiments, 2 g of HL was mixed with water to make a mixture of 60 wt.% solid content. The polymerization reaction was performed at different reaction temperatures (70, 80, and 90°C), times (1, 2, and 3 h), Na₂S₂O₈ dosages (0.75 wt.% and 1.5 wt.% based on lignin mass) and cationic monomer (METAC or MAPTAC)/lignin mole ratios (0.4, 0.8, 1.2, 1.6 and 2.4 mol/mol).

To obtain the CHLs with similar charge densities and molecular weights, the polymerization reaction was initiated by adding sodium persulfate (1.5 wt%) to the lignin suspension to generate sulfite radicals. The conditions for HL-METAC production were METAC/HL ratio of 0.8 mol/mol, 70 °C reaction temperature, and 2 h reaction time; and for HL-MAPTAC production were MAPTAC/HL ratio of 1.6 mol/mol, 3 h reaction time and 80 °C reaction temperature. The pH of the reactions was adjusted to 3.6 \pm 0.2, and the systems were deoxygenated by purging nitrogen gas for several minutes before the polymerization reactions. Upon completion, the systems were cooled to room temperature and their cationic lignin polymers were precipitated via

mixing the reaction products with 80 wt.% ethanol. The mixtures were then centrifuged at 3500 rpm for 10 min to separate the CHL from the rest of the suspensions. After that, the precipitates were mixed with deionized water, neutralized and kept in membrane tubes for 48 h of dialysis to remove any inorganic salts and unreacted cationic agents. Subsequently, the purified CHLs were dried in an oven at 60°C and used in this study.

5.3.4 Characterization of HL and CHL

Charge density determination

CHLs were partly soluble in water. In this experiment, 0.2 g of dried CHLs was mixed with 20 mL of deionized water and shaken for several hours. After centrifugation at 1000 rpm for 5 min, the supernatants (i.e., the soluble part of CHLs) were collected and titrated against the PVSK solution (0.005 M) using a Particle Charge Detector, PCD (Mütek PCD 04 titrator, Herrsching, Germany) for determining their charge density. The charge density of the insoluble part of CHLs was also measured by the PCD instrument following the back titration method according to previously established work. Finally, the overall charge densities of CHLs considering the soluble and insoluble charge densities of CHLs were reported in this study.²⁹

Phenolic hydroxy group analysis

The phenolic hydroxy group of CHLs was measured using an automatic potentiometric titrator, 785 Titrino. In this analysis, 0.06 g of CHLs was dissolved in 1 mL of KOH (0.8 M) and then 4 mL of para-hydroxybenzoic acid (0.5 wt %) was added to the system as an internal standard. Afterward, 100 mL of deionized water was added to the system and mixed for 2 h. The solutions were then titrated against the 0.1 M HCl standard solution.⁴⁷

Molecular weight analysis

Gel permeation chromatography (Malvern, GPCmax VE2001 Module + Viscotek TDA305) was used for determining the molecular weight of CHL. This instrument was equipped with multi-detectors (UV, RI, viscometer, low and right-angle laser detectors), and 5 wt.% acetic acid was used as eluent/solvent. Polyanalytic PAA206 and PAA203 columns were used, and the temperature of columns and their flow rates were adjusted to 35°C and 70 mL/min, respectively. In this analysis, 35 mg of CHLs were dissolved in 10 mL of a 5% acetic acid solution and mixed for 24 h at room temperature. Afterward, the filtration of the samples was carried out using a 0.2 µm nylon filter (13 mm diameter) and the samples were used for the molecular weight analysis.

Nitrogen content analysis

The organic elements of CHL and HL were determined via an elemental analyzer (Vario EL Cube, Elemental Analyzer, Germany). In this experiment, 2 mg of dried samples were transferred into the carousel chamber of the instrument and combusted at 1200 °C to reduce the generated gasses to determine their carbon, hydrogen, nitrogen, sulfur, and oxygen contents. Based on the nitrogen content of the samples, which was originated from the cationic monomer of CHLs, the grafting ratio of samples was identified according to a previous study:³⁰

$$\text{Grafting ratio (mol\%)} = \frac{\frac{N}{14} \times Mw}{100 - (\frac{N}{14} \times Mw)} \times 100 \quad (1)$$

where N is the nitrogen content of CHL or HL (%wt.), and Mw is the molecular weight of METAC or MAPTAC (207.7 or 220.74 g/mol, respectively).

The chemical structures of HL and CHL polymers were also analyzed using the Fourier Transformed Infrared (FTIR) and ^1H NMR as explained in the supporting information.

Hydrodynamic radius

Dynamic light scattering (DLS) instrument, BI-200SM Brookhaven Instruments, USA, was used for measuring the hydrodynamic radius (H_y) of the HL and CHL polymers. In this set of experiments, 1 g/L of HL and CHLs were prepared with deionized water. The solutions were then stirred at 300 rpm for 24 h and room temperature. In another set of experiments, lignin samples were mixed with KCl or urea solutions (10mM) to produce 1 g/L of salt or urea containing lignin solutions. Afterward, 20 mL of CHLs were filtered using a 0.45 μm disposable syringe filter. Then, the hydrodynamic radius of lignin samples was determined using the method described by Yan and coworkers.³¹ The light source of the instrument was set at the maximum power of 35 mW and the wavelength of 637 nm. The scattering angle was also fixed at 90°. The reported data of this analysis was the average value of three repetitions.

Radius of gyration

Static light scattering (SLS) instrument that was attached to a goniometer (Brookhaven BI-200SM, Holtsville, NY, USA) was used to measure the radius of gyration (R_g) of HL and CHLs. Lignin solutions with different concentrations (0.2-2 wt.%) were prepared in an alkaline aqueous solution (0.5 M NaOH) at room temperature. Sodium hydroxide solution was used as a solvent to solubilize lignin polymers since they were not completely soluble in water at pH 7. Moreover, NaOH solvent yielded the largest difference between refractive indices providing the best signal at a given sample concentration in this analysis (i.e., more accuracy).³² In another set of analyses, the predetermined amount of salt or urea was added to the aforementioned lignin solutions to study the effect of salt

and urea on R_g of HL or CHL. A nylon syringe filter (30 mm diameter and 0.45 μ m pore size) was then used for sample filtration. The intensities of lignin samples at various angles (15 ° - 155 °) were analyzed using the SLS instrument, while the wavelength of laser polarized light was set at 637 nm. BIC Zimm Plot software (Holtsville, NY, USA) was used to obtain the R_g of the polymers.³³

Also, ³¹P-NMR was acquired to analyze the chemical structures of lignin polymers. In this analysis, phosphitylation reaction of HL and CHL samples were conducted with 2-chloro-4,4',5,5'-tetramethyl-1,3,2-dioxaphospholane. First, 36 mg of the samples were dissolved in a 1.6/1 v/v CDCl₃ and C₅H₅N solvent mixtures. After several minutes of mixing, the appropriate amounts of cyclohexanol (0.2 mmol/mL) and chromium (III) acetylacetonate (0.20 mmol/mL) solutions were added to the mixtures, while the former one was used as an internal standard and the latter one was used as the relaxation agent in the NMR analysis. Finally, 102 μ L of phosphitylation agent was added to the dissolved solutions to initiate the phosphitylation reaction. ³¹P-NMR spectra were acquired with a 90° pulse width and a 5 sec relaxation delay following 512 scans.⁴⁶

5.3.5 Adsorption test

To study the adsorption of CHL samples on kaolin particles, different dosages (2-128 mg/g based on kaolin) of HL and CHLs (1 g/L) were added to the kaolin suspension. The pH of kaolin suspension was adjusted to 6. Then, the prepared samples stirred at 150 rpm and 30 °C in a water bath shaker for one hour. After that, the mixtures were centrifuged (4500 rpm for 10 min) and filtered. The concentration of HL and CHL remained in the supernatants was measured using a UV-Vis spectrophotometer (Genesys 10S UV-vis, Thermo Fisher Scientific, USA) at the wavelength of 205 nm using a predetermined calibration curve. To study the impact of salt and

urea on the adsorption performance of CHLs, the optimum dosage of 80 mg/g (based on kaolin) of CHLs was maintained in the kaolin suspension (0.5 g/L) at various salt and urea concentrations (i.e., 0.01-1000 mM) and the above-mentioned analysis was repeated for these samples.

5.3.6 Flocculation analysis via photometric dispersion analyzer (PDA)

The aggregation of kaolin particles was monitored using a photometric dispersion analyzer (PDA 3000, Rank Brothers Ltd). In this setup, the PDA instrument was connected to a dynamic drainage jar (DDJ) and fitted with a 70-mm mesh screen. The kaolin suspension was added to the DDJ cell containing water to make a 1 g/L concentration while stirring at 300 rpm and pH 6. Kaolin suspension was pumped from DDJ cell through a 3 mm transparent plastic tube into the photocell of the PDA that measured the fluctuations of transmitted light. Changes in the intensity of transmitted light identify two major components: V_{DC} that represents average transmitted light intensity and V_{RMS} that defines the root mean square of the fluctuations in the transmitted light. The considerable increase in the proportion of V_{RMS} to V_{DC} signal, known as a ratio (R) or flocculation index, is an indicator of particle growth.³⁴

After kaolin suspension reaching equilibrium in the light transmission, the CHLs were added to the system (0.2-20 mg/g of CHL in kaolin system) and R was measured every second until it reached a plateau. By elapsing time, a significant increase in the size of flocs occurred and the flocculation rate, ki , was determined (i.e., the maximum flocculation growth rate ratio). The stability ratio (W) for a specific flocculation rate was defined according to equation 2:

$$W = \frac{K_{fast}}{K_i} \approx \frac{(\frac{dR}{dt})_{fast}}{(\frac{dR}{dt})_i} \quad (2)$$

where k_{fast} is the fastest maximum growth rate in the flocculation process defined by $\log W=0$. In this system, $\log W=\infty$ represents a stable kaolin suspension.³⁵ In this analysis, the fastest aggregation rate of kaolin was selected as the reference K_{fast} , with which the initial aggregation rate, K_i , of kaolin particles in the presence of CHL polymers was compared.

5.3.7 Flocculation analysis via focused beam reflectance measurement (FBRM)

The flocculation behavior of CHL in the kaolin suspension and the properties of formed flocs were studied at different CHL/kaolin ratios by monitoring the chord length of the flocs in real-time using an FBRM instrument, G400, Mettler Toledo, E25, Switzerland. The focal point position of the laser beam was set at $-20 \mu\text{m}$.^{36,37} In this experiment, 200 mL of kaolin suspension (25 g/L) was dispensed in a 500 mL beaker at pH 6. Then, the probe was inserted into the suspension 20 mm below its surface. The impeller intensity was adjusted at 200 rpm. After reaching a steady-state mixing status, the desired amounts of CHLs (i.e., based on the optimum dosage from PDA analysis) were added to the system and the chord length of particles was measured every 5 s. The analysis of the experimental results was conducted using 90 log channels over the range of 1 and 1000 μm using the IC-FBRM software. To investigate the effect of KCl and urea on CHLs/kaolin flocculation, a similar analysis was conducted using different concentrations of salt and urea (0.1-1000 mM) under the experimental conditions stated in this section.

5.4 Results and Discussion

5.4.1 Structure of lignin polymer

In this work, HL-METAC and HL-MAPTAC were produced following free radical polymerization (Scheme 5.1).^[7,17] As both CHL polymers had asymmetric molecular structures, the dipole

moment (μ) vectors on each polymer cannot cancel each other creating polar molecules. As seen in Scheme 5.1, the larger electronegativity of the oxygen atom in the METAC structure of HL-METAC makes this macromolecule interact more with colloidal particles in an aqueous solution (i.e., electrostatic interactions). Moreover, the MAPTAC monomer contains an extra non-polar group of CH_2 in its molecule (Scheme 5.1), which would make the overall polarity of HL-MAPTAC less than that of HL-METAC. To quantify the polarity of CHLs, Gaussian 09 software was used to simulate the structure of CHLs. The source of lignin used in this study was hardwood, which consists of both sinapyl and coniferyl alcohol units.³⁸ Hardwood lignin (also known as guaiacyl (G) - syringyl (S) lignin), composed of primary monolignols coniferyl alcohol and sinapyl alcohol-derived units in different ratios.³⁸ The ^{31}P NMR spectrum and hydroxy groups of HL (Figure A14 and Table A3 in supporting information) confirmed that lignin macromolecule was composed of 4.13 mmol/g aliphatic OH, 0.95 mmol/g phenolic OH and 0.17 mmol/g COOH. The phenolic OH of HL was composed of 0.66, 0.27, and 0.02 mmol/g syringyl, guaiacyl, and phenolic diphenyl (5-5') subunits, respectively. Therefore, the S type lignin with the highest amount of OH in the phenolic part was chosen for this molecular simulation. After the attachment of the first monomer, the repeating monomer units of METAC and MAPTAC in HL-METAC and HL-MAPTAC are the same. Hence, for measuring the polarity of CHL molecules, the dipole moment of syringyl lignin that has only one group of attached METAC or MAPTAC was considered for the simulation. A similar assumption was also considered in the literature for analyzing the adsorption behavior of lignin-based polymers.³⁹ The dipole moment is an important physical property of a molecule that is vital in determining molecular polarity and is a key factor for understanding and quantifying the intermolecular interactions.^{40,41} Dipole moments occur when there is a charge separation between two ions in an ionic bond or between atoms in a covalent bond

due to the differences in their electronegativity, which tends to orient a molecule in a polarized dielectric.^{42,43} The overall polarity of a molecule not only depends on the polarity of its bonds but also on its molecular shape and geometry. Accordingly, the dipole moments of METAC and MAPTAC monomers attached to one unit of lignin were calculated and the magnitude of their μ were 25.9 and 16.7 D, respectively. The higher value of dipole moment showed a higher polarity of HL-METAC than HL-MAPTAC.⁴⁴

5.4.2 Characterization of lignin polymer

Proposed reaction scheme

The chemical structures of CHLs are proposed in Scheme 5.1. The hydrolysis lignin is rich in carbohydrates and it usually extracts in the form of lignin-carbohydrate complex (LCC) after enzymatic hydrolysis of biomass.⁴⁵ Hence, a phenylpropane unit (i.e., Sinapyl alcohol) of lignin attached to a carbohydrate unit (i.e., Sugar) represents the hydrolysis lignin in Scheme 5.1. The polymerization reaction of lignin and METAC or MAPTAC was carried out in an aqueous solution following a free radical polymerization mechanism. In this reaction, sodium persulfate was considered as the initiator. The sulfate radicals can initially be produced by heat decomposition, which can react with the phenolic OH groups of lignin to form phenoxy radicals (Scheme 5.1). The formation of these radicals on the lignin structure, which are the reaction sites for polymerization, facilitate their reactions with the cationic monomers (METAC or MAPTAC) or propagate monomers to form HL-METAC or HL-MAPTAC.

However, sulfate radicals can initiate the homopolymerization of cationic monomers to form polyMETAC and polyMAPTAC, which are identified as undesirable side reactions (Scheme 5.1).

NMR analysis

The ^{31}P -NMR spectra of HL and CHLs are depicted in Fig S1 and the quantitative data on various $-\text{OH}$ groups of lignin samples are also listed in Table A3. The results confirmed that after polymerization of HL with METAC and MAPTAC, the amount of aliphatic hydroxy groups present in the final products reduced to 0.65 and 0.46 mmol/g (from 0.95 mmol/g) and the $-\text{OH}$ groups originated from phenolic moieties decreased to 1.81 and 1.38 mmol/g (from 4.13 mmol/g), respectively (Table A3). Hence, it can be claimed that the polymerization proceeded through the participation of hydroxyl groups of lignin in the radical polymerization reaction as it was reported previously.⁴⁶ However, almost half of the $-\text{OH}$ groups remained intact. ^{31}P -NMR results also postulated that 67% and 52% of total aliphatic and phenolic hydroxy groups of HL participated in the polymerization reaction with MAPTAC, while the aliphatic and phenolic hydroxy groups of HL involved in the radical polymerization with METAC monomer were 56 and 32%, respectively. The ^1H NMR spectra of HL and CHLs are shown in Figure A15. The broad peak at 7.3-8 ppm was associated with the lignin's aromatic structure.⁴⁷

The peak at 5.15 ppm was attributed to the aliphatic protons and the signals at 4.01 ppm were assigned to the methoxy protons ($-\text{OCH}_3$) of lignin.^[7] Additionally, the observed signal at about 3.15 ppm could be assigned to the protons of hemicelluloses anhydroxylose units.⁴⁸ The peak at 4.75 and 3.5 ppm were also belonged to D_2O and DMSO-d_6 , respectively.

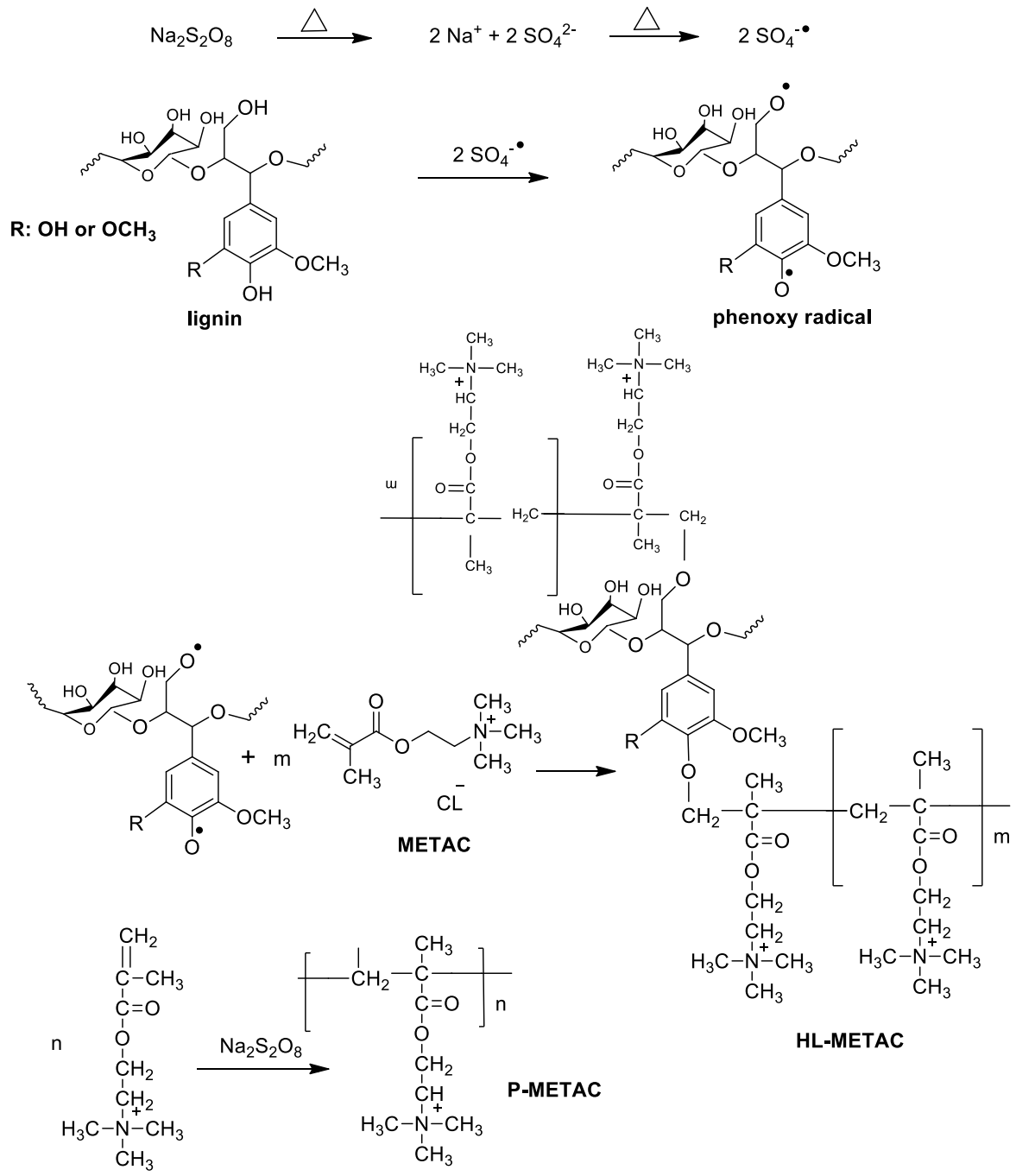
The characteristic peaks for CHL polymers appeared at 1.6-2.2 ppm, 2.8 ppm, 4.1 ppm, 4.5 ppm, and 5.2 ppm. Peaks at 1.6-2.2 ppm were associated with the protons of methyl group of METAC or MAPTAC monomer and the peak at 2.8 ppm was assigned to the methylene protons of cationic monomers. The intense peak of $-\text{N}^+(\text{CH}_3)_3$ was also observed at 4.1 ppm for both monomers. The

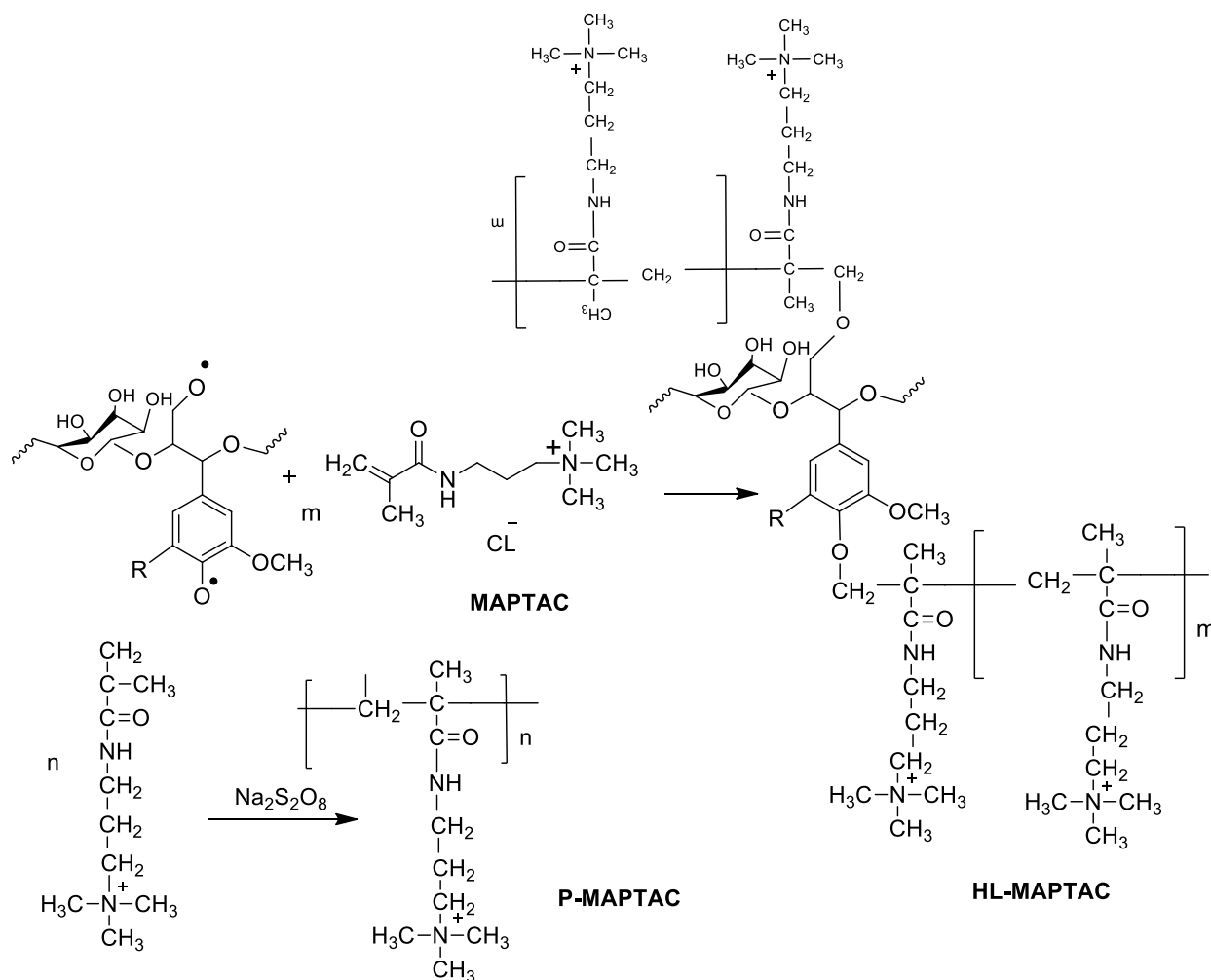
protons of amide groups (C=O —NH) was evidenced by the peaks around 5.2-5.7 ppm.^[7] Moreover, the peak at around 4.5 ppm in the spectra of HL-METAC and HL-MAPTAC, which is absent in that of unmodified hydrolysis lignin corresponded to the protons of —CH₂ attached to the phenolic hydroxy group of HL via ether bond (—CH₂— O—C₆H₅).^{46,49} The ¹H NMR analysis confirmed that the phenolic hydroxyl groups of lignin were the active sites for the polymerization of HL and METAC or MAPTAC monomers.

FTIR Analysis

The FTIR spectra of HL and CHL polymers are presented in Figure A16. The wide peak around 3400 cm⁻¹ was attributed to the O—H stretching absorption in the phenolic and aliphatic compounds of both HL and CHL, and a band around at 2900 cm⁻¹ was assigned to the C—H stretching in the methyl groups.⁵⁰ Since the hydrolysis lignin contains carbohydrates fractions, the observed signal at around 1035 cm⁻¹ was originated from the stretching vibration of ether bond in the polysaccharide compound of HL.⁵¹

In the spectrum of CHLs, the new peaks appeared at 1461 cm⁻¹ and around 960 cm⁻¹, which were assigned to C—N bending, and methyl groups of quaternary ammonium in cationic monomers, respectively. HL-METAC spectrum indicated an absorption peak at 1724 cm⁻¹, which was attributed to the C=O stretching vibration.⁷ The displayed band of NH—CO (amide group) at 1630 cm⁻¹ was also observed in the spectrum of HL-MAPTAC polymer.⁵² Therefore, the existence of new peaks on CHL polymers illustrated that the polymerization of lignin with METAC or MAPTAC was successfully achieved.





Scheme 5. 1Chemical structure of CHL polymers. “m” represents the number of cationic groups attached to lignin.

5.4.3 Properties of CHLs

The quaternary ammonium group in METAC and MAPTAC structure provides the cationic charge density of CHL. The properties of HL and CHL are shown in Table 5.1. As seen, both CHLs were produced to have a similar charge density, molecular weight, solubility and grafting ratio. However, the properties of HL are substantially different from those of CHLs. The charge density of HL was -0.47 mmol/g, and it reached to $+2.1$ and $+2.2$ mmol/g after polymerization with METAC and MAPTAC, respectively. The nitrogen content of CHLs is originated from METAC

and MAPTAC attached to the lignin backbone in CHLs. Although HL-MAPTAC had a higher nitrogen content stemming from two nitrogen elements in its structure, the grafting ratio and molecular weight of HL-METAC were very close to those of HL-MAPTAC. As HL was insoluble in acetic acid, it was not possible to measure its molecular weight in this work. Similar molecular weight distribution curves for HL-METAC and HL-MAPTAC were also observed in Figure A17. A slightly higher molecular weight of HL-MAPTAC (60×10^3 g/mol) than HL-METAC (54×10^3 g/mol) could be attributed to the higher grafting of MAPTAC monomer to HL (Table 5.1). It is worth mentioning that the phenolic OH group of lignin can inevitably induce a radical reaction for its polymerization with METAC or MAPTAC.⁵³ The phenolic OH group of lignin was reduced from 1.2 mmol/g for HL to 0.71 and 0.66 mmol/g for HL-METAC and HL-MAPTAC, respectively. However, since the OH groups of HL were mostly composed of aliphatic hydroxy groups (Figure A14 and Table A3), which was less reactive than phenolic OH,⁵⁴ the polymerization reaction was not performed effectively. As a result, the increase in the molecular weight of CHLs was not significant. It is also obvious that HL-METAC and HL-MAPTAC had the polydispersity of 1.4 and 1.6, respectively. The low polydispersity could be attributed to the small relative differences in the chains of CHLs as polymerization process could proceed (i.e., enhancement of polymeric chain length).⁵⁵ Moreover, after the polymerization reaction, the hydrodynamic radius of HL was increased from 21.9 nm to 32.4 and 27.1 nm for HL-METAC and HL-MAPTAC, respectively.

Table 5. 1 Properties of HL and CHLs.

Sample	HL	HL-METAC	HL-MAPTAC
Charge density, mmol/g	-0.47±0.1	+2.1±0.12	+2.2±0.11

Solubility, wt. %	45±1.2	51±1.3	55±0.8
Nitrogen, wt. %	-	3±0.1	5.7±0.2
Grafting ratio, mol %	-	78.5±0.1	82.5±0.2
Phenolic OH, mmol/g	1.20±0.03	0.71±0.04	0.66±0.02
M _w , g/mol	-	55±6.3 × 10 ³	60±3.1 × 10 ³
M _n , g/mol	-	37±4.2 × 10 ³	47±2.2 × 10 ³
M _w /M _n	-	1.4±0.05	1.3±0.06
H _y , nm	21.93±0.9	32.4±1.2	27.1±1.34
R _g , nm	44.3±3.2	60.0±1.8	51.6±4.1
R _g /H _y	2.02±0.10	1.85±0.21	1.90±0.14

It was reported that the hydrodynamic radius, H_y, of lignin is correlated with its molecular shape.^{56,57} The grafted METAC or MAPTAC monomers onto the lignin backbone changed the compact shape and conformation of lignin molecules owing to the dissociation of its ionizable ammonium group, thus increasing the molecular weight of lignin macromolecules.⁷

Increasing the radius of gyration (R_g) of HL from 44 nm to 60 and 51 nm for HL-METAC and HL-MAPTAC, respectively, also confirms the conformational changes of HL structure after the polymerization reactions. As R_g is sensitive to the geometry and structure of the molecules,⁵⁸ the larger R_g of HL-METAC than HL-MAPTAC can be attributed to the structure of METAC

monomers. In this case, the larger R_g of HL-METAC can be correlated to its greater dipole moment. This observation was similar to the previous results reported by *Petridis* and *Smith*, in which the R_g of simulated non-polar lignin was lower than that of polar lignin.⁵⁹ To have a greater insight into the configuration of CHLs in an aqueous solution, the shape factor (R_g/H_y) of the CHLs was determined, which describes the morphology of lignin polymers in aqueous solutions.^{60,61} This ratio reflects the polymer chain architecture and spatial density distribution of colloidal particles.⁶² In general, for a uniform hard-sphere, the value of R_g/H_y is approximately 0.774, for a hyperbranched polymer cluster or a soft sphere, this value is 1.0-1.3, and for flexible random coil chains, the value is 1.5-1.8.⁶³⁻⁶⁵ The shape factor value >2 corresponds to a rigid-rod structure.⁶³⁻⁶⁵ As seen in Table 5.1, HL displayed a rigid-rod shape structure with R_g/H_y of 2.02. However, after the polymerization reaction, the morphology of HL-METAC and HL-MAPTAC slightly transformed from a rod-like to flexible random coil chains. The less coiled structure of HL-MAPTAC can be attributed to the existence of less polar atom (i.e., nitrogen) attached to the carbon in the MAPTAC structure. Hence, HL-METAC with higher polarity created larger H_y and R_g resulting in the bulkier and a more three-dimensional HL-METAC compared to HL-MAPTAC.

Size effect

To probe the molecular architecture of CHLs in salt and urea solutions, the hydrodynamic radius, radius of gyration, and shape factor (R_g/H_y) of the polymers were analyzed in these solutions, and the results of this analysis are tabulated in Table 5.1. As discussed in the previous section, CHLs created larger R_g and H_y than did HL indicating that HL possessed a more extended structure after polymerization. In a salt-containing solution, the R_g and H_y of CHLs were reduced significantly, which is ascribed to the screening of repulsive electrostatic interactions of the quaternary

ammonium group of CHLs by salt.⁶⁶⁻⁶⁸ Results also showed that HL-METAC was more sensitive to the salinity (i.e., its structure was affected more significantly) as it was more polar. The results also revealed that R_g/H_y of CHLs dropped in salt-containing solutions. Such a decrease indicates the tendency of the polymer to form more compact conformations.⁶³ Also, HL-METAC had a smaller shape factor than did HL-MAPTAC indicating that its mass distribution was centered towards the core of the lignin macromolecule creating smaller less-branched polymer clusters in the presence of salt.^{65,69}

In the urea solution, HL/CHLs demonstrated swollen configurations (Table 5.1). It was previously observed that the addition of urea to aqueous solutions dropped the number of intramolecular hydrogen bonds of Protein L (obtained from *Peptostreptococcus magnus*) and hence it enlarged its R_g and H_y .⁷⁰ This effect probably induced a loose structure of CHLs with larger diameters. It was also seen that the more polar polymer (HL-METAC) created larger R_g with more three-dimensional conformation in the urea containing solution. Urea molecules have one carbonyl and two amino groups⁷¹ and CHLs have plenty of hydroxy groups on their structures (Table 5.1). Thus, urea can be adsorbed by lignin macromolecules through hydrogen bonding leading to enhancement of CHLs' chain flexibility. Since the oxygen atom in the METAC monomer structure can develop stronger hydrogen bonding compared to the nitrogen atom in MAPTAC monomer, the addition of urea has a more significant effect on HL-METAC conformation.⁷² As a result, the hydrodynamic radius and radius of gyration of HL-METAC increased to a greater extent (i.e., more three-dimensional configuration) than those of HL-MAPTAC.

The results indicated that lignin polymers underwent a morphological evolution with flexible chains ($R_g/H_y \sim 1.5-1.8$) and a more three-dimensional conformation in the urea containing solution.

Table 5. 2 Configurational changes of lignin polymers in presence of salt and urea (10mM).

Sample	Salt			Urea		
	HL	HL- METAC	HL- MAPTAC	HL	HL- METAC	HL- MAPTAC
H_y , nm	16.7±1.1	17.6±0.85	18.24±0.91	27.32±1.12	66.3±1.3	42.5±1.2
R_g , nm	23.5±2.4	16.3±1.6	20.6±0.47	50±2.5	119±3.8	75±1.2
R_g/H_y	1.40±0.05	0.93±0.02	1.13±0.055	1.83±0.04	1.79±0.031	1.76±0.026

5.4.4 Adsorption analysis

The adsorption isotherm of CHLs on kaolin particles was studied, and the results are shown in Figure A18. Since the adsorbed amount of HL on the surface of kaolin particles was insignificant, it illustrated that HL molecules minimally adsorbed on the surface of particles through hydrophobic interaction, van der Waals or hydrogen bonding. The CHL polymers had a similar adsorption efficiency on the particles in the dosage range of 1- 32 mg/g, and almost all of the polymers adsorbed on the kaolin particles. The maximum adsorption of CHL was 66 and 41 mg/g for HL-METAC and HL-MAPTAC at the dosage of 80 mg/g, respectively. As stated earlier, the only difference of CHLs was their polarity and overall structural configurations (Table 5.1). The

results confirmed that the higher polarity and more three-dimensional structure of HL-METAC contributed to its higher adsorption than HL-MAPTAC on the surface of the particles.

Salt-induced adsorption

In order to compare the impact of polarity and structure of CHLs on their adsorption performance on kaolin particles, their maximum adsorption efficiency at different salt concentrations was analyzed. Figure 5.1 shows the effect of CHL adsorption as a function of KCl concentration. The maximum adsorption amount of HL-METAC and HL-MAPTAC was 66 and 41 mg/g, respectively, at 80 mg/g of CHL/kaolin in a salt-free system (Figure A18). Therefore, those two points were considered as the complete adsorption of CHLs on kaolin particles in Figure 5.1. As seen, the addition of KCl declined the adsorption of CHLs. Generally, salts screen the charges of polyelectrolytes, reduce the interaction of cationic charges of CHL and negatively charge of kaolin particles, and compress the diffuse double layer thickness of CHL hampering the adsorption of CHLs.⁷³ Considering the additional amount of CHLs and their charge densities, the number of charges required for screening the charges of CHLs was theoretically calculated. Results showed that, at 33.8 and 35.4 mM KCl concentrations, the cationic charges of polymers were totally screened. However, the experimental results revealed that CHLs were adsorbed even at a higher than theoretical charge neutralization concentration of KCl (i.e., higher than 33-35 mM KCl concentration). At the highest ionic strength (100 mM), the adsorption efficiency of HL-METAC and HL-MAPTAC were reduced by 88 and 84%, respectively.

These findings showed that the electrostatic charge interaction was not the only driving force involved in the adsorption of CHLs; and hydrogen bonding, hydrophobic/hydrophobic and van der Waals interactions were indeed contributed to CHL adsorption on the surface of the particles.

Another conjecture on the reduced adsorption at higher ionic strength can be the conformational change of adsorbed CHL on the particles (Table 5.1). Salt may shield the repulsion forces between the charged group of CHL chains and make CHL coil up into a tighter, less extended configuration as H_y and R_g of CHLs decreased in the salt-containing system (Table 5.1). In other words, salt would change the loose structure of CHLs to be more compact. Therefore, the bridging capability of lignin macromolecules with clay particles decreased, and its respective adsorbed amount was reduced.

According to Figure 5.1, the adsorption capacity of HL-METAC polymer decreased to a larger extent than that of HL-MAPTAC. In this case, as both polymers have a similar charge density, the adsorption efficiency of the more polar polymer (HL-METAC) was affected more significantly in the presence of salt.

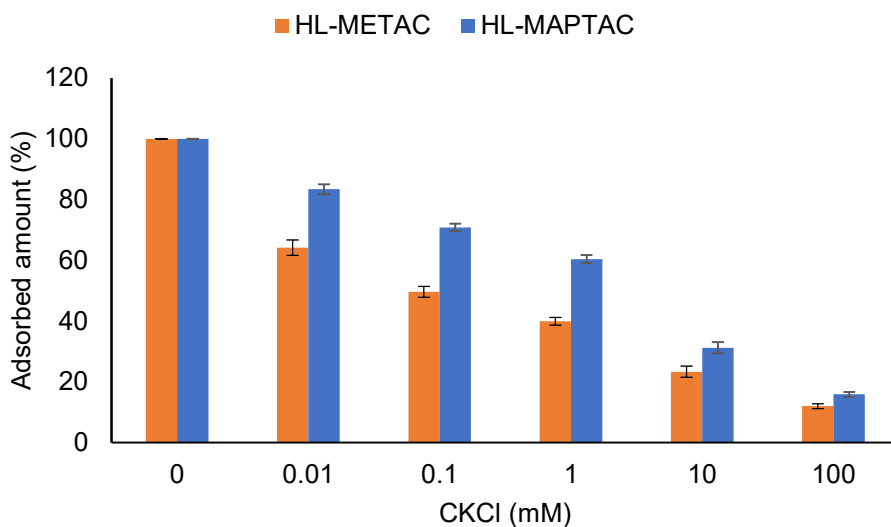


Figure 5. 1 Adsorption of CHLs on kaolin particles in the presence of salt. (100% adsorbed amount was considered with respect to the highest adsorbed amount of CHLs on kaolin; 66 and 41 mg/g for HL-METAC and HL-MAPTAC).

Urea-induced adsorption

In the absence of urea, CHL polymers can interact with the octahedral sheets of kaolin particles, which contains hydroxy groups on the interlayer surface of kaolin particles through hydrogen bonding.⁷⁴ The adsorption amount of CHLs on the particles was also studied in the presence of urea in Figure 5.2. As seen, the small amount of urea (0.01 mM) decreased the adsorption of CHLs on kaolin particles significantly. At a higher concentration of urea, the adsorbed amount of CHLs increased slightly. In this case, urea denatures CHLs and exposes their hydrophobic groups, which favors their adsorption onto the hydrophobic surface of the particles. As HL-MAPTAC was less polar than HL-METAC, it adsorbed more favorably on the particles through hydrophobic interaction in the urea containing system. The addition of urea increased the solubility of hydrophobic (i.e., less polar) molecules in water.⁷⁵ Hence, it created a more random coil structure in the urea solution ($R_g/H_y = 1.76$). As a result, the adsorption affinity of HL-MAPTAC dropped to a less extent. The adsorption of CHLs/kaolin in the urea environment (Figure 5.2) depicted that the hydrogen bonding and hydrophobic interactions were responsible for approximately 63% of HL-METAC adsorption and 23% of HL-MAPTAC adsorption on the particles even at very low urea concentration (0.01 mM). To examine whether charges of CHLs play any role in the urea-induced adsorption, the effect of urea addition on the electrophoretic mobility of CHLs was also investigated and results presented in Figure A19. As seen, altering the urea concentration in the range of 0-10 mM slightly increased the mobility of the particles due to the slight change in the electrical double layer thickness around the particles. However, the high dosage of urea (more than 10 mM) slightly decreased the mobility of particles (Figure A19). The reason for this phenomenon could be the conversion of urea to NH_3 and CO_2 at a high concentration generating ammonium ions and increasing the pH of the system.⁷⁶

The slight increase in the adsorbed amount of CHLs above 1 mM urea concentration may be due to the pH increment of the suspension. Overall, the results revealed that, in the urea-induced adsorption system, charges of CHLs played a minor role in the adsorption of CHLs on the particles in the presence of urea.

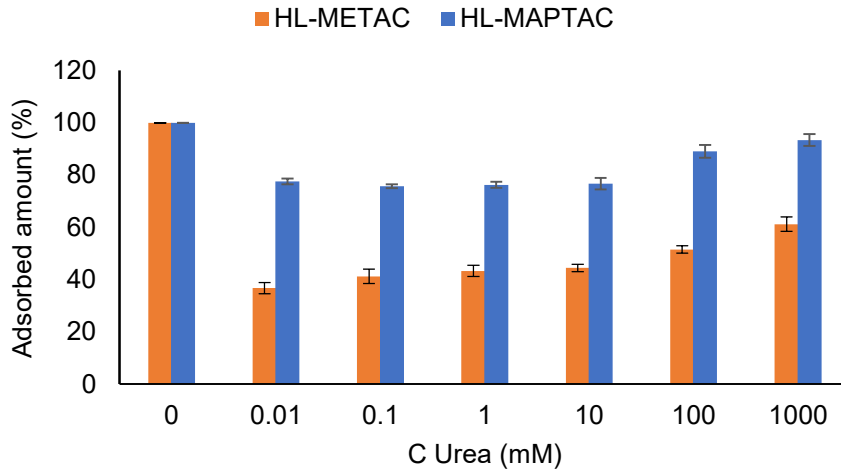


Figure 5. 2 Adsorption of CHLs on kaolin particles in the presence of urea. (100% adsorbed amount was considered with respect to the highest adsorbed amount of CHLs on kaolin; 66 and 41 mg/g dosages for HL-METAC and HL-MAPTAC).

5.4.5 Flocculation analysis

Stability ratio

Figure 5.3 shows the stability ratio ($\log W$) of the kaolin system in the presence of CHLs. It was reported that the largest flocs corresponded to the fastest kinetics of flocculation.⁷⁷ In the present work, the system stability ($\log W$) was analyzed based on the maximum growth rate of the V_{rms}/V_{dc} ratio (R) because it is a clear indication of the particle aggregation at a given time.⁷⁸ In the absence of salt/urea and CHLs, the kaolin particles were stable in the suspension due to the repulsion forces

originated from their negatively charged double layers with the electrophoretic mobility of around -3.4 ($\mu\text{cm/Vs}$) at pH 6. The fastest kaolin aggregation rate, K_{fast} , at the dosage of 1.2 mg/g of HL-METAC/kaolin was considered as a reference aggregation rate, with respect to which the initial aggregation rate, K_i , of kaolin particles was determined. As seen in Figure 5.3, the maximum aggregation rate was obtained for HL-METAC at 1.2 mg/g dosage ($W=1$). However, the apparent stability ratio of HL-MAPTAC reached 0.038 at 1.2 mg/g dosage. The extra amount of CHL (i.e., dosages higher than 1.2 mg/g) made the system stable ($\log W \rightarrow \infty$). The decrease in the stability ratio of kaolin suspension by adding different dosages of CHLs reflects the flocculation of particles and thus their removal from the suspension most likely via charge neutralization and bridging mechanisms.⁷⁸ However, the slight increase in the $\log W$ at a higher polymer dosage was probably corresponded to the electrostatic repulsion forces between the generated flocs.⁷⁸ This fact shows the importance of the polymer dosage in the flocculation process. At a similar charge density and molecular weight, the better performance of HL-METAC was attributed to its higher polarity (25.9 D) and more three-dimensional structure ($R_g/R_h \sim 1.85$), which facilitated its more efficient bridging performance. As the minimum $\log W$ and maximum flocculation efficiency ($\alpha = 1/W$ in Table A4) of kaolin/CHL system was achieved at 1.2 mg/g CHL/kaolin, the aforementioned dosage was selected as an optimum flocculant dosage for further analysis in this study. It is noteworthy that the relative turbidity results were in harmony with the stability ratio data, and the lowest relative turbidity of the kaolin suspension was achieved when 1.2 mg/g CHL adsorbed on kaolin particles (Figure A20).

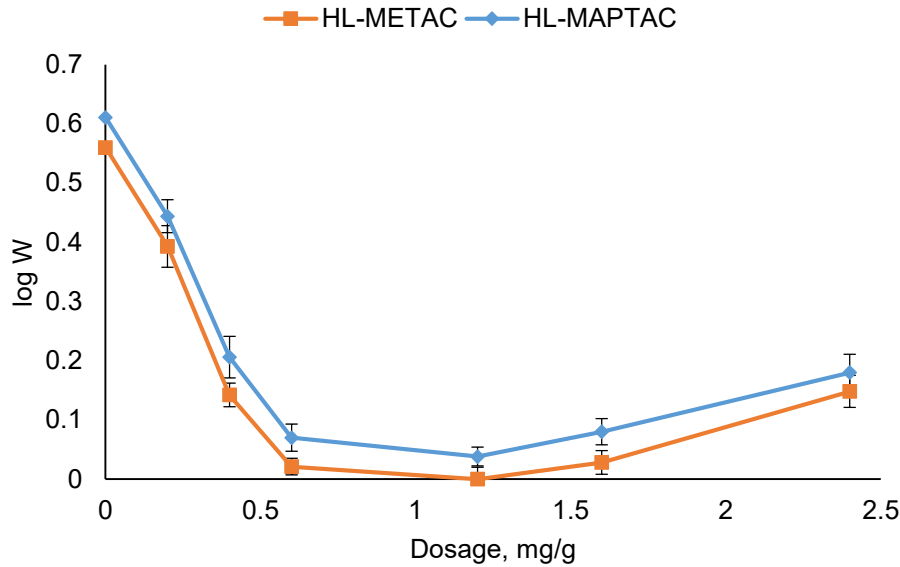


Figure 5. 3 Stability ratio ($\log W$) as a function of CHL dosage.

The addition of CHLs also changed the electrophoretic mobility of the kaolin suspension as presented in Figure A21. The mobility of kaolin suspension increased from negative to positive in the presence of different concentrations of CHLs. Furthermore, the particles attained similar electrophoretic mobility in the presence of CHLs, which is due to their similar charge densities (Table 5.1). However, the particles reached neutral charges when the dosage of HL-MAPTAC and HL-METAC were 16 and 22 mg/g, respectively. Since the aforementioned dosages were far over the optimum dosage for the lowest W (1.2 mg/g), the predominant flocculation mechanism cannot be the charge neutralization mechanism, and bridging or patching would have contributed to a larger extent in the flocculation process.⁷⁹ Focused beam reflectance measurements (FBRM) instrument was also used for monitoring the real-time changes of flocs size (i.e., chord length of particles) and floc formation during the flocculation process.⁸⁰ The mean chord length (MCL) of flocs is plotted in Figure A22 as a function of time. After 100 s of stabilizing the system (at 250 rpm), CHLs were added to the kaolin suspension and MCL increased from 7.80 μm to 10.97 and

9.17 μm for HL-METAC and HL-MAPTAC, respectively. The maximum MCL value of CHL/kaolin was attributed to the minimum stability ($\log W$) of the system. As discussed earlier, HL-METAC was more polar than HL-MAPTAC, which improved its charge interaction with the kaolin particles. In the flocculation process, HL-METAC with higher polarity than HL-MAPTAC can interact more effectively with kaolin particles and entrap clay particles more dramatically. Previously, the flocculation behavior of various asphaltene samples having different polarities that stemmed from their structural and compositional characteristics was compared, and results demonstrated that the higher polar samples decreased the stability of the asphaltenes more greatly.⁸¹

Salt induced flocculation

The fast flocculation started when 0.01M KCl was added to the system (Figure A23). The different dosages of KCl were added (0.01-1000 mM) to the system, which indicated that the critical coagulation concentration (CCC) of kaolin particles (i.e., the minimum concentration of salt leading to rapid coagulation)^{78,82} was less than 0.01M KCl. Since FBRM measures the distribution of hundreds of thousands of particles per second very accurately,⁸³ the device was selected to evaluate the flocculation behavior of CHL/kaolin system in the presence of salt and urea. Figure A24 indicates the changes in MCL and non-weighted counts of particles as a function of time when different amounts of KCl were added to the CHL/kaolin suspension. It is noted that the MCL of both CHLs were raised with an increase in the salt concentration, while the number of counts dropped. However, at high salinity (i.e., 10 and 100 mM), the flocculation efficiency of CHLs was reduced significantly (especially in case of HL-METAC), as it is observable from lower MCL and a higher number of counts (Figure A24). The decrease in MCL with the ionic strength

corresponded to the reduction in the R_g and H_y of CHLs (Table 5.1) confirming the direct correlation of CHL size and floc size.

Figure 5.4 presents the correlation between MCL and adsorbed mass of CHL on particles at different dosages of KCl. As discussed earlier, the addition of salt diminished the adsorption of CHLs on kaolin. However, it was seen in Figure 5.4 that there was no monotonic correlation between the adsorbed amount of CHLs and particle size of flocs in the presence of salt. At the maximum adsorption of CHLs, MCL was 10.97 and 9.17 μm for HL-METAC/particles and HL-MAPTAC/particles, respectively. However, the highest MCL was obtained when only 40% of HL-METAC and 60% of HL-MAPTAC were adsorbed on the particles (MCL reached 16.7 and 11.4 μm , respectively). According to Figure 5.4, at a lower amount of CHL adsorption in the saline system (except for the lowest level of adsorption at the highest ionic strength), the flocculation of CHL/particles occurred more efficiently than that in the absence of salt. The electrophoretic mobility of adsorbed CHLs on the particles could also be enhanced by increasing the salt concentration (Figure A25). This enhanced electrophoretic mobility could allow the adsorbed CHL to possess more flocculation efficiency even if the total charge of adsorbed CHL suppressed with increasing the salt concentration.⁷⁸ It was discussed previously that increasing the ionic strength could decrease the bridging affinity of CHLs (as seen as the reduction in the adsorbed amount of CHLs on clay particles). However, salt probably reduced the double layer thickness around the particles, which decreased the bridging distance a polymer must span to induce flocculation. Therefore, the effect of ionic strength on the colloidal flocculation is not straightforward and the force balance of all interactions need to be considered.

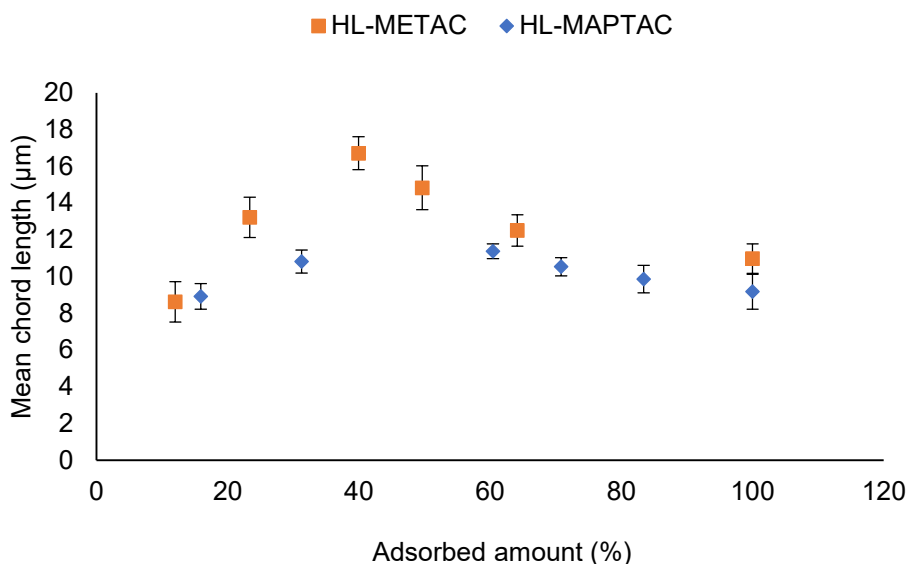


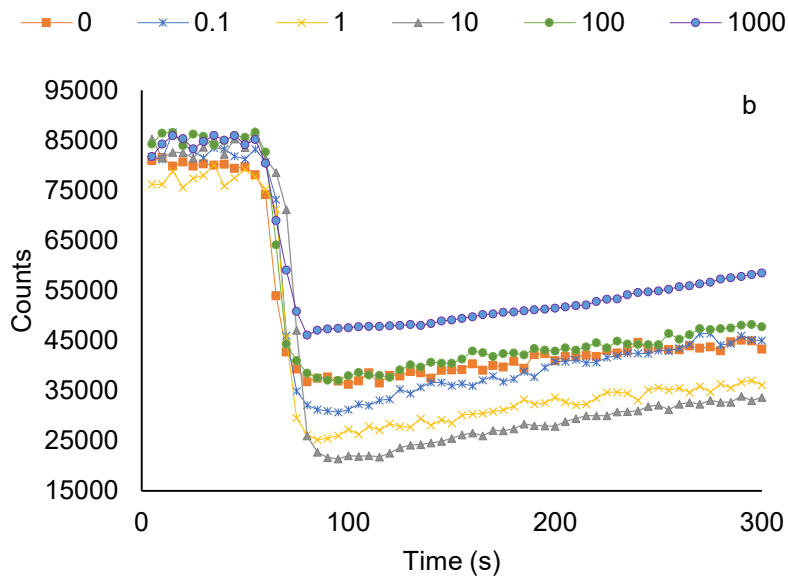
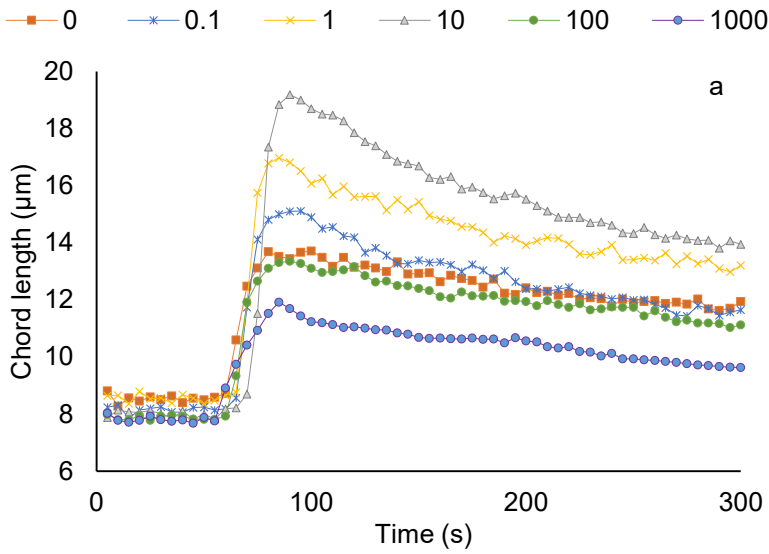
Figure 5. 4 The relationship between chord length and adsorbed mass

According to the results shown in Figure A24, the sensitivity of HL-METAC to ionic strength to form the largest MCL (at 1 mM salt concentration compared to the salt-free system) was about 1.2 times as much as that of HL-MAPTAC. The reasons for this phenomenon were 1) more compression of the electric double layer of the HL-METAC (Figure A25),⁸⁴ and 2) a more three-dimensional structure of HL-METAC (Figure A14). Moreover, as the hydrophobic interaction of CHLs was improved in saline systems, the interaction and flocculation efficiency of the more hydrophobic (i.e., less polar) polymer, HL-MAPTAC, was improved more greatly than that of the other polymer, HL-METAC.

Urea induced flocculation

The MCL and non-weighted counts of particles are shown as a function of time for different dosages of urea in the CHL/particle systems in Figure 5.5. Generally, the HL-METAC contained fewer particles with larger chord length than did HL-MAPTAC. By adding urea (0-10 mM), the chord length of particles

increased, and the number of counts dropped. Since CHLs possessed more three-dimensional configuration in the urea solution, they were very efficient in entrapping kaolin particles, even though the adsorption of CHLs on the particle surface decreased with increasing the urea concentration (as a result of hydrogen bonding breakage).



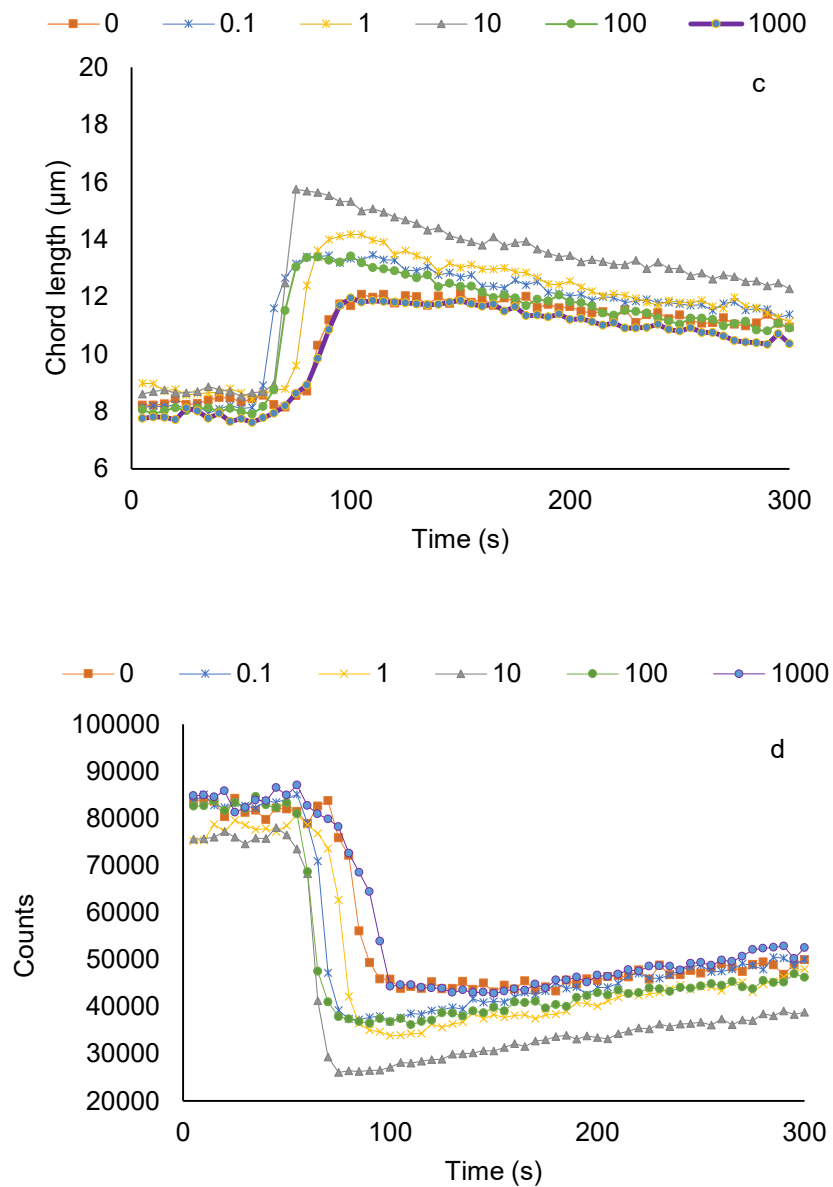


Figure 5. 5 Influence of urea concentration (0-1000 mM) on the mean chord length and number of counts of the a,b) HL-METAC, and c,d) HL-MAPTAC samples as a function of time (pH 6, 25 °C and 25 g/L of kaolin concentration).

However, the larger R_g and H_y of HL-METAC (Table 5.1) led to a larger bridging efficiency and thus more efficient flocculation in the urea system. However, the higher dosages of urea (10-1000 mM) suppressed the growth of MCL and resulted in smaller flocculated particles. In a similar

work, the effect of urea on the flocculation of a bio-flocculant, CBF-256 (microbial flocculants), was investigated and a similar trend was reported to affect the flocculation of printing and dyeing wastewater in the presence of urea.⁸⁵ As stated earlier, at a higher concentration, the generation of ammonium ions increased the pH of the suspension and hampered the flocculation.

5.5 Conclusions

Cationic hydrolysis lignin (CHL) polymers were successfully produced via free radical polymerization. The dipole moment of CHLs were 25.9 and 16.7 D for HL-METAC and HL-MAPTAC, respectively, indicating the higher polarity of the former CHL. The charge density, molecular weight, and grafting ratio of CHLs were controlled to be similar after the polymerization. The higher Rg and Hy of HL-METAC showed the more three-dimensional configuration of this polymer than that of HL-MAPTAC. The Rg/Hy results also revealed that the structure of HL was changed from a rigid rod to a more flexible random coil chain for CHLs. In the absence of salt and urea, HL-METAC adsorbed more than HL-MAPTAC on the surface of kaolin particles. Compared with the findings in the literature,^[7,9,10,24] our work proved that the higher polarity and configuration of polymers impacted the better flocculation efficiency in aqueous solution. The state of the kaolin system, characterized by stability ratio (W), confirmed the better flocculation performance of HL-METAC, which is ascribed to its higher polarity and more three-dimensional structure. Moreover, our results provided the experimental observation for polarity differences of macromolecules rather than an only molecular simulation of dipole moment.^[30,33] The addition of KCl to the system provided evidence for the stronger charge interaction of HL-METAC than HL-MAPTAC for its adsorption on the kaolin particles. The more compact structure was observed for CHLs in the saline system, which led to less flocculation

efficiency of CHLs for kaolin particles. The non-monotonic correlation was observed for adsorbed mass and flocculation performance of CHLs in the salt-containing system. In the presence of urea, the hydrophobic interaction of CHLs and the particles were highlighted, and HL-MAPTAC had a higher adsorption efficiency than HL-MAPTAC even though the adsorption of CHLs generally dropped in the presence of urea. The larger R_g and H_y of HL-METAC in the urea containing system led to its better flocculation than HL-MAPTAC. The results shed light on the impact of the structure of lignin-based polymers on the adsorption and flocculation efficiency of the clay suspension systems. The results presented in this study are limited to adsorption and flocculation properties of lignin macromolecules with different polarities.

5.6 References

- (1) Madan, S., Shaw, R., Tiwari, S. Tiwari, S.K., 2019. Adsorption dynamics of Congo red dye removal using ZnO functionalized high silica zeolitic particles. *Appl. Surf. Sci.* 487, 907-917.
- (2) Liu, L., Min, F., Chen, J., Lu, F. Shen, L., 2019. The adsorption of dodecylamine and oleic acid on kaolinite surfaces: Insights from DFT calculation and experimental investigation. *Appl. Surf. Sci.* 470, 27-35.
- (3) Konduri, M.K. Fatehi, P., 2017. Dispersion of kaolin particles with carboxymethylated xylan. *Appl. Clay Sci.* 137, 183-191.
- (4) Nasim, T., Pal, A. Bandyopadhyay, A., 2018. Flocculation of aqueous kaolin suspension using a biodegradable flocculant system of poly (vinyl alcohol)-Acacia nilotica gum blends. *Appl. Clay Sci.* 152, 83-92.

- (5) Razali, M.A.A. Ariffin, A., 2015. Polymeric flocculant based on cassava starch grafted polydiallyldimethylammonium chloride: flocculation behavior and mechanism. *Appl. Surf. Sci.* 351, 89-94.
- (6) Wang, S., Konduri, M.K.R., Hou., Q., Fatehi, P. 2016. Cationic xylan-METAC copolymer as a flocculant for clay suspensions. *RSC Adv.* 6, 40258-40269.
- (7) Wang, S., Kong, F., Gao, W. Fatehi, P., 2018. Novel process for generating cationic lignin based flocculant. *Ind. Eng. Chem. Res.* 57(19), 6595-6608.
- (8) Shuaiyang, W., Huiling, L., Junli, R., Chuanfu, L., Feng, P. Runcang, S., 2013. Preparation of xylan citrate—A potential adsorbent for industrial wastewater treatment. *Carbohydr. Polym.* 92(2), 1960-1965.
- (9) Wei, Y., Cheng, F. Zheng, H., 2008. Synthesis and flocculating properties of cationic starch derivatives. *Carbohydr. Polym.* 74(3), 673-679.
- (10) Kong, F., Parhiala, K., Wang, S. Fatehi, P., 2015. Preparation of cationic softwood kraft lignin and its application in dye removal. *Eur Polym J.* 67, 335-345.
- (11) Chakar, F.S. Ragauskas, A.J., 2004. Review of current and future softwood kraft lignin process chemistry. *Ind. Crops Prod.* 20(2), 131-141.
- (12) Ponnusamy, V.K., Nguyen, D.D., Dharmaraja, J., Shobana, S., Banu, J.R., Saratale, R.G., Chang, S.W. Kumar, G., 2019. A review on lignin structure, pretreatments, fermentation reactions and biorefinery potential. *Bioresour. Technol.* 271, 462-472.
- (13) Jin, Y., Cheng, X. Zheng, Z., 2010. Preparation and characterization of phenol–formaldehyde adhesives modified with enzymatic hydrolysis lignin. *Bioresour. Technol.* 101(6), 2046-2048.

- (14) Xie, Y., Lü, Q.F., Jin, Y.Q. Cheng, X.S., *Enzymatic hydrolysis lignin epoxy resin modified asphalt*. In *Advanced Materials Research*; Trans Tech Publications Ltd: 2011, 239, 3346-3349.
- (15) Lü, Q.F., Huang, Z.K., Liu, B. Cheng, X., 2012. Preparation and heavy metal ions biosorption of graft copolymers from enzymatic hydrolysis lignin and amino acids. *Bioresour. Technol.* 104, 111-118.
- (16) Ruihua, H., Bingchao, Y., Zheng, D. Wang, B., 2012. Preparation and characterization of a quaternized chitosan. *J. Mater. Sci.* 47(2), 845-851.
- (17) Sabaghi, S. Fatehi, P., 2019. Phenomenological Changes in Lignin Following Polymerization and Its Effects on Flocculating Clay Particles. *Biomacromolecules*, 20(10), 3940-3951.
- (18) Dorresteyn, R., Billecke, N., Parekh, S.H., Klapper, M. Müllen, K., 2015. Polarity reversal of nanoparticle surfaces by the use of light-sensitive polymeric emulsifiers. *J Polym Sci A Polym Chem.* 53(2), 200-205.
- (19) Sedlacek, O., Monnery, B.D., Filippov, S.K., Hoogenboom, R. Hruby, M., 2012. Poly (2-Oxazoline) s–Are They More Advantageous for Biomedical Applications Than Other Polymers?. *Macromol Rapid Commun.* 33(19), 1648-1662.
- (20) Wan, C. Chen, B., 2012. Reinforcement and interphase of polymer/graphene oxide nanocomposites. *J. Mater.Chem.* 22(8), 3637-3646.
- (21) Shi, L., Yu, Y., Chen, Z., Zhang, L., He, S., Shi, Q. Yang, H., 2015. A label-free hemin/G-quadruplex DNAzyme biosensor developed on electrochemically modified electrodes for detection of a HBV DNA segment. *RSC Adv.* 5(15), 11541-11548.

- (22) Kang, X., Xia, Z., Chen, R., Sun, H. Yang, W., 2019. Effects of inorganic ions, organic polymers, and fly ashes on the sedimentation characteristics of kaolinite suspensions. *Appl. Clay Sci.* 181, p.105220.
- (23) Mazzeo, C.P., Stedille, F.A., Mansur, C.R., Ramos, A.C. Lucas, E.F., 2018. Flocculation of asphaltenes by polymers: influence of polymer solubility conditions. *Energy Fuel* 32(2), 1087-1095.
- (24) Chen, Y., Liu, S. Wang, G., 2007. Flocculation properties and adsorption kinetics of cationic starches in kaolin suspensions. *J. Appl. Polym. Sci.* 105(5), 2841-2849.
- (25) Wang, S., Zhang, L., Yan, B., Xu, H., Liu, Q. Zeng, H., 2015. Molecular and surface interactions between polymer flocculant chitosan-g-polyacrylamide and kaolinite particles: Impact of salinity. *J. Phys. Chem. C.* 119(13), 7327-7339.
- (26) Jackson, N.E., Brettmann, B.K., Vishwanath, V., Tirrell, M. de Pablo, J.J., 2017. Comparing solvophobic and multivalent induced collapse in polyelectrolyte brushes. *ACS Macro Lett* 6(2), 155-160.
- (27) Liu, C.G., Chen, X.G. Park, H.J., 2005. Self-assembled nanoparticles based on linoleic-acid modified chitosan: Stability and adsorption of trypsin. *Carbohydr. Polym.* 62(3), 293-298.
- (28) Gaussian09, R.A., 2009. 1, mj frisch, gw trucks, hb schlegel, ge scuseria, ma robb, jr cheeseman, g. Scalmani, v. Barone, b. Mennucci, ga petersson et al., gaussian. Inc., Wallingford CT, 121, 150-166.
- (29) Liu, L., Parameswaran, S., Sharma, A., Grayson, S.M., Ashbaugh, H.S. Rick, S.W., 2014. Molecular dynamics simulations of linear and cyclic amphiphilic polymers in aqueous and organic environments. *J. Phys. Chem. B.* 118(24), 6491-6497.

- (30) Fang, R., Cheng, X.S., Fu, J. Zheng, Z.B., 2009. Research on the graft copolymerization of EH-lignin with acrylamide. *Nat. Sci.* 1(01), p.17.
- (31) Yan, M., Yang, D., Deng, Y., Chen, P., Zhou, H. Qiu, X., 2010. Influence of pH on the behavior of lignosulfonate macromolecules in aqueous solution. *Colloids Surf A Physicochem Eng Asp.* 371(1-3), pp.50-58.
- (32) Schärfl, Wolfgang. *Light scattering from polymer solutions and nanoparticle dispersions*; Springer Science & Business Media: 2007.
- (33) Lucey, J.A., Srinivasan, M., Singh, H. Munro, P.A., 2000. Characterization of commercial and experimental sodium caseinates by multiangle laser light scattering and size-exclusion chromatography. *J Agric Food Chem.* 48(5), 1610-1616.
- (34) Chen, D. van de Ven, T.G., 2016. Flocculation kinetics of precipitated calcium carbonate induced by electrosterically stabilized nanocrystalline cellulose. *Colloids Surf A Physicochem Eng Asp.* 504, 11-17.
- (35) Porubská, J., Alince, B. van de Ven, T.G., 2002. Homo-and heteroflocculation of papermaking fines and fillers. *Colloids Surf A Physicochem Eng Asp.* 210(2-3), 223-230.
- (36) Greaves, D., Boxall, J., Mulligan, J., Montesi, A., Creek, J., Sloan, E.D. Koh, C.A., 2008. Measuring the particle size of a known distribution using the focused beam reflectance measurement technique. *Chem. Eng. Sci.* 63(22), 5410-5419.
- (37) Boxall, J.A., Koh, C.A., Sloan, E.D., Sum, A.K. Wu, D.T., 2012. Droplet size scaling of water-in-oil emulsions under turbulent flow. *Langmuir* 28(1), 104-110.
- (38) Ragauskas, A.J., Beckham, G.T., Biddy, M.J., Chandra, R., Chen, F., Davis, M.F., Davison, B.H., Dixon, R.A., Gilna, P., Keller, M. Langan, P., 2014. Lignin valorization: improving lignin processing in the biorefinery. *science* 344(6185).

- (39) Qiao, D., Yang, C., Chen, J., Guo, Y., Li, Y., Niu, S., Cao, K. Chen, Z., 2019. Comprehensive identification of the full-length transcripts and alternative splicing related to the secondary metabolism pathways in the tea plant (*Camellia sinensis*). *Sci. Rep.* 9(1), 1-13.
- (40) Hickey, A.L. Rowley, C.N., 2014. Benchmarking quantum chemical methods for the calculation of molecular dipole moments and polarizabilities. *J Phys Chem A.* 118(20), 3678-3687.
- (41) Singh, H., Sindhu, J. Khurana, J.M., 2014. Determination of dipole moment, solvatochromic studies and application as turn off fluorescence chemosensor of new 3-(4-(dimethylamino) phenyl)-1-(5-methyl-1-(naphthalen-1-yl)-1H-1, 2, 3-triazol-4-yl) prop-2-en-1-one. *Sens. Actuators B Chem* 192, 536-542.
- (42) Oxtoby, D.W., Gillis, H.P. Butler, L.J. *Principles of modern chemistry*; Cengage learning: 2015.
- (43) Likhatsky, V.V. Syunyaev, R.Z., 2010. New colloidal stability index for crude oils based on polarity of crude oil components. *Energ Fuel* 24(12), 6483-6488.
- (44) Joshi, S., Kumari, S., Bhattacharjee, R., Sarmah, A., Sakhuja, R. Pant, D.D., 2015. Experimental and theoretical study: Determination of dipole moment of synthesized coumarin-triazole derivatives and application as turn off fluorescence sensor: High sensitivity for iron (III) ions. *Sens. Actuators B Chem* 220, 1266-1278.
- (45) Zhang, Y. Fatehi, P., 2019. Periodate oxidation of carbohydrate-enriched hydrolysis lignin and its application as coagulant for aluminum oxide suspension. *Ind. Crops Prod.* 130, 81-95.

- (46) Ghavidel, N. Fatehi, P., 2019. Synergistic effect of lignin incorporation into polystyrene for producing sustainable superadsorbent. *RSC Adv.* 9(31), 17639-17652.
- (47) Bahrpaima, Khatereh, Pedram Fatehi. "Synthesis and characterization of carboxyethylated lignosulfonate." *ChemSusChem* 11, no. 17 (2018): 2967-2980.
- (48) An, L., Wang, G., Jia, H., Liu, C., Sui, W. Si, C., 2017. Fractionation of enzymatic hydrolysis lignin by sequential extraction for enhancing antioxidant performance. *Int. J. Biol. Macromol.* 99, 674-681.
- (49) Kang, Y., Chen, Z., Wang, B. Yang, Y., 2014. Synthesis and mechanical properties of thermoplastic films from lignin, sebacic acid and poly (ethylene glycol). *Ind. Crops Prod.* 56, 105-112.
- (50) Kong, F., Wang, S., Gao, W. Fatehi, P., 2018. Novel pathway to produce high molecular weight kraft lignin–acrylic acid polymers in acidic suspension systems. *RSC Adv.* 8(22), 12322-12336.
- (51) Kacurakova, M., Capek, P., Sasinkova, V., Wellner, N. Ebringerova, A., 2000. FT-IR study of plant cell wall model compounds: pectic polysaccharides and hemicelluloses. *Carbohydr. Polym.* 43(2), 195-203.
- (52) Toletay, G., Dauletbekova, M., Shakhvorostov, A. Kudaibergenov, S. *Quenched Polyampholyte Hydrogels Based on (3-Acrylamidopropyl) trimethyl Ammonium Chloride and Sodium Salt of 2-Acrylamido-2-methyl-1-Propanesulfonic Acid.* In *Macromolecular Symposia*: 2019, June, 385, 1800160.
- (53) Cui, C., Sadeghifar, H., Sen, S. Argyropoulos, D.S., 2013. Toward thermoplastic lignin polymers; part II: thermal & polymer characteristics of kraft lignin & derivatives. *BioResources*, 8(1), 864-886.

- (54) Berlin, A. Balakshin, M. *Industrial lignins: analysis, properties, and applications*. In *Bioenergy Research: Advances and Applications*; Elsevier, 2014, 315-336.
- (55) Mastan, E. Zhu, S., 2015. A molecular weight distribution polydispersity equation for the ATRP system: quantifying the effect of radical termination. *Macromolecules* 48(18), 6440-6449.
- (56) Garver, T.M. Callaghan, P.T., 1991. Hydrodynamics of kraft lignins. *Macromolecules* 24(2), 420-430.
- (57) Gilardi, G. Cass, A.E., 1993. Associative and colloidal behavior of lignin and implications for its biodegradation in vitro. *Langmuir* 9(7), 1721-1726.
- (58) Kaasalainen, M., Aseyev, V., von Haartman, E., Karaman, D.Ş., Mäkilä, E., Tenhu, H., Rosenholm, J. Salonen, J., 2017. Size, stability, and porosity of mesoporous nanoparticles characterized with light scattering. *Nanoscale Res. Lett.* 12(1), p.74.
- (59) Petridis, L. Smith, J.C., 2016. Conformations of Low-Molecular-Weight Lignin Polymers in Water. *ChemSusChem*, 9(3), 289-295.
- (60) Ruckdeschel, P., Dulle, M., Honold, T., Förster, S., Karg, M. Retsch, M., 2016. Monodisperse hollow silica spheres: an in-depth scattering analysis. *Nano Res.* 9(5), 1366-1376.
- (61) Li, W., Cui, S.W. Wang, Q., 2006. Solution and conformational properties of wheat β -D-glucans studied by light scattering and viscometry. *Biomacromolecules* 7(2), 446-452.
- (62) Melas, A.D., Isella, L., Konstandopoulos, A.G. Drossinos, Y., 2014. Morphology and mobility of synthetic colloidal aggregates. *J. Colloid Interface Sci.* 417, 27-36.
- (63) Barthel, M.J., Rinkenauer, A.C., Wagner, M., Mansfeld, U., Hoepfener, S., Czaplowska, J.A., Gottschaldt, M., Träger, A., Schacher, F.H. Schubert, U.S., 2014. Small

- but powerful: co-assembly of polyether-based triblock terpolymers into sub-30 nm micelles and synergistic effects on cellular interactions. *Biomacromolecules* 15(7), 2426-2439.
- (64) Baek, J., Wahid-Pedro, F., Kim, K., Kim, K. Tam, K.C., 2019. Phosphorylated-CNC/modified-chitosan nanocomplexes for the stabilization of Pickering emulsions. *Carbohydr. Polym.* 206, 520-527.
- (65) Niu, A., Li, C., Zhao, Y., He, J., Yang, Y. Wu, C., 2001. Thermal decomposition kinetics and structure of novel polystyrene clusters with mtempo as a branching agent. *Macromolecules* 34(3), 460-464.
- (66) Alarcón, F., Pérez-Hernández, G., Pérez, E. Goicochea, A.G., 2013. Coarse-grained simulations of the salt dependence of the radius of gyration of polyelectrolytes as models for biomolecules in aqueous solution. *Eur Biophys J.* 42(9), 661-672.
- (67) Wong, G.C. Pollack, L., 2010. Electrostatics of strongly charged biological polymers: ion-mediated interactions and self-organization in nucleic acids and proteins. *Annu. Rev. Phys.* 61, 171-189.
- (68) Sim, A.Y., Lipfert, J., Herschlag, D. Doniach, S., 2012. Salt dependence of the radius of gyration and flexibility of single-stranded DNA in solution probed by small-angle x-ray scattering. *Phys. Rev. E.* 86(2), p.021901.
- (69) Hu, Y., Crist, R.M. Clogston, J.D., 2020. The utility of asymmetric flow field-flow fractionation for preclinical characterization of nanomedicines. *Anal. Bioanal. Chem.* 412(2), 425-438.

- (70) Rocco, A.G., Mollica, L., Ricchiuto, P., Baptista, A.M., Gianazza, E. Eberini, I., 2008. Characterization of the protein unfolding processes induced by urea and temperature. *Biophys. J.* 94(6), 2241-2251.
- (71) Yu, Q., Wu, Y., Li, D., Cai, M., Zhou, F. Liu, W., 2017. Supramolecular ionogel lubricants with imidazolium-based ionic liquids bearing the urea group as gelator. *J. Colloid Interface Sci.* 487, 130-140.
- (72) Cai, S., He, X., Liu, K., Zhang, R. Chen, L., 2015. Interaction between HPAM and urea in aqueous solution and rheological properties. *Iran. Polym. J.* 24(8), 663-670.
- (73) Fatehi, P., Ryan, J. Ni, Y., 2013. Adsorption of lignocelluloses of model pre-hydrolysis liquor on activated carbon. *Bioresour. Technol.* 131, 308-314.
- (74) Lee, K.E., Morad, N., Poh, B.T. Teng, T.T., 2011. Comparative study on the effectiveness of hydrophobically modified cationic polyacrylamide groups in the flocculation of kaolin. *Desalination* 270(1-3), 206-213.
- (75) Hüsecken, A.K., Evers, F., Czeslik, C. Tolan, M., 2010. Effect of urea and glycerol on the adsorption of ribonuclease A at the air– water interface. *Langmuir* 26(16), 13429-13435.
- (76) Nair, L.V., Philips, D.S., Jayasree, R.S. Ajayaghosh, A., 2013. A Near-Infrared Fluorescent Nanosensor (AuC@ Urease) for the Selective Detection of Blood Urea. *Small* 9(16), 2673-2677.
- (77) Gaudreault, R., Di Cesare, N., Weitz, D. van de Ven, T.G., 2009. Flocculation kinetics of precipitated calcium carbonate. *Colloids Surf A Physicochem Eng Asp.* 340(1-3), 56-65.

- (78) Peng, P. Garnier, G., 2010. Effect of cationic polyacrylamide adsorption kinetics and ionic strength on precipitated calcium carbonate flocculation. *Langmuir* 26(22), 16949-16957.
- (79) Lü, T., Zhang, S., Qi, D., Zhang, D. Zhao, H., 2018. Enhanced demulsification from aqueous media by using magnetic chitosan-based flocculant. *J. Colloid Interface Sci*, 518, 76-83.
- (80) Vajihinejad, V. Soares, J.B., 2018. Monitoring polymer flocculation in oil sands tailings: A population balance model approach. *Chem Eng J*. 346, 447-457.
- (81) Wattana, P., Fogler, H.S., Yen, A., Carmen Garcia, M.D. Carbognani, L., 2005. Characterization of polarity-based asphaltene subfractions. *Energ Fuel* 19(1), 101-110.
- (82) Gaudreault, R., van de Ven, T.G. Whitehead, M.A., 2005. Mechanisms of flocculation with poly (ethylene oxide) and novel cofactors. *Colloids Surf A Physicochem Eng Asp*. 268(1-3), 131-146.
- (83) Cadotte, M., Tellier, M.E., Blanco, A., Fuente, E., Van De Ven, T.G. Paris, J., 2007. Flocculation, retention and drainage in papermaking: a comparative study of polymeric additives. *Can. J. Chem. Eng.* 85(2), 240-248.
- (84) Barbot, E., Dussouillez, P., Bottero, J.Y. Moulin, P., 2010. Coagulation of bentonite suspension by polyelectrolytes or ferric chloride: Floc breakage and reformation. *Chem Eng J*. 156(1), 83-91.
- (85) Ren, D., Li, H., Pu, Y. Yi, L., 2013. Medium optimization to improve the flocculation rate of a novel compound bioflocculant, CBF-256, using response surface methodology and flocculation characters. *Biosci. Biotechnol. Biochem.* 130479.

Chapter 6: Dual Lignin-derived Polymeric Systems for Ions Removal

6.1 Abstract

The functionalization of lignin derivatives for ion removals is a promising method to expedite their use in treating industrial wastewater. In this work, kraft lignin (KL) was polymerized with [2-(methacryloyloxy)ethyl]trimethylammonium methyl sulfate (METAM) or acrylic acid (AA) in an acidic aqueous suspension system to produce cationic and anionic water-soluble lignin polymers with high molecular weights. Then, the interaction of soluble ions and KL-METAM and KL-AA was investigated using a Quartz crystal microbalance (QCM) and a vertical scan analyzer (VSA). The QCM, X-ray photoelectron spectroscopy (XPS) and contact angle measurement results showed that the adsorption and flocculation efficiencies of KL-AA were better than KL-METAM for ions due to the stronger electrostatic interaction, cationic π -interaction, and chelation between ions and KL-AA. Based on adsorption, sedimentation, and floc size analyses, the dual polymer systems of KL-AA/KL-METAM was more effective than KL-METAM/KL-AA in removing ions since KL-AA addition. Among Zn^{2+} , Cu^{2+} , and K^+ ; Zn^{2+} interacted more effectively with polymers in all scenarios because it has higher reactivity for interacting with other elements. As the efficiency of ion removals was more remarkable than past reported findings, the system of KL-AA/KL-METAM may be a promising alternative for the removal of dissolved ions from solutions.

Keywords: Lignin; Ions; Adsorption; Flocculation; Polymer

6.2 Introduction

Industrial and municipal wastewater effluents contain numerous pollutants such as toxic metals, micro and macroparticles, bacteria, toxic dyes, and organic materials.¹ Among potential pollutants, copper (Cu) and zinc (Zn) metals are the most toxic elements.^{2,3} The trace amount of such elements causes chronic health disorders, phytotoxicity, and bioaccumulation in the human body.^{3,4} Currently, it is of the utmost importance to minimize the concentration of heavy metals dissolved in water resources.⁵ Recently, extensive efforts were made in developing efficient and cost-effective water treatment systems. Adsorption and flocculation have gained considerable attention for the removal of heavy metals from various wastewater resources, owing to their excellent performance and simple operation procedures.^{6,7} For instance, ionic polyacrylamides exhibited excellent removal efficiency for chromium (III) oxide suspension.⁸ Amidoxime (AO) modified poly(acrylonitrile-*co*-acrylic acid) (poly(AN-*co*-AA)) was found to be highly efficient for Cd²⁺ and Pb²⁺ removals.⁹ However, the synthetic polymers may pose several environmental concerns owing to their toxicity and non-biodegradability.²

On the other hand, there has been an increasing demand for the implementation of natural polymeric flocculants in wastewater treatment processes due to their numerous offered advantages, such as biodegradability, low price, and high efficiency. Among natural polymers, lignin is the second most abundant aromatic polymer after cellulose, offering a complex three-dimensional amorphous structure. Despite its complicated molecular structure, its inherent properties with various functional groups, e.g., methoxy, carboxylate, and hydroxy groups, promote its chemical alteration to generate anionic/cationic polymers.^{10,11}

In this work, we studied the adsorption of ions (i.e., KCl, CuCl₂, and ZnCl₂) on cationic and anionic lignin derivatives fundamentally with the aid of a Quartz crystal microbalance with dissipation (QCM-D). These salts constitute the main sources of contamination in municipal and industrial wastewater effluents.^{12,13} In the past, QCM-D was utilized for investigating the deposition behavior of various substances, such as soluble pollutants (e.g., sodium alginate and bovine serum albumin),^{14,15} dissolved organic matters (e.g., humic acid and fulvic acid),¹⁶ or ions of Na⁺ and Ca²⁺ on the bare crystal surfaces of polyvinylidene fluoride (PVDF),¹³ SiO₂, polystyrene and polyamide.^{13,16} However, it was not utilized for studying the deposition of ions on lignin derivatives.

Generally, the complex properties of municipal wastewater (e.g., heavy metal, salts, volatile suspended solid) complicate the flocculation processes. The previous studies proved that lignin polymers could improve the settling performance of suspended particles in wastewater treatment systems.^{17,18} In order to achieve even greater separation efficiency of suspended particles and to further enhance the flocculation performance of lignin macromolecule, multicomponent flocculation procedures have been suggested.¹⁹⁻²¹ Previously, lignin-based flocculant (LNF) was synthesized by grafting amine groups (epichlorohydrin, N, N-dimethylformamide, and ethylenediamine) onto alkali lignin, and the product was used with aluminum sulfate (AS) and polyaluminum chloride (PAC) to treat humic acid solution.²² However, to the best of our knowledge, a dual polymeric system containing lignin-based macromolecules for heavy metal removals have not been studied.

In the present work, [2-(methacryloyloxy)ethyl]trimethylammonium methyl sulfate (METAM) and acrylic acid (AA) were utilized for the polymerization of lignin to produce cationic and anionic

lignin polymers.^{10,23} Here, we aim to apply the anionic/cationic lignin polymers to treat synthetic wastewater models containing ionic compositions (i.e., ZnCl₂, CuCl₂, and KCl) in singular and dual polymer systems. Since in many practical wastewater treatment systems, more than one element is present, the adsorption and destabilization performance of lignin-based polymers was also conducted in a mixture of selected elements (ZnCl₂, CuCl₂, KCl). However, as the dual polymer systems used for ions removals were the combination of synthetic materials and lignin,¹⁹⁻²² little attention has been devoted to exploring the use of combined anionic and cationic lignin in a dual polymer system, as a green and effective flocculation system, for ion removals. Therefore, the primary novelties of the present work are 1) the systematic investigation of ion removals by functionalized lignin-based polymers in different polymer/ion systems (singular, dual, and multi-component), and 2) the exploration of underlying ion removal mechanisms.

6.3 Materials and Methods

6.3.1 Materials

Softwood kraft lignin (KL) was received from FPIinnovations' pilot plant facilities, which produces lignin via LignoForce technology and is located in Thunder Bay, ON, Canada. Copper (II) chloride, zinc chloride, poly diallyl dimethyl-ammonium chloride (PDADMAC, 100,000–200,000 g/mol, 20 wt % in water), sodium persulfate (Na₂S₂O₈) and potassium persulfate (K₂S₂O₈) (analytical grade), sulfuric acid, sodium hydroxide (97%, reagent grade), sodium nitrate (NaNO₃, 99%), potassium hydroxide (8 M), hydrochloric acid (37%, reagent grade), acrylic acid (AA) and para-hydroxybenzoic acid were obtained from Sigma-Aldrich Company and used as received. Potassium poly (vinyl sulfate) (PVSK, 100000–200000 g/ mol, 97.7 wt % esterified) was supplied

by Wako Pure Chemical Co., Japan. Dialysis membrane with 1000 g/mol cut-off was received from Spectrum Laboratories and used for product purification. Acetic acid, potassium chloride (KCl), and ethanol (95 vol %) were purchased from Fisher Scientific Co. Also, BOC Sciences company, USA, supplied [2-(Methacryloyloxy)ethyl]- trimethylammonium methyl sulfate (METAM). Mili-Q water (resistivity $\geq 18 \text{ M}\Omega \text{ cm}$) was used throughout the experiments. Piezoelectric Quartz crystal sensors (5 MHz resonant frequency) were obtained from Biolin Scientific Inc.

6.3.2 Characterization of lignin polymers

In this study, kraft lignin was polymerized with [2-(Methacryloyloxy)ethyl] trimethylammonium methyl sulfate (METAM) or acrylic acid (AA) in an acidic environment, and the details of the reaction mechanism are available in the supporting information. The molecular weight, phenolic hydroxyl and carboxylate groups, elemental analysis, and charge density of KL, KL-METAM, and KL-AA were determined by the methods described in the literature²⁴⁻²⁶ and the details of this analysis were explained in the supporting information.

The hydrodynamic radius (R_h) of lignin samples was measured using a dynamic light scattering (DLS), BI-200SM Brookhaven Instruments, USA. About 20 mg of dried lignin polymers was firstly dissolved in a 1mM KCl solution (20 mL). The prepared samples were then filtered by a 0.45 μm syringe filter. The experiment was conducted under isothermal conditions (25 °C), while the scattering angle and the laser wavelength were set at 90° and 637 nm, respectively.²⁷

6.3.3 Coating lignin derivatives on QCM sensor

KL-METAM and KL-AA were coated on the clean dried gold sensors of the QCM instrument using a spin coater (WS-400B-NPP) spin-processor (Laurell Technologies Corp). First, lignin polymers were dissolved in ammonium hydroxide (1 wt% concentration) at 300 rpm overnight at room temperature. Then, the solutions were spin-coated on the gold sensors at 500 rpm for 10 seconds, 1000 rpm for 20 seconds, and 2000 rpm for 30 seconds under a nitrogen environment.²⁸ The coated samples were dried and kept covered prior to adsorption analysis.

6.3.4 Synthetic ion solutions

In this set of experiments, KCl, CuCl₂, and ZnCl₂ solutions were mixed with deionized water at different concentrations of 1, 10 and 100 mM to prepare ionic model solutions. These model wastewater samples were synthesized according to the compositions of municipal and industrial wastewater effluents.^{13-16,29,30}

6.3.5 Adsorption studies

The adsorption mechanisms of the components of synthetic model effluent on the lignin coated surface and the properties of the adsorbed layer were assessed by a Quartz crystal microbalance with dissipation (QCM-D 401, E1, Q-Sense Inc. Gothenborg, Sweden). The principle of this instrument was discussed elsewhere³¹ and briefly described in the supporting information.

In the singular component adsorption system, the adsorption test was monitored by introducing a buffer solution (i.e., Mili-Q water) to lignin coated surfaces (i.e., KL-METAM and KL-AA) at a controlled temperature of 22±0.1 °C to establish an equilibrated baseline. After reaching a constant baseline, the buffer solution was changed to different ionic compositions namely copper (II) chloride, zinc (II) chloride, and potassium chloride at desired ionic strength (1-100 mM). The

buffer solution was applied after the adsorption experiment for another 2 min to wash any loosely adsorbed ionic composition from the substrate. After completion, the sensors used in the adsorption experiment of 10 mM effluent concentration were collected and dried with nitrogen gas for the XPS analysis (Section 2.8).

In the dual-component adsorption system, a cationic coated sensor (KL-METAM) was first exposed to the buffer solution and then to the one type of ionic model effluent (i.e., ZnCl₂, CuCl₂, or KCl) at 10 mM concentration containing anionic lignin (KL-AA) with 10 g/L concentration. The opposite scenario was also tested on the KL-AA coated sensors for adsorbing the ionic solution containing the same concentration of salts and KL-METAM at 10 g/L concentration.

In another set of experiments, the adsorption analysis of the model solution containing all ionic salts (i.e., ZnCl₂, CuCl₂, and KCl) at 10 mM each and KL-AA (10 g/L) was carried out on the KL-METAM coated sensor. Similarly, the adsorption of the model solution containing the same concentration of salts and KL-MTAM (10 g/L) was studied on the KL-AA coated sensor. The shifts in frequency and dissipation of the sensors were recorded, and the surface was buffer rinsed after adsorption. A flow rate of 0.15 mL/min was used throughout all experiments. Normalized frequency and dissipation shift at the 5th harmonic (n = 5) are presented throughout this work.

6.3.6 Contact angle measurement

The contact angle of a droplet of CuCl₂, ZnCl₂, and KCl solution (10 mM) on lignin coated slides (KL-METAM and KL-AA) was determined using a Theta Lite Optical tensiometer, TL100 (Biolin Scientific, USA) equipped with USB2 digital camera and Attension software. In this set of analyses, 1 mL of KL-MEAM or KL-AA samples (10 g/L) was coated on glass slides using a spin coater WS-650 (Laurell Technologies Corp), while rotating at 1000 rpm with 60 psi pressure for

60 s under vacuum (by purging N₂ gas). Then, a droplet of ionic solution (5 μm) was placed on the coated surface and the contact angle of each droplet was determined following the sessile drop method according to Young's equation,³² and the mean value of measurements on 3 different spots on the coated glass slides was reported. In another set of experiment, a droplet of mixed solutions containing CuCl₂, ZnCl₂, KCl (10 mM), and lignin polymer (10 g/L) deposited on the lignin coated surface with the oppositely charged density for measuring the contact angle of lignin macromolecules in the mixed system.

6.3.7 Zeta potential analysis

The zeta potential (ζ) of ionic solutions in a single polymer system was characterized by a NanoBrook Zeta PALS (Brookhaven Instruments Corp, USA) in the absence and presence of lignin polymers. This analysis was performed at a constant electric field (8.4 V/cm) at room temperature, and the average value of three repetitions was reported in this study. The sample preparation for the zeta potential analysis of the dual polymer system was carried out by adding different dosages of KL-METAM and KL-AA polymer to ZnCl₂, CuCl₂, and KCl solutions with 30 min time interval between polymer addition. In the same way, for measuring ζ of a mixed system, all model effluent solutions (i.e., ZnCl₂, CuCl₂, and KCl) stirring with KL-AA followed by KL-METAM, and then the prepared sample was poured into the instrument cuvette to determine its zeta potential. It should be noted that the model solutions had a salt concentration of 10 mM and lignin polymer concentration of 10 g/L.

6.3.8 X-ray Photoelectron Spectroscopy

The surface compositions of the crystal sensors before and after conducting the QCM-D analysis were investigated using XPS. First, a high-purity conductive double-sided adhesive carbon tape

was used to fix samples to the sample holder of the XPS instrument.³³ X-ray photoelectron spectroscopy (XPS) analysis was performed with a Kratos Analytical AXIS 165 electron spectrometer using a high-resolution monochromatic Al KR (15 keV, 25 mA emission current, VSW MX10 700 mm Rowland circle monochromator) as the X-ray source. Data analysis and atomic quantification were performed using the ESCAPE software from the XPS peak areas of high-resolution narrow scans.

6.3.9 Vertical scan analyzer

The stability of the ionic (i.e., CuCl₂, ZnCl₂, KCl) solutions at 10 mM concentration in the presence of KL-METAM and KL-AA (10 g/L) was analyzed using a vertical scan analyzer, Turbiscan Lab Expert, Formulacion, France. In the singular polymer system, the different dosages of lignin samples were added to the model solutions while stirring at 300 rpm for 2 min. Afterward, 20 mL of prepared samples were poured into a flat-bottomed cylindrical glass cell of the instrument and scanned from the bottom to the top at 40 μm height intervals. The analysis was conducted for 30 min at 30 °C, and the sample scanning was conducted every 25s to report the kinetic stability of the suspension.²⁴ To monitor the suspension stability in the dual polymer system, the first ionic solution was poured into the glass cell and then the optimum dosage of KL-METAM or KL-AA (10 g/L) (obtained from the destabilization index of singular polymer system) was mixed with the model solutions. After 30 min scanning, the optimum dosage of the other lignin polymer with the opposite charge density was added and mixed in the system, and samples were scanned for another 30 min. The analysis was repeated following the same procedure but with a mixture of all ionic solutions.

Turbiscan stability index (TSI) and the aggregate mean diameter (d) were determined using Turbisoft 2.1 software considering the difference in transmittance signals generated by the samples with those generated by the standard silicon oil (i.e., calibration chemical).³⁴ The destabilization index of the samples was determined following equation 1:

$$TSI = \sum_i \frac{\sum_h |Scan_i(h) - Scan_{i-1}(h)|}{H} \quad (1)$$

where $scan_i(h)$ and $scan_{i-1}(h)$ are the transmission signals for two consecutive time intervals at a given height (h) and H is the entire height of measuring samples.

The mean aggregate size (d) was also determined following equation 2:^{8,35}

$$V(t) = \frac{|\rho_p - \rho_c| g d^2}{18\nu} \cdot \frac{[1 - \varphi]}{\left[1 + \frac{4.6\varphi}{(1 - \varphi)^3}\right]} \quad (2)$$

wherein; V(t) represents the migration velocity of aggregates, ρ_c , and ρ_p express the continuous phase and particle density, d is the mean diameter of aggregates, ν shows the dynamic viscosity of continuous phase, g is the gravity field and φ refer to every volume fraction of particles.

6.4 Results and Discussions

6.4.1 Properties of lignin polymers

The properties of lignin polymers are listed in Table 6.1. KL-METAM had a positive charge density of 2.5 meq/g and high molecular weight (690×10^3 g/mol). As the nitrogen element was initially absent in KL, the nitrogen content of KL-METAM (3 wt.%) was directly related to the grafting of METAM monomer to the lignin backbone; hence the grafting ratio of KL-METAM macromolecule was determined to be 58.1 mol %.

The charge density of KL-AA, on the other hand, was -2.6 meq/g while its molecular weight was 593×10^3 g/mol. As seen, the carboxylate content of unmodified lignin was 0.36 mmol/g (Table 6.1), and an increase in the carboxylate content of lignin to 4.01 mmol/g is attributed to the grafting of acrylic acid on the phenolic OH of lignin. Therefore, the grafting ratio of 61.3 mol % for KL-AA depicted that the polymerization reaction was performed successfully.

Based on the phenolic OH of KL and those of KL-METAM or KL-AA, the degree of substitution (DS) of 65 and 79 mol/mol was obtained for KL-METAM and KL-AA, respectively, demonstrating the successful attachment of METAM or AA monomer to lignin core via polymerization reaction. It is well-known that steric effects play a vital role in monomer reactivity in the free radical polymerization. In other words, by increasing the length of the alkyl chain or carbon content of monomers, the steric effect would increase, which would reduce the reactivity of the monomer.³⁶ Thus, AA monomer with a lower molecular weight (72 g/mol) and carbon content may be more reactive than METAM monomer (Mw of 283 g/mol), thus decreasing the phenolic OH of KL more greatly and mimicking a higher DS.

The larger polydispersity index (PDI) of KL-METAM and KL-AA than KL reveal that the polymerization increased the PDI of the polymer, which is a characteristic of free radical polymerization.^{37,10} Moreover, the hydrodynamic diameter of both cationic and anionic lignin polymers (34.3 nm for KL-METAM and 28 nm for KL-AA) was larger than that of KL (14.3 nm). It was reported that the hydrodynamic diameter of the kraft lignin is related to its molecular shape.³⁸ Accordingly, the higher hydrodynamic diameter of the lignin polymer is attributed to its looser molecular shape. Also, the larger R_h value of K-METAM is ascribed to its more three-dimensional structure and looser shape. Therefore, the grafted AA or METAM monomer onto

lignin backbone not only increased the molecular weight but also altered the compact shape and structure of lignin macromolecules owing to dissociation of its ionizable ammonium or carboxylic groups.³⁹

Table 6. 1 Properties of KL, KL-METAM, and KL-AA

Sample	KL	KL- METAM	KL-AA
Charge density, meq/g	-0.4±0.11	+2.5±0.1	-2.6±0.2
Nitrogen, wt. %	-	3.01±0.1	-
Carbon, wt. %	62.6±1.8	48.9±2.1	54.4±1.2
Hydrogen, wt. %	5.69±1.2	8.47±1.3	5.36±0.06
Oxygen, wt. %	27.04±1.3	39.16±1.6	38.9±0.45
Phenolic hydroxyl group, mmol/g	1.63±0.1	0.57±0.08	0.34±0.04
Carboxylate content, mmol/g	0.36±0.08	0.30±0.05	4.01±0.1
Grafting ratio, mol %	-	58.1±0.7	61.3±0.2
Degree of substitution, mol/mol	-	65±0.4	79±0.3
M _w , g/mol	49±6.4× 10 ³	690±107.5× 10 ³	593±55× 10 ³
M _n , g/mol	28±6.02× 10 ³	242±51.6 × 10 ³	180±16.8× 10 ³
M _w /M _n	1.7±0.15	2.6±0.091	3.2±0.1
R _h , nm	14.28±1.9	34. 3±2.7	28±1.1

6.4.2 Adsorption analysis of single KL-METAM or KL-AA

To understand the adsorption performance of ions on KL-METAM and KL-AA surfaces, we first investigated the responsive behavior of the singular ion/lignin system using QCM-D. Figure A26 shows the shift in frequency (Δf translated to mass changes) for the surfaces of coated lignin derivatives as a function of ionic strength concentration (I) for different ionic composition solutions. For all the cations, Δf decreased with ionic strength in the range of $1.0 \leq I \leq 100$ mM on both surfaces of KL-METAM in Figure A26a and KL-AA in Figure A26c. As the concentration increased to 100 mM, the number of available ions in the system interacting with the available charges of KL-METAM or KL-AA enhanced, leading to greater frequency changes. In other words, upon the continuous deposition of ions on both lignin surfaces, the electrostatic inter/intrachain interaction inside the charged lignin chains was weakened and gradually dominated by the interaction between the charged groups of ions and lignin to promote the adsorption.⁴⁰ Furthermore, dissipation reflects the structural changes of the polymeric surface upon adsorption.³⁹ Similar to frequency variations, the ΔD of both surfaces increased by ionic strength revealing enhanced viscoelasticity and coupling of ions and water molecules to the surface at higher adsorbed mass (Figure A26b and S1d).

According to the literature, the concentration of the ionic composition (KCl, CuCl₂, and ZnCl₂) in wastewater was reported to be approximately 10 mM.¹³ Therefore, the changes in D/F ratio, as well as the adsorption kinetics of model solution on the lignin surface, were studied at an ionic strength of 10 mM, and results were shown in Figure 6.1. The slope of dissipation over frequency depicts how much energy is dissipated for a unit of adsorbed mass (Figures 1a and 1b). Accordingly, a graph with a smaller slope was observed for the adsorption of the ionic composition

on the surface of KL-METAM compared to that of KL-AA. These results may reveal a less viscous adsorbed layer on the KL-METAM surface. The adsorption of ionic solutions was observed to be more on the KL-AA anionic surface.

The interaction of KL-AA with oppositely charged K^+ , Cu^{2+} , and Zn^{2+} was more detectable than that of Cl^- with KL-METAM. This may ascribe to the low chaotropic nature of Cl^- ,⁴¹ which is inclined to be less polarizable with less energy of dissolution.^{42,43} The strength of ion pairing between the weakly hydrated quaternary ammonium group of KL-METAM⁴⁴ and monovalent Cl^- ion (as the common anions in KCl , $CuCl_2$, and $ZnCl_2$) was lower than that of the carboxylate group of KL-AA and positive K^+ , Cu^{2+} , Zn^{2+} .

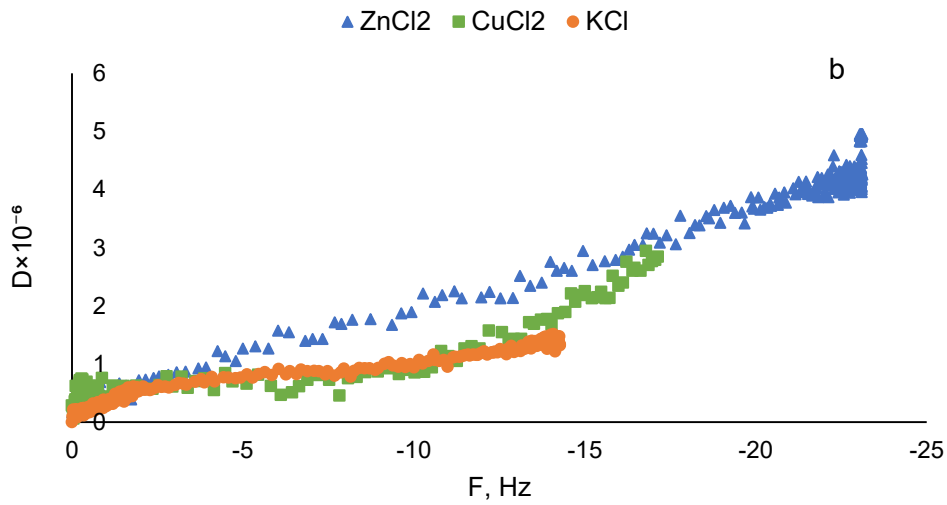
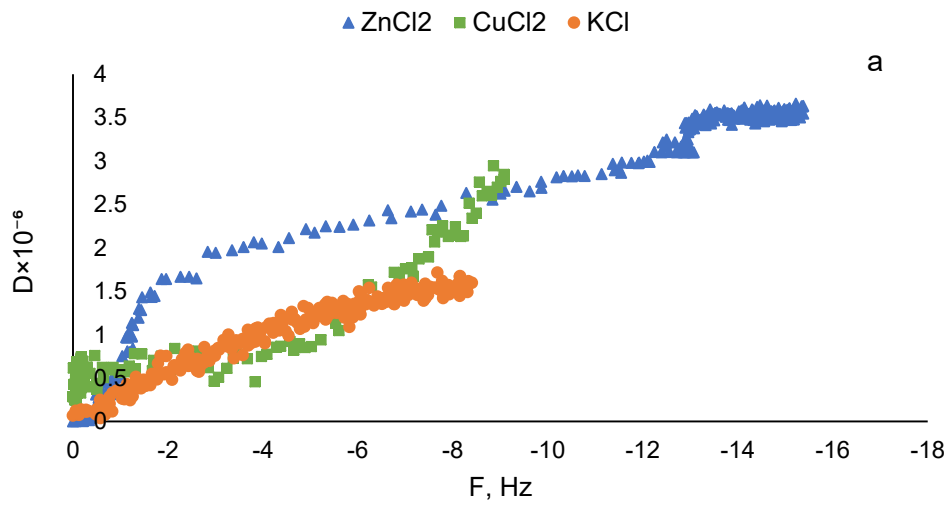
Also, the extent of ion-pairing on the KL-AA increased from monovalent K^+ to divalent Cu^{2+} and Zn^{2+} . Hence, a stronger interaction between the divalent ions on the KL-AA coated surface caused a greater electrostatic interaction, leading to higher frequency changes on the anionic surface (Figure 6.1b).

The deposition kinetics of soluble ions were also shown in Figures 1c and 1d. The large value of the dissipation of the sensor after adsorbing ions suggested the viscoelastic properties of the adsorbed layer and the Voigt model was valid for modeling adlayer mass variations as a function of time. In KL-METAM coated surface, the highest adsorbed mass (300 ng/cm^2) was achieved for $ZnCl_2$ and the adsorption affinity was faster at the initial stage (first 100 s). However, the adsorption of $ZnCl_2$ was gradually increased by prolonging the adsorption time. The maximum adsorbed mass of 267 ng/cm^2 was obtained for $CuCl_2$ at the time of 350s. Further extending the adsorption time (up to 500 s) resulted in the desorption of adlayer due to the weak adsorption energy of $CuCl_2$ toward the surface.¹³ Moreover, the maximum rate of adsorption for KCl on the

KL-METAM surface occurred at the first 150 s. However, a slight decrease in the overall adsorbed mass was observed by prolonging the adsorption time.

Similar to the KL-METAM surface, the increasing order of the adsorption rates on the KL-AA coated surface followed the sequence of $\text{ZnCl}_2 > \text{CuCl}_2 > \text{KCl}$, and the overall adsorbed mass of 455, 371, and 230 ng/cm^2 was achieved, respectively. The higher affinity of ZnCl_2 than CuCl_2 to adsorb on the lignin coated surface can be attributed to the less significant reactivity of copper and higher reactivity of zinc for interacting with other elements.⁴³ In other words, the higher tendency of copper to delocalize the outer electron (the last suborbital associated with copper is $4s^1$ and that of zinc is $4s^2$) would induce a stronger metallic bond than zinc. Evidently, breaking the greater metallic bond in copper when interacting with other elements requires more energy than that in zinc.⁴⁴ Hence, copper was deposited less when exposed to charged lignin surfaces and a longer time was needed for its adsorption.

It is worth noting that, after saturation of ions-adsorption via KL-AA and KL-METAM polymers, the solution could be acidified using 0.1 M H_2SO_4 to recover the lignin-based polymers from the ions solution. Since the main focus of this study was to investigate the maximum removal efficiency of metal ions from model waste solution we did not study the isolation of lignin macromolecules after adsorption process.



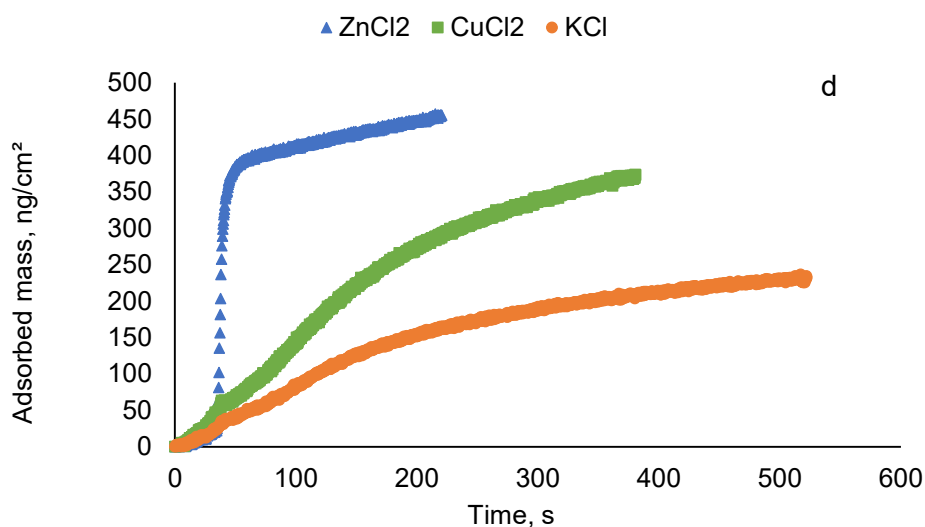
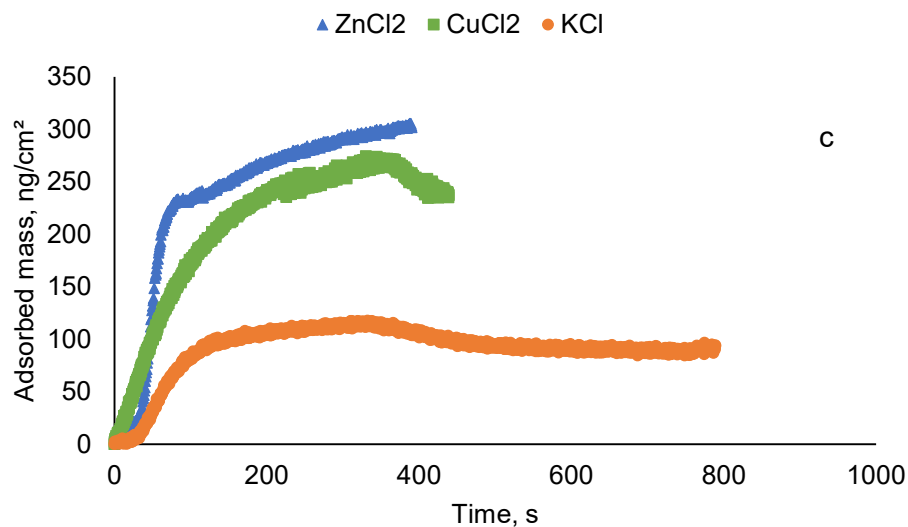


Figure 6. 1 Dissipation change of the sensors as a function of frequency changes in the adsorption of ions on a) KL-METAM and b) KL-AA; the adsorbed mass of ions on c) KL-METAM and d) KL-AA as a function of time (experiments were conducted with ionic composition at 10 mM)

6.4.3 Surface wettability of model surfaces

KL-METAM and KL-AA coated surfaces exhibited different hydrophilic natures as presented in Table 6.2. A water droplet on the bare glass slide generated the contact angle of 21°, which was in harmony with previous work.⁴⁵ The contact angle of the water droplet on KL-METAM and KL-

AA coated glass slides were 14.4° and 15.8°, respectively. These results suggest that the hydrophilicity of the glass surface was enhanced upon the polymer coating, which is attributed to the more interactions of water molecules with hydrophilic groups of KL-METAM or KL-AA (i.e., -COOH, -OH and NR₄⁺, which R can be alkyl or aryl groups)

Generally, the deposition of ion-containing droplets on the polymer-coated surfaces (i.e., cationic or anionic) further improved the hydrophilicity of the surface due to the electrostatic interaction of polymer and ionic compositions.¹³ Also, the association of divalent cations (Cu²⁺ and Zn²⁺) and monovalent K⁺ seems to reduce the contact angles on KL-AA and KL-METAM (Table 6.2). This behavior can be attributed to shielding some of the electrostatic charges of KL-AA by cations, decreasing the polarity and attraction forces of the surface, and thus suppressing the hydrophilicity of the surface.⁴⁶ The higher hydrophilicity of KL-METAM/ions than KL-AA/ions (10.5°, 11.9°, and 12.2° in case of ZnCl₂, CuCl₂, and KCl, respectively) may arise from the higher polarity of surface and formation of stronger hydrogen bonding between quaternary ammonium groups (or OH) of KL-METAM and water molecules than water and KL-AA.

Table 6. 2 Contact angles of water and model solutions (10mM) on lignin coated surfaces.

Coated surface	Contact angle (θ), °				
	Water	CuCl ₂	ZnCl ₂	KCl	Mixed model (CuCl ₂ , ZnCl ₂ and KCl)
KL-METAM	14.4±0.27	11.9±2.0	10.5±1.05	12.2±1.9	10.2° ± 0.2
KL-AA	15.8±0.9	13.6±1.3	12.7±1.5	12.6±1.03	11.6° ± 0.3

6.4.4 Surface composition changes

Figure A27 represents the wide XPS spectra of adsorbed ions on KL-METAM or KL-AA surfaces obtained from QCM-D analysis as compared with the bare surface of KL-METAM and KL-AA coated surfaces. The XPS technique was used to probe the binding energy (BE) of each element, which can be considered as a ‘fingerprint’ of each element.⁴⁷ The results confirmed that Zn^{2+} , Cu^{2+} , and K^+ were present on the surface of KL-METAM and KL-AA providing evidence for their adsorption on the coated surface, which were absent in those of KL-METAM or KL-AA coated surfaces. In KL-METAM coated surface, the peak at 934.20, 1021.40 and 284.4 eV corresponded to the $\text{Cu}_{2p_{3/2}}$ of the cupric forms,⁴⁸ $\text{Zn}_{2p_{3/2}}$, and K_{2p} as the results of their chemical bonds (i.e., ionic bonds) or electrostatic forces between Cu^{2+} , Zn^{2+} , and K^+ and the amino groups of KL-METAM. According to Table 6.3, Zn^{2+} was present more (17.69 %) on KL-AA than on KL-METAM (7.62%) coated surface, which was consistent with the QCM results. As shown in Figure A27, the N1s binding energies of the N–C bond in ionic composition/KL-METAM were 399.4 eV for Cu or K, and 402.2 eV for Zn, respectively. The reason for the higher binding energy of the Zn element could be ascribed to the chelating site formation between Zn^{2+} and the N atom of the amino group,⁴⁹ which led to the transfer of electrons from the N atom of the amino group (in KL-METAM) to metal ions.⁵⁰

Also, the highest mass concentration of $\text{Zn}_{2p_{3/2}}$ photoelectron (17.69%) indicated the highest adsorption of Zn^{2+} on KL-AA compared to the other elements (13.99% and 8.89%). Moreover, comparing the O_{1s} XPS spectra of KL-AA surface before and after ions adsorption, it was observed that after the binding of COO^- with Zn^{2+} , Cu^{2+} and K^+ ; the binding energy of C=O in the carboxylate group would shift from 531.0 to 532.4 eV; but the intensity of the peak dropped. The signal shift from 535.2 to 532.9 eV is attributed to the binding energy of C–O in carboxylate groups

indicating the donation of electrons in the oxygen atom to the shared bond between the oxygen of the carboxylate group and Zn^{2+} , Cu^{2+} , and K^+ ions.⁵¹

The adsorption of monovalent K^+ on both surfaces (KL-AA and KL-METAM) were lower than other cations, which was attributed to 1) the weaker charge interaction of K^+ with the carboxylate group of KL-AA (compared with divalent elements) and 2) the repulsive electrostatic interactions of the quaternary ammonium group of KL-METAM and K^+ .

As seen in Figure A27, the peaks at binding energies of 197.4-199.6 eV corresponded to Cl_{2p} .⁵² Compared to the KL-AA surface, the greater mass concentration of Cl^- on the surface of KL-METAM confirmed the higher adsorption of chloride ion on the quaternary ammonium group of KL-METAM surface. Moreover, the peaks of Cl_{2p} shifted to the position of lower binding energy when adsorbed on KL-METAM as compared with that of KL-AA, suggesting the higher interaction between Cl^- and KL-METAM (i.e., electrostatic forces).⁵²

Table 6. 3 XPS characterization of the lignin films before and after ionic adsorption

Sample	Properties	
	Component	Mass concentration, %
KL-METAM surface	O_{1s}	24.91
	N_{1s}	5.47
	C_{1s}	69.38
KL-METAM/ions	$Cu_{2p3/2}$, Cl_{2p}	5.38±0.59, 9.33±0.66
	$Zn_{2p3/2}$, Cl_{2p}	7.62±0.68, 23.8±0.48
	K_{2p} , Cl_{2p}	5.33±0.53, 4.09±0.40
KL-AA surface	O_{1s}	24.66

	C _{1s}	56.11
KL-AA/ions	Cu _{2p3/2} , Cl _{2p}	13.99±0.86, 7.81±0.57
	Zn _{2p3/2} , Cl _{2p}	17.69±0.28, 10.48±0.30
	K _{2p} , Cl _{2p}	8.89±0.53, 3.6±0.41

6.4.5 Mechanism of adsorption of ions on lignin derivatives

The adsorption of ions on the lignin-coated surfaces is mainly controlled by the electrostatic charge interactions. Figure 6.2 shows the possible mechanism for ions adsorption on KL-METAM and KL-AA. The monovalent Cl⁻ ion of salt solutions can attach to the quaternary ammonium group of KL-METAM via electrostatic attraction forces as confirmed by XPS results. As K⁺, Cu²⁺, Zn²⁺, and METAM part of KL-METAM would electrostatically repel each other, the amount of adsorbed ions on KL-METAM was limited. Instead, the binding of the ions on the KL-METAM surface would only be restricted to the deposition of ions on the lignin part of the KL-METAM due to its negative dipole moment of lignin.⁵³ The carboxylate and hydroxy groups on lignin structure (Table 6.1) can promote the interaction of lignin and Cu²⁺, Zn²⁺, which increases the stability of the metal-ligand complexes. Moreover, the formation of cation- π interaction between low electron density ions and high electron density of the π system in the aromatic structure of lignin macromolecules has been suggested to play a role in the adsorption mechanism of cations on lignin.⁵⁴

However, in the case of KL-AA, the ions can easily adsorb on both lignin and attached acrylic acid monomer through charge interaction/ion exchange leading to the higher adsorbed amount of ions on the KL-AA surface as evident by the QCM and XPS results. Another possible mechanism for

ions adsorption on the KL-AA polymer can be complexation/chelation with the carboxyl group of the AA chain of KL-AA.⁵⁵ In such a case, a chelate formation can easily occur between divalent Cu^{2+} and Zn^{2+} ions and the lone pair of electrons present on the carboxylate group of KL-AA,⁵⁶ resulting in the adsorption of ions on lignin polymers.⁵⁵ As seen in Figure 6.2b, the carboxylate group on the surface of KL-AA acted as active sites for the adsorption of divalent cations. Then, part of cationic ions was captured by two carboxylate groups simultaneously through complexation. This phenomenon was previously observed for the adsorption of Cu^{2+} ion on carboxymethylated cellulose nanofibrils.⁵¹ The Cl^- ion can also entrap within the chains of the KL-AA macromolecule.

As seen in Figure 6.2, the magnitude of cation adsorption on KL-METAM and KL-AA was in the order of $\text{Zn}^{2+} > \text{Cu}^{2+} > \text{K}^+$. However, the higher deposition of ions, and in particular Zn^{2+} , (Figure 6.1d and Table 6.3) along with more water molecule entrapment (i.e., higher dissipation value in Figure A26) created a thicker and more viscoelastic adsorbed layer on KL-AA (Figure 6.2a).

Also, the higher strength of electrostatic interaction between ions and KL-AA along with π -interaction and chelation resulted in higher adsorption on KL-AA than KL-METAM.

a



b

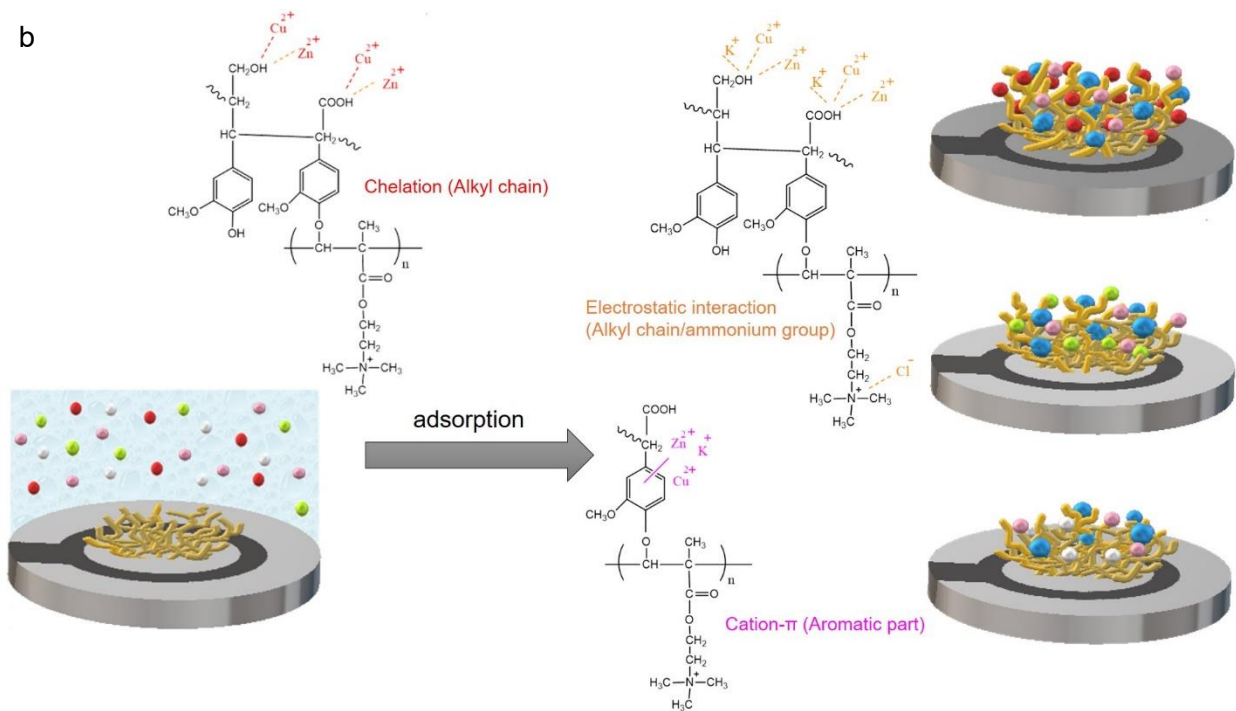




Figure 6. 2 Mechanism model of ions adsorption using a) KL-AA and b) KL-METAM coated surface.

6.4.6 Flocculation analysis

The kinetics of destabilization index of different model effluents upon addition of KL-METAM and KL-AA polymer was shown in Figures A28 and A29, respectively. The ionic composition solutions and pure KL-METAM or KL-AA polymer solution (10 g/L) were selected as control samples. In the absence of lignin polymers, the ionic solutions had approximately zero transmission in 30 min of the experiment. However, the destabilization index of the solutions containing only lignin macromolecules (i.e., KL-AA or KL-METAM) slightly increased in 30 min of analysis. This behavior would imply that the lignin macromolecules self-assembled during the test and formed clusters that were relatively stable in the solutions.

As illustrated in Figures A28 and A29, the different dosages of KL-METAM and KL-AA were added to the model samples to investigate their stability as a function of time. As time elapsed, the produced complexes and aggregates started to settle and gradually clarified the system (i.e., increased the TSI value). Lower transmission represents the existence of a larger number of suspended particles, while a higher transmission indicates a larger number of settled particles as a result of flocculation.⁵⁷ The anionic KL-AA promoted significant TSI changes in CuCl₂, ZnCl₂, and KCl systems in the 30 min test (Figure A29). The adsorption of ions on the KL-AA polymer following the mechanisms discussed in section 3-5 promoted the generation of large flocs. These heavy flocs are settled with a high settling velocity.⁵⁸ Moreover, the higher concentration of ionic

composition/KL-AA polymer (i.e., 10 g/L) increased the destabilization index of the ionic solutions due to the introduction of more negative charges by the KL-AA. Results also depicted that the ZnCl₂ solution reached the equilibrium level in 500s and no significant changes in the clarified zone were observed by prolonging time. However, the maximum transmittance zone was obtained in 1000 s for the CuCl₂ solution due to less reactivity of Cu than Zn⁴⁴ as also seen in (Figure 6.1d). The continuous increase in the TSI values was observed for KCl treated samples throughout the experiment.

However, this clarification marginally occurred for the systems treated with cationic KL-METAM (10g/L). In this case, the smaller slope obtained from the flocculation curves indicated the limited affinity of KL-METAM to destabilize the ionic solution compared to that of KL-AA. This effect was more highlighted in ionic solutions containing Cu⁺² and Zn⁺² due to an enhanced mutual repulsion between the cations and ammonium group of KL-METAM polymer in the solution, which was in harmony with the adsorption results (Figure 6.1). The initial ζ values of CuCl₂, ZnCl₂, and KCl solutions were observed to be 4 mV, 5 mV, and 1 mV, respectively. Upon the addition of KL-METAM polymer to the model solutions, the ζ increased (Figure A30) and their TSI reached the maximum values of 1.9, 4.9, and 2.6 for CuCl₂, ZnCl₂, and KCl solutions, respectively. Limited TSI value changes pointed to an ineffective interaction among monovalent/divalent ions and KL-METAM.

6.4.7 Dual polymer system

Competitive adsorption in a dual polymer system

To study the effect of a dual adsorption system, the cationic and anionic lignin coated surface was treated by the ion solutions mixed with the lignin derivative with an opposite charge. For example,

the KL-METAM surface was treated with the solution of ions and KL-AA and vice versa. Figure 6.3 shows the dissipation versus frequency of the films. Compared with the single polymeric system (Figure 6.1), the adsorption capacities of all three ionic compositions in the dual system were remarkably higher. As illustrated in Figure 6.3, KL-METAM polymer and KL-AA had limited interaction and thus adsorption, in which the ΔF values were raised only to -6.7 and -21.3 Hz for KL-METAM and KL-AA coated surfaces, respectively. However, the adsorption of lignin polymers on the oppositely charged lignin surface facilitates the adsorption of ions on the coated surfaces (Figure 6.3). This finding is in line with previous reports stating that the adsorption capacity for heavy metal ions was improved significantly in a dual system compared with the singular system.⁵⁹⁻⁶¹

As charged polymers may not stoichiometrically interact with each other, there might be unoccupied charges on the surface of KL-METAM or KL-AA, and the available charges will contribute to the adsorption of ions, such as K^+ . Also, KL-METAM and KL-AA would adsorb ions, as observed earlier, and thus their combination in the dual polymer system would promote the overall adsorption of ions. As seen in Figure 6.3, the adsorption on the KL-AA surface was more than the KL-METAM surface. The adsorption exhibited the most rapid deposition of $ZnCl_2$ followed by $CuCl_2$ solution on KL-AA surface that created a thicker and more viscoelastic adlayer compared to that on KL-METAM coated surface (Figure 6.2a). However, the impact of electric double layer compression, screening chain substrate interactions, and insufficient adsorption site for the deposition of K^+ developed a denser adlayer.¹³

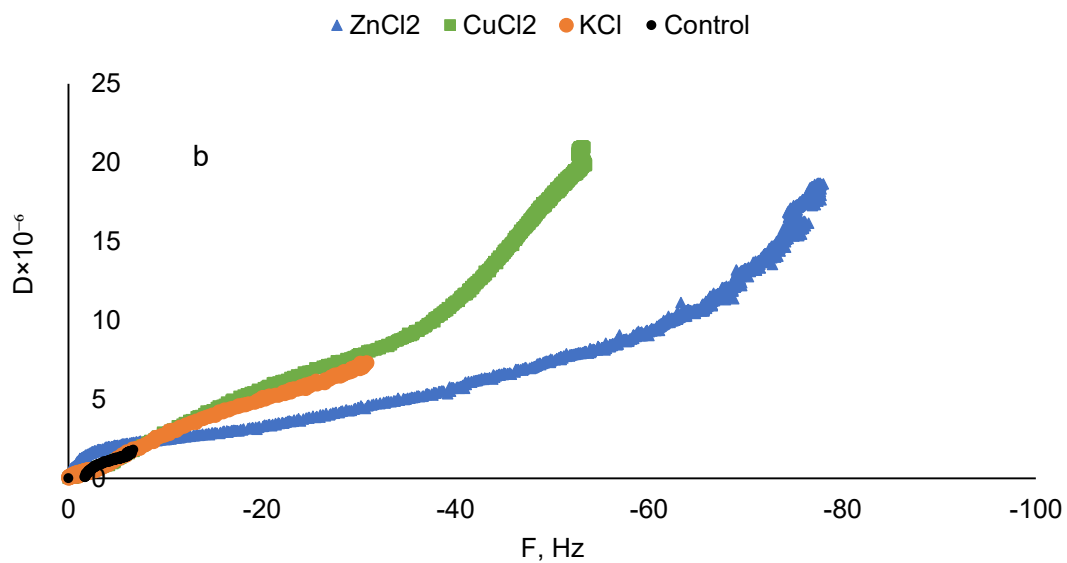
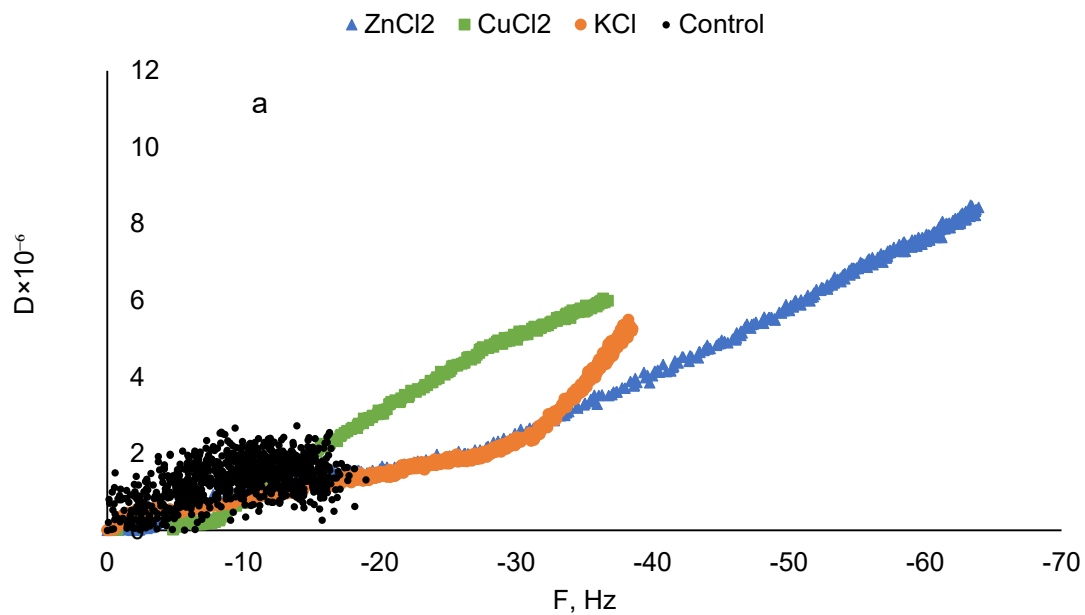


Figure 6. 3 Dual component adsorption of CuCl₂, ZnCl₂, and KCl on a) KL-METAM surface, b) KL-AA surface (10 mM salt concentration, the control solution contained lignin derivative with the opposite charge to the lignin coated surface)

Competitive flocculation in a dual polymer system

A two-step flocculation process in ionic solutions using oppositely charged polymers (KL-METAM and KL-AA polymers) are presented in Figure 6.4. To ensure the maximum interaction between polymers and ions and to minimize the competitive interaction of KL-METAM and KL-AA in the flocculation process, the polymers were sequentially added to the ion solutions (i.e., first KL-METAM, then KL-AA and vice versa in the other scenario). The optimum dosage of cationic and anionic polymers was selected based on the results presented in Figures A28 and A29. The first scenario was the addition of KL-METAM to the ion solution followed by KL-AA (after 30 min) (Figure 6.4a). Results showed that the TSI value of ZnCl₂ containing solution reached the maximum of 51, while the TSI of KCl and CuCl₂ solutions were almost identical (20 and 23, respectively). The addition of both polymers also resulted in the changes of ζ potential of ZnCl₂, CuCl₂, and KCl solutions from 12, 32, and 13 to 5, 15, and 9, respectively. The results are in line with adsorption behavior in the dual polymer system shown in Figure 6.3a.

Figure 6.4b exhibited the dual system, in which KL-AA was added first to the different salt solutions in which the TSI values changed from 0 to 26, 15, and 5.5 for treated ZnCl₂, CuCl₂, and KCl solutions, respectively. The addition of the KL-AA reduced the ζ potential of ZnCl₂ and CuCl₂ systems (-15 and -12 mV, respectively). After 30 min, KL-METAM was added to the system. In this case, the TSI value of ZnCl₂ and CuCl₂ solutions reached 83 and 45, respectively, which also changed the ζ potential of ZnCl₂ and CuCl₂ systems to -3 and -7, respectively. These results confirmed that both charge neutralization and patching mechanisms were involved in the flocculation of ions.⁸ However, the destabilization index of the KCl solution decreased to 14 when the system was treated with KL-AA and then KL-METAM.

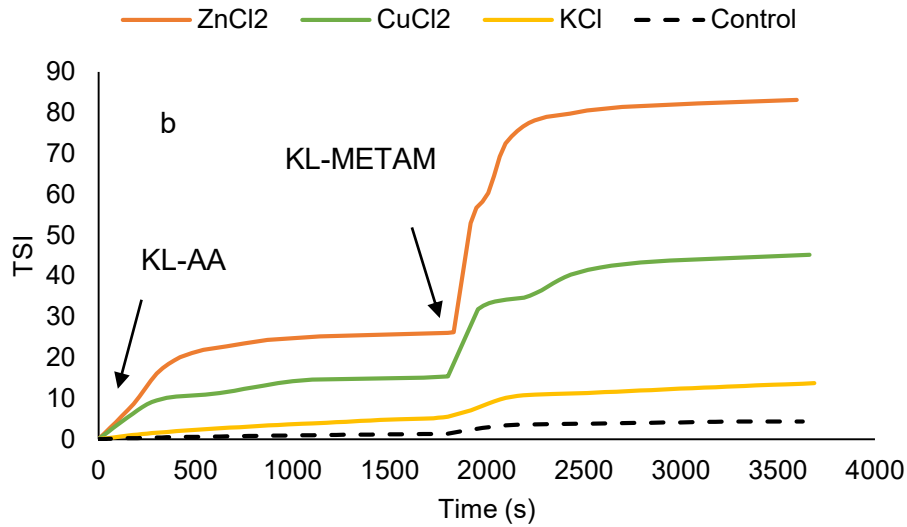
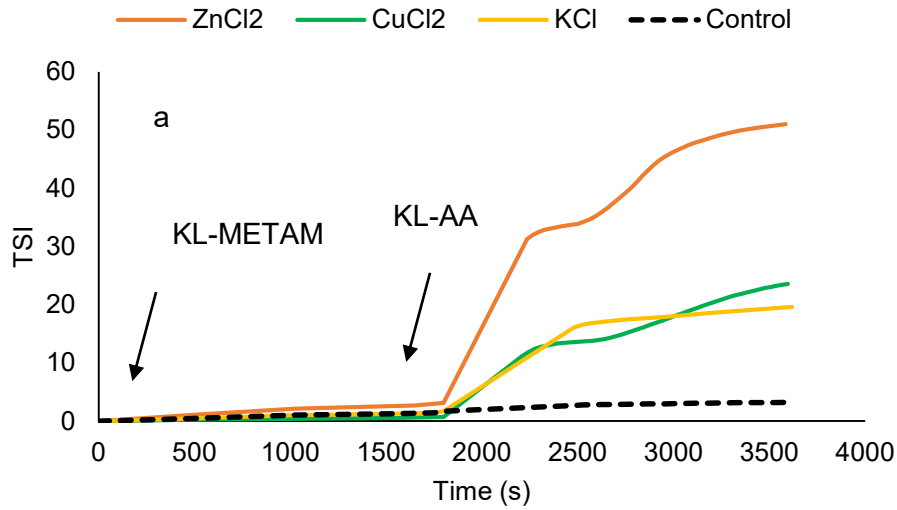


Figure 6. 4 The effect of dual polymer system on the destabilization index of the model solutions (control solution contained lignin derivative with the opposite charge and no salt)

To further validate the flocculation results, the mean aggregate sizes (d) of lignin polymer/ion solutions were measured in the flocculation process and results are tabulated in Table 6.4. In the salt-free system, the d of mixed KL-METAM and KL-AA increased significantly compared to

those in the singular system. The coagulation of KL-METAM and KL-AA expanded the molecular coils of the polymers by enhancing the loop and tail formations resulted in large open flocs and promoting flocculation.

The KL-METAM or KL-AA altered the d of ions solutions from $170 < \text{picometer (pm)}^{62}$ up to 0.7-1.8 μm , which favored the formation of complexes between ions and lignin macromolecules, leading to more flocculation and settling (more TSI value in Figure 6.4). In the dual system, the subsequent addition of the second polymer led to a remarkable alteration in d . However, the combined KL-AA/KL-METAM system generated the largest aggregates in ZnCl_2 solution (d of 4.44 μm) due to the more efficient interaction of Zn^{2+} with KL-AA/KL-METAM (Figure 6.4), which supports the results presented in Figure 6.3.

Table 6. 4 Mean aggregate sizes (d) obtained for the model solutions in the single and dual polymer systems (conducted under the conditions of 10 g/L polymer solution, and 0 or 10 mM model effluent).

Sample	d (μm)				
	CuCl ₂	ZnCl ₂	KCl	No salt	All salts
KL-METAM	0.74	0.86	0.787	0.03	-
KL-AA	0.97	1.86	1.03	0.02	-
KL-METAM/KL-AA	1.62	3.60	1.31	0.71	-
KL-AA/KL-METAM	2.27	4.44	1.28	0.86	5.33

Error was $<5\%$.

6.4.8 Adsorption and flocculation in a mixed system

The negligible changes were found between the contact angles of mixed model solution (ZnCl_2 , CuCl_2 , and KCl) on both KL-METAM and KL-AA coated surfaces compared to that of single solution systems reported (Table 6.2).

The normalized frequency and dissipation in the adsorption of mixed model solutions on lignin derivatives are presented in Figure 6.5. Similar to the previous adsorption results (Figures 1 and 3), more adsorption was achieved on the KL-AA surface than on the KL-METAM surface (5390 ng/cm² on KL-AA vs 3410 ng/cm² on KL-METAM). The cartoon model of ion removals using KL-AA and KL-METAM coated surface is proposed in Figure 6.6. Accordingly, the mutual electrostatic attraction between KL-AA and KL-METAM considerably increased the possibility of the formation of polymer bridges between the coated polymers and approaching polymers as well as ions.

It is worth mentioning that the viscoelastic properties of the adsorbed layer in the mixed solution was slightly less than the adlayer of the single solution system on the surface of KL-AA (Figure 6.3b). This might be due to the more diffusion of mixed solution into the KL-AA coated layer, which leads to reorganization and densification of the adsorbed layer.⁶³ However, no significant changes were observed between the viscoelastic properties of the adsorbed layer in the mixed solution and that of the single solution system for the KL-METAM surface.

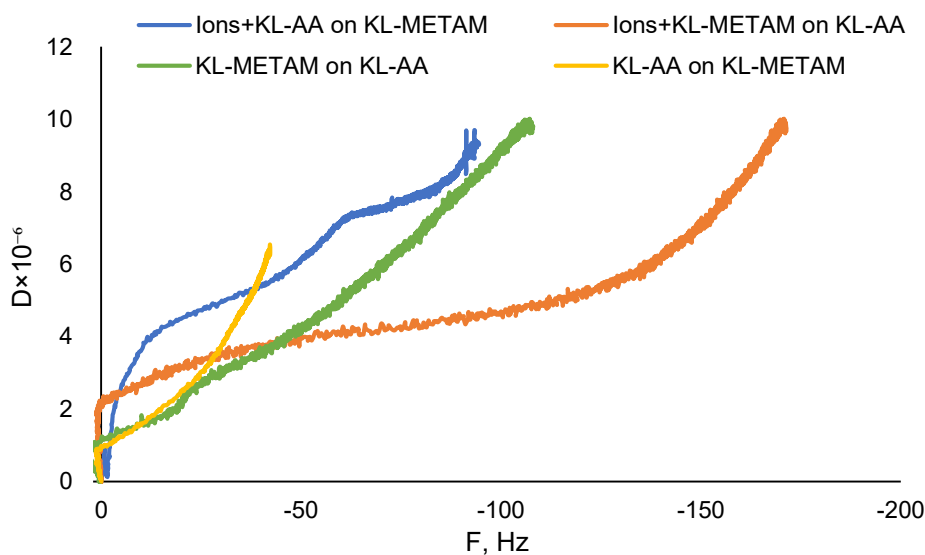


Figure 6. 5 Dual-component adsorption of mixed model solution (10 mM, 20 min, salt solutions are mixed with lignin polymer and adsorbed on the oppositely charged lignin coated surface)

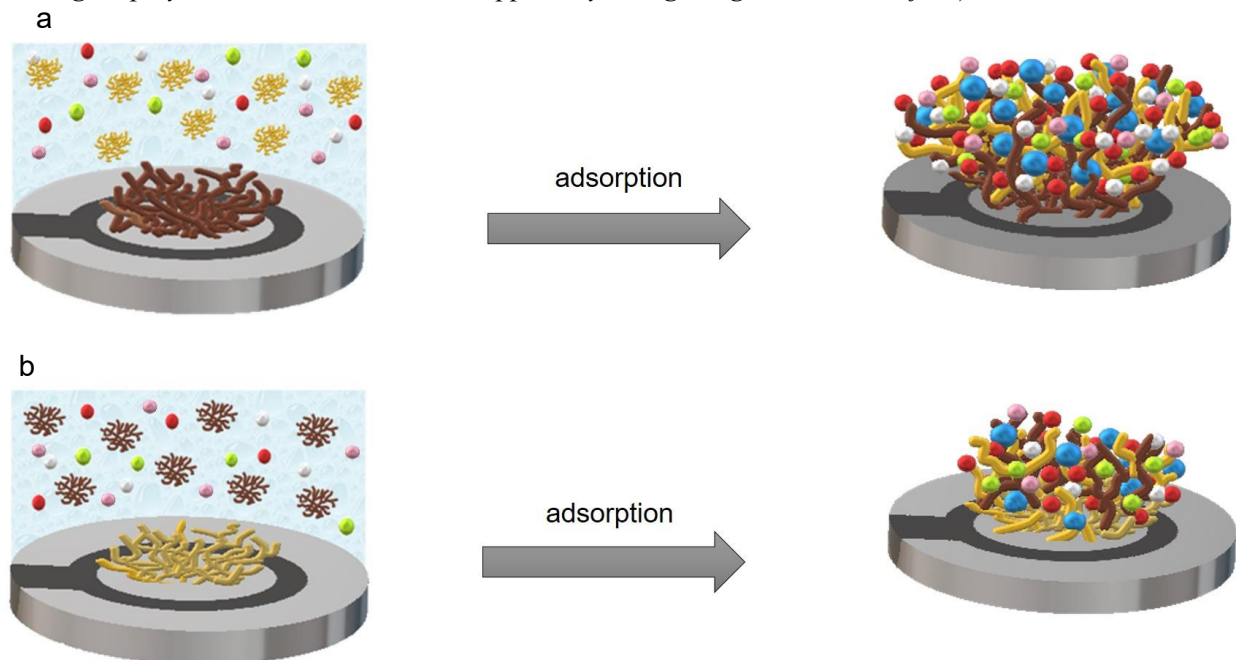


Figure 6. 6 Proposed adsorption mechanism of the dual-component adsorption in mixed model solution on QCM sensor coated with a) KL-AA and b) KL-METAM

The synergistic effect of binary mixtures of KL-AA and KL-METAM in the flocculation of mixed ion solution was shown in Figure 6.7. Since the presence of KL-AA followed by KL-METAM had the greatest effect on the adsorption and instability of ionic composition solutions, this sequence was employed in the mixed solution. The results revealed a drastic increase in the instability of model solutions in which the TSI value reached 95 in the presence of the polymers.

The better flocculation performance of the dual polymer system in the mixed model solution (Figure 6.7) compared to that of the single polymer flocculant (Figure A31) could be due to the mechanism involved in the flocculation of ions by lignin polymers. As stated earlier, each polymer could adsorb ions as illustrated in Figure 6.2 in the saline systems. Then, the oppositely charged lignin polymers could attract each other and adsorb in a dual polymer system. In this case, the rest

of the uninvolved charges of lignin polymers (if any) will be neutralized by extra ions. Additionally, there would be some ions physically trapped within the structure of the polymer flocs, and some ions could diffuse in the voids of the polymer flocs.

It should be pointed out that the ζ of the mixed solution reached 5.5 mV (from 8.4 mV) when KL-AA and KL-METAM were added, implying the higher flocculation efficiency and formation of larger flocs as compared with the singular solution system. In such a case, the larger aggregate diameter (5.33 μm) was attributed to the greater binding of ions and lignin macromolecules (Figure 6.6).

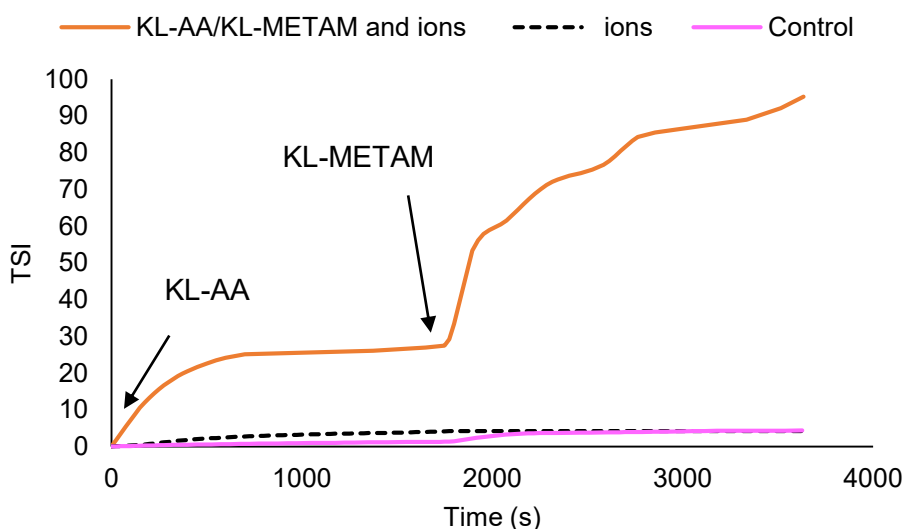


Figure 6. 7 The effect of the dual polymer system on the destabilization index of the mixed model solutions (10 mM)

6.4.9 Ion removal efficiency using different materials

The stability performance of KL-AA/KL-METAM was compared with other polymers (natural or synthetic), and the results are shown in Table 6.5. As seen, the removal efficiency of ions using KL-AA/KL-METAM polymers was much higher than those reported in other studies. Moreover,

the optimum dosage of KL-AA and KL-METAM used in this work was significantly lower than that stated in other reports. Superior enhancement of TSI value obtained at neutral pH can be another advantage of using lignin-based materials in the destabilization of ionic composition from aqueous solution. Overall, the results confirmed that the application of KL-AA/KL-METAM for ions removal is promising.

Table 6. 5 Comparison of various polymers for the destabilization of ions in water

Polymer	Ions	pH	Dosage	TSI
KL-AA and KL-METAM	Zn ²⁺ , Cu ²⁺ , K ⁺	7	10 mg/L + 0.2 mg/L	95
Coffee lignin ⁶⁴	Cr ³⁺ , Zn ²⁺ , Pb ²⁺ ,	5.5	95 mg/L	55
Tule lignin	Ni ²⁺ , Ca ²⁺ , Cd ²⁺ , Cu ²⁺		155–185 mg/L	40
Chitosan-graft-poly(N-vinylcaprolactam) ⁶⁵	Cr ³⁺ , Pb ²⁺ , Cu ²⁺ , Ni ²⁺ , Zn ²⁺ , Ca ²⁺ , Cd ²⁺	4.7	97 mg/L	70
Anionic polyacrylamide ⁶⁶	Cr ³⁺	9	100 mg/L	45.5
Anionic polyacrylamide and cationic polyacrylamide ⁸	Cr ³⁺	6	100 mg/L	50

Poly(L-aspartic acid Cr ³⁺ sodium salt)-block-poly(ethylene glycol) ⁶⁷	3	200 mg/L	52
--	---	----------	----

6.5 Conclusions

Various scenarios were examined for the removal of heavy metal ions using lignin derivative polymers. Results showed that KL-AA was more efficient than KL-METAM for removing ions from the solution due to the greater electrostatic attraction as well as cation- π interaction and chelation/complexation mechanism developed between the polymer and ions. QCM and XPS analyses proved that divalent ions tended to adsorb via chelation/complexation mechanism on both alkyl chains and carboxylic groups of KL-AA coated films. Cationic- π interactions between ions and the aromatic part of lignin macromolecules were also responsible for the uptake of cationic ions from the aqueous solutions. Compared to the single polymer system, the dual polymer system had higher adsorption and flocculation capacity for ions when KL-AA was introduced as a first polymer followed by KL-METAM because KL-AA had a stronger affinity to adsorb ions, and then KL-METAM could form bridges to entrap the unattached ions. Moreover, the diffusion of ions into the voids of polymer flocs enhanced the flocculation efficiency of the dual system compared to the single polymer system, which manifested by larger aggregate size. Compared with the reported findings, the present work indicated that KL-AA/KL-METAM polymers were more efficient for eliminating ions from the model solutions. Among the ion solution studied, the removal efficiency of Zn²⁺ was more significant than other ions due to its higher reactivity for

interacting with other elements. The QCM results also revealed that the deposition of ions on the KL-AA coated surface generated a bulkier and more viscoelastic adlayer compared to that on the KL-METAM surface. A similar trend was also observed in the multi-component systems.

6.6 References

- (1) Dey, K.P., Mishra, S. Sen, G., 2017. Synthesis and characterization of polymethylmethacrylate grafted barley for treatment of industrial and municipal wastewater. *J. Water Process. Eng.* 18, 113-125.
- (2) Hargreaves, A.J., Constantino, C., Dotro, G., Cartmell, E. Campo, P., 2018. Fate and removal of metals in municipal wastewater treatment: a review. *Environ. Technol. Rev.* 7(1),1-18.
- (3) Darko, G., Azanu, D. Logo, N.K., 2016. Accumulation of toxic metals in fish raised from sewage-fed aquaculture and estimated health risks associated with their consumption. *Cogent Environ. Sci.* 2(1), 1190116.
- (4) Alhadrami, H.A., Mbadugha, L. Paton, G.I., 2016. Hazard and risk assessment of human exposure to toxic metals using in vitro digestion assay. *Chem. Speciat. Bioavailab.* 28(1-4), 78-87.
- (5) Peters, A., Merrington, G., De Schampelaere, K. Delbeke, K., 2011. Regulatory consideration of bioavailability for metals: Simplification of input parameters for the chronic copper biotic ligand model. *Integr. Environ. Assess. Manag.* 7(3), 437-444.
- (6) Feng, L., Zheng, H., Gao, B., Zhang, S., Zhao, C., Zhou, Y. Xu, B., 2017. Fabricating an anionic polyacrylamide (APAM) with an anionic block structure for high turbidity water separation and purification. *RSC Adv.* 7(46), 28918-28930.

- (7) Teh, C.Y., Budiman, P.M., Shak, K.P.Y. Wu, T.Y., 2016. Recent advancement of coagulation–flocculation and its application in wastewater treatment. *Ind. Eng. Chem. Res.* 55(16), 4363-4389.
- (8) Wiśniewska, M., Chibowski, S., Urban, T. Terpiłowski, K., 2019. Investigations of chromium (III) oxide removal from the aqueous suspension using the mixed flocculant composed of anionic and cationic polyacrylamides. *J. Hazard. Mater.* 368, 378-385.
- (9) Zahri, N.A.M., Jamil, S.N.A.M., Abdullah, L.C., Huey, S.J., Yaw, T.C.S., Mobarekeh, M.N. Rapeia, N.S.M., 2017. Equilibrium and kinetic behavior on cadmium and lead removal by using synthetic polymer. *J. Water Process. Eng.* 17, 277-289.
- (10) Sabaghi, S. Fatehi. P. 2019. Phenomenological changes in lignin following polymerization and its effects on flocculating clay particles, *Biomacromolecules* 20, 3940-3951.
- (11) Kong, F., Wang, S., Gao, W. Fatehi, P., 2018. Novel pathway to produce high molecular weight kraft lignin–acrylic acid polymers in acidic suspension systems. *RSC Adv.* 8(22), 12322-12336.
- (12) Boeije, G., Corstanje, R., Rottiers, A. Schowanek, D., 1999. Adaptation of the CAS test system and synthetic sewage for biological nutrient removal: Part I: Development of a new synthetic sewage. *Chemosphere* 38(4), 699-709.
- (13) Huang, H., Ding, L.L., Ren, H.Q., Geng, J.J., Xu, K. Zhang, Y., 2015. Preconditioning of model biocarriers by soluble pollutants: a QCM-D study. *ACS Appl. Mater. Interfaces.* 7(13), 7222-7230.
- (14) Orgad, O., Oren, Y., Walker, S.L. Herzberg, M., 2011. The role of alginate in *Pseudomonas aeruginosa* EPS adherence, viscoelastic properties and cell attachment. *Biofouling* 27(7), 787-798.

- (15) Li, Y., Su, Y., Zhao, X., He, X., Zhang, R., Zhao, J., Fan, X. Jiang, Z., 2014. Antifouling, high-flux nanofiltration membranes enabled by dual functional polydopamine. *ACS Appl. Mater. Interfaces*. 6(8), 5548-5557.
- (16) Armanious, A., Aeppli, M. Sander, M., 2014. Dissolved organic matter adsorption to model surfaces: adlayer formation, properties, and dynamics at the nanoscale. *Environ. Sci. Technol.* 48(16), 9420-9429.
- (17) Guo, K., Gao, B., Wang, W., Yue, Q. Xu, X., 2019. Evaluation of molecular weight, chain architectures and charge densities of various lignin-based flocculants for dye wastewater treatment. *Chemosphere* 215, 214-226.
- (18) Liu, Z., Lu, X., Xie, J., Feng, B. Han, Q., 2019. Synthesis of a novel tunable lignin-based star copolymer and its flocculation performance in the treatment of kaolin suspension. *Sep. Purif. Technol.* 210, 355-363.
- (19) Al-Dawery, S.K., 2017. Degree of flocculation and Interparticles charges of conditioned Municipal Activated Sludge using Mixed Polymers. *J. Macromol. Sci. B.* 56(8), 578-594.
- (20) Lu, Q., Yan, B., Xie, L., Huang, J., Liu, Y. Zeng, H., 2016. A two-step flocculation process on oil sands tailings treatment using oppositely charged polymer flocculants. *Sci. Total Environ.* 565, 369-375.
- (21) Glover, S.M., Jameson, G.J. Biggs, S., 2004. Dewatering properties of dual-polymer-flocculated systems. *Int. J. Miner. Process.* 73(2-4), 145-160.

- (22) Li, R., Gao, B., Sun, S., Yue, Q., Li, M., Yang, X., Song, W. Jia, R., 2015. Amine-Cross-Linked lignin-based polymer: modification, characterization, and flocculating performance in humic acid coagulation. *ACS Sustain. Chem. Eng.* 3(12), 3253-3261.
- (23) Kong, F., Wang, S., Price, J.T., Konduri, M.K. Fatehi, P., 2015. Water soluble kraft lignin–acrylic acid copolymer: Synthesis and characterization. *Green Chem.* 17(8), 4355-4366.
- (24) He, W., Gao, W. Fatehi, P., 2017. Oxidation of kraft lignin with hydrogen peroxide and its application as a dispersant for kaolin suspensions. *ACS Sustain. Chem. Eng.* 5(11), 10597-10605.
- (25) Bayazeed, A., Elzairy, M.R. Hebeish, A., 1989. Synthesis and Application of New Thickeners Part I: Preparation of Poly (Acrylic Acid)-Starch Graft Copolymer. *Starch* 41(6), 233-236.
- (26) Jahan, M.S., Chowdhury, D.N., Islam, M.K. Moeiz, S.I., 2007. Characterization of lignin isolated from some nonwood available in Bangladesh. *Bioresour. Technol.* 98(2), 465-469. (27) Yan, M., Yang, D., Deng, Y., Chen, P., Zhou, H. Qiu, X., 2010. Influence of pH on the behavior of lignosulfonate macromolecules in aqueous solution. *Colloid Surf. A Physicochem. Eng. Asp.* 371(1-3), 50-58.
- (28) Tammelin, T., Österberg, M., Johansson, L.S. Laine, J., 2006. Preparation of lignin and extractive model surfaces by using spincoating technique–Application for QCM-D studies. *Nord. Pulp Pap. Res. J.* 21(4), 444-450.
- (29) Ying, W., Yang, F., Bick, A., Oron, G. Herzberg, M., 2010. Extracellular polymeric substances (EPS) in a hybrid growth membrane bioreactor (HG-MBR): viscoelastic and adherence characteristics. *Environ. Sci. Technol.* 44(22), 8636-8643.

- (30) Liu, S.X. Kim, J.T., 2009. Application of Kelvin—Voigt model in quantifying whey protein adsorption on polyethersulfone using QCM-D. *JALA*. 14(4), 213-220.
- (31) Sakai, K., Quartz Crystal Microbalance with Dissipation Monitoring (QCM-D). In *Measurement Techniques and Practices of Colloid and Interface Phenomena*; Springer, Singapore: 2019, 45-50.
- (32) Maximova, N., Österberg, M., Laine, J. Stenius, P., 2004. The wetting properties and morphology of lignin adsorbed on cellulose fibres and mica. *Colloids Surf. A Physicochem. Eng. Asp.* 239(1-3), 65-75.
- (33) Korin, E., Froumin, N. Cohen, S., 2017. Surface analysis of nanocomplexes by X-ray photoelectron spectroscopy (XPS). *ACS Biomater. Sci. Eng.* 3(6), 882-889.
- (34) Mengual, O., Meunier, G., Cayre, I., Puech, K. Snabre, P., 1999. Characterisation of instability of concentrated dispersions by a new optical analyser: the TURBISCAN MA 1000. *Colloid Surf. A Physicochem. Eng. Asp.* 152(1-2), 111-123.
- (35) Mills, P. Snabre, P., 1994. Settling of a suspension of hard spheres. *Europhys. Lett.* 25(9), 651.
- (36) Bisht, H.S., Ray, S.S. Chatterjee, A.K., 2003. Resonance, polar, and steric effects of substituent on monomer reactivity in radical polymerization of alkyl 4-vinylbenzoate and butylacrylate. *J. Polym. Sci. A Polym. Chem.* 41(12), 1864-1866.
- (37) Sun, Y., Ma, Z., Xu, X., Liu, X., Liu, L., Huang, G., Liu, L., Wang, H. Song, P., 2020. Grafting lignin with bioderived polyacrylates for low-cost, ductile, and fully biobased poly (lactic acid) composites. *ACS Sustain. Chem. Eng.* 8(5), 2267-2276.

- (38) Li, H., Deng, Y., Liu, B., Ren, Y., Liang, J., Qian, Y., Qiu, X., Li, C. Zheng, D., 2016. Preparation of nanocapsules via the self-assembly of kraft lignin: A totally green process with renewable resources. *ACS Sustain. Chem. Eng.* 4(4), 1946-1953.
- (39) Deng, Y., Feng, X., Zhou, M., Qian, Y., Yu, H. Qiu, X., 2011. Investigation of aggregation and assembly of alkali lignin using iodine as a probe. *Biomacromolecules* 12(4), 1116-1125.
- (40) Wang, T., Wang, X., Long, Y., Liu, G. Zhang, G., 2013. Ion-specific conformational behavior of polyzwitterionic brushes: exploiting it for protein adsorption/desorption control. *Langmuir* 29(22), 6588-6596.
- (41) O'Neal, J.T., Dai, E.Y., Zhang, Y., Clark, K.B., Wilcox, K.G., George, I.M., Ramasamy, N.E., Enriquez, D., Batys, P., Sammalkorpi, M. Lutkenhaus, J.L., 2018. QCM-D investigation of swelling behavior of layer-by-layer thin films upon exposure to monovalent ions. *Langmuir* 34(3), 999-1009.
- (42) Volodkin, D. von Klitzing, R., 2014. Competing mechanisms in polyelectrolyte multilayer formation and swelling: Polycation–polyanion pairing vs. polyelectrolyte–ion pairing. *Curr. Opin. Colloid Interface Sci.* 19(1), 25-31.
- (43) Kunz, W., 2010. Specific ion effects in colloidal and biological systems. *Curr. Opin. Colloid Interface Sci.* 15(1-2), 34-39.
- (44) Schmidt-Rohr, K., 2018. How Batteries Store and Release Energy: Explaining Basic Electrochemistry. *J. Chem. Edu.* 95(10), 1801-1810.
- (45) Binks, B.P. Clint, J.H., 2002. Solid wettability from surface energy components: relevance to Pickering emulsions. *Langmuir* 18(4), 1270-1273.

- (46) Al-Yaseri, A.Z., Lebedev, M., Barifcani, A. Iglauer, S., 2016. Receding and advancing (CO₂+ brine+ quartz) contact angles as a function of pressure, temperature, surface roughness, salt type and salinity. *J. Chem. Thermodyn.* 93, 416-423.
- (47) Xi, Y., Mallavarapu, M. Naidu, R., 2010. Reduction and adsorption of Pb²⁺ in aqueous solution by nano-zero-valent iron—a SEM, TEM and XPS study. *Mater. Res. Bull.* 45(10), 1361-1367.
- (48) Biniak, S., Pakuła, M., Szymański, G.S. Świątkowski, A., 1999. Effect of activated carbon surface oxygen-and/or nitrogen-containing groups on adsorption of copper (II) ions from aqueous solution. *Langmuir* 15(18), 6117-6122.
- (49) Orozco-Guareño, E., Santiago-Gutiérrez, F., Morán-Quiroz, J.L., Hernandez-Olmos, S.L., Soto, V., De la Cruz, W., Manríquez, R. Gomez-Salazar, S., 2010. Removal of Cu (II) ions from aqueous streams using poly (acrylic acid-co-acrylamide) hydrogels. *J. Colloid Interf. Sci.* 349(2), 583-593.
- (50) Ge, Y., Li, Z., Kong, Y., Song, Q. Wang, K., 2014. Heavy metal ions retention by bi-functionalized lignin: Synthesis, applications, and adsorption mechanisms. *J. Ind. Eng. Chem.* 20(6), 4429-4436.
- (51) Qin, F., Fang, Z., Zhou, J., Sun, C., Chen, K., Ding, Z., Li, G. Qiu, X., 2019. Efficient Removal of Cu²⁺ in Water by Carboxymethylated Cellulose Nanofibrils: Performance and Mechanism. *Biomacromolecules* 20(12), 4466-4475.

- (52) Zhou, Z., Liu, X., Hu, Y., Liao, Z., Cheng, S. Xu, M., 2018. An efficient sorbent based on CuCl₂ loaded CeO₂-ZrO₂ for elemental mercury removal from chlorine-free flue gas. *Fuel* 216, 356-363.
- (53) Kasprzyk-Hordern, B., 2004. Chemistry of alumina, reactions in aqueous solution and its application in water treatment. *Adv. Colloid Interf. Sci.* 110(1-2), 19-48.
- (54) Pillai, K.V. Rennekar, S., 2009. Cation- π interactions as a mechanism in technical lignin adsorption to cationic surfaces. *Biomacromolecules* 10(4), 798-804.
- (55) Liang, F.B., Song, Y.L., Huang, C.P., Li, Y.X. Chen, B.H., 2013. Synthesis of novel lignin-based ion-exchange resin and its utilization in heavy metals removal. *Ind. Eng. Chem. Res.* 52(3), 1267-1274.
- (56) Kumar, R., Sharma, R.K. Singh, A.P., 2017. Cellulose based grafted biosorbents-Journey from lignocellulose biomass to toxic metal ions sorption applications-A review. *J. Mol. Liq.* 232, 62-93.
- (57) Dwari, R.K., Angadi, S.I. Tripathy, S.K., 2018. Studies on flocculation characteristics of chromite's ore process tailing: Effect of flocculants ionicity and molecular mass. *Colloid Surf. A Physicochem. Eng. Asp.* 537, 467-477.
- (58) Grenda, K., Arnold, J., Gamelas, J.A., Cayre, O.J. Rasteiro, M.G., 2020. Flocculation of silica nanoparticles by natural, wood-based polyelectrolytes. *Sep. Purif. Technol.* 231, 115888.
- (59) Liu, Q., Li, Y., Chen, H., Lu, J., Yu, G., Möslang, M. Zhou, Y., 2020. Superior adsorption capacity of functionalised straw adsorbent for dyes and heavy-metal ions. *J. Hazard. Mater.* 382, 121040.
- (60) Gu, H., An, R. Bao, J., 2018. Pretreatment refining leads to constant particle size distribution of lignocellulose biomass in enzymatic hydrolysis. *Chem. Eng. J.* 352, 198-205.

- (61) Simair, A.A., Qureshi, A.S., Simair, S.P., Khushk, I., Klykov, S.P., Ali, C.H. Lu, C., 2018. An integrated bioprocess for xylanase production from agriculture waste under open non-sterilized conditions: Biofabrication as fermentation tool. *J. Clean. Prod.* 193, 194-205.
- (62) Shannon, R.D., 1976. Revised effective ionic radii and systematic studies of interatomic distances in halides and chalcogenides. *Acta Cryst. A.* 32(5), 751-767.
- (63) Höök, F., Rodahl, M., Brzezinski, P. Kasemo, B., 1998. Measurements using the quartz crystal microbalance technique of ferritin monolayers on methyl-thiolated gold: dependence of energy dissipation and saturation coverage on salt concentration. *J. Colloid Interf. Sci.* 208(1), 63-67.
- (64) López-Maldonado, E.A., García, H.H., Aguilar, M.A.M.Z., Oropeza-Guzmán, M.T., Ochoa-Terán, A., Martínez, L.M.L., Martínez-Quiroz, M., Valdez, R. Olivas, A., 2020. Chemical issues of coffee and Tule lignins as ecofriendly materials for the effective removal of hazardous metal ions contained in metal finishing wastewater. *Chem. Eng. J.* 125384.
- (65) García, O.G.Z., Oropeza-Guzmán, M.T., Monal, W.M.A. López-Maldonado, E.A., 2019. Design and mechanism of action of multifunctional BPE's with high performance in the separation of hazardous metal ions from polluted water Part I: Chitosan-poly (N-vinylcaprolactam) and its derivatives. *Chem. Eng. J.* 359, 840-851.
- (66) Wiśniewska, M., Chibowski, S. Urban, T., 2015. Impact of polyacrylamide with different contents of carboxyl groups on the chromium (III) oxide adsorption properties in aqueous solution. *J. Hazard. Mater.* 283, 815-823.

(67) Wiśniewska, M., Ostolska, I. Sternik, D., 2016. Impact of adsorption of poly (aspartic acid) and its copolymers with polyethylene glycol on thermal characteristic of Cr₂O₃. *Therm. Anal. Calorim.* 125(3), 1171-1184.

Chapter 7: Production and Application of Triblock Hydrolysis Lignin-based Anionic Copolymer in Aqueous Systems

7.1 Abstract

Although lignin is currently an under-utilized biopolymer, it has the potential to be valorized through different modification pathways to yield alternative products to petroleum-based ones. In this work, hydrolysis lignin (HL) was copolymerized with acrylamide (AM) and acrylic acid (AA) under acidic conditions to generate lignin-AM polymer (HM), lignin-AA polymer (HA), and lignin-AM-AA copolymer (HAM) with different negative charge densities and molecular weights. Lignin-based polymers characterized by advanced tools, such as proton nuclear magnetic resonance ($^1\text{H-NMR}$), gel permeation chromatography (GPC), and elemental analysis confirmed the successful polymerization of HL with AM, AA, or AM/AA monomers. The adsorption analysis using Quartz crystal microbalance (QCM) revealed that, compared to diblock HM and HA, the triblock copolymers of HAM adsorbed more on the Al_2O_3 surface and generated a bulkier adsorbed layer, which is important for lignin-based coating formulation. HAM1 with lower charge density yielded higher surface excess density, while HAM2 with a larger R_h occupied more space (153.7 \AA^2) at the interface of water and Al_2O_3 . In suspension systems, because of the higher M_w , R_h , and adsorption affinity; the bridging performance of HAM2 was more remarkable than the other lignin derivatives for Al_2O_3 particles via forming stronger flocs (with deflocculation parameter, T_{df} , of 80.6 s). However, the diblock lignin-acrylic acid (HA1) polymer showed the fastest floc regrowth capability after reducing the shear forces (with reflocculation parameter, T_{rf} , of 62.5 s). The high thermal stability, T_g , and rheological characteristics of the HAM copolymer proved that it can be an excellent material for coating formulations and flocculant for wastewater treatment systems.

Keywords: Lignin, Biorefining, Polymer, Sustainability, Flocculation

7.2 Introduction

Lignin, a highly branched aromatic polymer, is now considered the main aromatic renewable resource with attractive properties, such as biodegradability as well as antimicrobial and UV activities.^{1,2} Enzymatically hydrolyzed lignin (HL) is derived from the biofuel production process and has been recognized to have poor hydrophilicity and low reactivity, which impedes its conversion to value-added products.³⁻⁵ Therefore, the advancement in the applications of hydrolysis lignin necessitates the modification of its chemical structure. Numerous studies demonstrated that the polymerization of lignin with functional monomers is a promising approach for lignin valorization, which can enhance both the molecular weight and charge density of the lignin macromolecule.⁶⁻⁸ Previously, the polymerization reaction of kraft lignin with acrylamide⁹ and acrylic acid (AA)^{10,11} was studied for producing lignin-based material with multifunctional applications. However, the production of HL with both AM and AA monomers in a ternary reaction system has not been investigated, which is covered in the present study.

The industrial wastewaters generally contain dissolved colloids, organic matter, and other impurities.^{12,13} The removal of these suspended particles is recognized as a serious challenge. The flocculation process has extensively been adapted to treat various wastewaters, which exhibited many advantages including the low cost of operation and effectiveness.^{12,13} Previously, novel lignin- acrylic acid polymer was synthesized, which was very efficient for flocculating the aluminum oxide suspension.¹¹ Similarly, the hydrolysis lignin- polyacrylamide showed promising results for flocculating azo dye particles from model wastewater.¹⁴ Although the attachment of

polyAM to natural polymers (i.e., lignin) can improve the grafting efficiency and bridging effectively of lignin in the flocculation process, it may have some disadvantages, such as long dissolution time and low efficiency for charge neutralization.^{15,16} It was reported that the lignin-based flocculant prepared through grafting two monomers to lignin can significantly increase the solubility, molecular weight, and flocculation efficiency of lignin compared with that prepared through grafting one monomer to the lignin backbone.¹⁷ For instance, the charge density, molecular weight, and solubility of kraft lignin (KL) was increased significantly via copolymerizing lignin with AM and [2-(methacryloyloxy)ethyl]trimethylammonium chloride (DMC), which showed a high flocculation efficiency for both kaolin and bentonite suspensions.⁸ However, there is no information available for the potential application of a triblock copolymer of hydrolysis lignin, AM, and AA as a flocculant for solid particles in suspensions, which is the second objective of this work.

The adsorption of polymers on particles is an important factor in the flocculation process of the suspension systems. Previous studies showed that the adsorption of high molecular weight (M_w) lignin polymer was greater than that of the low M_w on a model substrate.¹⁸⁻²² It is also evident that the high charge of lignin polymers can develop more electrostatic attraction forces with particles leading to a higher level of adsorption, which is crucial for solid/liquid separation processes.²³ However, it is not clear how both high negative charge density and molecular weight of lignin-based copolymers can affect the viscoelastic behavior of the adsorbed layer on particles, which is studied in this work.

The thermal stability of a flocculant is governed by its chemical architecture, molecular composition, and molecular weight properties, which are essential for wastewater treatment

systems of the chemical processes operating at an elevated temperature (i.e., mining process).^{24,25} In this regard, thermogravimetry analysis (TGA) and differential thermogravimetry (DTG) analysis can provide information on the thermal decomposition profiles of lignin macromolecule,²⁶ which facilitate the investigation on the physiochemical alternation of lignin polymer that occurs at a high temperature.²⁷ Moreover, high molecular weight flocculants have a high softening point and glass transition temperature (T_g).²⁸ It was stated that, at a temperature higher than the T_g , the molecular structure of lignin started to soften due to the Brownian motion, which would subsequently alter the physicochemical properties of lignin in solution and thus its performance as a flocculant.²⁸ Thus, the thermal properties of lignin-based polymers were fundamentally investigated in this study to probe if the lignin copolymers can be used as flocculants in wastewater treatment systems at an elevated temperature.

It should be stated that hydrolysis lignin is physiochemically different from kraft lignin: hydrolysis lignin has covalently bound carbohydrates but kraft lignin does not, hydrolysis lignin has larger particles and is more insoluble than kraft lignin. Therefore, the results available on the polymerization of kraft lignin would not be representative of the hydrolysis lignin. To valorize hydrolysis lignin, its polymerization should be delicately assessed. The main novelty of the present study was the copolymerization of hydrolysis lignin, acrylamide, and acrylic acid in a ternary reaction system. The adsorption behavior and flocculation efficiency of the triblock HL-AM-AA copolymers (HAM) were evaluated and compared with those of diblock HL-AA polymer (HA) and HL-AM polymer (HM). In addition, the structural, thermal, and rheological properties of the produced lignin-based copolymers in the threefold reaction system were compared with those produced in the twofold systems.

7.3 Materials and methods

7.3.1 Materials

Enzymatically produced hardwood hydrolysis lignin was supplied by FPInnovations (Thunder Bay, ON). Acrylic acid (AA), acrylamide AM (99.0%), KOH, parahydroxy benzoic acid, potassium persulfate ($K_2S_2O_8$) (analytical grades), sodium hydroxide and sulfuric acid, hydrochloric acid (37%, reagent grade), potassium hydroxide (8 M), potassium chloride (KCl), polydiallyldimethyl-ammonium chloride (PDADMAC, the molecular weight of 100–200 kg/mol 20 wt% in water), sodium azide (NaN_3 , 99.5%), trimethylsilyl propanoic acid (TSP), d₆-dimethyl sulfoxide (d₆-DMSO), deuterium oxide (D_2O), and aluminum oxide (Al_2O_3) were all purchased from Sigma-Aldrich company. Potassium polyvinyl sulfate (PVSK) was provided by Wako company. Fisher Scientific company provided ethanol (95 vol %). Cellulose acetate dialysis membrane tubes (molecular weight cut off of 1000 g/mol) was obtained from Spectrum Laboratories. Deionized water with a resistivity of less than 18 M Ω /cm was produced by a Millipore water purification system and used throughout this work.

7.3.2 Synthesis and purification of HAM copolymer

A 2 g sample of lignin was suspended in 20 mL of deionized water at room temperature and 300 rpm for 20 min in a 250 mL three-neck glass flask. After that, the desired amounts of AA (AA to lignin molar ratio of 3.8 and 10.1), and AM (AM to lignin molar ratio of 5.1) were added to the flasks, and the pH of the medium was adjusted to 3 using 1.0 M NaOH solution. Subsequently, the predetermined amount of $K_2S_2O_8$ (0.03 g) was added to the flasks as an initiator, and the medium was deoxygenated by purging with nitrogen gas for 20 min. The polymerization reaction was

carried out at 80 °C for 3 h, while a continuous purging of N₂ was supplied during the reaction. After completion, the reaction medium was firstly cooled to ambient temperature, and then acidified to a pH of 1.5 to collect the final product from the solution. After mixing, the mixture was centrifuged at 3500 rpm for 10 min to precipitate the HL-AM-AA copolymer (HAM) and to remove the homopolymers (i.e.; PAM, PAA) and unreacted monomers (i.e.; AM, AA) present in the supernatants. Further purification of the HAM polymer macromolecules was achieved using membrane dialysis for 48 h to remove any unreacted monomers and salts from the HAM polymer. Then, the dialyzed anionic lignin was dried at 105 °C. In another set of experiments, HL was polymerized with AA or AM and they were named HA and HM, respectively, using the above-mentioned method, and the final products were considered as the control samples to compare with HAM copolymers.

7.3.3 Characterization of lignin polymers

The charge density of the lignin copolymers was measured using a Particle Charge Detector, Mütek PCD 04 titrator (Herrsching, Germany). In this analysis, the lignin samples (1 mL) at a 1 wt.% concentration were titrated against the PDADMAC solution (0.0050 M) at pH 7. The charge density of the samples was then determined according to the previously established procedure.¹⁰

The molecular weight of the HL, HM, HA, and HAM polymers was analyzed by a gel permeation chromatography (Malvern, GPCmax VE2001 Module + Viscotek TDA305) equipped with multi-detectors. In this measurement, the organic columns of PolyAnalytic PAS106M, PAS103, and PAS102.5 were used, and NaNO₃ (0.1 mol/L) was used as solvent and eluent. The flow rate and column temperature were set at 0.7 mL/min and 35 °C, respectively. Poly (ethylene oxide) was

used as the standard solution for the aqueous system, and the refractive index (RI) detector of the instrument was used to determine the molecular weight of the polymers.

The phenolic hydroxy group and carboxylate group contents of lignin samples were measured using an automatic potentiometer, Metrohm, 905 Titrand, Switzerland. In this analysis, 0.06 g of samples were mixed with 1 mL of KOH (0.8 M), and 4 mL of para-hydroxybenzoic acid (0.5 wt %) as an internal standard solution. The prepared samples were then titrated against 0.1 M HCl solution and the mean value of three measurements was reported.²⁹

The elemental analysis was performed for lignin polymers using an Elemental Analyzer (Vario EL Cube, Elemental Analyzer, Germany). Approximately, 5 mg of the oven-dried samples were transferred into the carousel chamber of the instrument and combusted at 1200 °C to reduce the generated gasses to examine their carbon, hydrogen, and oxygen contents. Considering the carboxyl group content of the samples, the grafting ratio of HM, HA, and HAM polymers was calculated according to the equation described by Bayazeed and coworkers.³⁰

The molecular structure of HL, HM, HA, and HAM polymers were analyzed using ¹H NMR spectroscopy. In this set of experiments, 30 mg of dried samples and 8 mg of trimethylsilyl propanoic acid (TSP) were dissolved in 450 μL DMSO-d₆ and 50 μL D₂O stirring overnight at room temperature. The ¹H-NMR spectra of samples were acquired using INOVA-500 MHz instrument (Varian, USA) with a 45° pulse after 64 scans and a relaxation delay time of 1.0 s.

The hydrodynamic radius (H_y) of the HL, HM, HA, and HAM polymers was measured via a dynamic light scattering (DLS) instrument, BI-200SM Brookhaven Instruments, USA, equipped with a 35 mW laser power source. In this analysis, 1 g/L of HL and HL-AM-AA were prepared in 1 mM KCl solution to avoid the aggregation and stirred at 300 rpm for 24 h and room temperature.

After mixing, 20 mL of sample were filtered using a 0.45 μm disposable syringe filter, and the hydrodynamic radius of lignin samples was determined using the method described previously.³¹ The scattering angle was set at 90° and the analysis was conducted at the wavelength of 637 nm. The average value of three repetitions was then reported in this study.

7.3.4 Quartz crystal microbalance with dissipation (QCM-D) Studies

The adsorption of lignin polymers (1 wt.%) on the aluminum oxide substrate was assessed using a Quartz crystal microbalance with dissipation (QCM)-D. The adsorption analysis was monitored by introducing the buffer solution (i.e., Mili-Q water) to the chamber of the QCM instrument at the controlled temperature of 22 \pm 0.1 °C to generate the baseline in the experiments. After reaching the equilibrated baseline, the buffer solution was switched to the lignin polymer solutions and the shifts in frequency and dissipation of the sensor at the 5th harmonic ($n = 5$) were recorded as a function of time. Solutions were pumped at the flow rate of 0.15 mL/min throughout the experiments. The viscoelastic properties of an adsorbed layer were also monitored by the dissipation of the sensor's energy in the oscillating Quartz crystal system following equation 1:

$$D = \frac{E_D}{2\pi E_S} \quad (1)$$

where E_D represents the energy dissipated during oscillation and E_S is the amount of energy stored in the oscillating system. For the rigid adsorbed layer, the dissipation value is very low. However, the viscoelastic film shows higher energy dissipated through the adsorbed layer indicating more deformation during the oscillation.³² The characteristic of the adsorbed lignin polymer on the aluminum oxide surface was determined by the Q-tools software in the QCM-D instrument.

7.3.5 Rheological studies

The rheological properties of lignin samples (HL, HM, HA, and HAM) were determined using a hybrid rheometer (TA Instruments) equipped with a cylindrical geometry (cone length, 41.96 mm; cone diameter, 28.03 mm; gap, 5500 μm ; angle, 1°) at 22°C . In this set of experiments, 25 mL of lignin solution (4 wt.%) was placed inside the cell of the instrument and a 3 min pre-shear at 100 1/s was applied to the samples prior to the measurement. To determine the linear viscoelastic region (LVR), the dynamic strain sweep measurement was carried out at the frequency of 6.28 rad/s. The frequency sweep measurements were then performed in the range of 0.01 and 100 rad/s, while the strain value from the linear viscoelastic region was set at 0.1%.

7.3.6 Zeta potential analysis

The zeta potential of aluminum oxide suspension was analyzed in the presence of various dosages (2 to 64 mg/L) of lignin polymers using a NanoBrook PALS (Brookhaven Inc.; USA). The zeta potential measurements were carried out at room temperature and a constant electric field (8.4 V/cm). The reported data in this experiment was the average of three repetitions.

7.3.7 Flocculation analysis

The flocculation behavior of the aluminum oxide suspension and the properties of the formed flocs were determined via monitoring the chord length distribution of particles in the suspension in a real-time scenario using a focused beam reflectance measurement (FBRM), Mettler Toledo, E25. In this experiment, 200 mL of aluminum oxide suspension (25 g/L at pH 6) was stirred at 200 rpm and then the laser probe (25 mm diameter) was submerged in the medium. After reaching the stable condition, the desired volume of lignin polymers was added to the suspension and the chord length distribution (CLD) was assessed by using 90 log-channels over the range of 1 and 1000 μm using the IC-FBRM software. To study the re-flocculation performance of flocs, the stirring rate of the

mixture was increased to 700 rpm for 1 min to break down the generated flocs (i.e.; deflocculation process). Subsequently, the agitation speed decreased to 200 rpm once again to analyze the reflocculation of broken flocs. The CLD of the particles in aluminum oxide suspension was recorded every 3 s.

7.3.8 Thermogravimetric Analysis (TGA)

The thermogravimetric analysis of HL, HM, HA, and HAM was evaluated by a thermogravimetric analyzer, Instrument Specialist, i1000, to determine the thermal behavior of lignin samples. In this set of experiments, the samples were first dried in an oven (105 °C) overnight prior to analysis. Then, they heated from room temperature to 700 °C under a 20 mL/min nitrogen flow rate. The heating flow rate was adjusted at 10 °C/min.

7.3.9 Differential scanning calorimetry (DSC)

The glass transition temperature (T_g) and heat capacity (C_p) values of the lignin samples were analyzed using a differential scanning calorimetry (DSC, TA Instruments Q2000). The experiment was conducted according to the methods published previously.^{33,34} First, a 5 mg dried lignin sample was placed in a DSC pan, and then the samples were treated in the temperature range of 0 °C and 200 °C, while the heating rate was set at 3 °C/min.³⁴ After heating the samples to 200 °C, they were cooled down to 0 °C and reheated again to 200 °C. The values of T_g and C_p of lignin samples were assessed in the second heating cycle.³³

7.4 Results and discussion

7.4.1 Characterization of lignin polymers

¹H NMR spectroscopy

The ¹H NMR spectra of HL, HM, HA, and HAM are depicted in Figure A32a. The broad resonance at 7-8.2 ppm is associated with the aromatic protons, including the vinyl protons, on the carbon atom next to the aromatic ring.³⁵ The peak between 3.7 and 4.4 ppm is attributed to protons in the methoxy group of lignin,^{36,37} and the signals at 3.38 ppm are assigned to the methylene protons in the β-β structure.³⁸ Moreover, the resonance at 3.1 ppm is attributed to the protons of anhydroxylose units of hemicelluloses.³⁹ The new peaks for the PAA chain segment (Figure A32-b,c) occurred at 1.5 ppm, 1.96 ppm, and 2.33 ppm, which were assigned to C-1, C-2, and hydroxyl end.⁴⁰ Moreover, the signal at around 4.15 ppm, which was absent in that of HL, corresponded to the protons of -CH₂ attached to the aromatic structure through ester bond (-CH₂-O-C₆H₅). In the case of HM polymer, the additional peaks presented at 1.6 and 2.1 ppm (Figure A32-d) were attributed to the protons of C_α and C_β, respectively, connecting to the amide group of HM.⁴¹ The peak at 4.3 ppm also corresponded to the -CH₂ protons connecting to the phenolic hydroxy group of lignin (i.e., via ester bonding) and indicating that the Ph-OH of lignin was the active site for the polymerization reaction.⁴²

Examining the ¹H NMR spectrum of HAMs illustrated that the resonance from the acrylamide and acrylic acid portions of the copolymers was observed at 1.5–1.8 ppm and 2.2-2.5 ppm, respectively. Moreover, a decline in the residual content of phenolic hydroxy group in HAMs was evident as a conclusion of the reduced peak intensity at 7-8.2 ppm, which confirmed that the Ph-OH group of HL was the active site for the polymerization of HL and AM/AA (Figure A32-e,f).

Properties of lignin polymers

In this work, the free radical copolymerization of hydrolysis lignin, acrylamide, and acrylic acid (HAM) was carried out in an aqueous solution. To find out how acrylamide or acrylic acid monomers work separately in a polymerization reaction with lignin, HL was polymerized with AA or AM to generate HA and HM, respectively. Since the amount of AM applied for producing HAMs was constant (5.1 mol/mol), but AA was used at different dosages (3.8 and 10.1 mol/mol), one HM and two HA (namely HA1 and HA2) were synthesized following the free radical polymerization. Then, HA and HM were considered as the control samples for HAM production throughout this work. The details of the polymerization mechanism and the proposed reaction scheme are available in Scheme A2.

Table 1 lists the properties of the HL derivatives. HL had a charge density of $-0.43 \mu\text{eq/g}$ and M_w of 6300 g/mol. It is evident that the charge density, solubility, and molecular weight of HA and HAM polymers were increased after polymerization confirming the successful grafting of the monomers onto the lignin structure. The successful polymerization of HL and AM was confirmed by enhancing the molecular weight of HM from 63×10^2 g/mol to 141×10^3 g/mol. Also, the high amount of nitrogen (1.09 wt.%) in the HM polymer, originating from the amide group ($-\text{CONH}_2$) of AM monomer, was also an indicator of the successful polymerization of HL and AM. Although the charge density increment of HM polymer was negligible, AM monomer increased the solubility of lignin polymer (from 25 to 47 wt.%) due to the attachment of the amide group to the lignin backbone. A decrease in the phenolic hydroxy group of HM and HAs was mainly attributed to the participation of Ph-OH of HL in the polymerization. Increasing the carboxylate group content of HAs, stemming from the acrylic acid monomer, was associated with the decrease in the Ph-OH group of lignin.¹¹ Compared to HA1, the lower amount of Ph-OH and higher amount carboxylate group, charge density, solubility, and molecular weight of HA2 reflected that the

polymerization reaction was accelerated more greatly for HA2. It is worth noting that, by increasing the carboxylate group and the molecular weight of HAs, their oxygen content increased, while the carbon and hydrogen contents decreased.

A comparison between the products of the three-component reaction systems showed that HAM1 had a higher charge density and nitrogen content than HAM2 did, indicating that the copolymerization reaction was performed more efficiently for HAM2 than HAM1. Moreover, the phenolic OH group content of lignin copolymer was reduced to 0.78 and 0.37 mmol/g (from 1.63 mmol/g) for HAM1 and HAM2, respectively, illustrating that the phenolic group of lignin was involved in the reaction with AM and AA monomers. Unmodified HL had a carboxylate content of 0.38 mmol/g. However, the carboxylate content of HAMs increased to 2.2 and 3.1 mmol/g for HAM1 and HAM2, respectively. As stated in the literature,¹¹ an increase in the carboxylic acid content of lignin is an indicator of grafting of AA group on the phenolic OH of lignin, improving the water solubility of lignin macromolecule. The AM facilitated more bridging of HL and AA, facilitating the water solubility of HAM polymers. Considering the constant amount of AM in the polymerization reaction, HAM2 with more attachment of AA had a higher molecular weight (351×10^3 g/mol) compared to HAM1 (277×10^3 g/mol). The results in Table 1 also revealed that the hydrodynamic radius of modified lignin was larger than that of HL due to the presence of AA and AM segments on lignin. However, in the ternary reaction system, the attachment of both AA/AM made these copolymers to have larger hydrodynamic sizes.

Table 7. 1 Properties of HL and HAM polymers.

Sample	HL	HM	HA1	HA2	HAM1	HAM2
--------	----	----	-----	-----	------	------

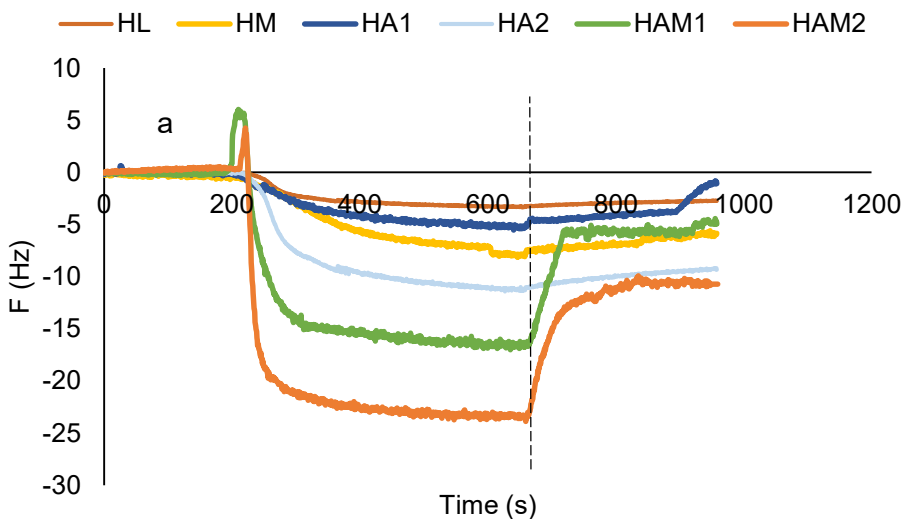
Charge density, meq/g	-0.43±0.11	-0.45±0.1	-0.8±0.07	-1.35±0.2	-1.6±0.2	-2.2±0.1
Carbon, wt. %	62.6±1.8	58.4±0.2	59.4±0.3	52.2±0.9	48.9±2.1	47.4±1.2
Hydrogen, wt. %	7.5±1.2	7.4±0.1	7.3±0.1	6.6±0.4	6.5±1.3	6.4±0.06
Nitrogen, w.t. %	0	1.09±0.1	0.3±0.1	0.3±0.1	1.09±0.1	1.09±0.1
Oxygen, wt. %	27.4±1.3	31.06±0.6	31.1±0.3	39.6±0.5	42.2±1.1	44.61±0.4
Phenolic hydroxyl group, mmol/g	1.6±0.3	0.9±0.1	0.85±0.04	0.66±0.03	0.58±0.05	0.37±0.03
Carboxylate content, mmol/g	0.38±0.05	0.38±0.05	1.07±0.04	1.45±0.02	2.2±0.03	3.1±0.2
Solubility, wt. %	25±0.5	47±1.1	52±0.9	64±1.2	73±2.3	81±2.5
M _w , g/mol	44±5.1×10 ²	141±3.7×10 ³	131±2.9×10 ³	228±5.5×10 ³	277±7.1×10 ³	351±4.2×10 ³
M _n , g/mol	28±1.3×10 ²	59±3.1×10 ³	59±2.5×10 ³	95±3.9×10 ³	124±4.4×10 ³	140±3.4×10 ³
M _w /M _n	1.6±0.3	2.4±0.6	2.2±0.7	2.4±0.5	2.2±0.3	2.5±0.2
R _h , nm	17.2±0.7	55±1.1	34.3±0.72	48.6±0.8	64.3±1.7	75±2.1

7.4.2 Adsorption Analysis

The adsorption kinetics of lignin polymers on the aluminum oxide-coated QCM sensors is shown as a function of time in Figure 1. The limited adsorption performance of HL implied that HL had limited interaction with aluminum oxide. However, by introducing the diblock lignin polymers (i.e., HM and HAs) to the surface, the frequency started to decrease due to the deposition of the polymer and water molecules on the surface. Of diblock polymers, the larger negative frequencies of the sensors (-11.4 Hz and -7.6 Hz) before buffer rinsing were recorded for HA2 and HM, respectively, which illustrated more adsorption affinity of those polymers on the Al_2O_3 surface. The greater deposition of HA2 can be due to the higher charge density and molecular weight (Table 1) of HA2 compared to that of HM. Additionally, the high dissipation values of 8.6 and 6 for HM and HA2, respectively, confirmed that they created a soft and viscoelastic adsorbed layer on the sensor upon the course of adsorption. In this case, HA2 generated a more packed adlayer. However, the lower adsorption affinity and the less dissipative adsorbed layer was observed for HA1, which was attributed to its limited surface functional groups to interact with the Al_2O_3 surface.

In contrast to diblock polymers, a higher adsorption rate was observed for HAM copolymers. Since HAM2 had a higher charge and molecular weight, it interacted more significantly than HAM1 with the cationically charged aluminum oxide surface.^{43,44} The adsorbed mass and adsorbed adlayer thickness were also illustrated in Table 2. The higher overall mass and thickness of the adsorbed layer of HAM2 on the aluminum oxide surface (68.5 mg/cm^2 , 108.2 nm) than those of HAM1 (48.3 mg/cm^2 , 72.2 nm) confirmed the more intense interaction and self-assembly of HAM2 polymer, which was probably due to the greater size ($R_h=75 \text{ nm}$) of this polymer than other

polymers.^{45,46} When the adsorption reached a saturation level (at the time of 650 s), buffer rinsing was initiated, which removed the weakly adsorbed mass of HAMs from the sensors and thus reduced the dissipation of the sensor. The desorption of HAM molecules from the aluminum oxide surface was due to the loose binding of HAM molecules to the surface in the presence of strong electrostatic repulsion forces developed between the negatively charged deposited HAM polymers on the surface. The insignificant changes in dissipation were the indicator of the flat configuration of lignin polymers on the surface that was more pronounced for diblock polymers.⁴⁷ The similar behavior was also observed in a study on the adsorption of carboxymethylated lignin particles on the gold surface, in which some of the loosely bound lignin polymers desorbed during the buffer rinsing stage.²³



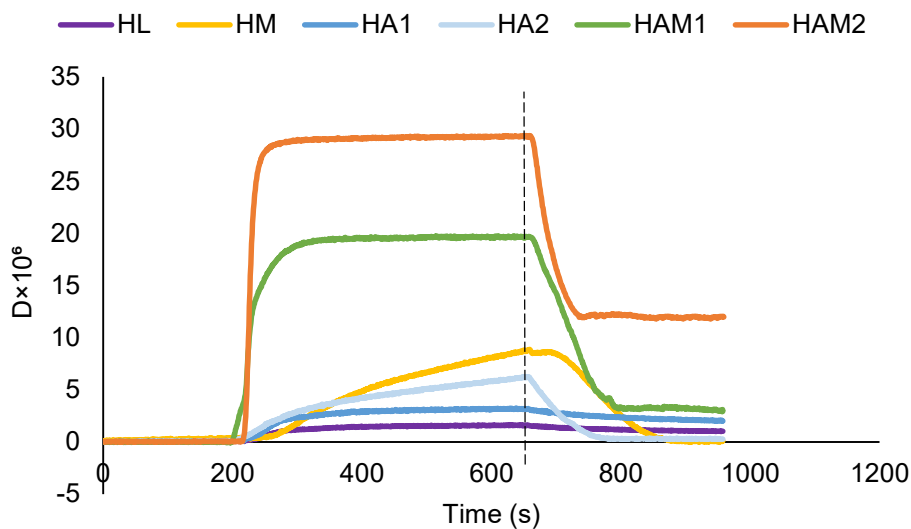


Figure 7. 1 Adsorption of HL, HAs, HM and HAMs on the aluminium oxide sensor: a) frequency changes, b) dissipation changes (vertical dash line shows buffer rinsing).

Table 7. 2 Adsorption properties of lignin macromolecules on aluminium oxide surface at equilibrium.

Sample	Δ_m (mg/ cm ²)	Δ_d (nm)
HL	7.3	7.8
HM	28.2	32.8
HA1	19.5	29
HA2	32.8	12.5
HAM1	48.3	72.2
HAM2	68.5	108.2

The changes in the frequency, Δf , and dissipation, ΔD , in the adsorption of lignin derivatives on the aluminum oxide sensor were illustrated in Figure A33 to understand the effect of polymer adsorption on the viscoelastic behavior of the adsorbed layer. Presenting $\Delta D/\Delta f$ ratio illustrates the induced energy dissipation per coupled unit mass.⁴⁸ The results depicted a less viscous adsorbed

layer for HM and HAs on the surface at a low adsorption level. However, HAM polymers with a steeper slope indicated a more viscous adsorbed layer on the sensor. According to the literature, the higher $\Delta D/\Delta f$ ratio may also imply the entrapment of water molecules within the adsorbed layer, which creates a more viscous film.⁴⁹ Thus, HAM2 with a more three-dimensional structure ($R_h=75$ nm) may entrap more water molecules within its adsorbed polymer and generate a bulkier adsorption portfolio on the surface.

The fundamentals of the HAM polymer adsorption on the aluminum oxide surface were further studied via the determination of the surface occupancy of the HAM molecule on the surface to develop the first layer of polymer on the sensor. To calculate the surface activity of each molecule on the desired surface, the surface excess density (Γ) of the molecule should be evaluated. Considering the slope of surface tension (σ) of water containing HAMs and the polymer concentration (C), the surface excess density can be calculated (Figure A34) following Gibbs adsorption isotherm (equation 2):

$$\Gamma = -(RT)^{-1} \times \left(\frac{d\sigma_{CKL}}{d \ln C} \right) \quad (2)$$

wherein R and T represent the universal gas constant (J/(mol K)) and absolute temperature (K), respectively.

The surface tension results (Figure A34) depicted that the surface tension of HAMs reduced linearly with rising the natural logarithm of polymer concentration. Accordingly, at a 7 g/L HAM concentration, ∂ of lignin copolymers reached 65.3 and 63.9 mN/m for HAM1 and HAM2, respectively (from $\partial_{\text{water}} = 72.8$ mN/m). Considering the results of Figure A34, the maximum surface concentration of polymers determined to be 1.24×10^{-6} and 1.08×10^{-6} mol/m² for HAM1

and HAM2 solutions at the air/water interface, respectively. As stated in the literature, the surface activity of a polymer is correlated with its surface access density (Γ).⁵⁰ Hence, the smaller the Γ value of HAM1, the smaller the surface activity of this polymer would be. The surface area occupied by each molecule (a) at the interface of the aluminum oxide sensor can be assessed following equation 3:

$$a = \frac{10^{20}}{\Gamma N} \quad (3)$$

where N is the Avogadro constant.

Owing to the larger R_h (Table 2), HAM2 polymer occupied a larger area (153.7 \AA^2) at the interface than did HAM1 (133.8 \AA^2). In other words, the extended configuration and higher surface occupancy of HAM2 reflected a more three-dimensional structure of this polymer compared to that of HAM1, when the first layer of polymer segments coat the surface.

7.4.3 Rheological Characteristics

The intermolecular forces of chemically modified lignin can significantly impact the rheological properties of the polymer due to its three-dimensional structure as well as molecular chain length and conformation.⁵¹ To understand how the structure of the lignin derivatives would impact their properties in solution, dynamic rheological studies of the polymers were carried out. Figure 2a illustrates the plot of storage modulus (G') and loss modulus (G'') over the frequency sweep (ω). It is generally suggested that G' represents the magnitude of the energy stored and recovered per cycle, which indicates the entropy elasticity for polymer chains.⁵² Also, the G'' is a measure of the energy dissipated in a cycle of deformation.⁵² All the lignin samples exhibited higher storage modulus than loss modulus at the higher range of frequency indicating their solid-like behavior

(Figure 2-a). At lower values of frequency (Figure 2b), the intersection points were present between G' and G'' of all lignin samples, illustrating that the studied systems at a lower frequency (≥ 20 rad/s) manifested weak gel-like structures. In other words, the intersection point between G' and G'' , namely crossover frequency, which shows the beginning of the elastic behavior of the gel state, was observed at a lower frequency value of lignin samples. At the crossover point, sample property changes from viscous to predominant elastic behavior due to the formation of an interconnected network of polymer chains. However, HAM2 polymer with a higher molecular weight showed the highest modulus compared with the other samples. Such behavior indicated strong interactions between HAM2 polymer chains, which reflected more elastic behavior and the existence of a three-dimensional network of HAM2 in an aqueous system.

The polymerization of lignin macromolecule as a biodegradable and abundant source of raw material with synthetic polymers (i.e., particularly acrylates as well as other vinyl monomers) has the potential of generating a new class of engineering plastics.^{53,54} Therefore, HAM copolymers can potentially be used as biodegradable plastics. However, substantial effort should be made to improve the mechanical properties and water resistance of HAM copolymers.⁵⁵

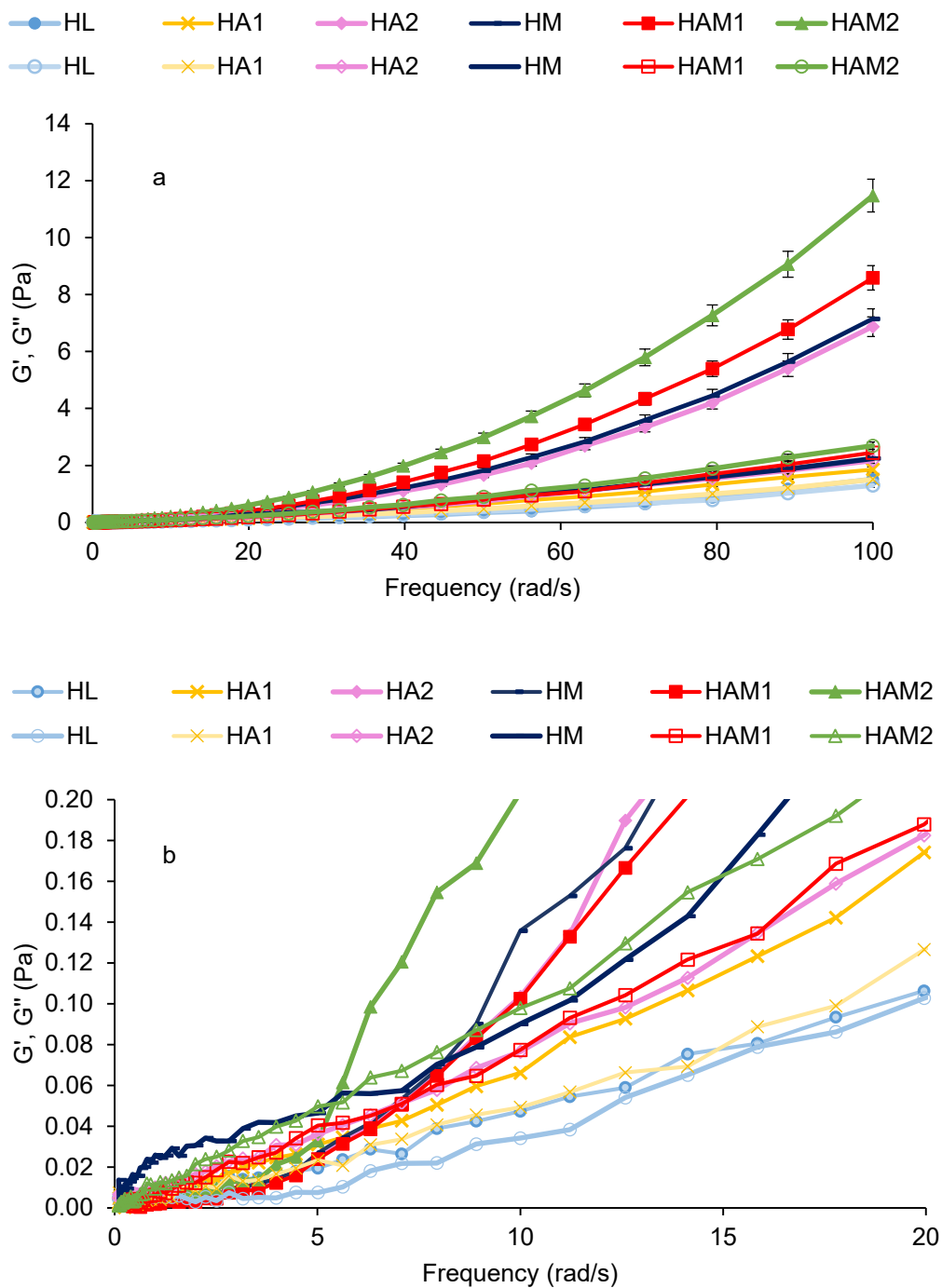


Figure 7. 2 Plot of storage and loss modulus as a function of angular frequency in the range of a) 0-100 (rad/s) and b) 0-20 (rad/s) for lignin samples (G' and G'' are respectively represented as solid and open symbols).

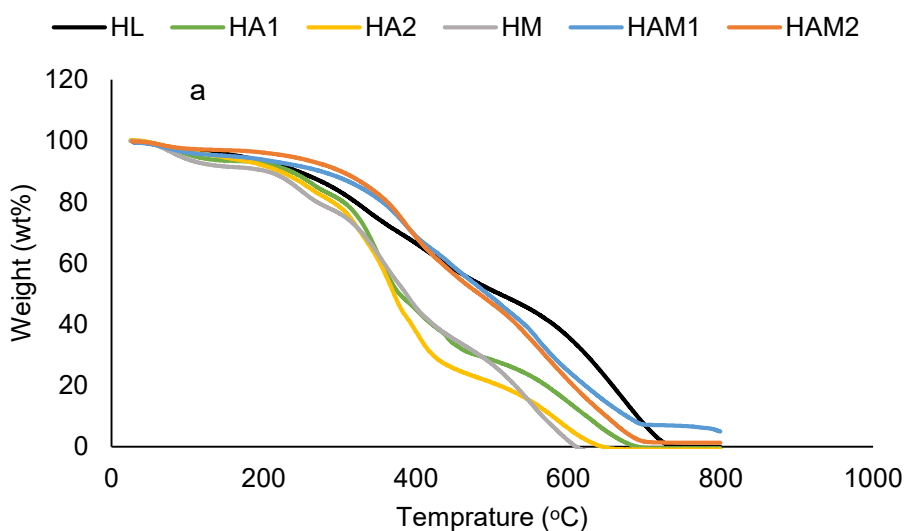
7.4.5 Thermal Properties

The weight loss and weight loss rate of HL, HM, HAs, and HAMs can be found in Figure 3. It was observed that HL had different stages of decomposition. The initial weight loss of HL below 200 °C is mainly due to the release of adsorbed and bound water. In the temperature range of 100-180 °C, the plasticization phenomenon occurred, which indicated the cleavage of weak ether or aryl-alkyl bonds.⁵⁶ Generally, the decomposition of the polymeric structure of lignin starts in the temperature range 120-275 °C, in which the propanoid side chains will degrade. Moreover, at a temperature around 275-350 °C, β - β and C-C linkages start to break down.^{57,58} According to Figure 3, the HL sample continuously decomposed above 200 °C with a 34% weight loss at 400 °C. Hydrolysis lignin was significantly more stable than HM and HAs; however, the HAM copolymers was slightly more thermally stable. The higher thermal stability of HAMs can be due to the more resistance of ether bond linkages formed during the polymerization reaction⁵⁹ as a result of the wrapping of lignin backbone by AM and AA chains. Compared to diblock polymers (i.e., HM and HAs), triblock HAM copolymers had three weight loss events in the temperature ranges of 200-350 °C, 350-450 °C, and 450-700 °C. The first decomposition event (200-350 °C) was linked to the loss of water, ammonia, and small quantities of CO⁶⁰ while the polymer network remained intact and the main degradation phenomenon arose at the pendant amide groups on the acrylamide part of the HAM copolymers.¹⁷ In the second weight-loss event (350-450 °C), the main polymeric chains started to decompose releasing carbon dioxide, nitrile compounds, acrylic acid from depolymerization, and imides.^{17,61,62} At a temperature above 700 °C, only 1.5% of HAM1 and 5% of HAM2 copolymer remained.

Table A5 lists the glass transition temperature (T_g) of lignin samples. It was observed that the HAM copolymers had higher T_g values compared with HM, HA1, and HA2 polymers. The higher T_g of HAM1 (181 °C) and HAM2 (160 °C) is related to the presence of a lignin macromolecule

that solidified the structure of the former copolymer. In other words, the free ends of AA and AM monomers attached to the rigid lignin macromolecule in HAMs can suppress the molecular motion of the grafted AA/AM chains, elevating the T_g values of HAM copolymers.⁶³

It is worth mentioning that the knowledge of thermal properties of lignin-based polymers might be beneficial for its use in wastewater treatment systems of some process, where oxidation or acid/alkaline treatments at a high temperature are required.^{64,25} In such a process, the functionality and integrity of polymers are crucial.²⁴



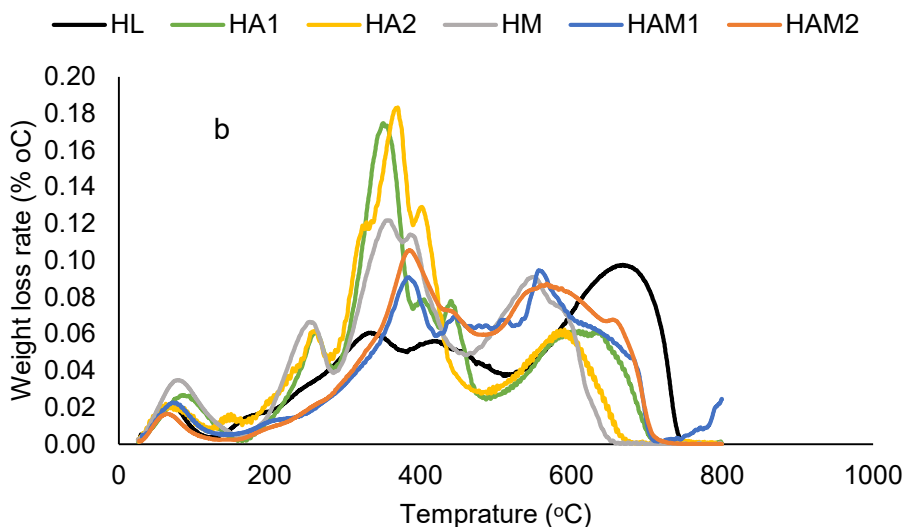


Figure 7. 3 a) Weight loss and b) weight loss rate of HL, HM, HAs and HAMs at a heating rate of 10 °C/min.

7.4.6 Behavior of lignin macromolecules in flocculation process

Zeta potential

The effect of HL, HM, HA, and HAM polymers on the zeta potential (ζ) of aluminum oxide suspension as a function of polymer dosages is demonstrated in Figure A35. The addition of HL and HM reduced the ζ of aluminum oxide suspension slightly due to the limited surface charge density of the polymers. The zeta potential of the aluminum oxide suspension increased significantly and changed from positive to negative when the concentration of HAs and HAMs increased in the suspension. However, the aluminum oxide particles attained a higher zeta potential in the presence of HAM2 than HAM1 owing to their higher charge density and adsorption of HAM2 (Figure 1), which created a more compact diffuse double layer around aluminum oxide particles.⁶⁵ It was also observed that the suspension reached the isoelectric point at a slightly lower dosage of HAM2 than that of HAM1.

Floc formation

The weighted chord length distributions of the formed flocs in the aluminum oxide suspension are depicted in Figure A36 when different dosages of lignin polymers were added. By increasing the dosage of the samples to the aluminum oxide suspension, the number of counts decreased, and the chord length distribution slightly shifted toward larger sizes. Moreover, considering the area under the count-chord length distribution curve, the total counts dropped by 25%, 24%, 37%, 45%, and 47% when 2.4 mg/g of HM, HA1, HA2, HAM1, and HAM2 was added to the aluminum oxide suspension, respectively. This behavior reflected the aggregation of small particles to larger ones.^{66,67} However, various dosages of HL did not change the chord length size of aluminum oxide particles implying that HL was not effective in flocculating the particles. Since the maximum increment in the chord length and reduction in the number of counts of aluminum oxide particles treated with HM, HAs, and HAMs occurred at the dosage of 2.4 mg/g, this dosage was selected as the optimum dosage for further flocculation analysis. The details of the FBRM results at 2.4 mg/g in various moments of the aggregate size distribution are available in Table A6.

Floc strength and recoverability

The variations in the mean chord length (MCL) of the suspension systems as a function of time for lignin samples at different shear rates were shown in Figure 4. The aluminum oxide suspension was stirred for 5 min at 200 rpm for stabilizing the system before initiating the trial. At the time of 300 s, different lignin polymers were added to the suspension, which induced larger flocs by increasing the chord length. HL did not impact the flocculation performance of the aluminum oxide suspensions owing to the limited anionic charge density and adsorption on the aluminum oxide surface (Figure 1). However, the addition of HM, HA1, and HA2 to the suspension slightly

increased the chord length of the aluminum oxide suspension to 14.4, 16.9, and 17.7 μm , respectively (from an initial size of 12.1 μm). Compared with diblock polymers, three-component HAM copolymers generated larger flocs at 2.4 mg/g, leading to the lower number of particles in the suspensions. HAM2 with the higher molecular weight (Table 1) created larger flocs with a larger chord length (28.5 μm) compared with that of HAM1 (22.8 μm). However, HAM1 created more stable flocs as the variation in the size of the formed flocs was less than that of HAM2 at 200 rpm. Considering the constant amount of the grafted acrylamide to HAM polymers, the higher content of acrylic acid monomers grafted to HAM2 increased the charge density, M_w , (Table 1) and three-dimensional structure (i.e., R_h) of HAM2 copolymer facilitating the adsorption of this copolymer on the aluminum oxide particles, which subsequently improved its flocculation performance. Moreover, the higher surface occupancy of the HAM2 polymer when adsorbing on the aluminum oxide particles could be another reason for better flocculation characteristics of the aluminum oxide/HAM2 system. As stated in the literature, the higher surface occupancy of the polymer could improve the flocculation efficiency most probably through bridging mechanism (i.e., tail and loop configurations).^{68,23}

After 700 s, the mixing speed in the FBRM analysis was increased to 700 rpm (from 200 rpm), which reduced the mean chord length of particles, providing evidence of deflocculation (i.e., flocs breakage). Once the shear force dropped to the initial level (200 rpm), the crushed particles agglomerated and chord length increased accordingly.^{69,70} As illustrated in Figure 4, by reducing the shear rate (i.e., from 700 to 200 rpm), the chord length of the aluminum oxide suspension treated with HM, HA1, and HA2 increased to 13.4, 15.9, and 16.7 μm , which were very similar to their chord length obtained at the flocculation step prior to the shear rate elevation. However, only partial reflocculation was achieved for the aluminum oxide/HAMs. To have further insight into

the deflocculation and reflocculation phenomenon, the obtained data from Figure 4 was fitted into equations 4 and 5, respectively:

$$Y = C_0 + Ae^{\frac{-t}{T_{df}}} \quad (4)$$

$$Y = C_\infty - Ke^{\frac{-t}{T_{rf}}} \quad (5)$$

herein C_0 and C_∞ are numerical constant (μm), A and K are pre-exponential factors, T_{df} represents the deflocculation parameter (s), T_{rf} stands for the reflocculation parameter (s), t is time (s), and Y shows the mean chord size.

Table 3 lists the parameters of the de-flocculation and re-flocculation processes. As stated in the literature, there is a dynamic equilibrium between the formation and the breakage of flocs in the flocculation process.⁷¹ According to Table 3, the higher value of T_{df} in aluminum oxide/HAM2 (80.6 s) is attributed to the higher strength of the generated flocs. The properties of flocs may be attributed to their main flocculation mechanism. Since the patching mechanism can form flocs with relatively weak strength, but bridging creates the stronger flocs,⁷² it might be implied that HAM2 copolymer formed flocs mainly through bridging than patching mechanism.

T_{rf} parameter elucidates the recovery of the broken flocs after reducing the shear rate. Accordingly, the lower T_{rf} value of aluminum oxide/HAM1 suspension indicates the higher tendency of this system to reflocculate and relatively faster regrowth capability.⁷³ However, the reformed flocs via HAM2 polymer in the aluminum oxide suspension could not reach their initial sizes after deflocculation process. In this case, the formed bridges between HAM2 and aluminum oxide particles may undergo scission, and hence, a part of the detached HAM2 would reconfigure on the surface of aluminum oxide particles and loose their bridging efficiency.^{8,74} Among lignin

polymers, HA1 polymer formed smaller flocs with more reversible affinity in the floc size after deflocculation and reflocculation process, which confirmed the patching flocculation mechanism.⁷⁵

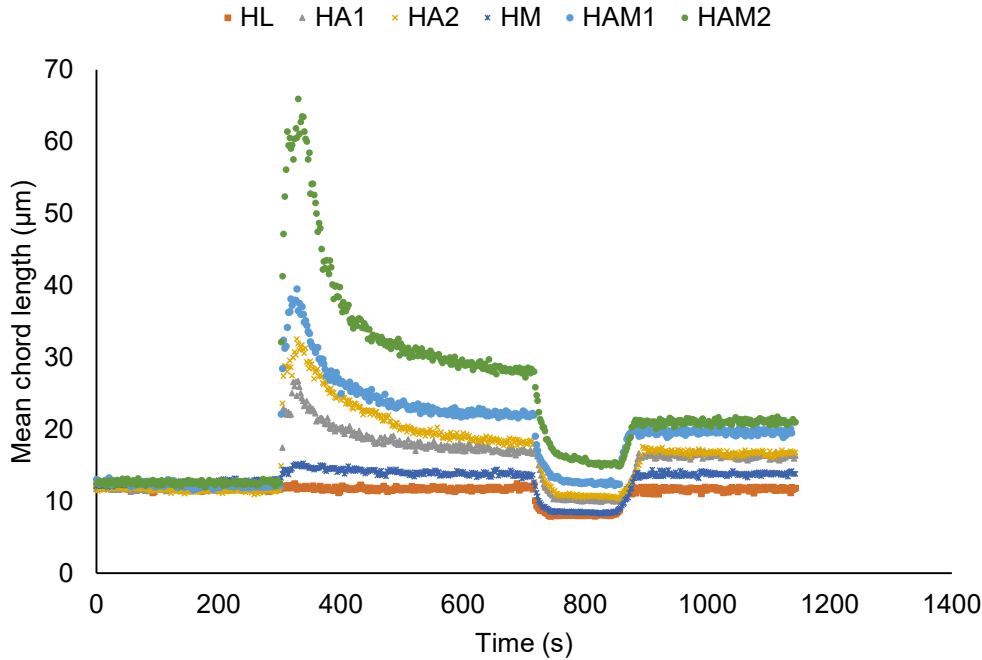


Figure 7. 4 The change in the chord length of flocs in aluminum oxide suspension in the presence of 2.4 mg/g polymers dosage at different shear rates.

Table 7. 3 The deflocculation and reflocculation parameters of aluminium oxide/HAMs systems under different shear rates.

Sample	T_{df} , s	R^2	T_{rf} , s	R^2
HL	58.1	$R^2 = 0.98$	48.5	$R^2 = 0.97$
HM	51.8	$R^2 = 0.96$	71.4	$R^2 = 0.98$
HA1	62.9	$R^2 = 0.98$	62.5	$R^2 = 0.99$
HA2	49.02	$R^2 = 0.97$	76.3	$R^2 = 0.96$

HAM1	71.4	$R^2 = 0.98$	78.7	$R^2 = 0.98$
HAM2	80.6	$R^2 = 0.99$	91.7	$R^2 = 0.97$

7.4.7 Comparison

The flocculation performance of HAMs was compared with other bio-based flocculants, and the results are tabulated in Table 4. Compared to our previous work,⁶ the molecular weight of hydrolysis lignin increased significantly after polymerizing with two monomers (i.e., AM and AA) and thus yielded higher particle removals by generating a larger chord length. Although cationic HL-METAC was used at a lower dosage, it was not as efficient as HAMs in particle removal from model wastewater.⁷⁶ The higher molecular weight of HAM than that of cationic cellulose (29×10^3 - 103×10^3 g/L) resulted in larger floc production when interacting with colloidal particles.

Despite the high molecular weight of cationic starch⁷⁶ ($1-2 \times 10^6$) and Chito-CTA⁷⁹ (10^7 g/mol), the chord length generated by those flocculants was smaller than that of HAM copolymers. Additionally, the optimum dosage of HAM1 and HAM2 achieved in this study was 50 times as much as that reported for Chito-CTA.⁷⁹ Interestingly, the high surface charge density of cationic chitosan⁷⁸ (3.8-5.4 meq/g) was not highly efficient in removing suspended particles (i.e., calcium carbonate) compared to HAM copolymers with medium charge density. Overall, the results elucidated that the application of HAM copolymers for different wastewater treatment systems is promising.

Table 7. 4 Comparison of various flocculants for wastewater treatment systems.

Flocculant	Charge density, meq/g	Mw, g/mol	Wastewater	pH	Dosage, mg/g	MCL, μm
HAM1	-1.6	277×10^3	Aluminium	7	2.4	22.8
HAM2	-2.2	351×10^3	oxide			28.5
HL- <i>graft</i> - (methacryloyloxy)ethyl] trimethyl ammonium chloride (HL-METAC)	[2- +2.1	55×10^3	Kaolin	6	1.2	10.9
Cationic starch ⁷⁶	+2.3	$1-2 \times 10^6$	Digested sludge	7.0 – 7.5	12	19.2
Cationic cellulose ⁷⁷	-	29×10^3 - 103×10^3	Digested sludge	7.5	4-12	15-20
Cationic chitosan (low, medium and high M_w) ⁷⁸	+3.8-5.4	77×10^3 - 444×10^3	Calcium carbonate	7.6	5-10.8	<20
Chitosan- <i>graft</i> - hydroxypropyltrimethylam monium chloride (Chito- CTA) ⁷⁹	3-chloro-2- -	10×10^6	Oil Sands Tailings	7	120	25

7.5 Conclusions

Hydrolysis lignin was copolymerized with AM and AA to synthesize anionic copolymerized HL based polymers. Compared with two-component HA and HM polymers, the hydrodynamic radius of three-component HAM polymers was significantly larger after polymerization, indicating its more three-dimensional structure. The QCM studies indicated the greater adsorption performance of HAM polymers with a higher charge density and molecular weight, which created a more dissipative adlayer (i.e., more viscoelastic properties). Owing to its greater adsorption performance and three-dimensional structure, the bridging affinity of HAM was more remarkable compared with HM and HAs. However, the larger surface occupancy (153.7 \AA^2) and R_h (75 nm) of HAM2 led to its higher flocculation performance than HAM1 for treating aluminum oxide suspension. Furthermore, HAM copolymers generated stronger flocs in aluminum oxide suspension, which were more resistant to the external shear forces (higher T_{df} values). However, the flocculation of aluminum oxide particles using diblock HM and HA polymers were more reversible (lower T_{rf} values). The more three-dimensional structure of HAMs, which was manifested by larger R_h and more intensive chain entanglement capability in aqueous solution resulted in the higher elastic characteristic of HAMs than diblock HM or HAs. HAM copolymers were more thermally stable than other polymers, which is advantageous for their application as flocculants for wastewater systems that partly operate at a high temperature (i.e., mining industry).

7.6 References

- (1) Thakur, V. K., Thakur, M. K., Raghavan, P., Kessler, M. R. 2014. Progress in green polymer composites from lignin for multifunctional applications: a review. *ACS Sustain. Chem. Eng.* 2(5), 1072-1092.
- (2) Ren, W., Pan, X., Wang, G., Cheng, W., Liu, Y. 2016. Dodecylated lignin-g-PLA for effective toughening of PLA. *Green Chem.* 18(18), 5008-5014.
- (3) Jin, Y., Cheng, X., Zheng, Z. 2010. Preparation and characterization of phenol–formaldehyde adhesives modified with enzymatic hydrolysis lignin. *Bioresour. Technol.* 101(6), 2046-2048.
- (4) Xie, Y., Lü, Q. F., Jin, Y. Q., Cheng, X. S. 2011. *Enzymatic hydrolysis lignin epoxy resin modified asphalt*. In *Advanced Materials Research*; Trans Tech Publications Ltd: 239, 3346-3349.
- (5) Lü, Q. F., Huang, Z. K., Liu, B., Cheng, X. 2012. Preparation and heavy metal ions biosorption of graft copolymers from enzymatic hydrolysis lignin and amino acids. *Bioresour. Technol.* 104, 111-118.
- (6) Sabaghi, S. Fatehi, P., 2020. Polarity of cationic lignin polymers: Physicochemical behavior in aqueous solutions and suspensions. *ChemSusChem*, 13(17), 4722-4734.
- (7) Alipoormazandarani, N., Fatehi, P. 2020. Lignin-methyl methacrylate polymer as a hydrophobic multifunctional material. *Ind Crops Prod.* 154, 112728.
- (8) Hasan, A., Fatehi, P. 2019. Cationic kraft lignin-acrylamide copolymer as a flocculant for clay suspensions:(2) Charge density effect. *Sep. Purif. Technol.* 210, 963-972.
- (9) Hasan, A. Fatehi, P., 2018. Synthesis and characterization of lignin–poly (acrylamide)–poly (2-methacryloyloxyethyl) trimethyl ammonium chloride copolymer. *J. Appl. Polym. Sci.* 135(23), p.46338.

- (10) Kong, F., Wang, S., Price, J. T., Konduri, M. K., Fatehi, P. 2015. Water soluble kraft lignin–acrylic acid copolymer: Synthesis and characterization. *Green Chem.* 17(8), 4355-4366.
- (11) Kong, F., Wang, S., Gao, W. Fatehi, P., 2018. Novel pathway to produce high molecular weight kraft lignin–acrylic acid polymers in acidic suspension systems. *RSC Adv.* 8(22), 12322-12336.
- (12) Singh, R. P., Pal, S., Ali, S. A. 2014. Novel biodegradable polymeric flocculants based on cationic polysaccharides. *Adv. Mater. Lett.* 5(1), 24-30.
- (13) Yang, R., Li, H., Huang, M., Yang, H., Li, A. 2016. A review on chitosan-based flocculants and their applications in water treatment. *Water Res.* 95, 59-89.
- (14) Fang, R., Cheng, X. S., Fu, J., Zheng, Z. B. 2009. Research on the graft copolymerization of EH-lignin with acrylamide. *Nat. Sci.* 1(01), 17.
- (15) Wang, H. F., Hu, H., Wang, H. J., Zeng, R. J. 2019. Combined use of inorganic coagulants and cationic polyacrylamide for enhancing dewaterability of sewage sludge. *J. Clean. Prod.* 211, 387-395.
- (16) Chen, N., Liu, W., Huang, J., Qiu, X. 2020. Preparation of octopus-like lignin-grafted cationic polyacrylamide flocculant and its application for water flocculation. *Int. J. Biol. Macromol.* 146, 9-17.
- (17) Price, J. T., Gao, W., Fatehi, P. 2018. Lignin-g-poly (acrylamide)-g-poly (diallyldimethyl-ammonium chloride): Synthesis, Characterization and Applications. *ChemistryOpen.* 7(8), 645-658.
- (18) Zhou, H., Yang, D., Wu, X., Deng, Y., Qiu, X. 2012. Physicochemical properties of sodium lignosulfonates (NaLS) modified by laccase. *Holzforschung*, 66(7), 825-832.

- (19) Li, R., Yang, D., Guo, W., Qiu, X. 2013. The adsorption and dispersing mechanisms of sodium lignosulfonate on Al₂O₃ particles in aqueous solution. *Holzforschung*, 67(4), 387-394.
- (20) Lin, X., Wu, L., Huang, S., Qin, Y., Qiu, X., Lou, H. 2019. Effect of lignin-based amphiphilic polymers on the cellulase adsorption and enzymatic hydrolysis kinetics of cellulose. *Carbohydr. Polym.* 207, 52-58.
- (21) Hong, N., Yu, W., Xue, Y., Zeng, W., Huang, J., Xie, W., Qiu, X. Li, Y., 2016. A novel and highly efficient polymerization of sulfomethylated alkaline lignins via alkyl chain cross-linking method. *Holzforschung*, 70(4), 297-304.
- (22) Qin, Y., Qiu, X., Liang, W., Yang, D. 2015. Investigation of adsorption characteristics of sodium lignosulfonate on the surface of disperse dye using a quartz crystal microbalance with dissipation. *Ind. Eng. Chem. Res.* 54(49), 12313-12319.
- (23) Alipoormazandarani, N., Fatehi, P. 2018. Adsorption characteristics of carboxymethylated lignin on rigid and soft surfaces probed by quartz crystal microbalance. *Langmuir*, 34(50), 15293-15303.
- (24) Saito, T., Brown, R.H., Hunt, M.A., Pickel, D.L., Pickel, J.M., Messman, J.M., Baker, F.S., Keller, M. Naskar, A.K., 2012. Turning renewable resources into value-added polymer: development of lignin-based thermoplastic. *Green Chem.* 14(12), 3295-3303.
- (25) Tang, X., Huang, T., Zhang, S., Wang, W. Zheng, H., 2020. The role of sulfonated chitosan-based flocculant in the treatment of hematite wastewater containing heavy metals. *Colloids Surf. A Physicochem. Eng. Asp.* 585, 124070.
- (26) Marcilla, A., García, A. N., Pastor, M. V., León, M., Sánchez, A. J., Gómez, D. M. 2013. Thermal decomposition of the different particles size fractions of almond shells and

- olive stones. Thermal behaviour changes due to the milling processes. *Thermochim. Acta.* 564, 24-33.
- (27) Chen, W. H., Tu, Y. J., Sheen, H. K. 2010. Impact of dilute acid pretreatment on the structure of bagasse for bioethanol production. *Int. J. Energy Res.* 34(3), 265-274.
- (28) Wang, B., Wang, S.F., Lam, S.S., Sonne, C., Yuan, T.Q., Song, G.Y. Sun, R.C., 2020. A review on production of lignin-based flocculants: Sustainable feedstock and low carbon footprint applications. *Renew. Sust. Energ. Rev.* 134, 110384.
- (29) Bahrpaima, K., Fatehi, P. 2018. Synthesis and characterization of carboxyethylated lignosulfonate. *ChemSusChem*, 11(17), 2967-2980.
- (30) Bayazeed, A., Elzairy, M. R., Hebeish, A. 1989. Synthesis and Application of New Thickeners Part I: Preparation of Poly (Acrylic Acid)-Starch Graft Copolymer. *Starke* 41(6), 233-236
- (31) Yan, M., Yang, D., Deng, Y., Chen, P., Zhou, H., Qiu, X. 2010. Influence of pH on the behavior of lignosulfonate macromolecules in aqueous solution. *Colloids Surf. A Physicochem. Eng. Asp.* 371(1-3), 50-58.
- (32) Feiler, A. A., Davies, P. T., Vincent, B. 2011. Adsorption of anionic gold nanoparticles by a layer of cationic microgel particles deposited on a gold-coated, quartz surface: studied by quartz crystal microbalance and atomic force microscopy. *Soft Matter*, 7(14), 6660-6670.
- (33) Sammons, R.J., Harper, D.P., Labbé, N., Bozell, J.J., Elder, T. Rials, T.G., 2013. Characterization of organosolv lignins using thermal and FT-IR spectroscopic analysis. *BioResources* 8 (2): 2752-2767, 8(2), 2752-2767.

- (34) Persson, J., Dahlman, O. Albertsson, A.C., 2012. Birch xylan grafted with PLA branches of predictable length. *Bioresources*, 7(3), 3640-3655.
- (35) Chen, R., Kokta, B. V., Valade, J. L. 1980. Study on the graft copolymerization of lignosulfonate and acrylic monomers. *J. Appl. Polym. Sci.* 25(10), 2211-2220.
- (36) El Mansouri, N. E., Yuan, Q., Huang, F. 2011. Characterization of alkaline lignins for use in phenol-formaldehyde and epoxy resins. *BioResources*, 6(3), 2647-2662.
- (37) Hu, L., Pan, H., Zhou, Y., Hse, C. Y., Liu, C., Zhang, B., Xu, B. 2014. Chemical groups and structural characterization of lignin via thiol-mediated demethylation. *J. Wood Chem. Technol.* 34(2), 122-134.
- (38) Savy, D., Piccolo, A. 2014. Physical–chemical characteristics of lignins separated from biomasses for second-generation ethanol. *biomass bioenergy*, 62, 58-67.
- (39) An, L., Wang, G., Jia, H., Liu, C., Sui, W., Si, C. 2017. Fractionation of enzymatic hydrolysis lignin by sequential extraction for enhancing antioxidant performance. *Int. J. Biol. Macromol.* 99, 674-681.
- (40) Witono, J. R., Marsman, J. H., Noordergraaf, I. W., Heeres, H. J., Janssen, L. P. 2013. Improved homopolymer separation to enable the application of ¹H NMR and HPLC for the determination of the reaction parameters of the graft copolymerization of acrylic acid onto starch. *Carbohydr. Res.* 370, 38-45.
- (41) Yang, Z. L., Gao, B. Y., Li, C. X., Yue, Q. Y., Liu, B. 2010. Synthesis and characterization of hydrophobically associating cationic polyacrylamide. *Chem. Eng. J.* 161(1-2), 27-33.

- (42) Kang, Y., Chen, Z., Wang, B., Yang, Y. 2014. Synthesis and mechanical properties of thermoplastic films from lignin, sebacic acid and poly (ethylene glycol). *Ind Crops Prod.* 56, 105-112.
- (43) Salmi, J., Nypelö, T., Österberg, M., Laine, J. 2009. Layer structures formed by silica nanoparticles and cellulose nanofibrils with cationic polyacrylamide (C-PAM) on cellulose surface and their influence on interactions. *BioResources*, 4(2), 602-625.
- (44) Hasan, A., Fatehi, P. 2019. Self-assembly of kraft lignin-acrylamide polymers. *Colloids Surf. A Physicochem. Eng. Asp.* 572, 230-236.
- (45) Long, Y., Wang, T., Liu, L., Liu, G., Zhang, G. 2013. Ion specificity at a low salt concentration in water–methanol mixtures exemplified by a growth of polyelectrolyte multilayer. *Langmuir*, 29(11), 3645-3653.
- (46) Merta, J., Tammelin, T., Stenius, P. 2004. Adsorption of complexes formed by cationic starch and anionic surfactants on quartz studied by QCM-D. *Colloids Surf. A Physicochem. Eng. Asp.* 250(1-3), 103-114.
- (47) Pillai, K. V., Renneckar, S. 2009. Cation– π interactions as a mechanism in technical lignin adsorption to cationic surfaces. *Biomacromolecules*, 10(4), 798-804.
- (48) Hahn Berg, I. C., Lindh, L., Arnebrant, T. 2004. Intraoral lubrication of PRP-1, statherin and mucin as studied by AFM. *Biofouling*, 20(1), 65-70.
- (49) Saarinen, T., Österberg, M., Laine, J. 2009. Properties of cationic polyelectrolyte layers adsorbed on silica and cellulose surfaces studied by QCM-D—effect of polyelectrolyte charge density and molecular weight. *J Dispers Sci Technol.* 30(6), 969-979.

- (50) Matsushita, Y., Imai, M., Iwatsuki, A., Fukushima, K. 2008. The relationship between surface tension and the industrial performance of water-soluble polymers prepared from acid hydrolysis lignin, a saccharification by-product from woody materials. *Bioresour. Technol.* 99(8), 3024-3028.
- (51) Collins, M.N., Nechifor, M., Tanasă, F., Zănoagă, M., McLoughlin, A., Strózyk, M.A., Culebras, M. Teacă, C.A., 2019. Valorization of lignin in polymer and composite systems for advanced engineering applications—a review. *Int. J. Biol. Macromol.* 131, 828-849.
- (52) Cao, C., Jiang, W., Lin, Y., Chen, X., Qian, Q., Chen, Q., Yu, D. Chen, X., 2020. Sensitive phase separation behavior of ultra-high molecular weight polyethylene in polybutene. *Polym. Test.* 81, 106243.
- (53) Mittal, H., Mishra, S.B., Mishra, A.K., Kaith, B.S., Jindal, R. and Kalia, S., 2013. Preparation of poly (acrylamide-co-acrylic acid)-grafted gum and its flocculation and biodegradation studies. *Carbohydr. Polym.* 98(1), 397-404.
- (54) Mai, C., Milstein, O. and Hüttermann, A., 2000. Chemoenzymatical grafting of acrylamide onto lignin. *J. Biotechnol.* 79(2), 173-183.
- (55) Yoon, S.D., Park, M.H. and Byun, H.S., 2012. Mechanical and water barrier properties of starch/PVA composite films by adding nano-sized poly (methyl methacrylate-co-acrylamide) particles. *Carbohydr. Polym.* 87(1), 676-686.
- (56) Ház, A., Jaslonsky, M., Orsagova, A. Surina, I., *Determination of temperature regions in thermal degradation of lignin.* In *4 th International Conference on renewable energy source, High Tatras, Slovak Republic:* 2013.

- (57) Fenner, R. A., Lephardt, J. O. 1981. Examination of the thermal decomposition of kraft pine lignin by Fourier transform infrared evolved gas analysis. *J. Agric. Food Chem.* 29(4), 846-849.
- (58) Brebu, M., Vasile, C. 2010. Thermal degradation of lignin—a review. *Cellul. Chem. Technol.* 44(9), 353.
- (59) Konduri, M. K., Kong, F., Fatehi, P. 2015. Production of carboxymethylated lignin and its application as a dispersant. *Eur. Polym. J.* 70, 371-383.
- (60) Van Dyke, J. D., Kasperski, K. L. 1993. Thermogravimetric study of polyacrylamide with evolved gas analysis. *J Polym Sci A Polym Chem.* 31(7), 1807-1823.
- (61) Domínguez, J. C., Oliet, M., Alonso, M. V., Rojo, E., Rodríguez, F. 2013. Structural, thermal and rheological behavior of a bio-based phenolic resin in relation to a commercial resol resin. *Ind Crops Prod.* 42, 308-314.
- (62) Dubinsky, S., Grader, G. S., Shter, G. E., Silverstein, M. S. 2004. Thermal degradation of poly (acrylic acid) containing copper nitrate. *Polym. Degrad. Stab.* 86(1), 171-178.
- (63) Liu, X., Xu, Y., Yu, J., Li, S., Wang, J., Wang, C., Chu, F. 2014. Integration of lignin and acrylic monomers towards grafted copolymers by free radical polymerization. *Int. J. Biol. Macromol.* 67, 483-489.
- (64) Wang, J.P., Yuan, S.J., Wang, Y. and Yu, H.Q., 2013. Synthesis, characterization and application of a novel starch-based flocculant with high flocculation and dewatering properties. *Water Res.* 47(8), 2643-2648.
- (65) Dryhurst, G. *Periodate oxidation of diol and other functional groups: analytical and structural applications*; Elsevier: 2, 2015.

- (66) Kail, N., Marquardt, W., Briesen, H. 2009. Process analysis by means of focused beam reflectance measurements. *Ind. Eng. Chem. Res.* 48(6), 2936-2946.
- (67) Vay, K., Frieß, W., Scheler, S. 2012. Understanding reflection behavior as a key for interpreting complex signals in FBRM monitoring of microparticle preparation processes. *Int. J. Pharm.* 437(1-2), 1-10.
- (68) Sabaghi, S. Fatehi, P., 2019. Phenomenological Changes in Lignin Following Polymerization and Its Effects on Flocculating Clay Particles. *Biomacromolecules*, 20(10), 3940-3951.
- (69) Yoon, S. Y., Deng, Y. 2004. Flocculation and reflocculation of clay suspension by different polymer systems under turbulent conditions. *J. Colloid Interface Sci.* 278(1), 139-145.
- (70) Zhang, Y., Fatehi, P. 2019. Periodate oxidation of carbohydrate-enriched hydrolysis lignin and its application as coagulant for aluminum oxide suspension. *Ind Crops Prod.* 130, 81-95.
- (71) Blanco, A., Fuente, E., Negro, C. Tijero, J., 2002. Flocculation monitoring: focused beam reflectance measurement as a measurement tool. *Can J Chem Eng.* 80(4), 1-7.
- (72) Yang, Z., Li, H., Yan, H., Wu, H., Yang, H., Wu, Q., Li, H., Li, A. Cheng, R., 2014. Evaluation of a novel chitosan-based flocculant with high flocculation performance, low toxicity and good floc properties. *J. Hazard. Mater.* 276, 480-488.
- (73) Antunes, E., Garcia, F. A. P., Blanco, A., Negro, C., Rasteiro, M. G. 2015. Evaluation of the flocculation and reflocculation performance of a system with calcium carbonate, cationic acrylamide co-polymers, and bentonite microparticles. *Ind. Eng. Chem. Res.* 54(1), 198-206.

- (74) Chen, W. J. 1998. Effects of surface charge and shear during orthokinetic flocculation on the adsorption and sedimentation of kaolin suspensions in polyelectrolyte solutions.
- (75) Zhu, Z., Li, T., Lu, J., Wang, D., Yao, C. 2009. Characterization of kaolin flocs formed by polyacrylamide as flocculation aids. *Int. J. Miner. Process.* 91(3-4), 94-99.
- (76) Vuoti, S., Narasimha, K., Reinikainen, K., 2018. Green wastewater treatment flocculants and fixatives prepared from cellulose using high-consistency processing and deep eutectic solvents. *J. Water Process. Eng.* 26, 83-91.
- (77) Sievänen, K., Kavakka, J., Hirsilä, P., Vainio, P., Karisalmi, K., Fiskari, J., Kilpeläinen, I., 2015. Cationic cellulose betainate for wastewater treatment. *Cellulose*, 22(3), 1861-1872.
- (78) Nicu, R., Bobu, E., Miranda, R. Blanco, A., 2013. Flocculation efficiency of chitosan for papermaking applications. *BioResources*, 8(1), 768-784.
- (79) Pennetta de Oliveira, L., Gumfekar, S.P., Lopes Motta, F. Soares, J.B., 2018. Dewatering of oil sands tailings with novel chitosan-based flocculants. *Energy Fuels*. 32(4), 5271-5278.

Chapter 8: Conclusions and Recommendations for Future Works

8.1 Conclusions

New cationic lignin-based macromolecules were synthesized via the radical polymerization of kraft lignin (KL) and [2-(acryloyloxy)ethyl]trimethylammonium chloride (ATAC) or [2-(methacryloyloxy)ethyl]trimethylammonium methyl sulfate (METAM) in a semidried condition for the first time, which had a similar charge densities (2.3-2.5 mmol/g) and different molecular weights (657×10^3 and 824×10^3 g/mol). The hydrodynamic radius (R_h) and radius of gyration (R_g) of lignin macromolecules enhanced after polymerization. The shape factor results (R_g/R_h) illustrated that the structure of lignin macromolecules changed from rigid-rod to more flexible random coil chain after the polymerization reaction. Moreover, a strong correlation between the conformation of lignin polymers and their flocculation behavior was observed. Owing to its large surface occupancy and three-dimensional structure, KL-METAM had greater flocculation performance in a kaolin suspension and created larger flocs that were more resistant to the external shear forces.

The conformational changes of KL-METAM and KL-ATAC also influenced the surface properties, self-assembly, adsorption capacity and viscoelastic characteristics of lignin polymers. The contact angle and surface tension of water containing KL-METAM were smaller compared to that of KL-ATAC. The self-assembly of KL-METAM with larger R_h was enhanced with time. Owing to its higher self-association capability, the destabilization index and settling velocity of KL-METAM solution increased progressively with increasing R_g at both regular and accelerated gravitations. Compared to KL-ATAC, KL-METAM deposited more greatly and generated a bulkier adsorbed layer on the SiO_2 surface. The higher elastic

characteristic (G') was observed for KL-METAM due to its higher chain entanglement. The higher T_g values of KL-ATAC proved that its molecular chain mobility was restricted due to the more compact conformation of the polymer, which was enhanced its rigidity.

Hydrolysis lignin was polymerized with [3-(methacryloylamino)propyl] trimethylammonium chloride (MAPTAC) or [2-(methacryloyloxy)ethyl] trimethyl ammonium chloride (METAC) in a semidried manner to produce cationic hydrolysis lignin polymers (CHL) with similar charge densities, molecular weights and grafting ratios. The successful polymerization reaction was confirmed by ^{31}P NMR, ^1H NMR and FTIR spectra. The dipole moments of HL-METAC and HL-MAPTAC, were 25.9 and 16.7 D for respectively, confirming the higher polarity of the former CHL. In the salt and urea free systems, HL-METAC adsorbed more than HL-MAPTAC on the surface of kaolin particles. The flocculation performance of HLMETAC was better than HL-MAPTAC, which was attributed to its higher polarity and more three-dimensional structure. The addition of KCl salt reduced the flocculation efficiency of CHLs, however, the stronger charge interaction was observed for HL-METAC than HL-MAPTAC for its adsorption on the kaolin particles. In the urea containing system, the hydrophobic interaction of CHLs and the particles were highlighted, and HL-MAPTAC with less polarity showed a higher adsorption efficiency than HL-METAC.

The polymerized kraft lignin with METAM or acrylic acid (AA) were examined for the removal of heavy metal ions. KL-AA was more efficient than KL-METAM for eliminating ionic composition (i.e., Zn^{2+} , Cu^{2+} , K^+) from the solution due to the stronger electrostatic interaction, cationic π -interaction, and chelation/complexation mechanism developed between the polymer and ions. The dual polymer systems of KL-AA/KL-METAM was highly efficient for ion removal from a model solution when KL-AA was introduced as a first polymer

followed by KL-METAM because KL-AA had a stronger affinity to adsorb ions, and then KL-METAM could form bridges to entrap the unattached ions. The diffusion of ions into the voids of lignin-based flocculants enhanced the flocculation efficiency of the dual system compared to the singular one, which manifested by a larger aggregate size. The QCM results also revealed that the adsorption of ions on the KL-AA coated surface was more remarkable and generated a bulkier and more viscoelastic adlayer compared to that on the KL-METAM surface.

The hydrolysis lignin (HL) was copolymerized with acrylamide (AM) and acrylic acid (AA) under acidic conditions to produce anionic HAM copolymers with various surface characteristics. The properties of the copolymers were characterized using ^1H NMR, elemental analyser, gel permeation chromatography (GPC), and thermogravimetry analysis (TGA). The triblock copolymer of HAM with higher charge density yielded lower surface excess density and adsorbed more on the Al_2O_3 surface, which generated a bulkier adsorbed layer. However, a larger surface occupancy was observed at the interface of water and QCM sensor (153.7 \AA^2) for the lower molecular weight HAM polymer, which had smaller R_h of 64.3 nm. Compared to diblock HL-AM (HM) and HL-AA (HA), three component HAM copolymers showed greater adsorption and bridging performance on aluminium oxide particles. In addition, high thermal stability, glass transition temperature (T_g) and rheological characteristics of the HAM copolymer proved its potential application as flocculant/adsorbent for wastewater treatment systems at a high temperature.

Overall, the results of this research thesis suggested that the lignin macromolecules, which is currently an under-utilized biopolymer has potential to be valorized through free radical polymerization with cationic or anionic monomers to yield alternative to petroleum-based products.

The finding of this work provided fundamental evidence on how a small group (i.e., a methyl group) on the structure of a cationic monomer can have a significant impact on its polymerization with lignin and subsequently on the physicochemical behavior lignin polymer in aqueous solutions. It was also revealed that the conformation of cationic lignin may alter from highly branched and dense structure to rigid-rod like shape by increasing the grafting density, which in turn have a substantial influence on their rheological properties and thermal behaviour. The results also proved that the polarity of lignin macromolecules originated from the structure of attached cationic monomers might affect their hydrogen bonding development and electrostatic interaction with other colloidal particles.

The detailed interaction and adsorption behavior of metal ions on lignin- derived polymeric surface was investigated, which indicated the superior adsorption performance of the lignin-based macromolecules for ions removal. This study also proved that the high molecular weight and charge density of triblock lignin-based polymers have great impacts on their flocculation performance, the properties of induced flocs and their viscoelastic performance in aqueous solutions and upon adsorptions.

8.2 Future work

The impact of reaction conditions on the graft polymerization of the lignin polymers should be investigated in detail. The results presented herein have focused mainly on the adsorption and flocculation performance of lignin macromolecules in model clay suspension and ion solutions. However, the kinetic of flocculation and floc's properties in actual wastewater system having different properties and compositions should be investigated to obtain more industrially attractive results.

Hydrolysis lignin can be fractionated into water soluble and water insoluble parts. Then, the water insoluble fraction should be employed for polymerization reaction to develop the functionality as well as water-solubility of final products. Since lignin-based polymers showed superior thermal stability and exceptional mechanical properties (i.e., high storage modulus), a systematic study should be conducted on their application in thermoplastic and composite production.

Chapter 9: Appendix

Characterization of polymers

The charge density of macromolecules was measured using a Particle Charge Detector (Mütek PCD 04 titrator, Herrsching, Germany). The samples were mixed with deionized water (20 g/L) overnight and then centrifuged at 1000 rpm for 5 min. Afterward, 1 mL of the supernatants were titrated against PVSK solution (0.005 M), which helped the charge density measurement of soluble macromolecules. The charge density of insoluble macromolecules was also measured by the PCD instrument following the back titration method.¹

The elemental analysis of unmodified lignin and cationic lignin macromolecules was carried out using an elemental analyser (Vario EL Cube, Elemental Analyzer, Germany). In this study, 2 mg of dried samples (at 105°C) was used to analyze their nitrogen contents. As unmodified kraft lignin (KL) did not have any nitrogen, the nitrogen content of the polymers is originated from cationic monomers attached to lignin macromolecules. The grafting ratio of ATAC and METAM to lignin correlates with the nitrogen content of lignin macromolecule and was calculated according to equation 1:

(1)

$$\text{Grafting ratio (mol\%)} = \frac{\frac{N}{14} \times Mw}{100 - \left(\frac{N}{14} \times Mw\right)} \times 100$$

Where N is the nitrogen content of polymers (wt.%), and Mw is the molecular weight of ATAC and METAM, which are 152 and 173 g/mol, respectively.

The phenolic hydroxyl group content of KL and CKL was measured using an automatic potentiometric titrator, 785 Titrino. In this analysis, 0.06 g of lignin polymer were added to 1 mL of potassium hydroxide (0.8 M). Afterwards, the sample were dissolved in 0.02 g of para-hydroxybenzoic acid (as internal standard) and then 100 mL of deionized water was added to the system. After mixing, the prepared solutions were titrated against 0.1 M HCl standard solution. The phenolic hydroxyl group contents were calculated following equation 2:²

(2)

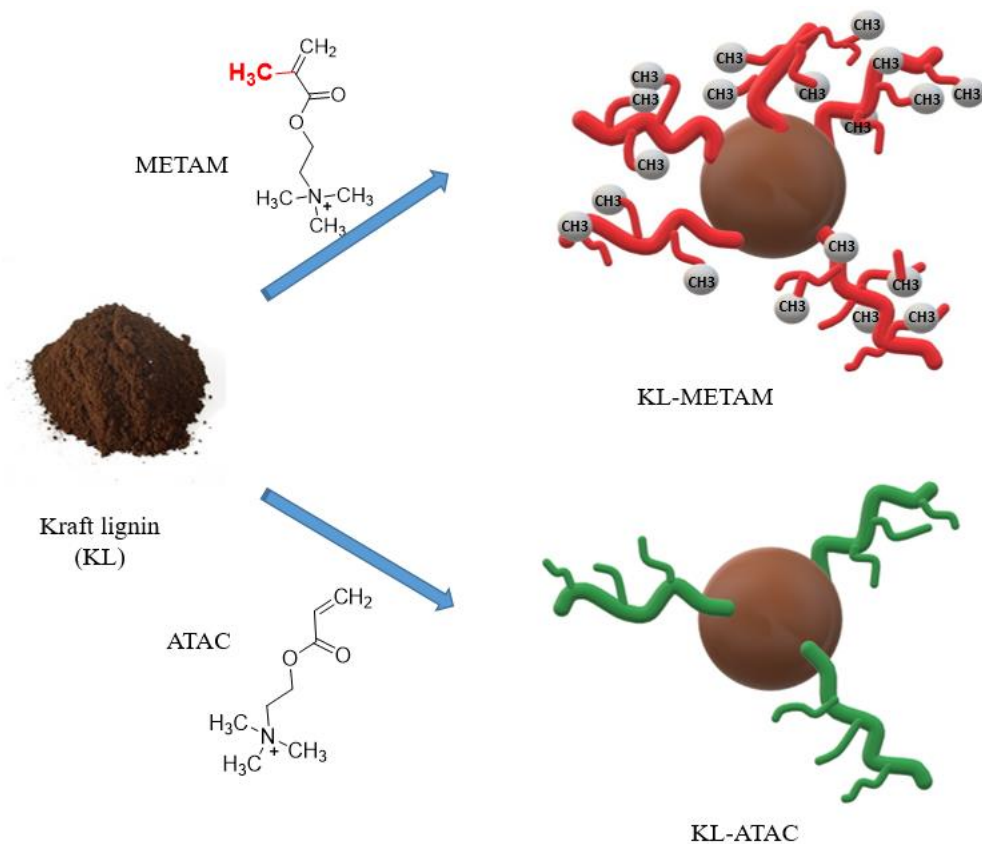
$$\text{Phenolic hydroxyl group} \left(\frac{\text{mmol}}{\text{g}} \right) = \frac{C_{\text{HCl}}[(V_2' - V_1') - (V_2 - V_1)]}{m}$$

Here C_{HCl} is the molar concentration of HCl, V_1 and V_2 are the consumed volume of HCl (mL) for titration of blank solutions where the first and second end points obtained, V_1' and V_2' are the consumed volume of HCl solution (mL) for the first and second end points when CKL solutions were titrated, and m stands for weight (g) of lignin samples.

The molecular weight of polymers was determined using a gel permeation chromatography (Malvern, GPCmax VE2001 Module + Viscotek TDA305) equipped with multi-detector (UV, RI, viscometer, low and right-angle laser detectors) using polyethylene oxide as standard samples. It should be noted that the polystyrene polymers were employed as standards for organic system, while poly (ethylene oxide) for the aqueous system. In this study, for cationic lignin measurements, PolyAnalytic PAA206 and PAA203 columns were used. A 0.1 mol/l

NaNO₃ solution was used as solvent and eluent, the flow rate and column temperature were adjusted to 0.70 mL/min and 35 °C, respectively.

The cartoon model of KL-ATAC and KL-METAM chemical structure and their reaction scheme are proposed in Scheme A1 and Scheme A2, respectively.



Scheme A. 1 Cartoon model of KL-ATAC and KL-METAM chemical structure

The hydrodynamic diameter of KL and CKLs was measured with the dynamic light scattering (DLS), BI-200SM Brookhaven Instruments, USA. The operating procedure was as stated by Yan et al.³ In this analysis, samples were dissolved in a 1mM KCl solution to keep the ionic strength of the solutions. Then, the 1 g/L of lignin solution was mixed overnight at 300 rpm and 25 °C. After that, the lignin samples were filtered using a 0.45 µm syringe filter. The laser wavelength and the scattering angle was set at 637 nm and 90°, respectively. Each analysis was repeated three times, and the average values were reported.

The Radius of gyration (R_g) of KL and CKLs was measured with a static light scattering (SLS) instrument that was attached to a goniometer, Brookhaven BI-200SM, Holtsville, NY, USA. In this set of experiments, different concentrations of lignin solution (0.2-2 wt.%) was prepared in alkaline aqueous solutions (using 0.75 M NaOH) at room temperature to completely solubilize the lignin samples. It should be pointed out that, since the lignin macromolecules were not completely soluble in deionized water specially at higher concentration (i.e. above 1 g/L) multiple solvents were used to disperse the lignin particles well, without changing their properties. Among them, sodium hydroxide solution was chosen to yield the largest difference between refractive indices. This provided the best signal at a given sample concentration.⁴

The solutions were then filtered using a nylon syringe filter (30 mm diameter and 0.45µm pore size). The wavelength of laser polarized light was 637 nm, and the intensities of different

samples were tested at different angles (15 ° - 155 °). BIC Zimm Plot software was then used for determining R_g of the samples.⁵

Characterization of clay particles

Surface Area

The total surface area of kaolin particles was measured using a Quantachrome surface area analyzer, Nova2200e, under N₂ atmosphere according to a previously established method.⁴ Initially, appropriate amount of sample (0.05 g) was preheated at 250 °C for 4 h. Then, the total specific surface area (SSA) of the samples was determined according to Brunauer–Emmett–Teller (BET) method via Nitrogen adsorption and desorption isotherms at -180 °C while the relative pressure was in the range of 0.01 and 0.99.⁶

Morphological analysis

The morphology of kaolin and kaolin/CKLs was monitored using a scanning electron microscopy (SEM) Hitachi SU-70 Field emission with energy dispersive X-Ray analysis (EDX). In this analysis, appropriate amount of CKLs was mixed with kaolin suspension at fixed rpm for several minutes to form aggregates. Then the mixture was filtered using filter paper and the filtrate was collected and dried using freeze- dryer. The freeze-dried sample was spread on a double side carbon tape on the specimen stubs and coated with gold. After scanning for 300 s, the specimen was analyzed at 5 kV for their microstructures.⁷

Adsorption

In this set of experiments, 25 g/L kaolin suspensions were prepared by dispersing kaolin powder in deionized distilled water at pH 6 and the suspension was shaken overnight. Different amounts of cationic macromolecules were then added to the suspension in order to analyse the adsorption of macromolecules on clay particles at different polymer dosages (1 to 128 mg/g).

The suspensions were agitated for 30 min at 150 rpm and 30 °C in a water bath shaker. After incubation, the mixture was centrifuged at 4500 rpm for 10 min.

The sample was then filtered by a filter (pore size 0.45 µm) to collect filtrate for adsorption test using Genesys 10 s UV–vis spectrophotometer at the wavelength of 205 nm. To satisfy statistical consistency, all the experiments were repeated in triplicates, and the average value was reported in this study.

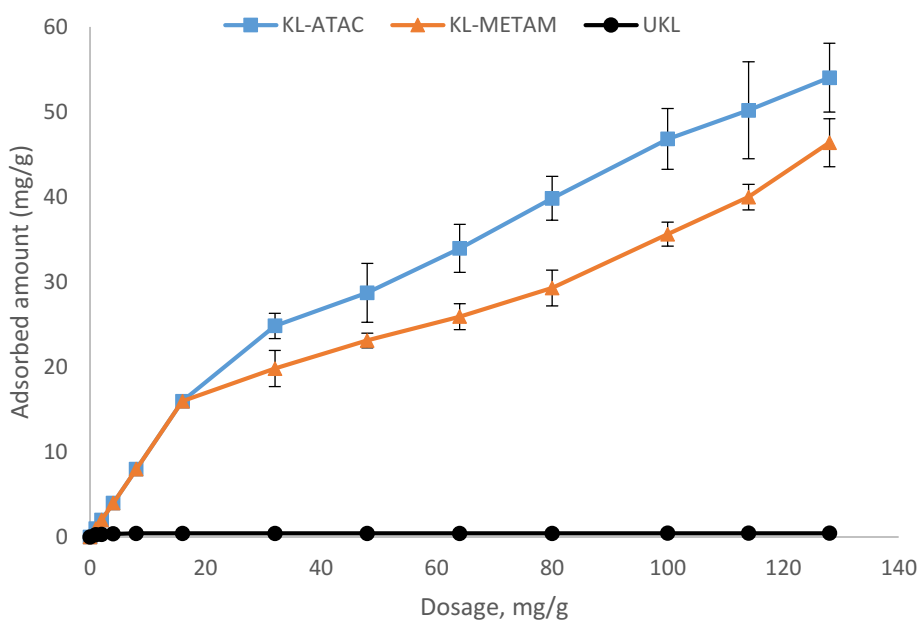


Figure A. 1 Adsorption of KL and CKLs on kaolin as a function of polymer dosage under the conditions of pH 6, 25 °C and 25 g/l of kaolin concentration.

Surface tension and contact angle measurement

The surface tension of KL and CKL samples were analyzed using a tensiometer (Attension sigma 700) equipped with a platinum loop. In this experiment, 1 g/L of CKL solution was prepared overnight at 300 rpm. Then, 20 mL of the prepared solutions were poured into the glass dish for analysing their surface tension following the ring method.^{8,9} All the

measurements were conducted at room temperature, neutral pH and the analysis was repeated 10 times to get an average value.

The wettability and contact angle of CKL macromolecules in 1 wt.% aqueous solution as well as diiodomethane solution were measured using an optical tensiometer instrument, Theta lite (Biolin Scientific, Finland), which was equipped with a camera. In this set of experiments, 1 mL of kaolin suspension (25 g/L, pH 6) was coated on glass slides using a spin coater WS-650 (Laurell Technologies Corp), while rotating at 800 rpm. The rotation was continued under vacuum environment (by purging N₂ gas) with 60 psi pressure for 60 s.¹⁰ Then, the kaolin coated glasses were dried in the oven at 60°C for 24 h. After that, a water or diiodomethane droplet (5µL) was placed on kaolin coated slides and the contact angle between water and kaolin were investigated. In another set of experiment, a droplet of CKL solutions (in 1 g/L) and diiodomethane was located on the kaolin coated slides (in separated runs) and the contact angle between droplets and coated slides was measured using the tensiometer. In this analysis, each test was repeated 3 times, and the average values of measurements were reported.

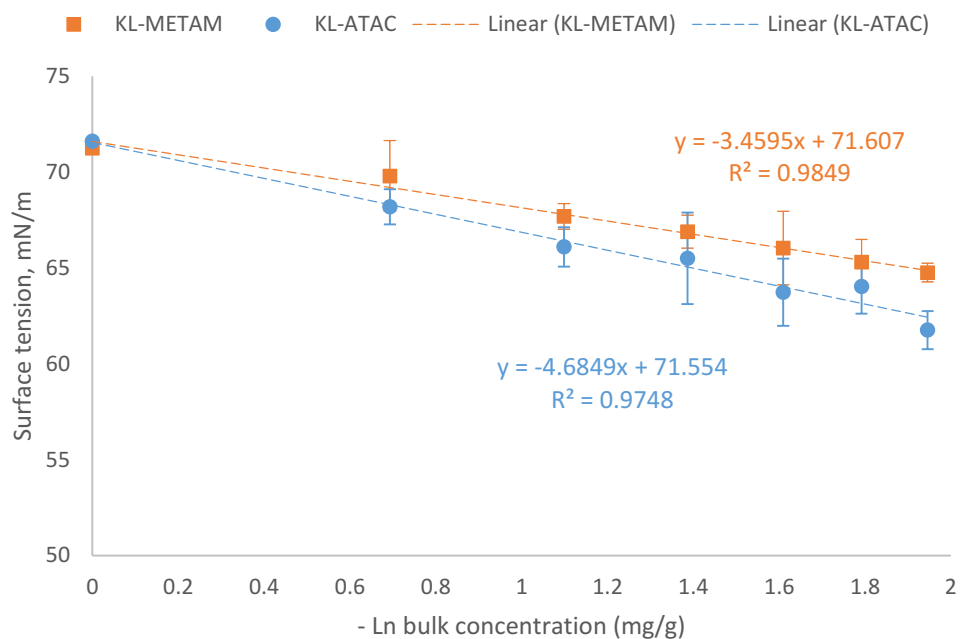


Figure A. 2 Plots of surface tension of aqueous solution against natural logarithm of concentration for KL-METAM and KL-ATAC

Zeta potential

The zeta potential of kaolin suspension in the presence of various dosages (2 to 64 mg/L) of cationic macromolecules was measured using a NanoBrook PALS (Brookhaven Inc., USA). All the measurements were carried out at a constant electric field (8.4 V/cm) and the reported data was the average of three repetitions.

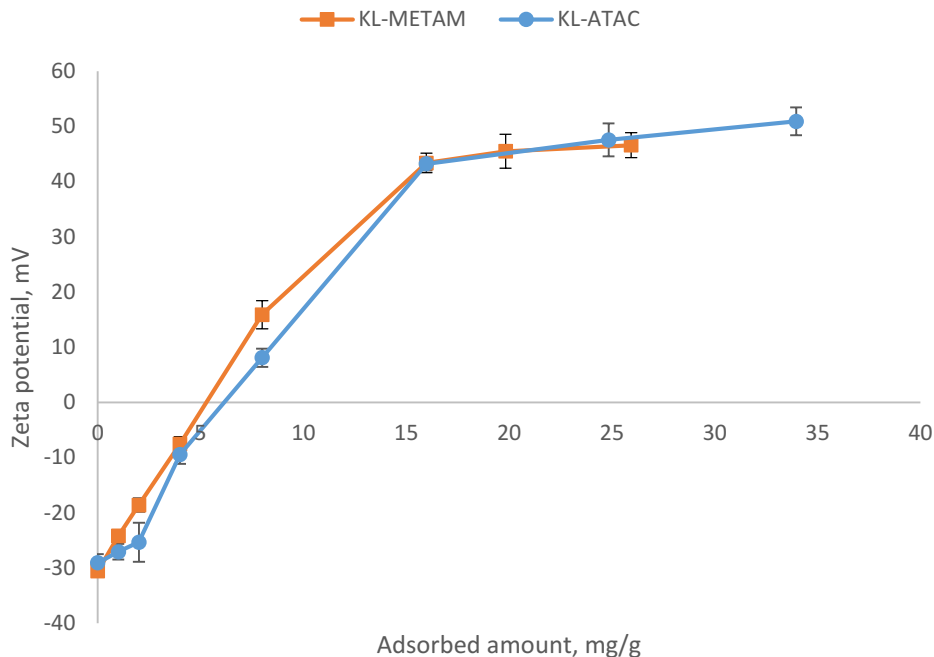


Figure A. 3 Effect of adsorbed CKLs on kaolin particles conducted under the conditions of pH 6, 25 °C and 25 g/L of kaolin concentration.

Flocculation

photometric dispersion analyser (PDA)

The flocculation analysis was performed using a photometric dispersion analyzer (PDA 3000, Rank Brothers Ltd), which was attached to a dynamic drainage jar (DDJ) and contained a 70 mm mesh screen. In this set of experiment, 480 mL of deionized water was poured into DDJ container and circulated from the DDJ to the PDA through a 3 mm plastic tube until a steady flow rate of 20 mL/min was obtained. Afterwards, 20 mL of a 25 g/L kaolin suspension was added into DDJ container while stirring at 300 rpm to achieve a total volume of 500 mL suspension. The pH of the total mixture was 6. The turbidity of the suspension was determined as elaborated in previous studies.¹¹⁻¹⁶ The effect of CKL adsorption on the relative turbidity of kaolin was presented in Fig S4.

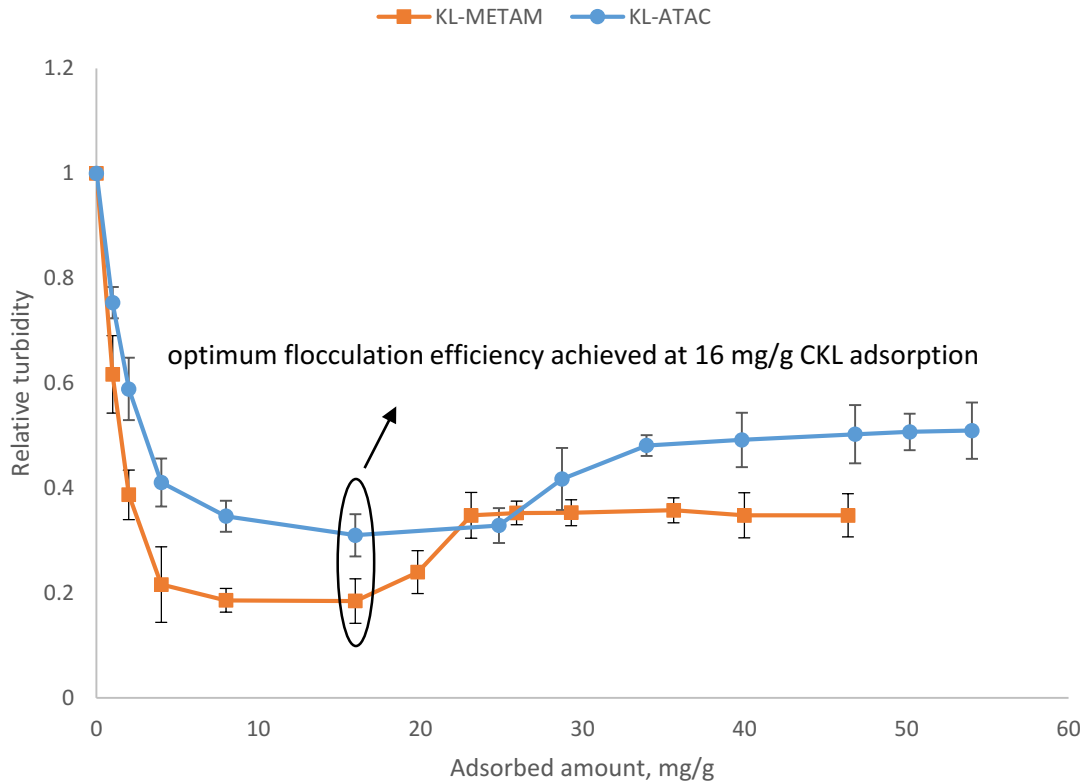


Figure A. 4 Effect of CKLs adsorption on the relative turbidity of kaolin suspension conducted under the condition of pH 6, 25 °C and 25 g/L of kaolin concentration.

Focused beam reflectance measurement (FBRM)

The flocculation behaviour of the suspension and floc properties were analysed under different conditions by monitoring the chord length distribution of particles in the suspension in real time using an FBRM, Mettler Toledo, E25. Chord length (CL) measures distance between the two edges of a particle in suspensions in the FBRM analysis. In this set of experiment, kaolin

suspension (25 g/L at pH 6) was stirred at 200 rpm and then the laser probe (25 mm diameter) was placed in the mixture. After reaching steady state conditions, a desired mass of cationic macromolecules was added to the suspension and the mixture was stirred at 200 rpm for 4-5 min. In order to study the re-flocculation affinity of flocs, the stirring rate of the mixture was increased to 700 rpm to break down the flocs, which is known as deflocculation process, and the agitation was subsequently decreased to 200 rpm to analyse reflocculation of broken flocs.

Particle size distribution

The particle size distribution of kaolin particles was determined using a MasterSizer 3000 (Malvern Instruments). First, 1 mL of kaolin suspension (25 g/L) or lignin solution (1 g/L – at dosage of 16 mg/g) was added to the cell of instrument, which contained 500 mL deionized water and stirred at 1000 rpm. After 15 min stirring, the particle size of the samples was identified.

Figure A5 displayed the particle size distribution of kaolin particles in the absence and presence of CKL macromolecules. Addition of CKLs increased the particle size of kaolin particles from 4.2 to 9.2 and 19.8 μm for KL-ATAC and KL-METAM, respectively. The adsorption of CKLs on kaolin particle was also broadened the size distribution of particles.

In this analysis the radius of kaolin particles was measured for further calculation (i.e. flocculation rate constant) in *Kinetic of flocculation* section.

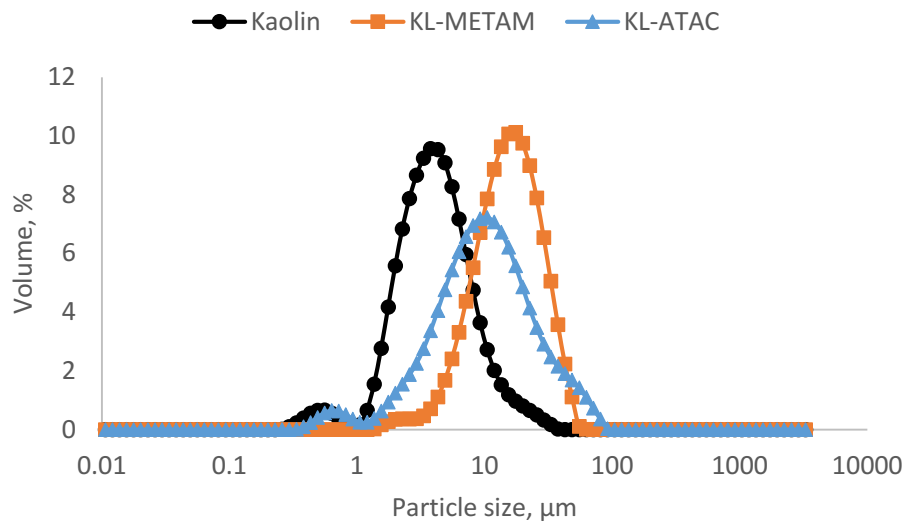


Figure A. 5 Volume fraction of kaolin particles as a function of their size

Adsorption time of flocculation

The required time for adsorption of CKLs at different macromolecule concentration are tabulated at Table A1.

Table A. 1 Theoretical predictions of CKLs adsorption times.

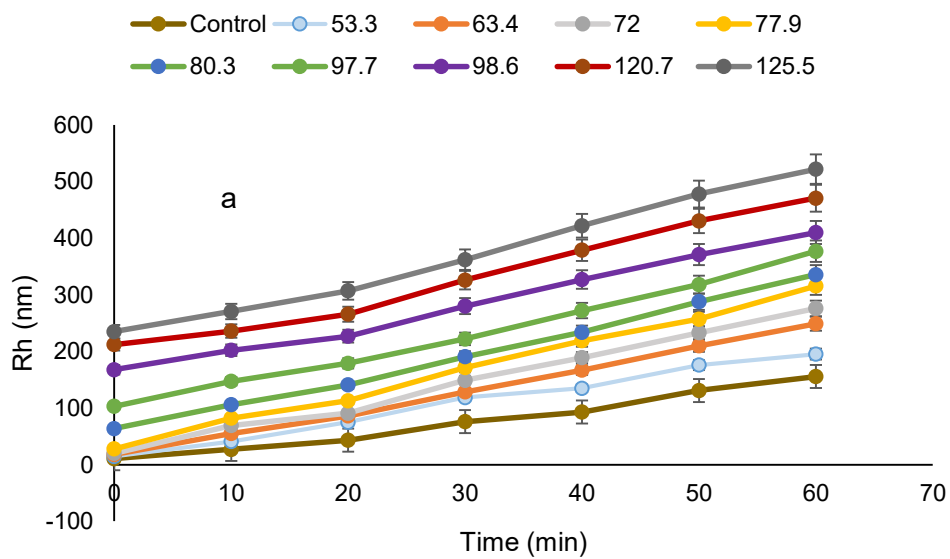
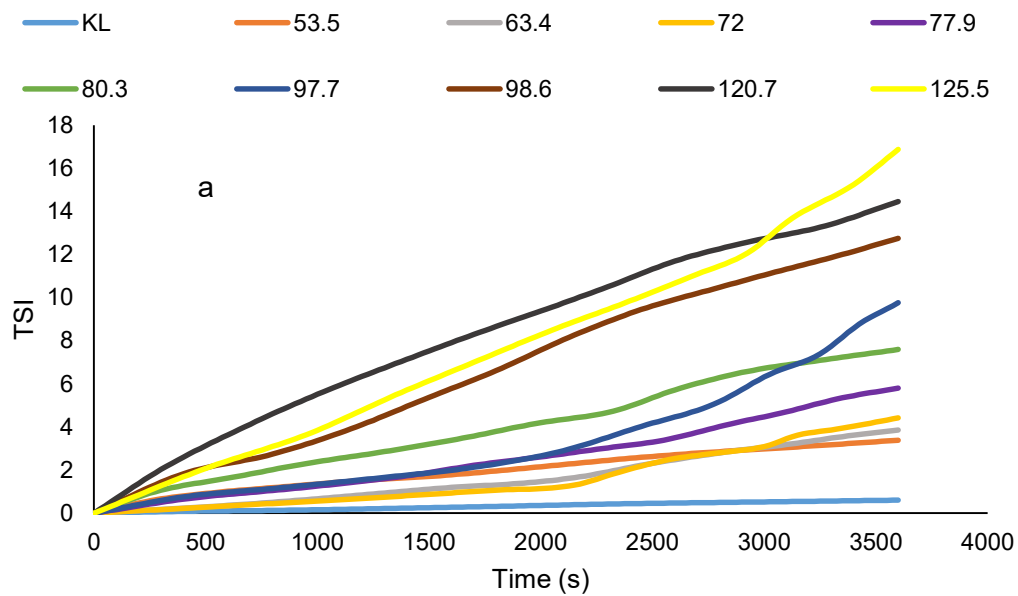
Dosage, (mg/g)	T_{ads} (s)	
	KL-MEAM	KL-ATAC
1	2.3	2.3
2	4.6	4.62
4	9.19	9.24
8	18.41	18.48
16	36.6	37
32	45.54	57.4

48	53.22	66.37
64	59.56	78.43
80	67.36	92.03
100	81.96	108.18
114	84.6	120.56
128	106.38	125.15

Table A. 2 The properties of KL, KL-METAM, and KL-ATAC

Sample	Properties					
	Charge density (mmol/g)	Nitrogen content (wt %)	Grafting ratio (mol %)	Phenolic hydroxide content (mmol/g)	M _w (g/mol)	R _g (nm)
KL	-0.7	0	0	1.64	4.1×10 ²	5.01
KL-METAM						
1	0.71	2.82	53.5	0.96	2.57×10 ³	16.2
2	0.95	3.14	63.4	0.82	4.8×10 ³	20.2
3	1.45	3.38	72	0.78	2.18×10 ⁴	22.8
4	1.57	3.53	77.9	0.73	8.65×10 ⁴	42.4
5	1.8	3.6	80.3	0.71	2.23×10 ⁵	102
6	2.45	4	97.7	0.67	8.82×10 ⁵	170.2

7	2.6	4.02	98.6	0.66	1.74×10^6	302.7
8	3.43	4.25	120.7	0.6	1.11×10^7	468.8
9	3.86	4.5	125.5	0.51	1.38×10^7	500
KL-ATAC						
1	0.27	2.4	35.2	1.04	1.59×10^3	11.4
2	0.55	2.91	46.2	0.99	4.5×10^3	14.6
3	0.72	3.64	65.3	0.95	1.73×10^4	16.9
4	1.23	3.93	74.4	0.91	5.47×10^4	26.8
5	1.67	4.1	80.2	0.88	1.41×10^5	32.3
6	1.92	4.5	95.5	0.83	5.56×10^5	85.9
7	2.63	4.75	106.5	0.77	1.38×10^6	126.3
8	3.02	5	118.7	0.71	1×10^7	187.4
9	3.34	5.1	124.06	0.69	1.09×10^7	301.1



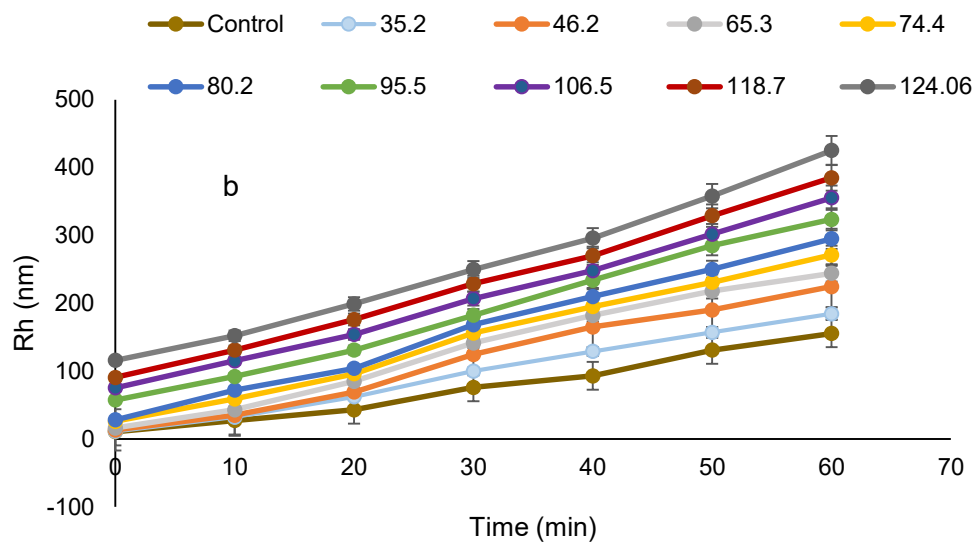


Figure A. 6 Effect of time on the hydrodynamic radius of a) KL-METAM and b) KL-ATAC at different grafting ratio (The Control sample is KL).

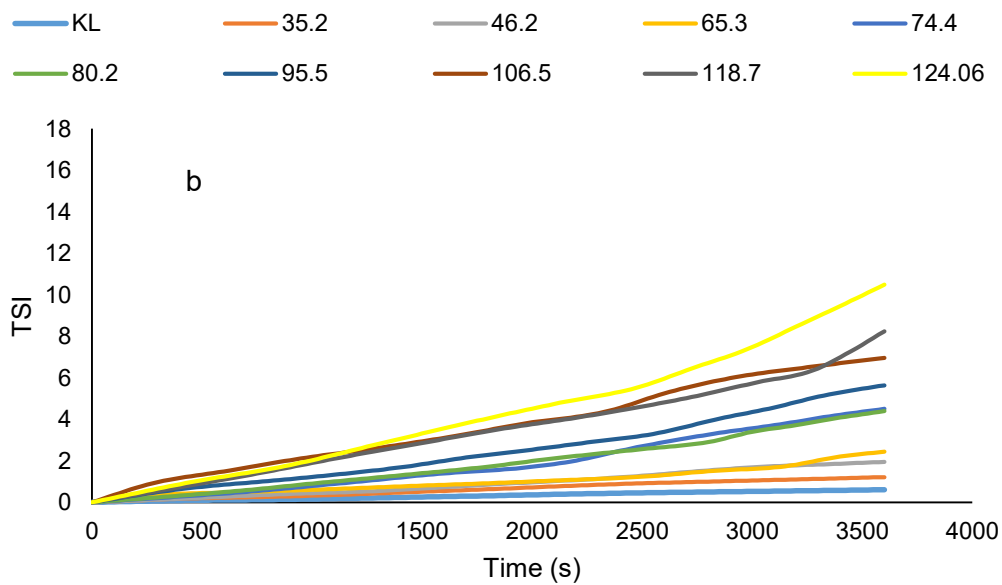


Figure A. 7 Effect of time on the destabilization index of a) KL-METAM and b) KL-ATAC at different grafting ratio

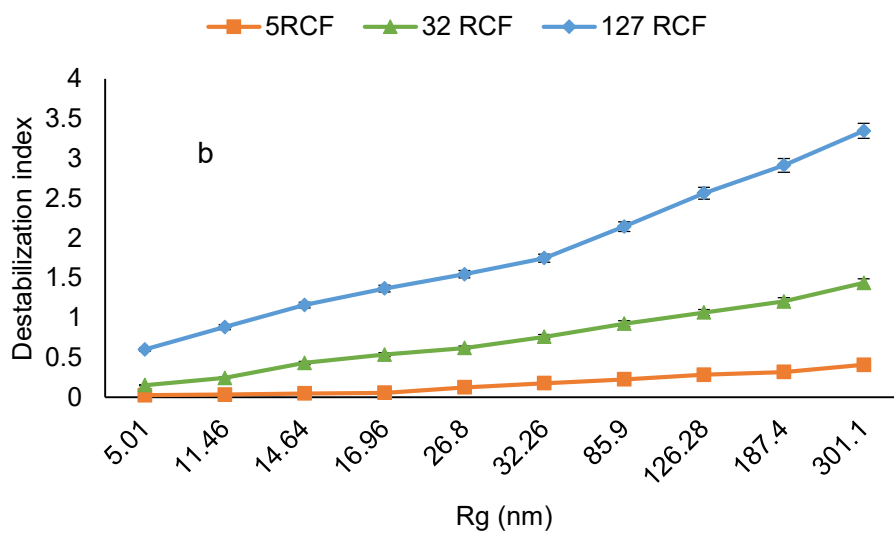
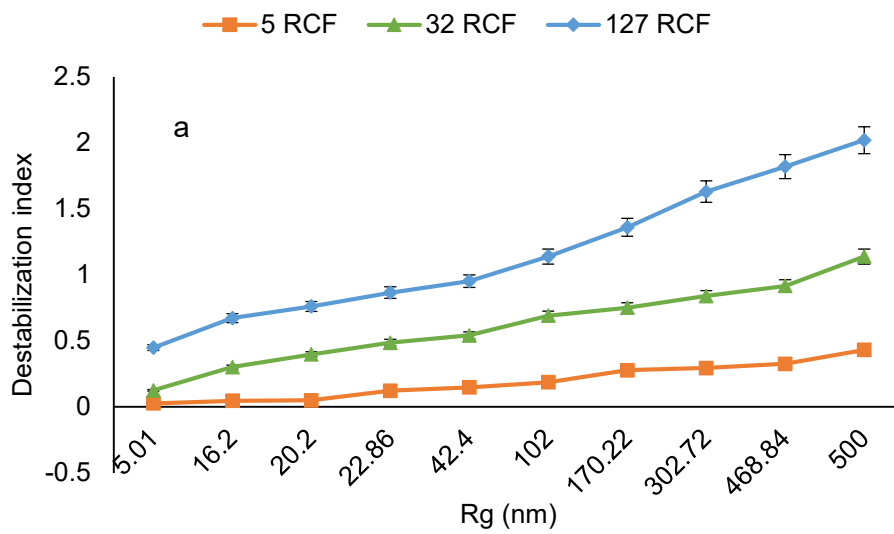


Figure A. 8 Stability of a) KL-METAM and b) KL-ATAC conducted under conditions of 1g/L CKL concentration, 25 °C at RCA of 5,32 and 127 (g).

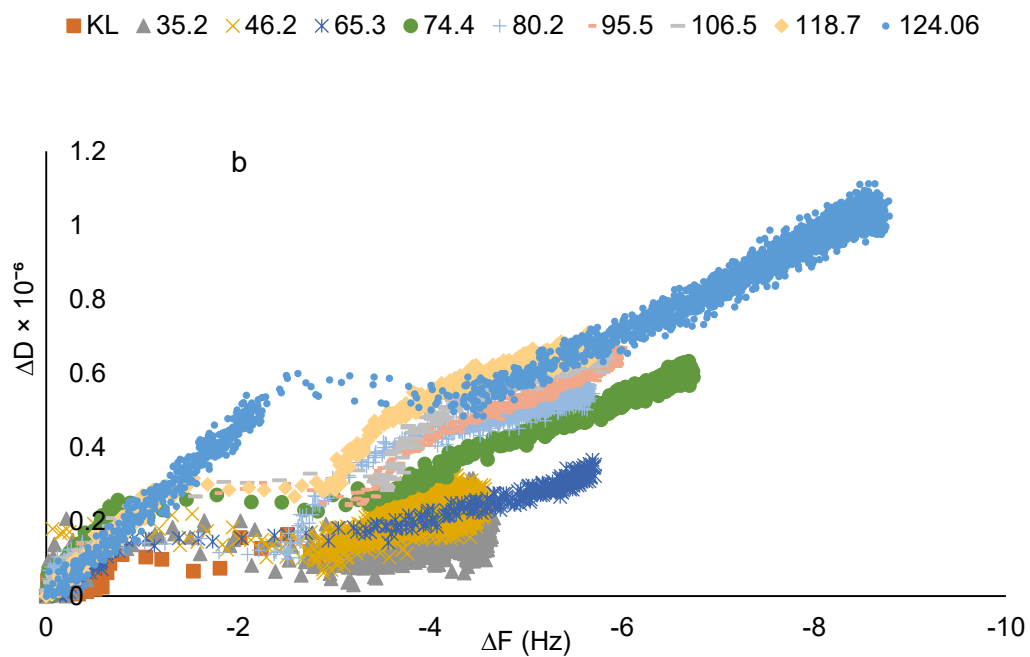
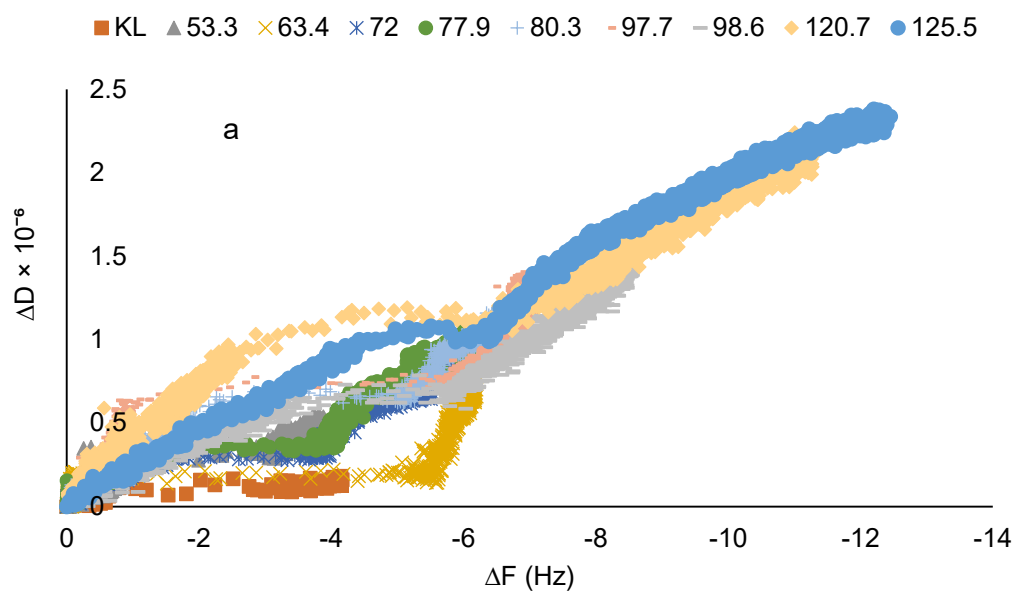


Figure A. 9 Dissipation change of the sensors as a function of frequency changes upon adsorption of a) KL-METAM and b) KL-ATAC on the SiO₂ surface at different grafting ratio.

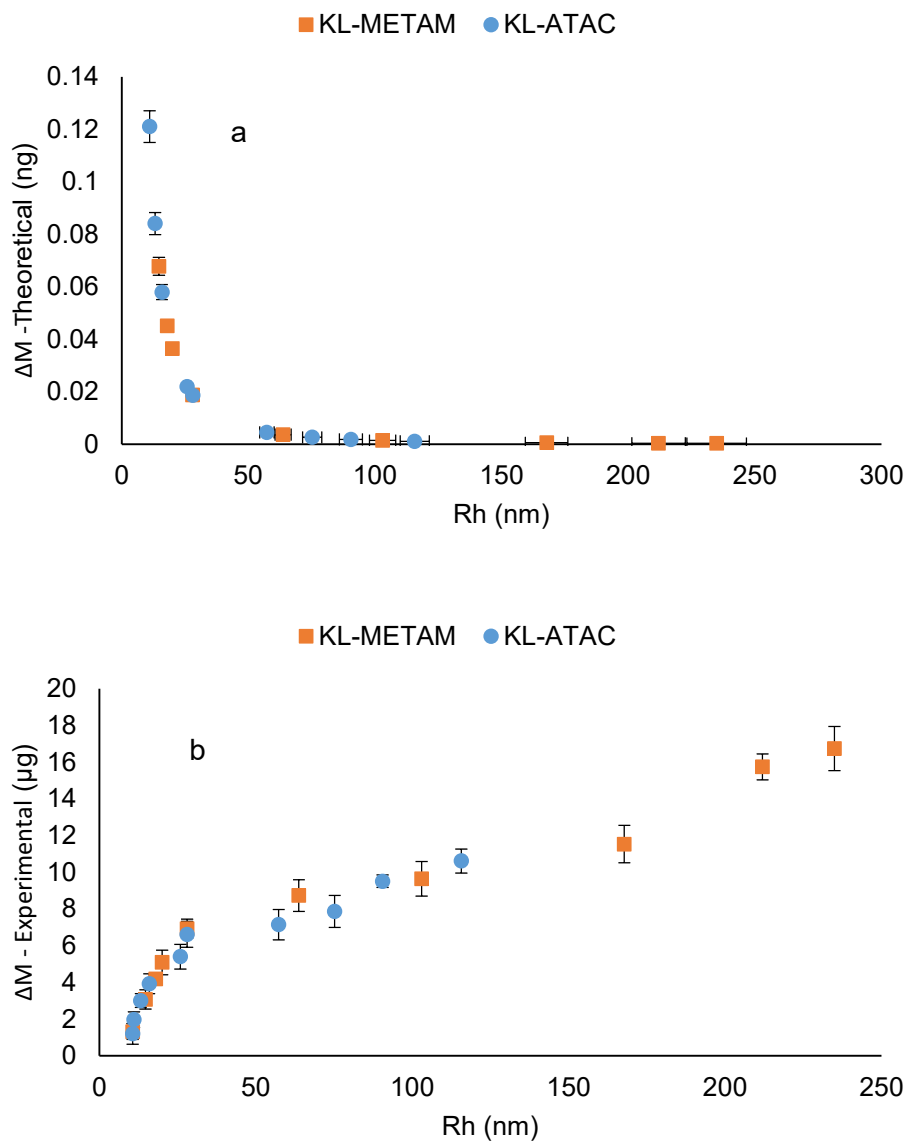


Figure A. 10 (a) Theoretical adsorbed mass required for developing a monolayer CKL coverage on QCM surface. (b) Experimental adsorbed mass of CKL on the SiO₂ surface.

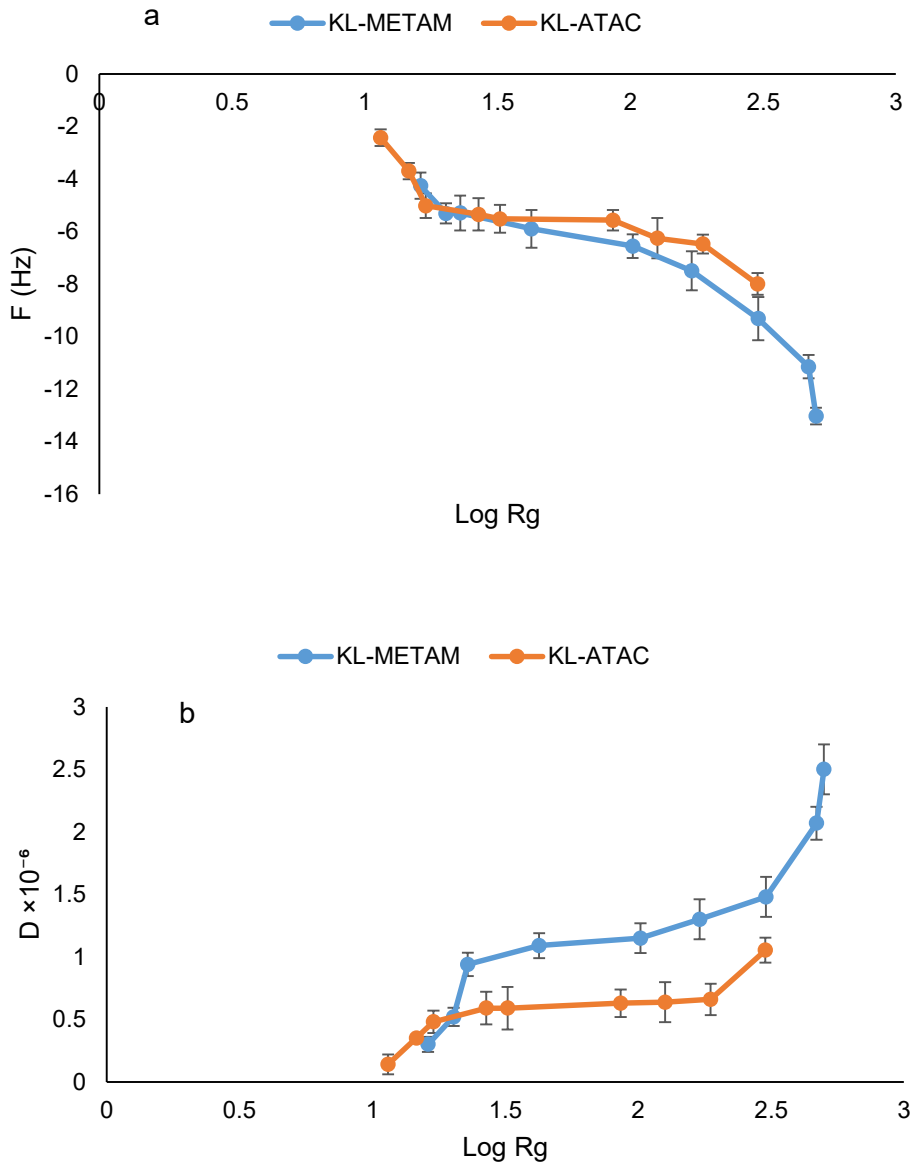


Figure A. 11 Changes in a) frequency and b) dissipation of the SiO₂ sensor for the adsorption of CKLs

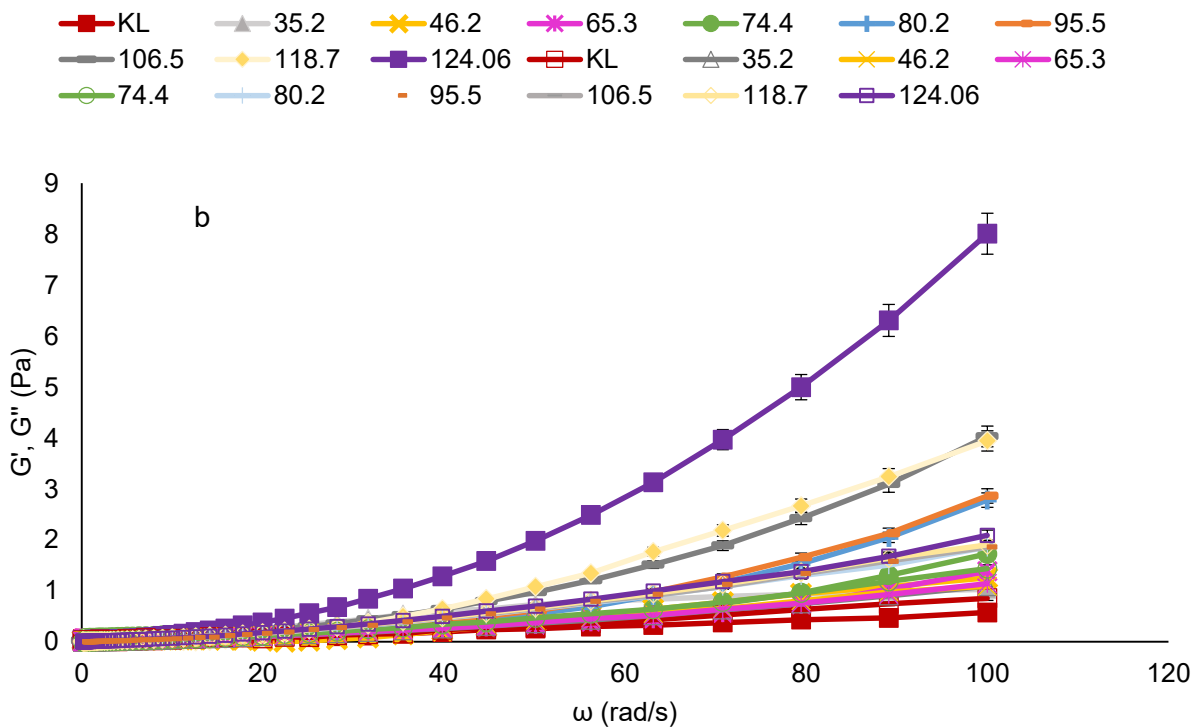
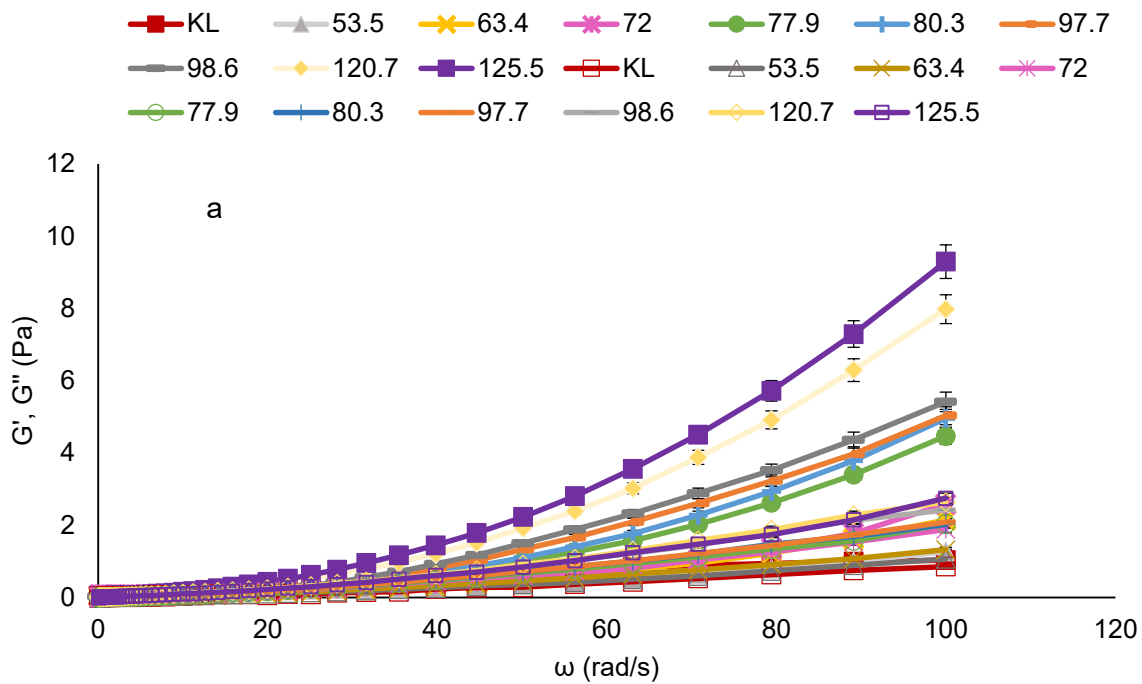


Figure A. 12 Storage and loss modulus of a) KL-METAM and b) KL-ATAC at different grafting ratio and 25 °C as a function of frequency (The G' and G'' are respectively represented as solid and open symbols)

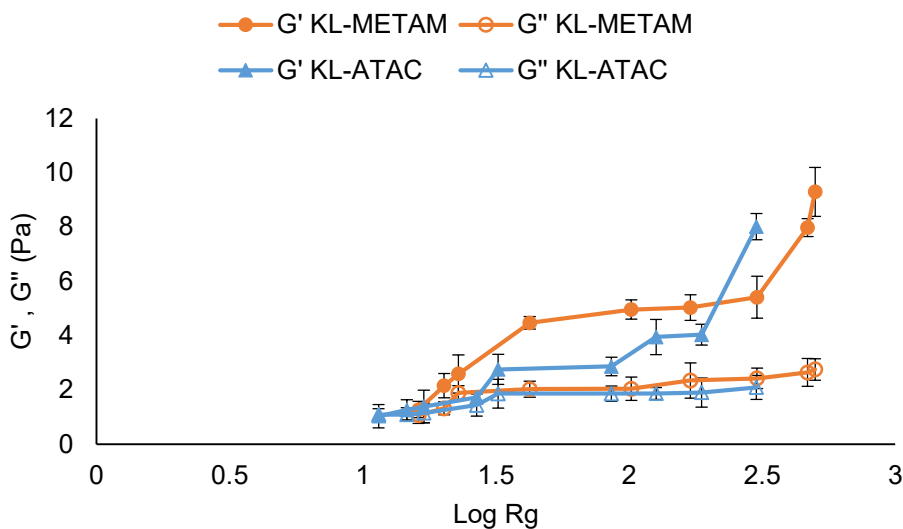


Figure A. 13 Semi log plot of storage (G') and loss modulus (G'') of CKLs at 25 °C as a function of radius of gyration.

HL characterization

Table A3 summarizes the results of quantitative ^{31}P NMR analysis and Figure A32 presents the ^{31}P NMR spectra of the samples. The concentration of OH groups was estimated based on the hydroxyl content of the cyclohexanol (internal standard) and its integrated peak area.¹⁷ Of the various hydroxy groups, aliphatic hydroxy group had the most influential signal as depicted in Figure A32 (4.13 mmol/g). A small amount of phenolic OH group (*i.e.*, 0.95 mmol/g) was observed in HL, which was very similar to the lignin of woody biomass with the following order: aliphatic OH > phenolic OH > carboxylic OH.¹⁸⁻²⁰ The lignin source was hardwood and ^{31}P NMR data (Table 1) illustrated that syringyl units (0.66 mmol/g) was more pronounced than guaiacyl units (0.27 mmol/g). However, *p*-hydroxyphenyl units was not detectable. Similar trends were also observed elsewhere.^{21,22} The minimum amount of OH group was originated from 5-5' phenolic OH and carboxylate group.

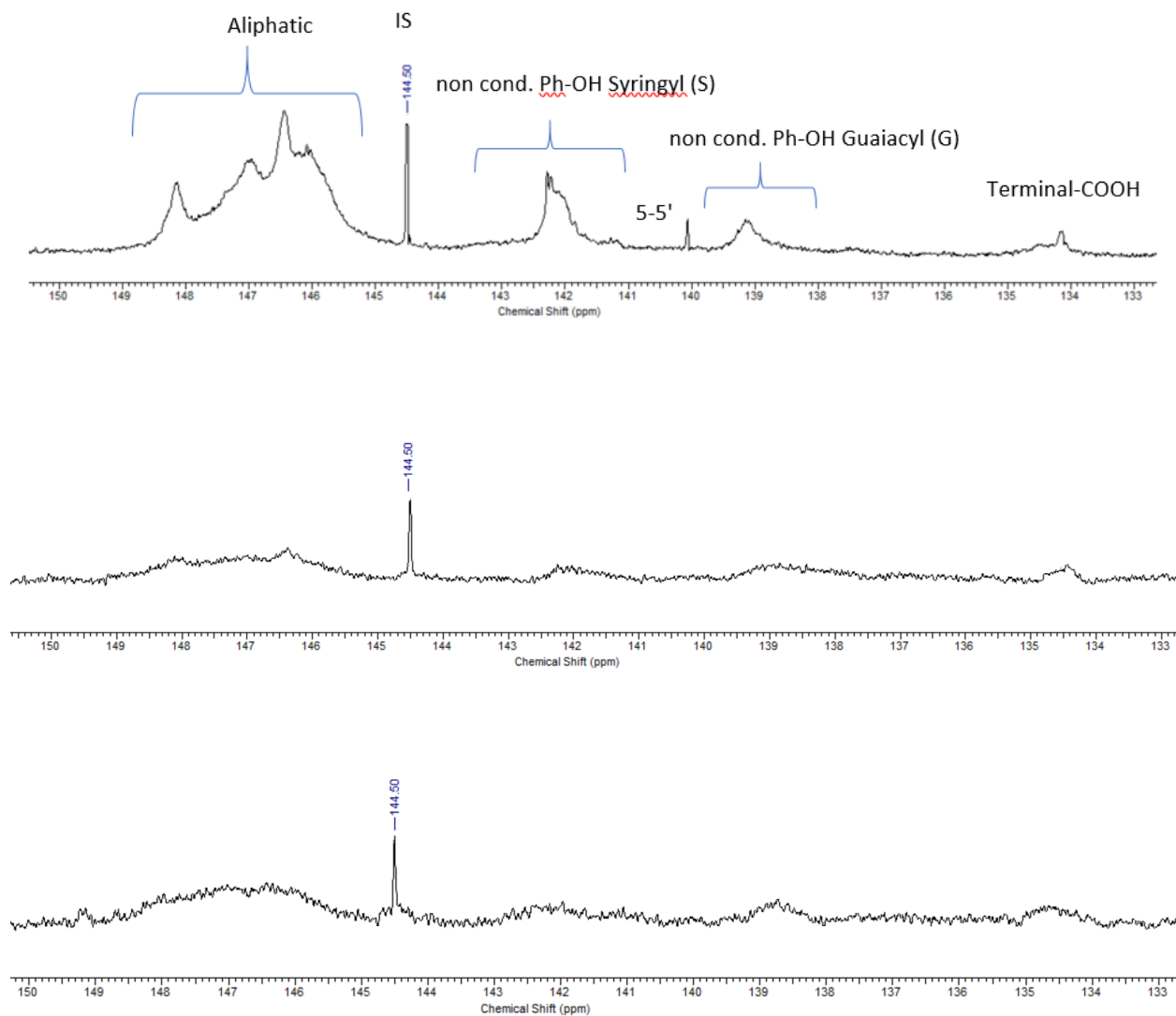


Figure A. ^{31}P -NMR spectrum of a) HL, b) HL-METAC and c) HL-MAPTAC

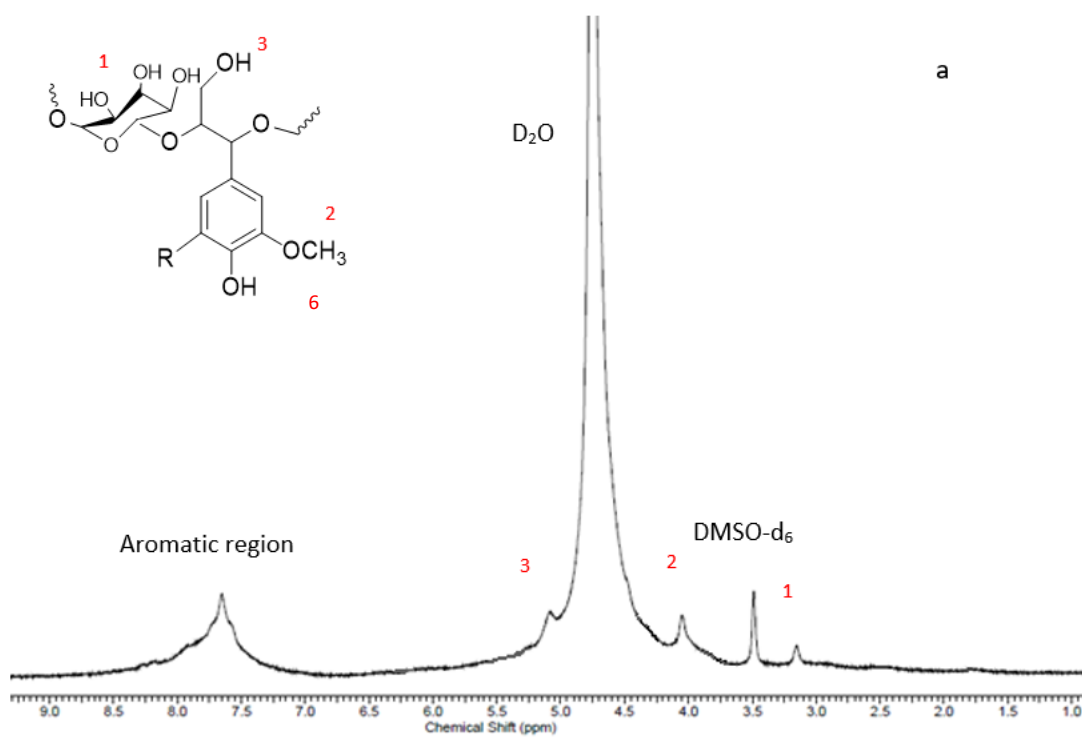
Table A. 3 Hydroxy group contents of HL and CHLs determined by ^{31}P NMR analysis

Sample	Phenolic OH, mmol/g				
	Aliphatic OH, mmol/g	Syringyl	Guaiacyl	5-5'	COOH mmol/g
HL	4.13	0.66	0.27	0.02	0.17

HL-	1.81	0.4	0.25	0	0.15
METAC					
HL-	1.38	0.24	0.22	0	0.15
MAPTAC					

¹H NMR analysis

The structures of unmodified and cationic hydrolysis lignin polymers were analyzed with ¹H NMR. The samples (30 mg) were dissolved in 500 μL D₂O and DMSO-d₆ under stirring overnight and ¹H-NMR spectra of samples were recorded using INOVA-500 MHz instrument (Varian, USA) with a 45° pulse, 64 number of scans and a 1 s relaxation delay time.



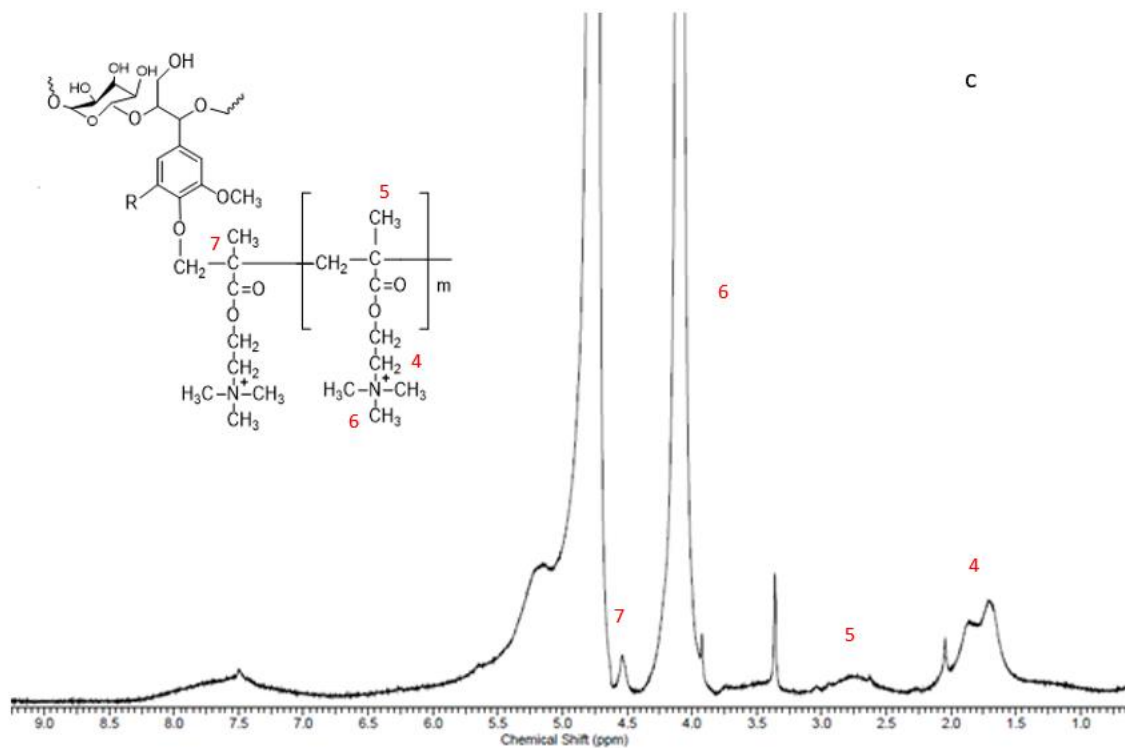
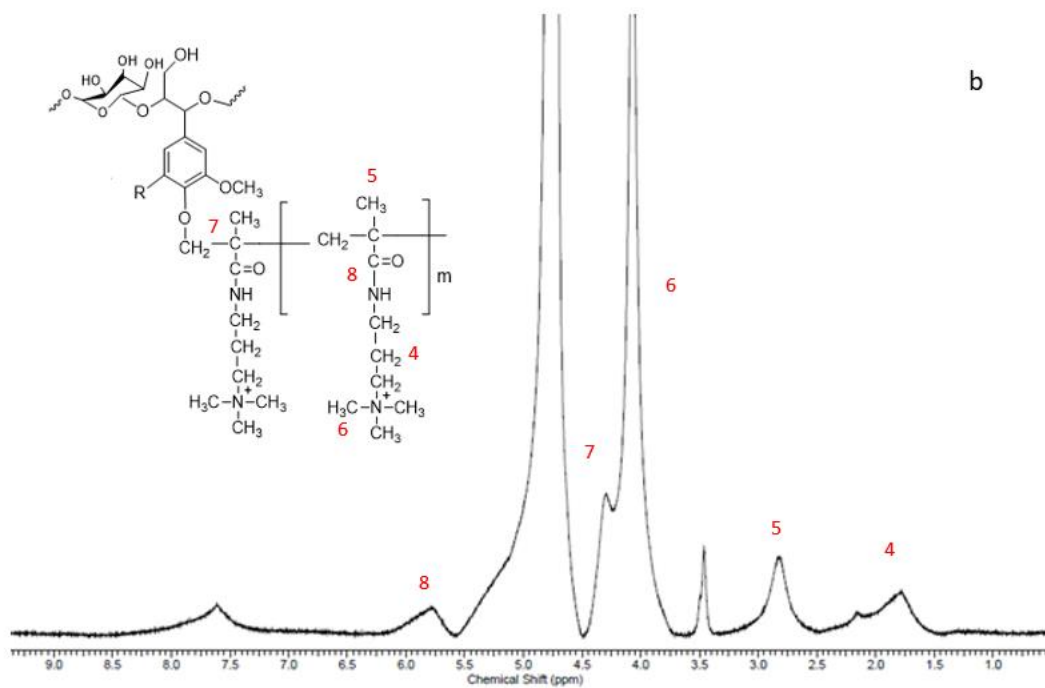


Figure A. 15 ^1H NMR spectra of a) HL, b) HL-MAPTAC, and c) HL-METAC.

FTIR analysis

The Fourier transformed infrared (FTIR) spectra of HL and CHL polymers was used in analyzing their structures in the transmittance mode in the range of 600 and 4000 cm^{-1} . Approximately, 0.05 g of dried sample was used for this analysis using a Bruker Tensor 37 (Germany, ATR accessory) FTIR instrument. The resolution was set at 4 cm^{-1} and each spectrum was recorded with 32 scans.

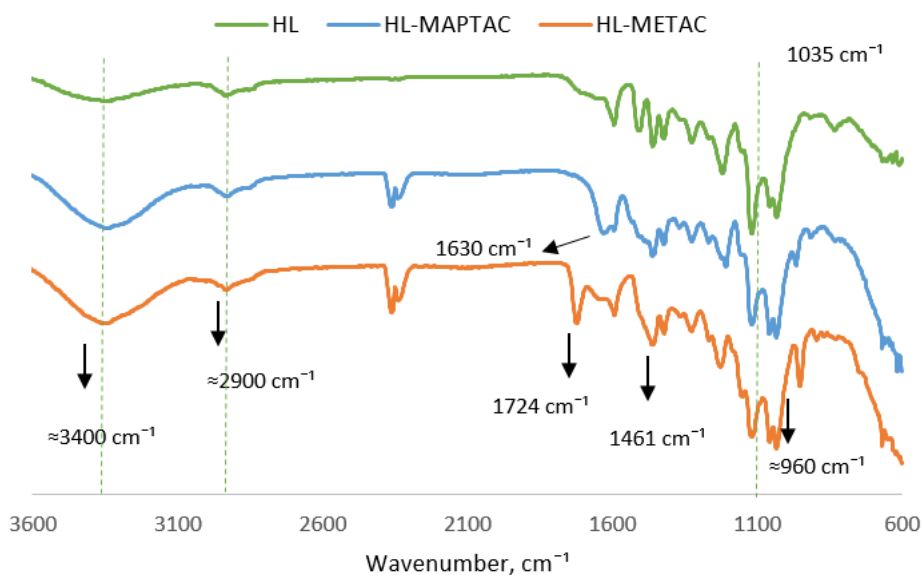


Figure A. 16 FTIR spectra of HL and CHL.

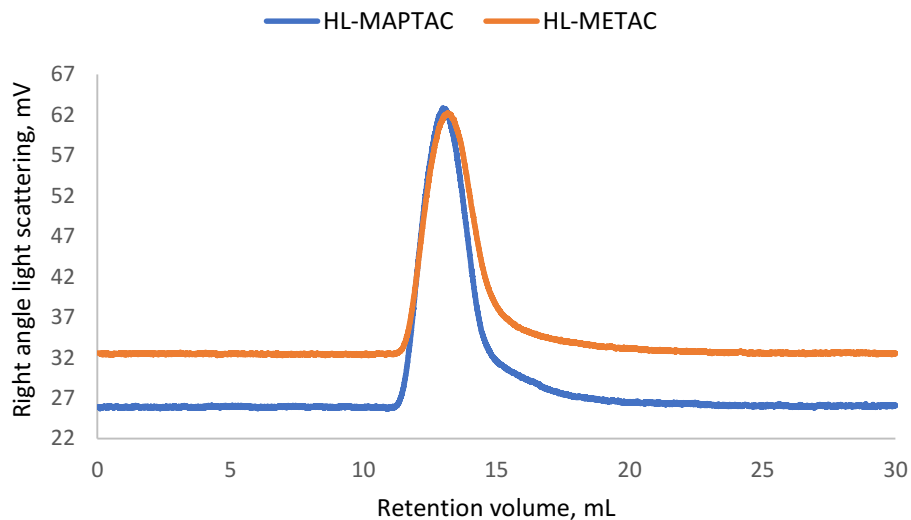


Figure A. 17 GPC traces for HL-MAPTAC and HL-METAC

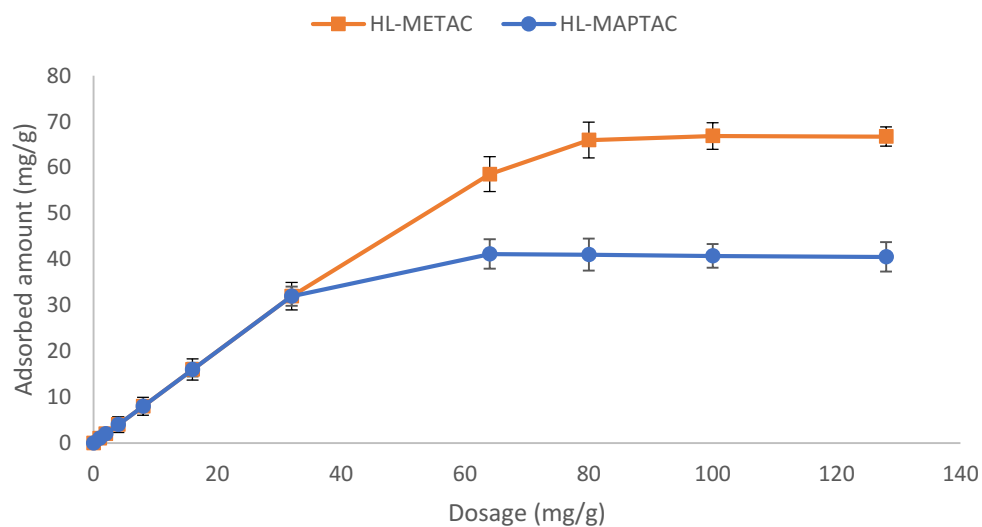


Figure A. 18 Adsorption of CHLs on kaolin particles as a function of polymer dosage under the conditions of pH 6, 25 °C and 25 g/L of kaolin concentration.

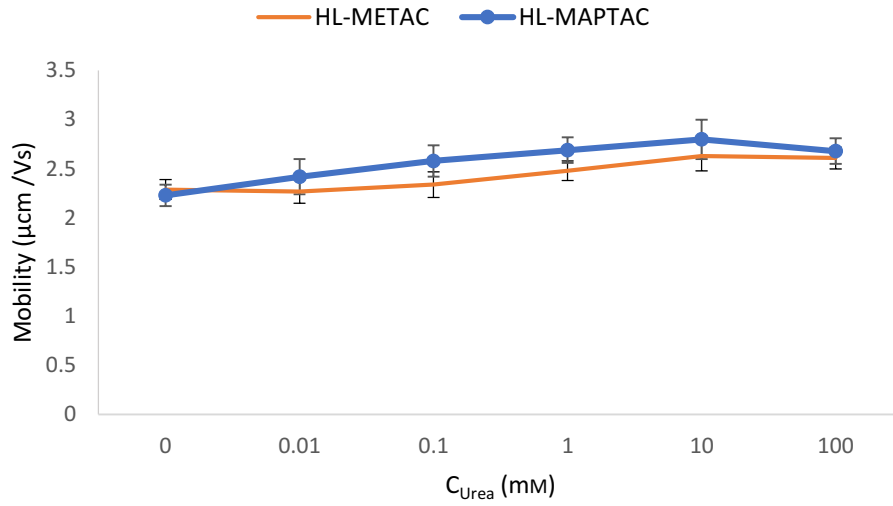


Figure A. 19 Effect of urea addition on the electrophoretic mobility of CHLs conducted under the conditions of pH 6, 25 °C and 25 g/L of kaolin concentration.

Table A. 4 Flocculation efficiency of kaolin particles in the HL-METAC, HL-MAPTAC/kaolin system (The flocculation efficiency was taken from Figure 2, $\alpha = 1/W$)²³

Polymer	Dosages	Flocculation efficiency (α)
HL-METAC	0.2	0.4
	0.4	0.72
	0.6	0.95
	1.2	1
HL-MAPTAC	0.2	0.36
	0.4	0.71
	0.6	0.85
	1.2	0.91

Relative turbidity analysis using Photometric dispersion analyser (PDA)

A variation in the direct current (DC) voltage of the PDA instrument expresses the flocculation behaviour of kaolin particles through changing the relative turbidity of the suspension. In this set of experiments, the addition of kaolin suspension (20 mL) to the photocell of PDA containing 480 mL water decreased the initial base DC voltage (V_0) to a new DC voltage (V_i). After 100 s, varying dosages of CHLs were added to the cell to induce flocculation. This caused an increment in the DC voltage (V_f) of the final dispersion. The relative turbidity of the system τ_r was measured using Eq. (S1):²⁴

$$\text{Relative turbidity, } \tau_r = \frac{\tau_f}{\tau_i} = \frac{\ln(V_0/V_f)}{\ln(V_0/V_i)}$$

Where τ_f and τ_i are the final and initial suspension turbidity, respectively.

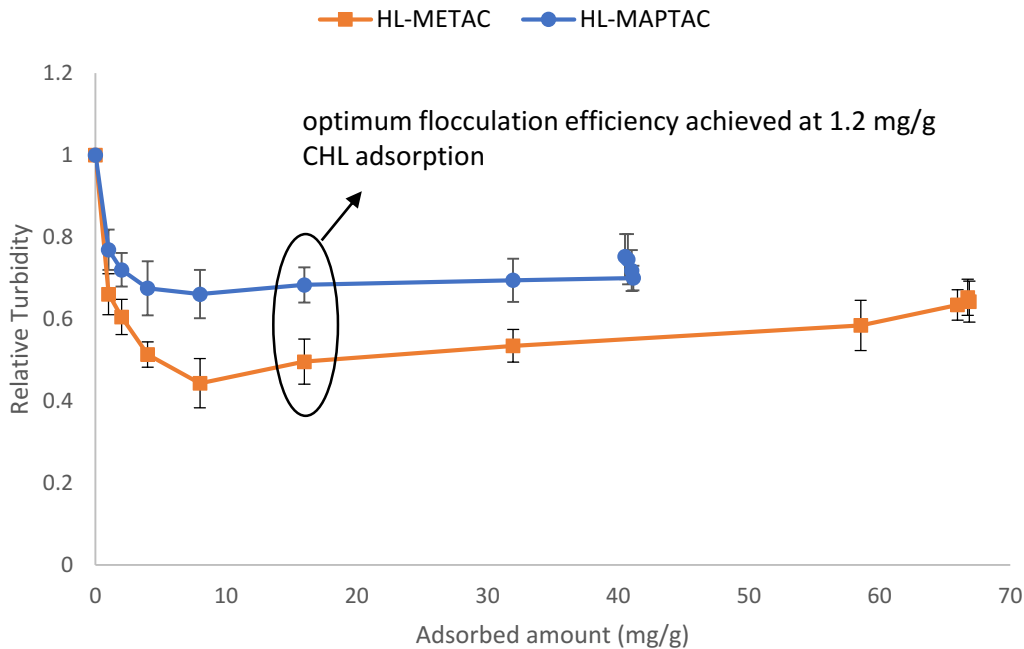


Figure A. 20 Effect of CHLs adsorption on the relative turbidity of kaolin suspension conducted under the condition of pH 6, 25 °C and 25 g/L of kaolin concentration.

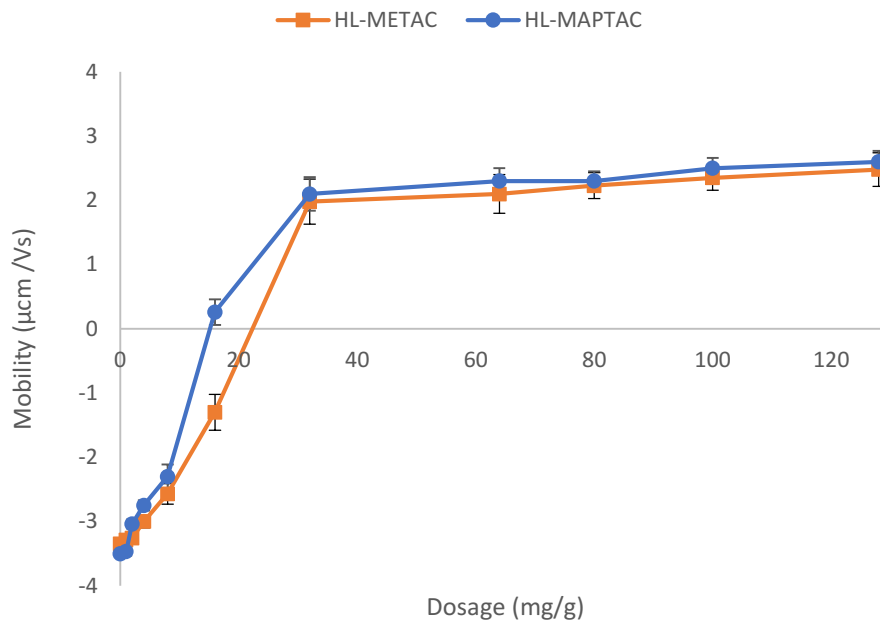


Figure A. 21 Electrophoretic mobilities of kaolin particles with CHLs in aqueous suspensions conducted under the conditions of pH 6, 25 °C and 25 g/L of kaolin concentration.

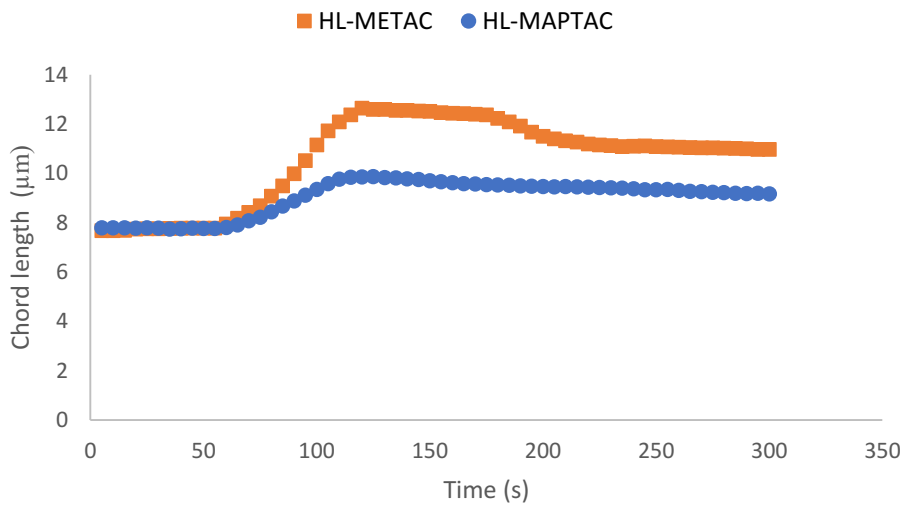


Figure A. 22 Evolution of flocculation process using different CHLs conducted under the conditions of pH 6, 25 °C and 25 g/L of kaolin concentration.

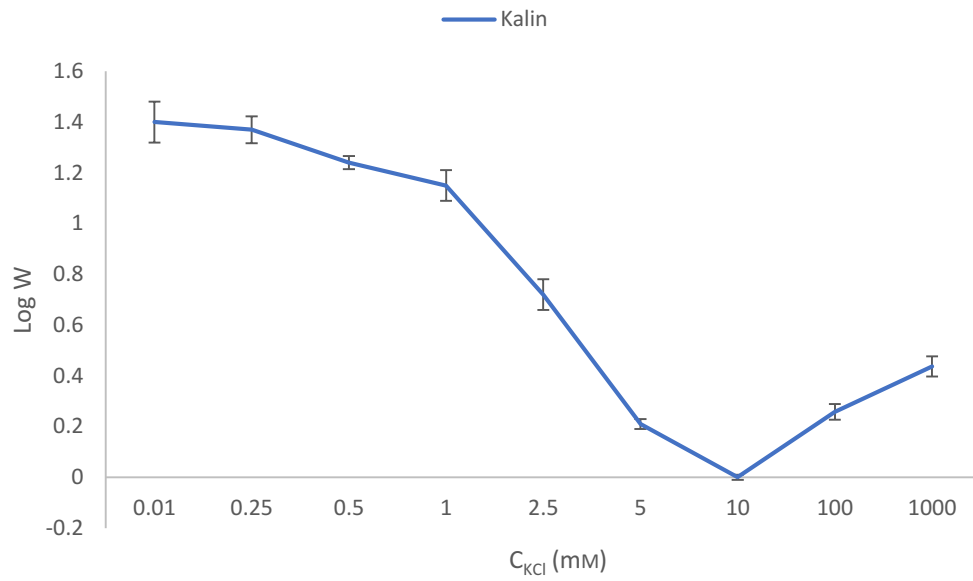
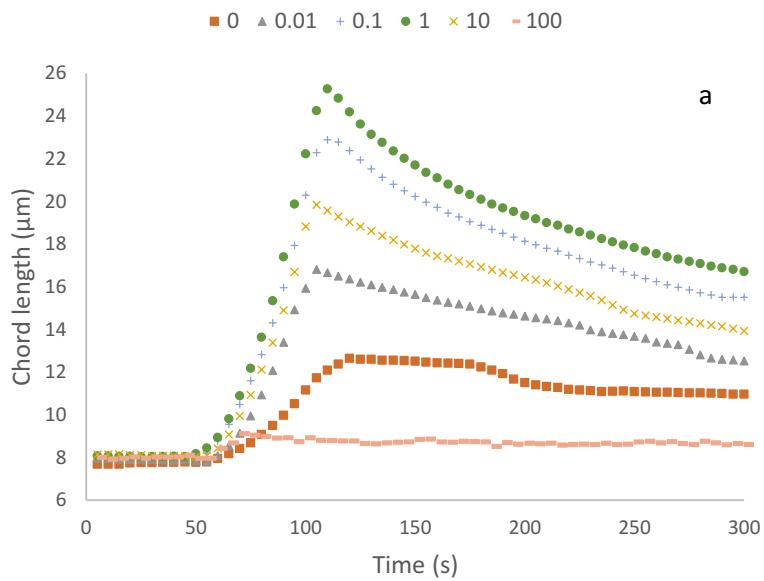
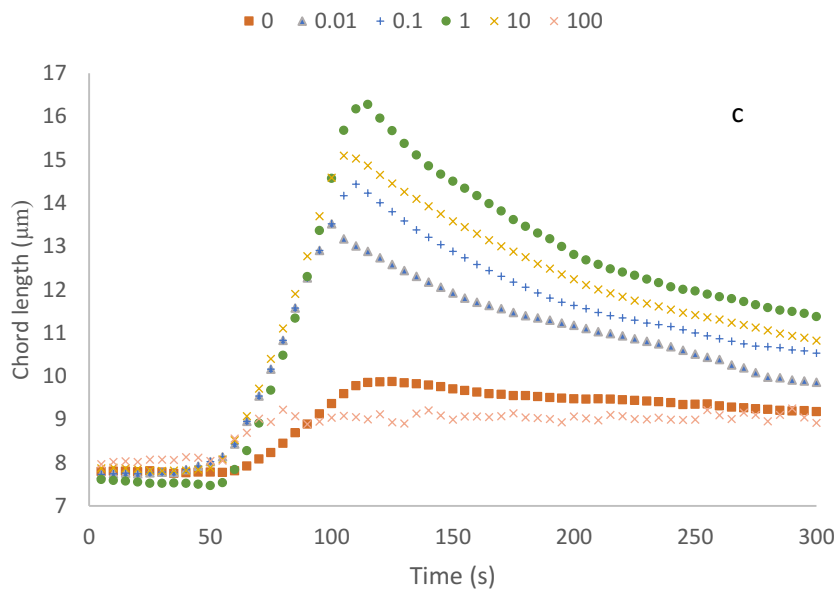
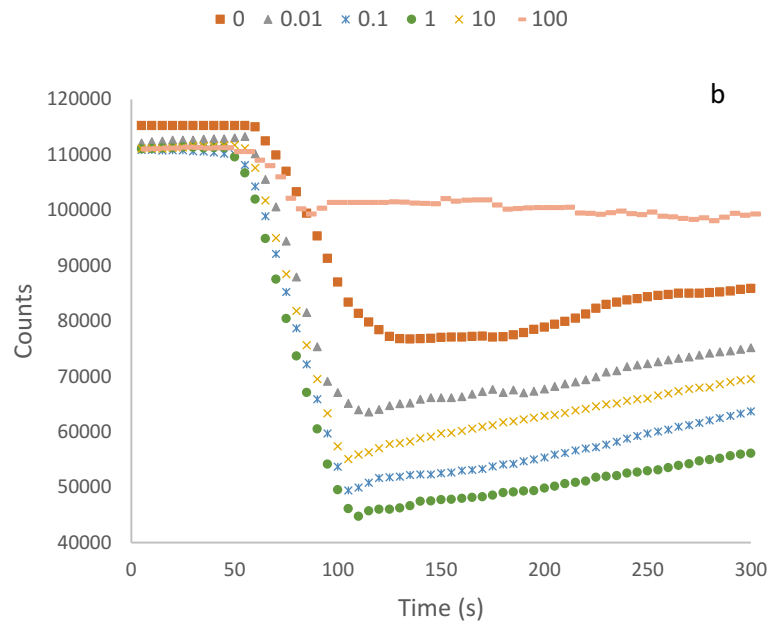


Figure A. 23 Stability ratio W of kaolin particles in the presence of salt conducted under the conditions of pH 6, 25 °C and 25 g/L of kaolin concentration.





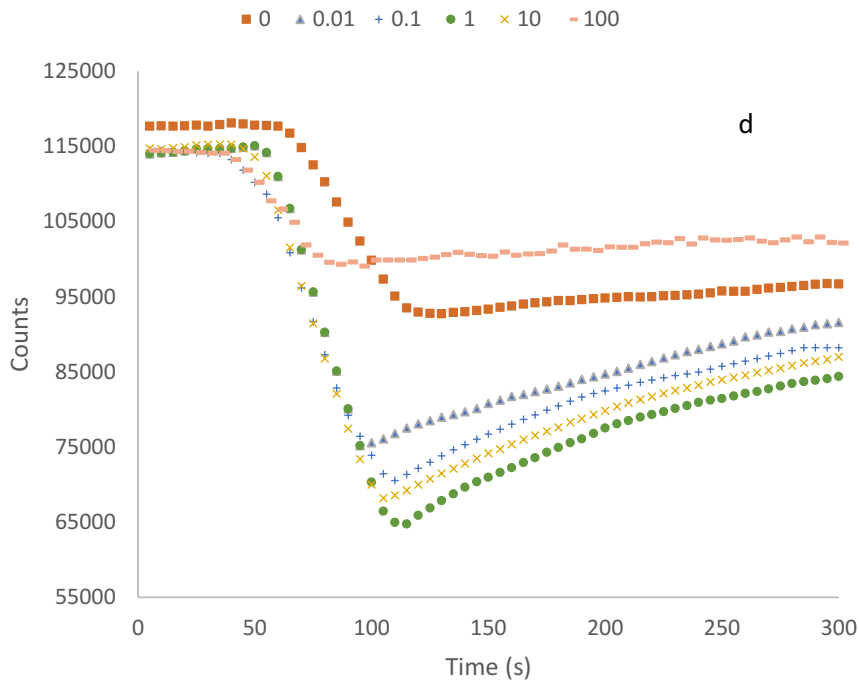


Figure A. 24 Influence of KCl concentration (0-100 mM) on the mean chord length and number of counts of the a,b) HL-METAC and c,d) HL-MAPTAC samples as a function of time (pH 6, 25 °C and 25 g/L of kaolin concentration).

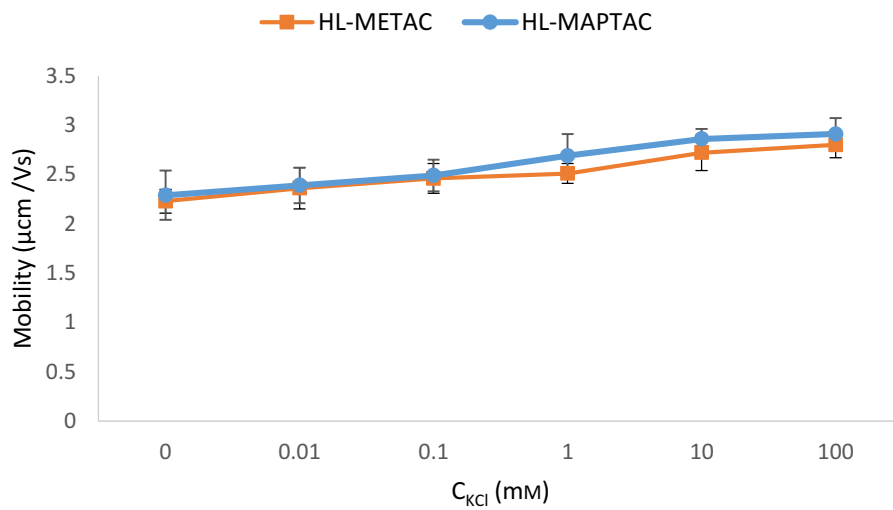


Figure A. 25 Effect of salt addition on the electrophoretic mobility of CHLs conducted under the conditions of pH 6, 25 °C and 25 g/L of kaolin concentration.

Cationic lignin polymerization

In this set of experiments, lignin was polymerized with a cationic monomer, [2-(Methacryloyloxy)ethyl] trimethylammonium methyl sulfate (METAM), in a semidry fashion (i.e., 60 wt % solid content). A 2 g sample of lignin was mixed with 4 g of water and cationic monomer (1.8 mol/mol METAM/lignin). Then, the pH of the lignin solution was adjusted to 3.6 ± 0.1 , and the polymerization reaction was carried out for 3 h at 80 °C.²⁵ After completion, the reaction mixture was cooled to room temperature and kraft lignin-METAM polymer (KL-METAM) was precipitated from the reaction medium using ethanol (80 vol % in water). Further purification of KL-METAM precipitate was conducted via membrane dialysis for 48 h to remove any unreacted METAM monomer and other impurities (salt). The final product was then extracted from dialysis tubes and dried with a freeze drier.

Anionic lignin polymerization

The polymerization reaction of lignin and acrylic acid (AA) was conducted in a nitrogen atmosphere. A 2.0 g sample of KL was dissolved in 50 mL of water and AA (10 mol/mol of AA/KL). After pH adjustment (pH = 3), a predetermined amount of potassium persulfate (1.5 wt.% based on the mass of lignin) was added to the mixture to initiate the polymerization reaction. The polymerization reaction of KL and AA reaction was conducted at 80 °C for 3 h in a nitrogen environment.²⁶ After reaction termination, the pH of the reaction solution was adjusted to 1.5 to precipitate the KL-AA from the reaction medium. The suspension was then centrifuged at 3500 rpm for 10 min to collect the anionic polymers and remove homopolymers. The samples were

further purified using a dialysis membrane for 48 h and dried at 60 °C, and the purified KL-AA was collected.

Molecular weight analysis

The molecular weight of lignin polymers was determined by a gel permeation chromatography (GPC) (Malvern, GPCmax VE2001 Module + Viscotek TDA305), which was equipped with a multi-detector unit using polyethylene oxide polymers as standard samples. NaNO₃ solution (0.1 mol/L) was used as a solvent and eluent in this analysis; the flow rate and column temperature were adjusted to 0.70 mL/min and 35 °C, respectively. To measure the molecular weight of the cationic sample, PolyAnalytic PAA206 and PAA203 columns were used. The cationic sample was dissolved in acetic acid solution (10 wt.%) and filtered using a 0.2 µm pore diameter nylon filter (13 mm diameter). However, the anionic sample (KL-AA) was dissolved in 10 mL of 0.1 mol/L NaNO₃ solutions. The columns of PAS106M, PAS103, and PAS102.5 were used in this analysis. The molecular weight of the polymers was determined using the refractive index detector of the GPC instrument.

Functional group analysis

The phenolic hydroxyl and carboxylate groups of KL, KL-METAM, and KL-AA were determined using an automatic potentiometric titrator, 785 Titrino. In this analysis, 0.06 g of lignin samples were dissolved in 1 mL of KOH (0.8 M) and then 4 mL of para-hydroxybenzoic acid (0.5 wt %) was added as an internal standard. Afterward, 100 mL of deionized water was added to the system and mixed for 2 h. The solutions were then titrated against 0.1 M HCl standard solution.²⁷ The grafting ratio of KL-AA was calculated based on its carboxylate group content according to the procedure described by Bayazeed and coworkers.²⁸

Elemental analysis

The elemental analysis of KL, KL-AA, and KL-METAM was performed using an Elementar Vario EL Cube elemental analyzer following the procedure described in the literature.²⁹ Approximately, 2 mg of oven-dried (at 105°C) samples were combusted at 1200 °C to reduce the generated gasses for determining carbon, hydrogen, and nitrogen contents of the samples. The oxygen content of the samples was determined based on mass balance. The grafting ratio of METAM to lignin in KL-METAM was correlated with the nitrogen content of lignin macromolecule according to equation 1:

$$\text{Grafting ratio (mol\%)} = \frac{\frac{N}{14} \times Mw}{100 - (\frac{N}{14} \times Mw)} \times 100 \quad (1)$$

Where N and Mw are the nitrogen content of KL-METAM polymers (wt.%) and the molecular weight of METAM monomer (173 g/mol), respectively.

Charge density analysis

The charge density of KL-METAM and KL-AA was determined using a Particle Charge Detector, Mütek PCD 04 titrator (Arzbergerstrae, Herrsching, Germany) via titrating against PDADMAC and PVSK (0.005 M) solutions, respectively.

The nitrogen content of KL-METAM can help calculate the theoretical charge density of macromolecule, assuming 1 mol of quaternary ammonium groups grafted onto lignin core has 1.0 meq charge density [2,6].^{26,30} Accordingly, the theoretical charge density of KL-METAM was 2.48 meq/g, which was close to the experimental value. The phenolic group content of lignin was

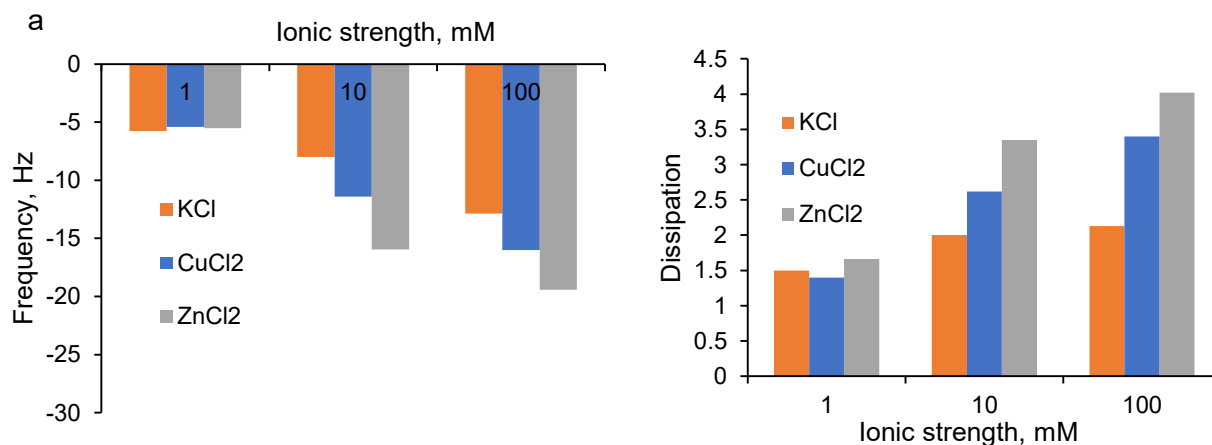
reduced from 1.63 to 0.57 mmol/g illustrating that the phenolic group of lignin was involved in the reaction with METAM.

Adsorption analysis using QCM

Briefly, the QCM-D technique monitors the simultaneous changes of the resonance frequency, f , caused by adsorption/desorption of polymer on the solid surfaces over time. The instrument monitors the changes of adsorbed mass related to frequency changes, according to equation 2:³¹

$$\Delta m = \frac{C}{n\Delta f} \quad (2)$$

where m is the adsorbed mass per unit surface, C is the mass sensitivity constant of the sensor and n is the frequency overtone number. This equation applies to the adsorbing thin films with limited viscoelastic coupling from the surrounding medium.³² However, Voigt viscoelastic model is applied to model soft and thick polymer in Q-Tools software, Q-sense, Gothenborg, Sweden.³³



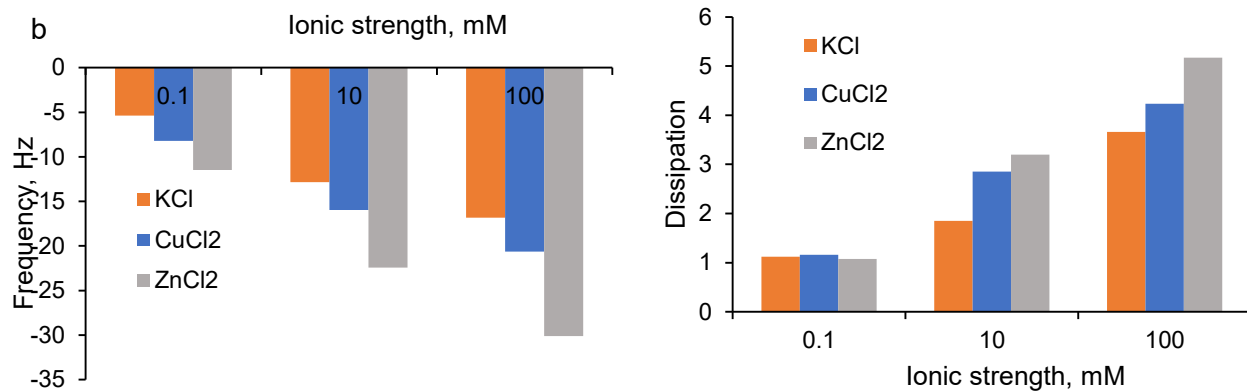


Figure A. 26 The changes in frequency and dissipation a result of model waste adsorption on a) KL-METAM and b) KL-AA coated sensor at different concentrations (1, 10 and 100 mM).

XPS analysis

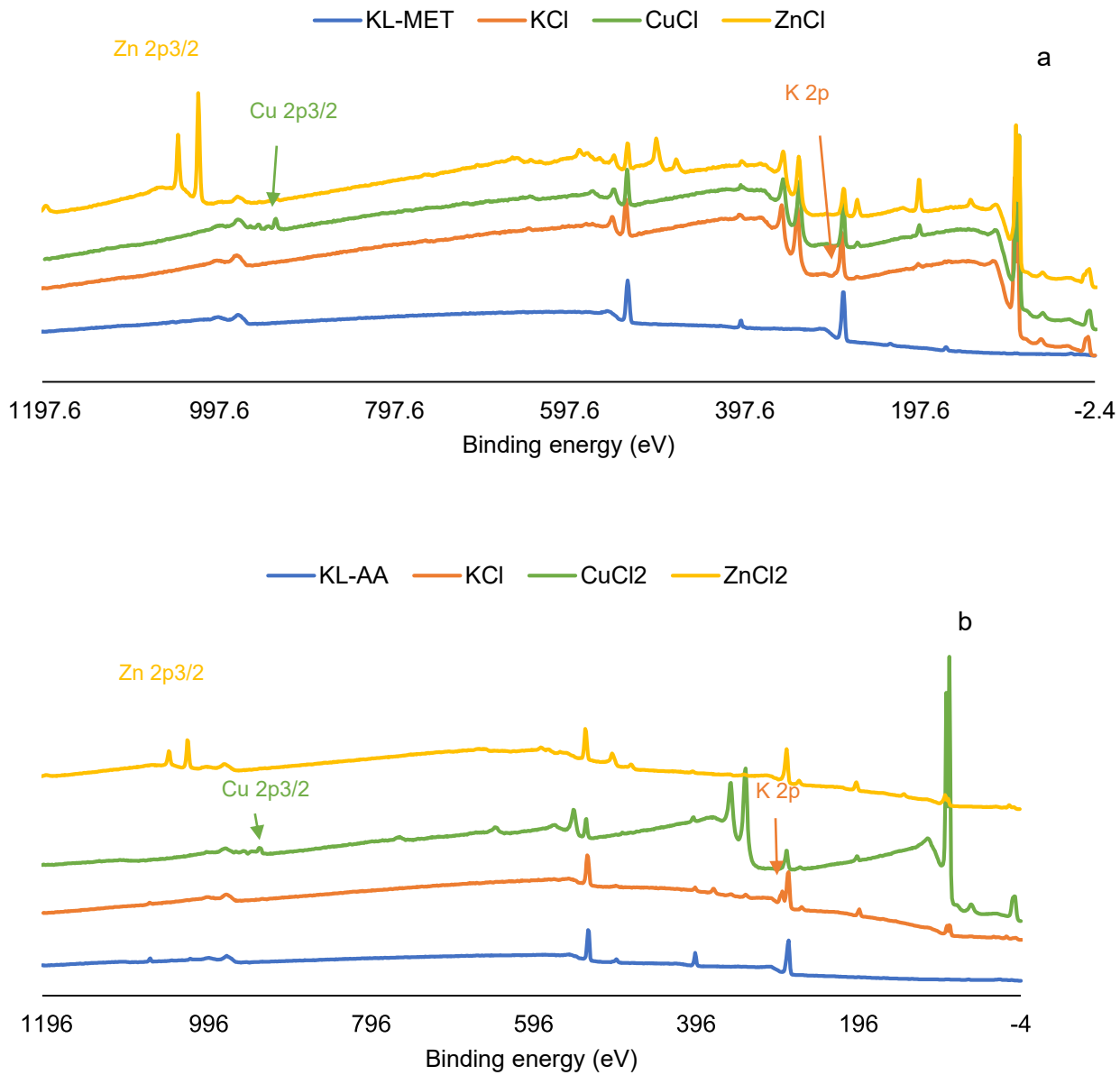
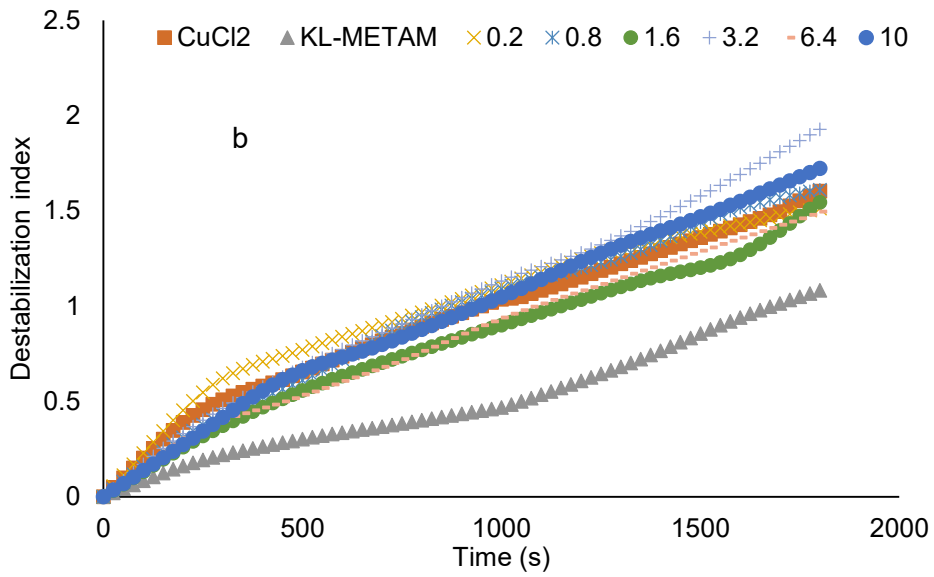
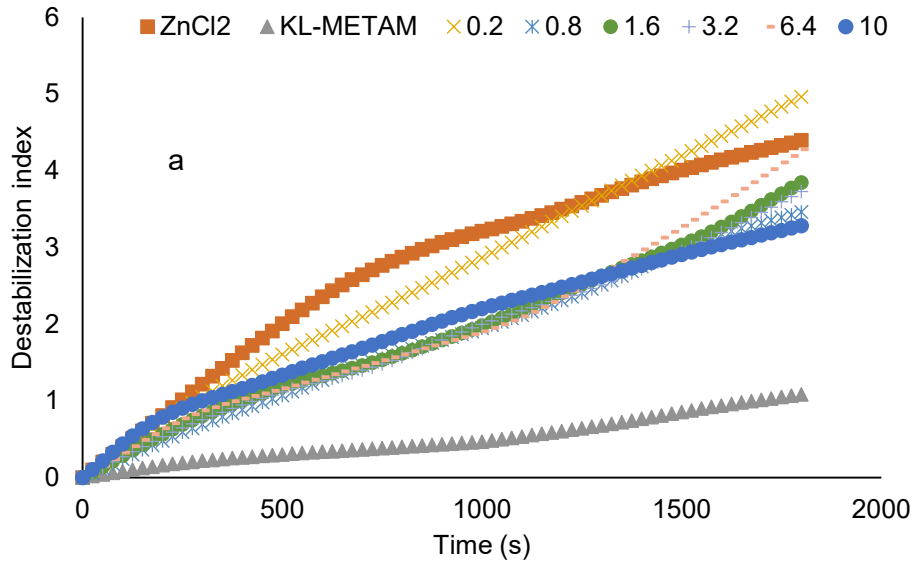


Figure A. 27 XPS survey spectra of a) KL-METAM and b) KL-AA



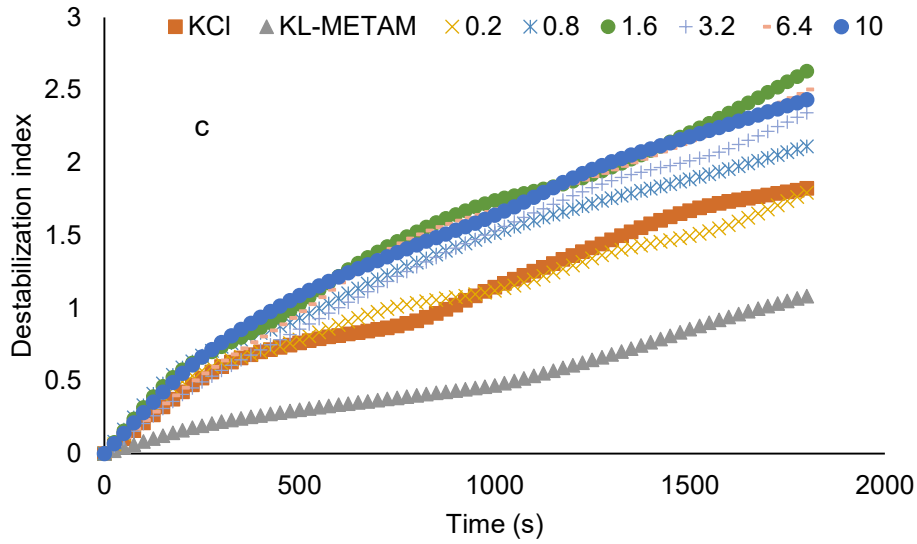
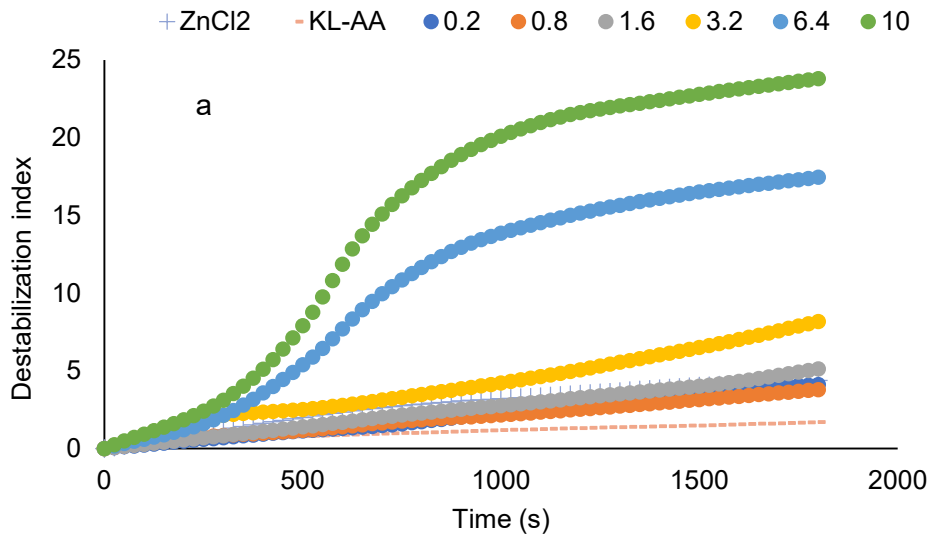


Figure A. 28 The effect of KL-METAM dosage (0-10 mg/L) on destabilization index of model wastewater a) ZnCl₂, b) CuCl₂, and c) KCl, (wastewater concentration 10mM, polymer concentration 10 g/L, 30 °C, 30min)



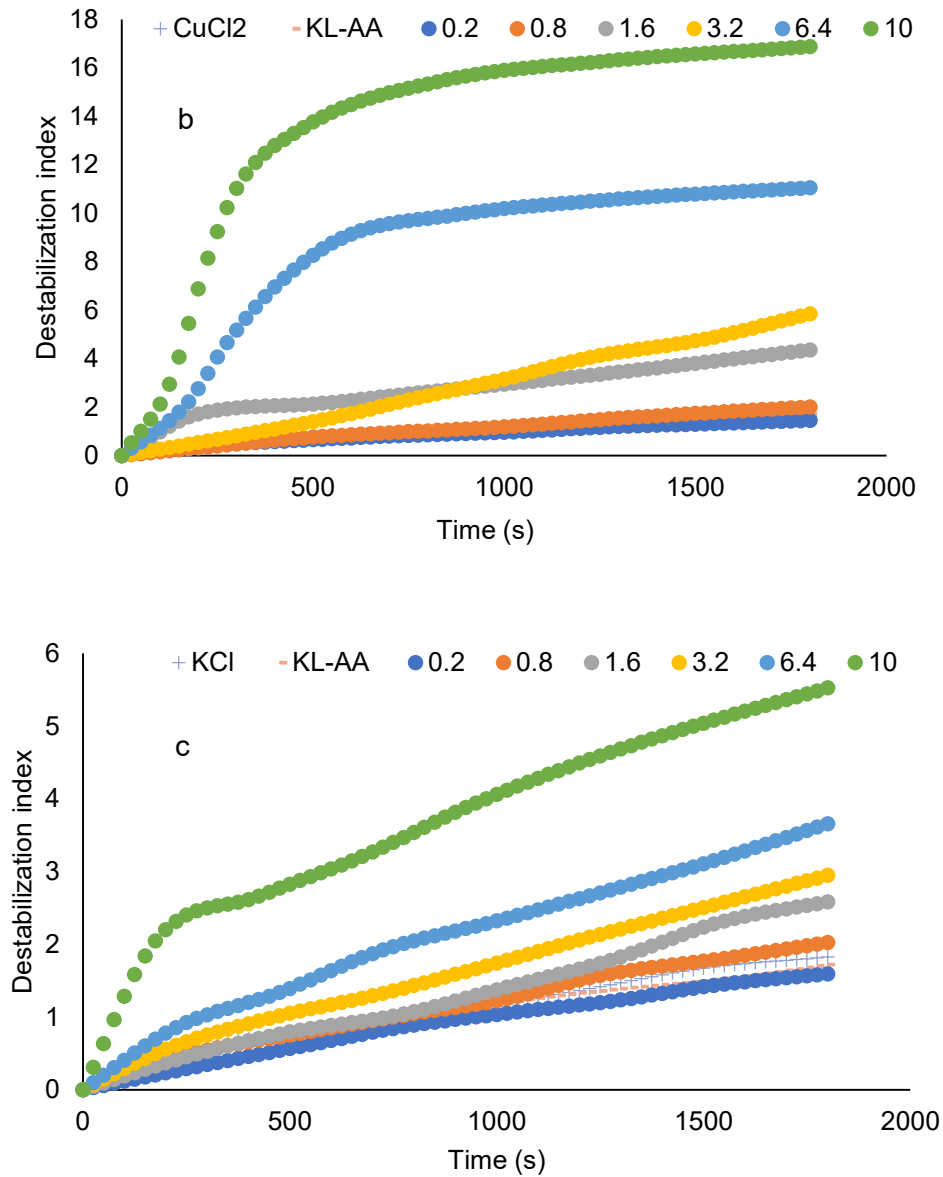
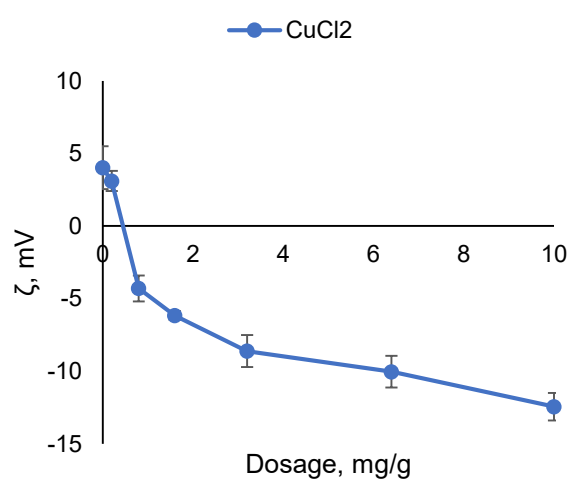
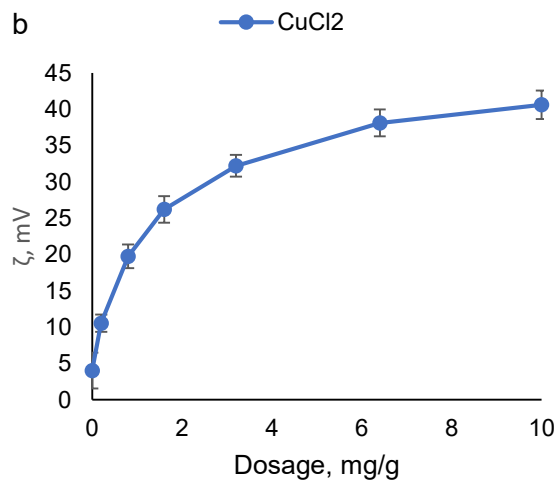
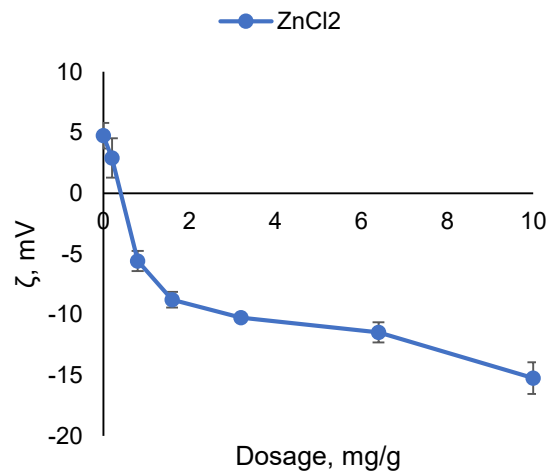
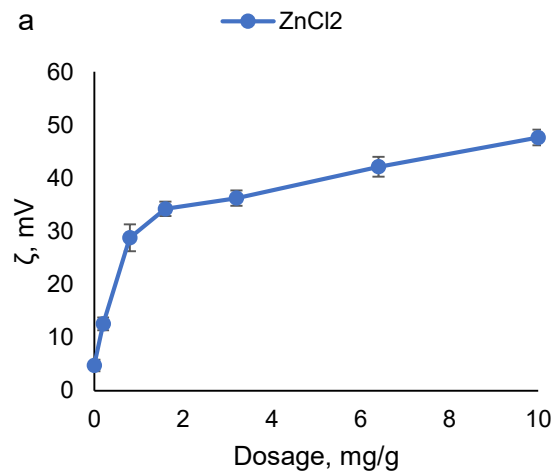


Figure A. 29 The effect of KL-AA dosage (0-10 mg/L) on destabilization index of model wastewater a) ZnCl₂, b) CuCl₂, c) and KCl (wastewater concentration 10mM, polymer concentration 10 g/L, 30 °C, 30min)

Zeta potential analysis



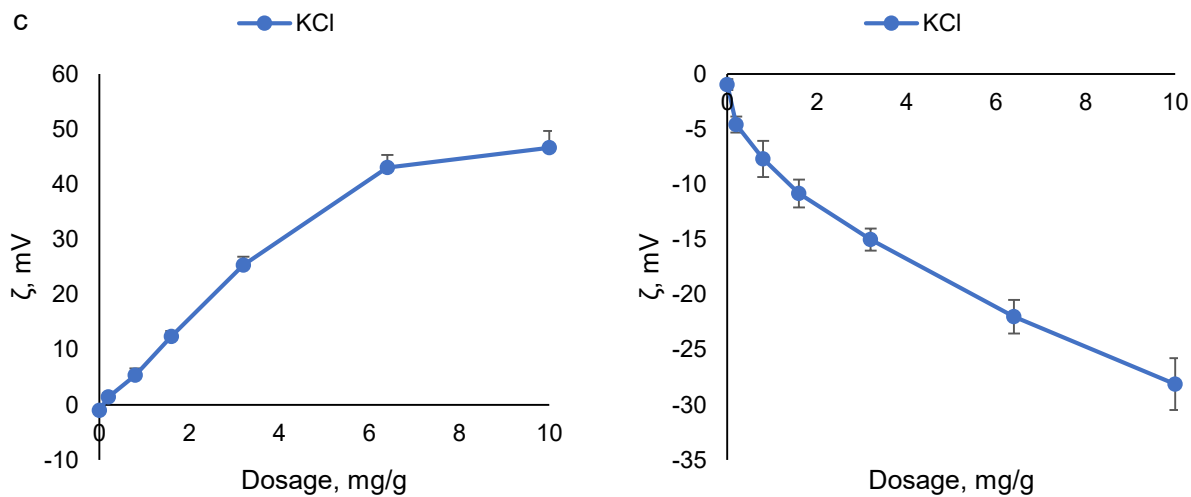


Figure A. 30 Zeta potential changes of adsorbed KL-METAM and KL-AA on a) ZnCl₂, b) CuCl₂, and c) KCl (wastewater concentration 10mM, 25 °C)

Stability analysis in a mixed system

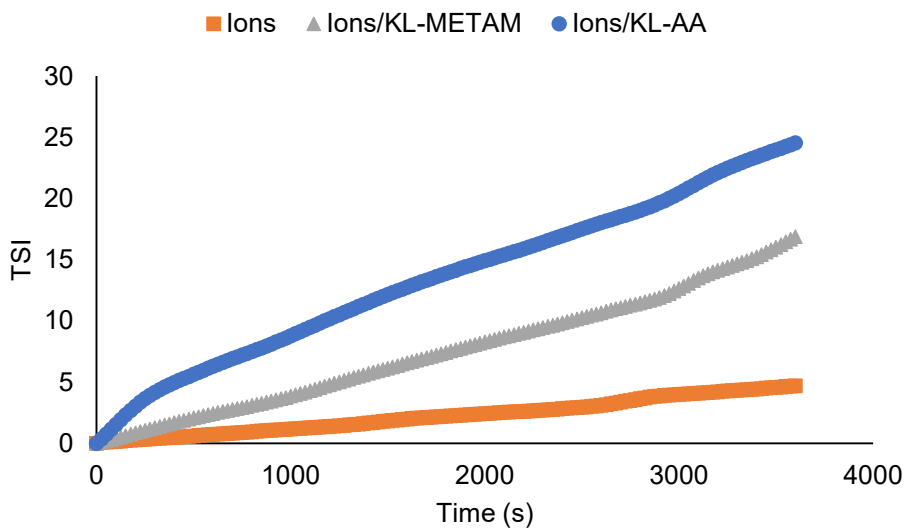
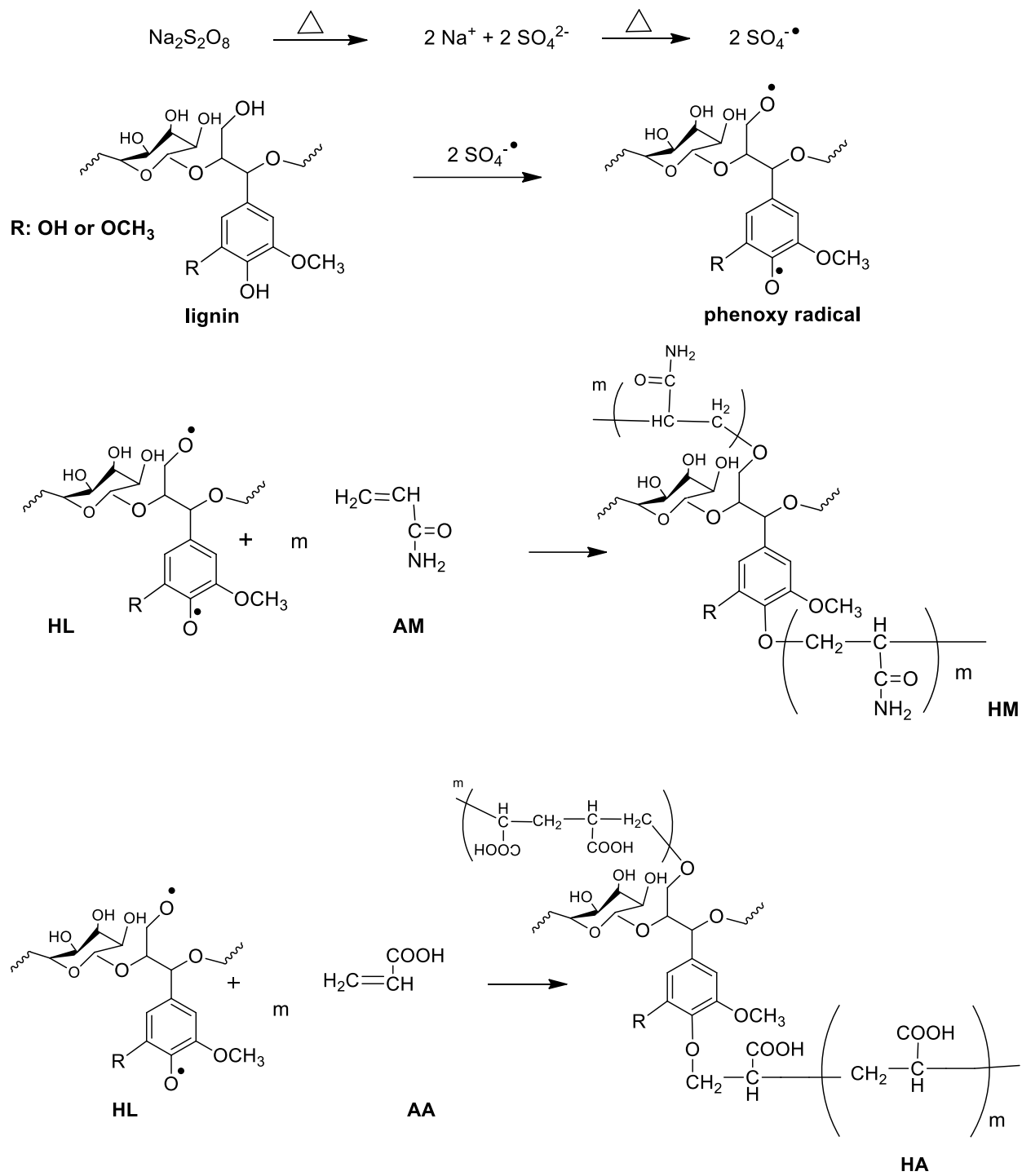
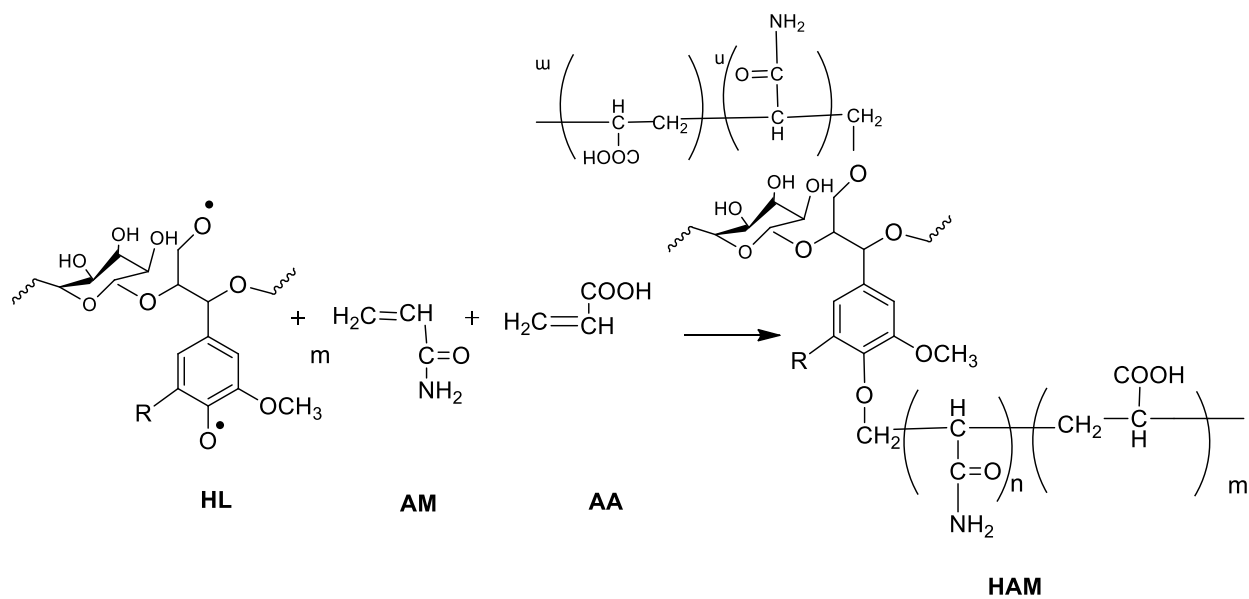
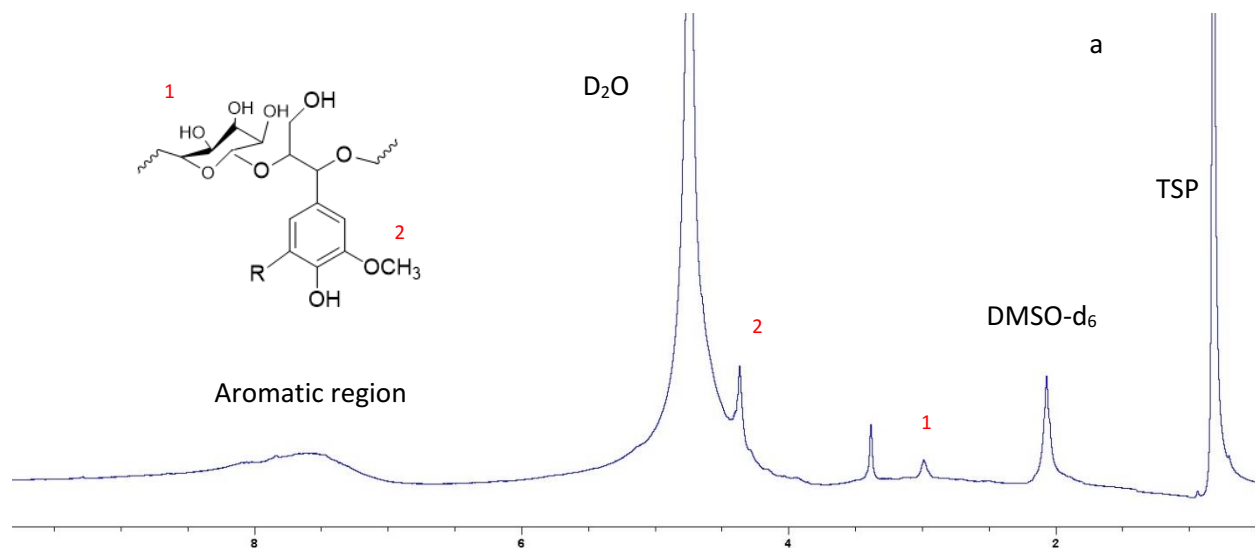


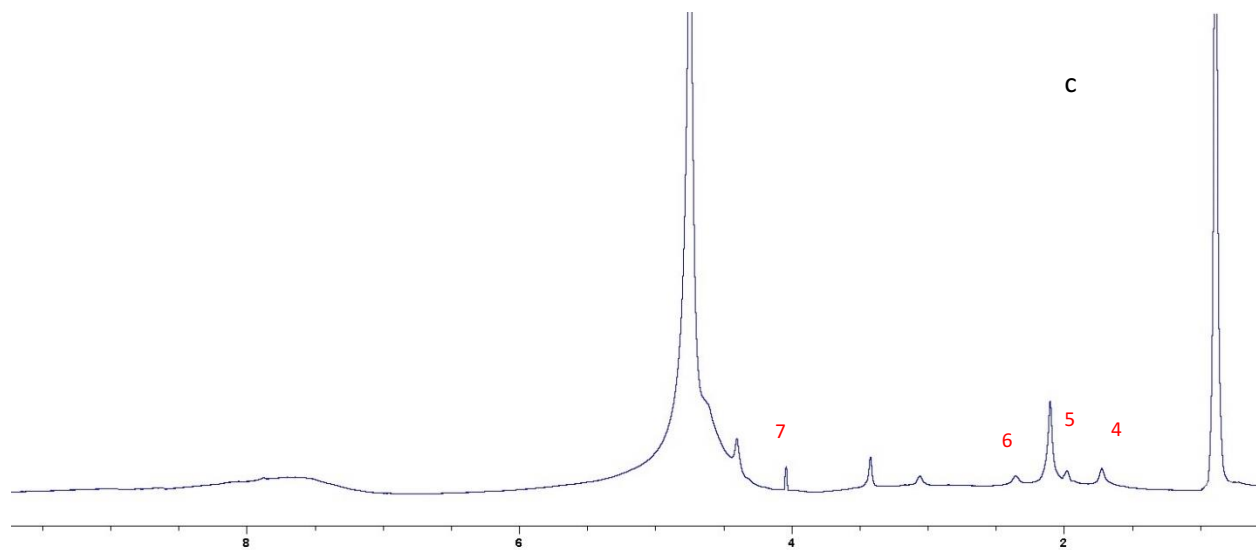
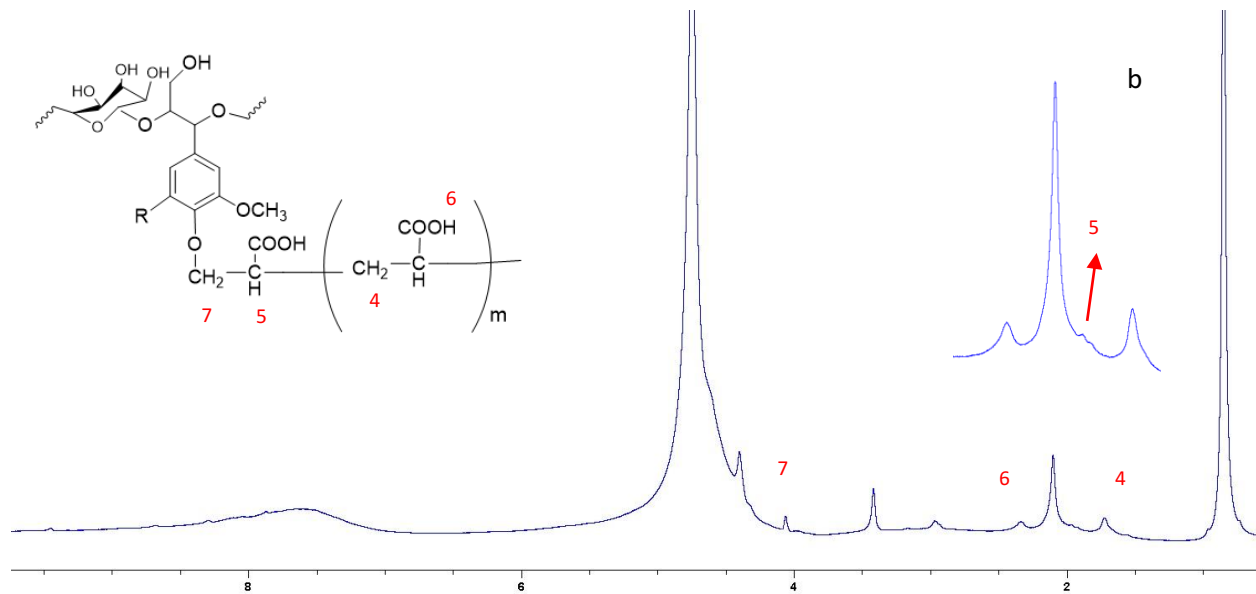
Figure A. 31 The effect of lignin-based polymers on destabilization index of mixed model wastewater containing ZnCl₂, CuCl₂, and KCl (wastewater concentration 10mM, polymer concentration 10 g/L)

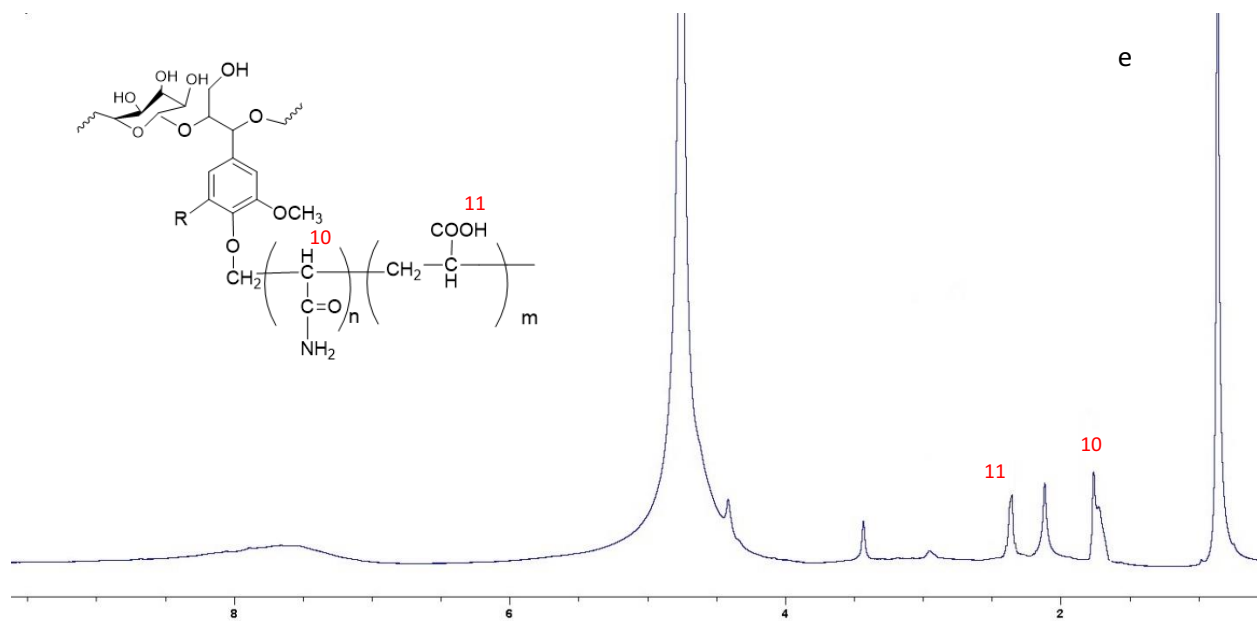
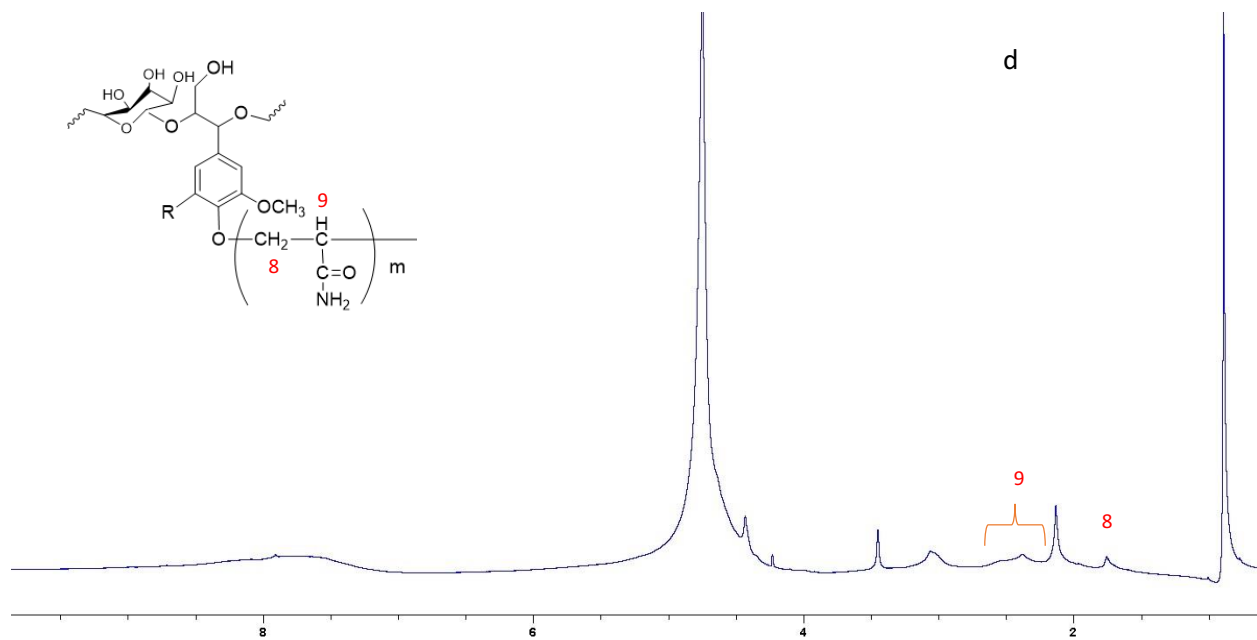




Scheme A. 2 Proposed reaction scheme of polymerization of HL with AA, AM and AA/AM initiated by $\text{Na}_2\text{S}_2\text{O}_8$ under acidic conditions.







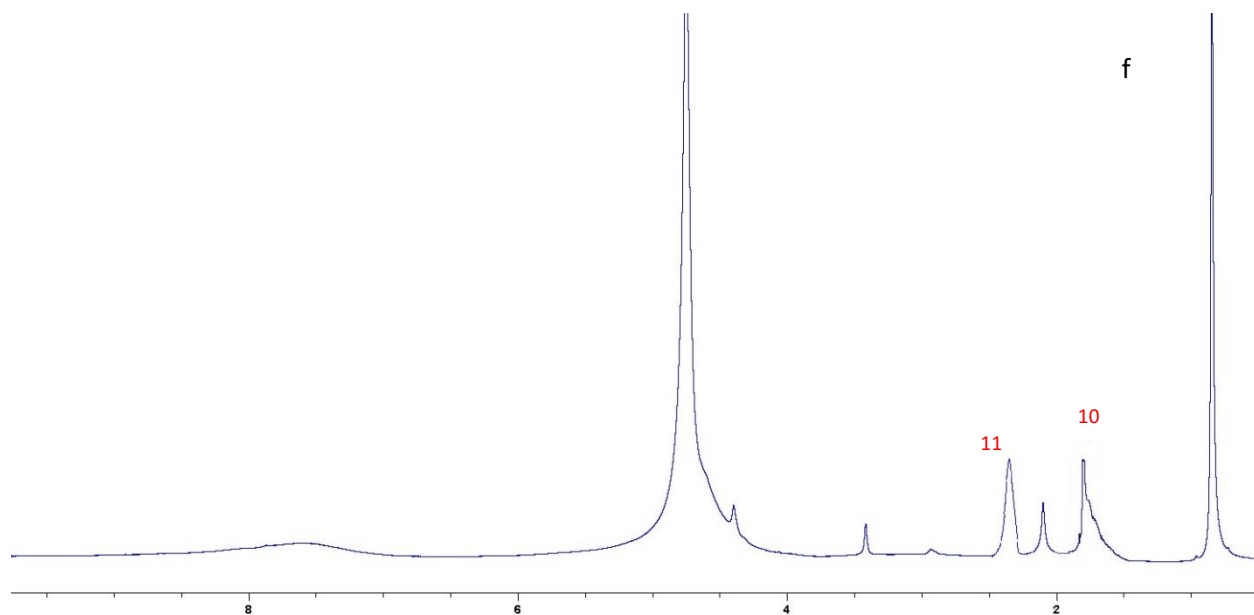


Figure A. 32 $^1\text{H-NMR}$ spectra of a) HL, b-c) HA, d) HM and e-f) HAM polymers.

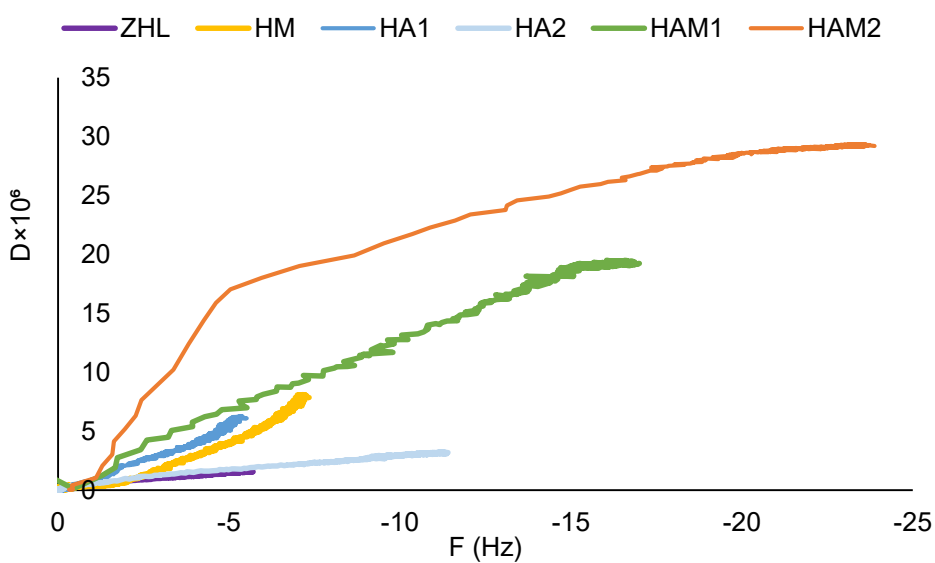


Figure A. 33 Dissipation change of the sensors as a function of frequency changes for adsorption of HMs on the aluminium oxide surface

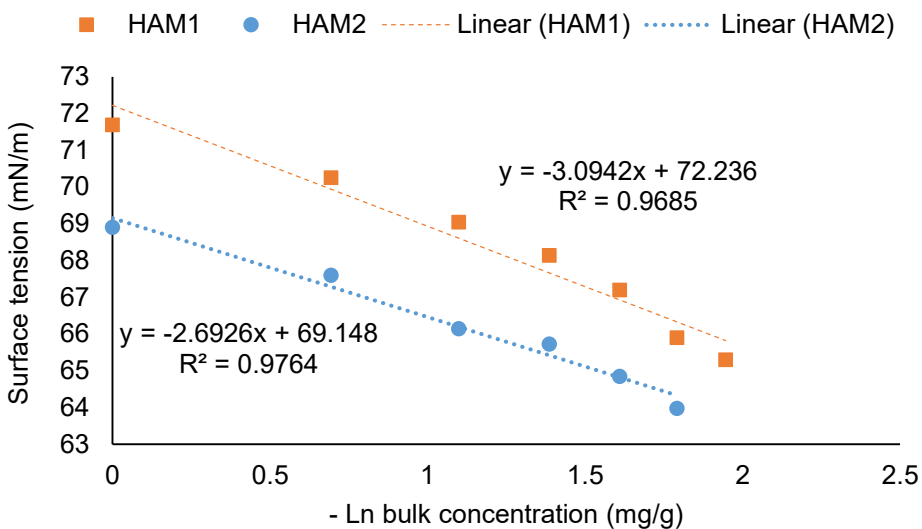


Figure A. 34 Surface tension of HAM polymer solution versus natural logarithm of concentration

Table A. 5 Properties of the DSC analysis.

Sample	T _g , °C	C _p , (J/g°C)
HL	137.67	0.2147
HM	151.23	0.1912
HA1	152.61	0.2125
HA2	150.34	0.1843
HAM1	181.74	0.0954
HAM2	160.6	0.1236

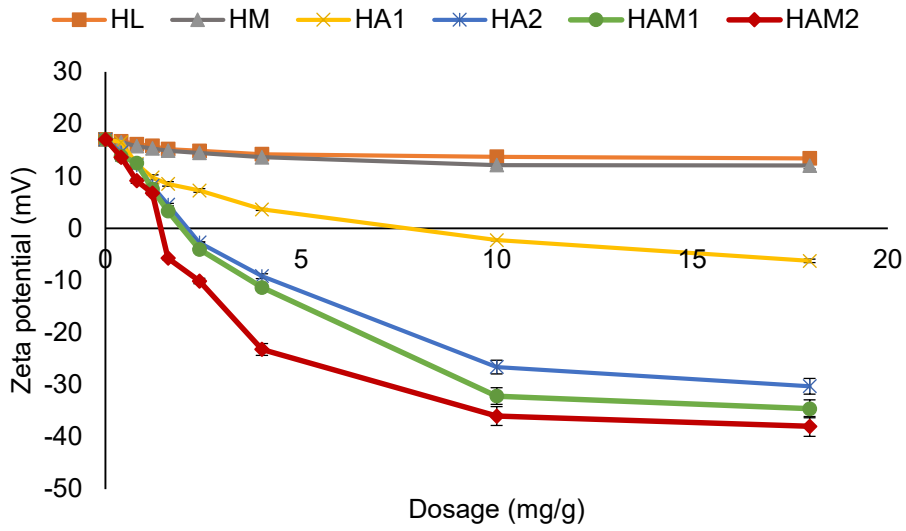
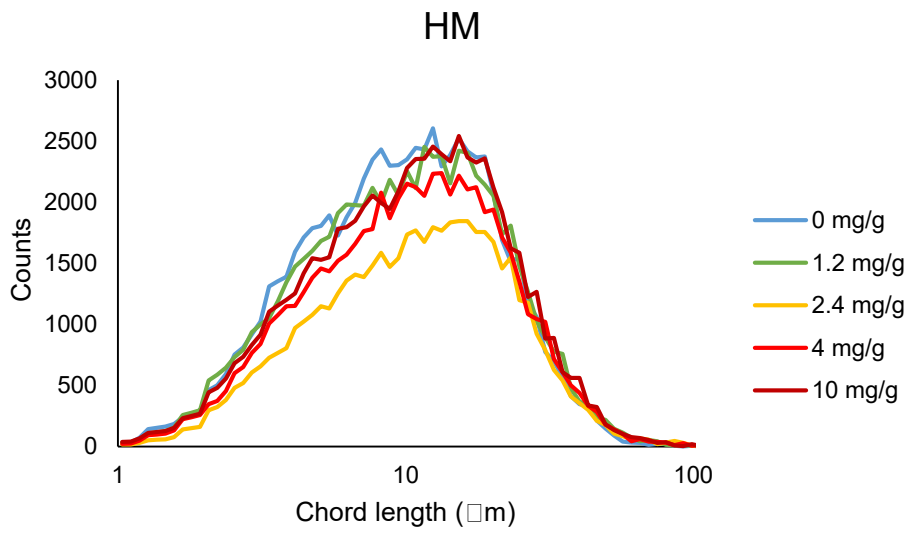
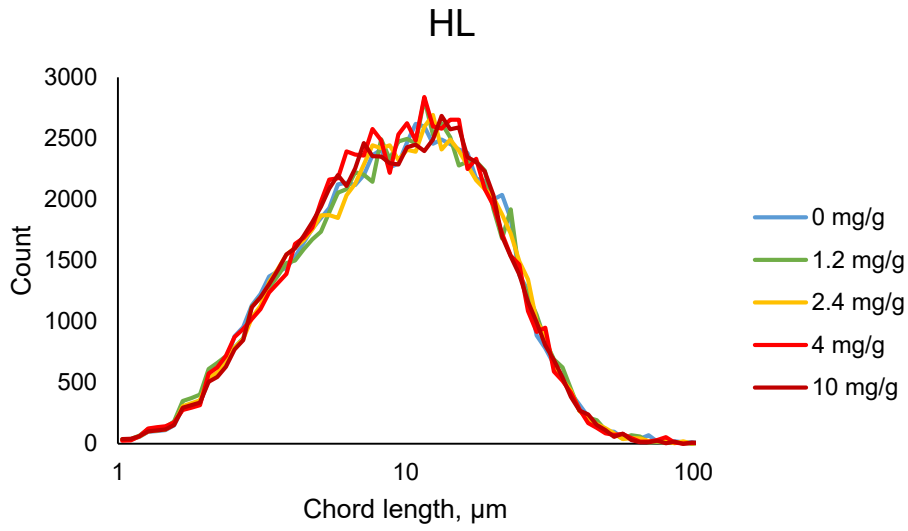
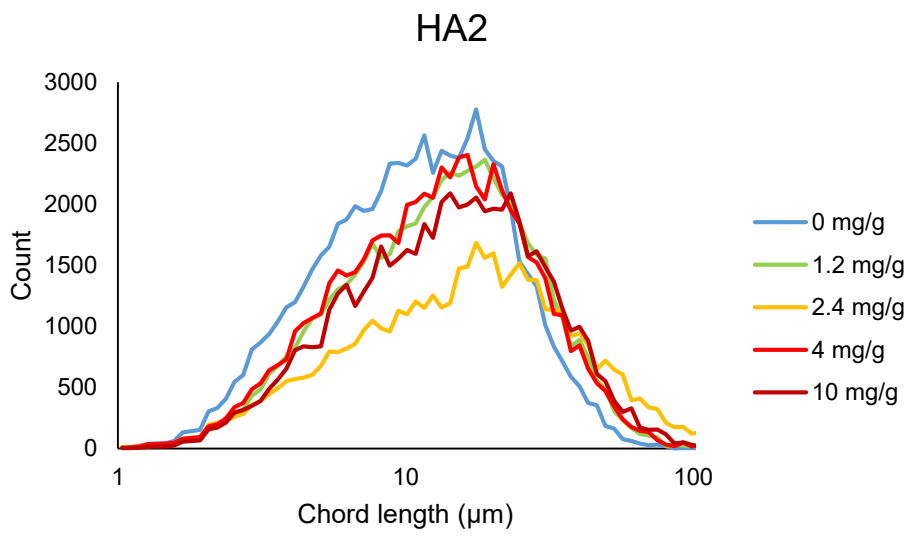
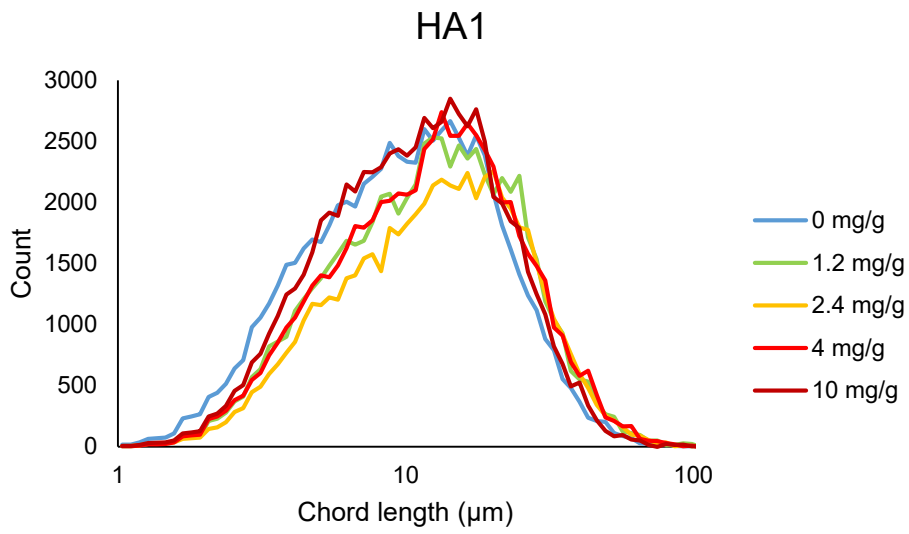


Figure A. 35 Zeta potential of aluminium oxide particles in the presence of HL, HM, HAs and HAMs as a function of polymer dosage (conducted under the conditions of pH 7, 25 C and 25 g/l of aluminium oxide concentration).





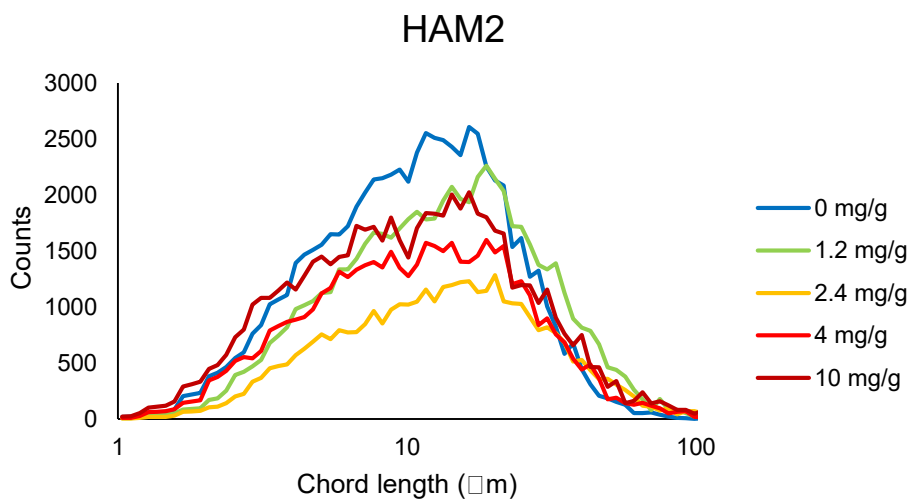
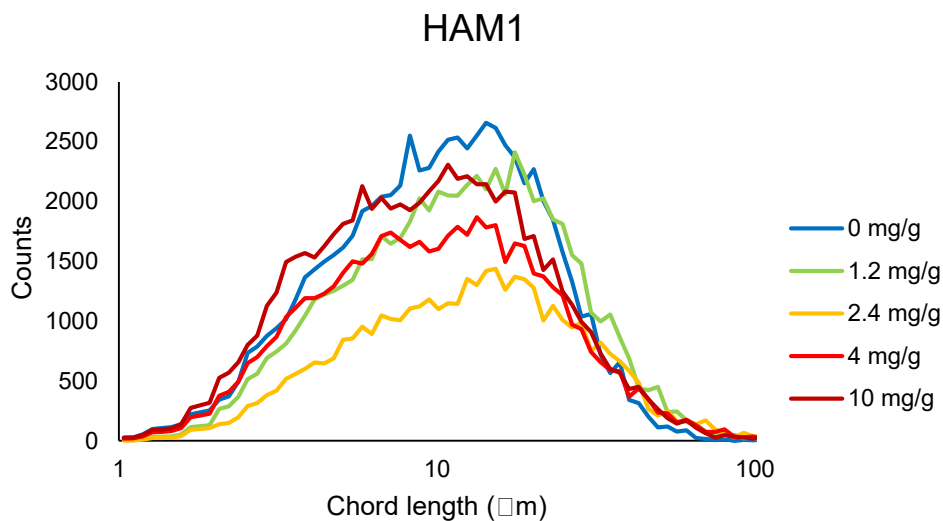


Figure A. 36 Normal-weighted chord length distribution of particles in aluminum oxide suspension at different dosages of a) HL and b) HM c) HA1 d) HA2 e) HAM1 f) HAM2 (25 g/L concentration, pH 7 and 200 rpm).

Table A. 6 Several weighting moments of the chord length distribution at 2.4 mg/g aluminium oxide/lignin polymers

Sample	Unweighted, μm	Square weighted, μm	Cube weighted, μm
HL	12.3	28	49.2
HM	15.7	39.9	60.7
HA1	14.2	38.5	54.8
HA2	16.8	48	84.2
HAM1	17.8	55	100.3
HAM2	18.5	57	126.2

11.1 References

- (1) Liu, Z., Ni, Y., Fatehi, P. A. 2011. Saeed, Isolation and cationization of hemicelluloses from pre-hydrolysis liquor of kraft-based dissolving pulp production process. *Biomass Bioenergy*, 35(5) 1789-1796.
- (2) Couch, R. L., Price, J. T., Fatehi, P. 2016. Production of flocculant from thermomechanical pulping lignin via nitric acid treatment. *ACS Sustain Chem Eng*, 4(4), 1954-1962.
- (3) Yan, M., Yang, D., Deng, Y., Chen, P., Zhou, H., Qiu, X. 2010. Influence of pH on the behavior of lignosulfonate macromolecules in aqueous solution. *Colloids Surf A Physicochem Eng Asp*, 371(1-3), 50-58.
- (4) W. Schärfl, Light scattering from polymer solutions and nanoparticle dispersions. *Springer Science & Business Media*. 2007.
- (5) Lucey, J. A., Srinivasan, M., Singh, H., Munro, P. A. 2000. Characterization of commercial and experimental sodium caseinates by multiangle laser light scattering and size-exclusion chromatography. *J Agric Food Chem*. 48(5), 1610-1616.

- (6) Yuan, Z., Cheng, S., Leitch, M., Xu, C. C. 2010. Hydrolytic degradation of alkaline lignin in hot-compressed water and ethanol. *Bioresour. Technol.* 101(23), 9308-9313.
- (7) Bang, J. H. 2011. Hollow graphitic carbon spheres for Pt electrocatalyst support in direct methanol fuel cell. *Electrochim Acta*, 56(24), 8674-8679.
- (8) Wells, O. C., Boyde, A., Lifshin, E., Rezanowich, A. Scanning electron microscopy. *McGraw-Hill Companies. New York.* 1974
- (9) Lunkenheimer, K., Wantke, K. D. 1981. Determination of the surface tension of surfactant solutions applying the method of Lecomte du Noüy (ring tensiometer). *Colloid Polym. Sci.* 259(3), 354-366.
- (10) Law, G., Watson, P. R. 2011. Surface tension measurements of N-alkylimidazolium ionic liquids. *Langmuir* 17(20), 6138-6141.
- (11) Konduri, M. K., Fatehi, P. 2018. Adsorption and dispersion performance of oxidized sulfomethylated kraft lignin in coal water slurry. *Fuel Process. Technol.* 176, 267-275.
- (12) Fatehi, P., Shen, J., Hamdan, F. C., Ni, Y. 2013. Improving the adsorption of lignocelluloses of prehydrolysis liquor on precipitated calcium carbonate. *Carbohydr Polym*, 92(2), 2103-2110.
- (13) Xiao, F., Huang, J. C. H., Zhang, B. J., Cui, C. W. 2009. Effects of low temperature on coagulation kinetics and floc surface morphology using alum. *Desalination*, 237(1-3), 201-213.
- (14) Wang, L. J., Wang, J. P., Zhang, S. J., Chen, Y. Z., Yuan, S. J., Sheng, G. P., Yu, H. Q. 2009. A water-soluble cationic flocculant synthesized by dispersion polymerization in aqueous salts solution. *Sep purif Technol*, 67(3), 331-335.
- (15) Wang, D., Gregory, J., Tang, H. 2008. Mechanistic difference of coagulation of kaolin between PACl and cationic polyelectrolytes: A comparative study on zone 2 coagulation. *Dry Technol*, 26(8), 1060-1067.

- (16) Yu, W., Gregory, J., Campos, L. 2010. The effect of additional coagulant on the re-growth of alum-kaolin flocs. *Sep purif Technol*, 74(3), 305-309.
- (17) Granata, A. Argyropoulos, D.S., 1995. 2-Chloro-4, 4, 5, 5-tetramethyl-1, 3, 2-dioxaphospholane, a reagent for the accurate determination of the uncondensed and condensed phenolic moieties in lignins. *J. Agric. Food Chem.* 43(6), 1538-1544.
- (18) Guerra, A., Filpponen, I., Lucia, L.A. Argyropoulos, D.S., 2006. Comparative evaluation of three lignin isolation protocols for various wood species. *J. Agric. Food Chem.* 54(26), 9696-9705.
- (19) Tohmura, S.I. Argyropoulos, D.S., 2001. Determination of arylglycerol- β -aryl ethers and other linkages in lignins using DFRC/³¹P NMR. *J. Agric. Food Chem.* 49(2), 536-542.
- (20) Vvu, S. Argyropoulos, D., 2003. An improved method for isolating lignin in high yield and purity. *J. Pulp. Pap. Sci.* 29(7), 235-240.
- (21) Hallac, B.B., Sannigrahi, P., Pu, Y., Ray, M., Murphy, R.J. Ragauskas, A.J., 2009. Biomass characterization of *Buddleja davidii*: a potential feedstock for biofuel production. *J. Agric. Food Chem.* 57(4), 1275-1281.
- (22) Pu, Y., Cao, S. Ragauskas, A.J., 2011. Application of quantitative ³¹P NMR in biomass lignin and biofuel precursors characterization. *Energy Environ Sci.* 4(9), 3154-3166.
- (23) Gaudreault, R., Di Cesare, N., van de Ven, T.G. Weitz, D.A., 2015. Structure and strength of flocs of precipitated calcium carbonate induced by various polymers used in papermaking. *Ind. Eng. Chem. Res.* 54(24), 6234-6246.
- (24) Wang, L.J., Wang, J.P., Zhang, S.J., Chen, Y.Z., Yuan, S.J., Sheng, G.P. Yu, H.Q., 2009. A water-soluble cationic flocculant synthesized by dispersion polymerization in aqueous salts solution. *Sep Purif Technol.* 67(3), 331-335.

- (25) Sabaghi, S. Fatehi, P., 2019. Phenomenological Changes in Lignin Following Polymerization and Its Effects on Flocculating Clay Particles. *Biomacromolecules* 20(10), 3940-3951.
- (26) Kong, F., Wang, S., Price, J.T., Konduri, M.K. Fatehi, P., 2015. Water soluble kraft lignin–acrylic acid copolymer: Synthesis and characterization. *Green Chem.* 17(8), 4355-4366.
- (27) He, W., Gao, W. Fatehi, P., 2017. Oxidation of kraft lignin with hydrogen peroxide and its application as a dispersant for kaolin suspensions. *ACS Sustain. Chem. Eng.* 5(11), 10597-10605.
- (28) Bayazeed, A., Elzairy, M.R. Hebeish, A., 1989. Synthesis and Application of New Thickeners Part I: Preparation of Poly (Acrylic Acid)-Starch Graft Copolymer. *Starch* 41(6), 233-236.
- (29) Jahan, M.S., Chowdhury, D.N., Islam, M.K. Moeiz, S.I., 2007. Characterization of lignin isolated from some nonwood available in Bangladesh. *Bioresour. Technol.* 98(2), 465-469.
- (30) Wang, S., Kong, F., Gao, W. Fatehi, P., 2018. Novel process for generating cationic lignin based flocculant. *Ind. Eng. Chem. Res.* 57(19), 6595-6608.
- (31) Edvardsson, M., Rodahl, M., Kasemo, B. Höök, F., 2005. A dual-frequency QCM-D setup operating at elevated oscillation amplitudes. *Anal. Chem.* 77(15), 4918-4926.
- (32) Reviakine, I., Johannsmann, D. Richter, R.P., *Hearing what you cannot see and visualizing what you hear; interpreting quartz crystal microbalance data from solvated interfaces*: 2011.

- (33) Yang, D., Yan, B., Xiang, L., Xu, H., Wang, X. Zeng, H., 2018. Understanding the surface properties and rheology of a silica suspension mediated by a comb-type poly (acrylic acid)/poly (ethylene oxide)(PAA/PEO) copolymer: effect of salinity. *Soft matter*, 14(23), 4810-4819.